Frictional Half-Plane Contacts in Partial Slip in the Steady-State



Hendrik N. Andresen

St Cross College

University of Oxford

A thesis submitted for the degree of

Doctor of Philosophy

Trinity 2020

Abstract

This thesis aims to understand how a number of real contact problems respond to local contact loads during cyclic loading and which combination of loads will give rise to a state of partial slip. At the core of this thesis lies a family of partial slip solutions for half-plane contact problems subject to different forms of periodic loading. This collection of partial slip solutions allows engineers and researchers alike to assess rapidly the contact behaviour, namely the position and extent of the zones of relative cyclic motion along the interface. While knowing the slip stick pattern, by itself, does not answer the question of whether an assembly is prone to fretting fatigue or not, it enables the user to set up simple laboratory experiments in order to determine the fretting fatigue strength of the design under consideration.

The thesis begins with a taxonomy of the different classes of contacts that can arise in mechanical assemblies. In many fretting fatigue problems, we encounter one particular contact class, the so-called *incomplete contact*, which is suited for being represented by half-planes. After exploring the properties and limitations of plane elasticity and half-plane theory, we look at half-plane partial slip contact problems under different types of loading. We will make use of three different solution approaches (a) an analytical description using a superposition of full sliding shear tractions, (b) an analytical description using glide dislocations starting from a fully adhered state, and (c) an asymptotic description of the contact edge behaviour. Where suitable, the research results are applied to example geometries in order to familiarise the reader with the methodologies presented. The thesis concludes with the proposal of a generalised approach to fretting fatigue strength utilising experimental results published in the literature. The test data is reinterpreted by applying the outlined asymptotic methods in order to provide generality and comparability across different geometries and loading scenarios.

This thesis is a collection of research performed by the author in the Department of Engineering Science at the University of Oxford under the supervision of Professor David A. Hills. This work is original and no part of it has been submitted for a degree at this university or elsewhere. Some of the work described in this thesis has been published or is under consideration for publication in the following journal articles or book chapters:

- **Andresen H.**, Hills D., Vázquez J. (2019b). Closed-form solutions for tilted three-part piecewise-quadratic half-plane contacts. *Int. J. Mech. Sci.*, **150**: 127–134.

- **Andresen H.**, Hills D., Barber J., Vázquez J. (2019a). Frictional half-plane contact problems subject to alternating normal and shear loads and tension in the steady state. *Int. J. Solids Struct.*, **168**: 166–171.

- **Andresen H.**, Hills D., Barber J., Vázquez J. (2020b). Steady state cyclic behaviour of a half-plane contact in partial slip subject to varying normal load, moment, shear load, and moderate differential bulk tension. *Int. J. Solids Struct.*, **182**: 156–161.

- **Andresen H.**, Hills D. (2020). A review of partial slip solutions for contacts represented by half-planes including bulk tension and moments. *Tribology Int.*, **143**: 106050.

- **Andresen H.**, Hills D., Moore M. (2020c). The steady state partial slip problem for half plane contacts subject to a constant normal load using glide dislocations. *Eur. J. Mech/A Solids*, **79**: 103868.

- Hills D., **Andresen H.** (2020). *Fundamentals of Elastic Contacts. In: M. Paggi and D. Hills, ed., Modeling and Simulation of Tribological Problems in Technology, 1st ed.. Springer International Publishing.*

- **Andresen H.**, Hills D., Moore M. (2020e). Representation of incomplete contact problems by half-planes. *Eur. J. Mech/A Solids*, *accepted for publication.*

- **Andresen H.**, Fleury R., Moore M., Hills D. (2020a). Explicit and asymptotic solutions for incomplete half-plane contacts subject to general loading. *J. Mech. Phys. Solids*, *under review.*

Some of the work described in this thesis has been presented at the following conferences:

- **Andresen H.**, Hills D. (2018). Unsymmetrical incomplete contacts subject to varying loads. 9th *Contact Mechanics International Symposium*, Biella, Italy.
- **Andresen H.**, Hills D. (2019c). Half-plane contacts under conditions of varying loads in the steady-state. 9th *International Symposium on Fretting Fatigue*, Seville, Spain.
- **Andresen H.**, Hills D., Moore M. (2019d). A rigorous matching procedure between prototype and laboratory test for highly loaded contacts. 1st *Tribomechadynamics Conference*, Houston, USA.
- **Andresen H.**, Hills D., Wormsen A., Macdonald K. (2020d). Fretting fatigue design of subsea connectors; a generalised approach to testing. 39th *International Conference on Ocean, Offshore & Arctic Engineering*, Virtual Conference.

Acknowledgements

Personal

I would like to take this opportunity to thank Professor David Hills for guiding, advising, and challenging me over the past three years and for the opportunities he has given me to grow as a person. I am grateful to have met Professor Jesús Vázquez from Seville, Spain, who was always willing to offer help and advice. I also would like to express my thanks to Professor James Barber at the University of Michigan for his invaluable feedback on different technical questions and Dr. Matthew Moore for his help with numerous mathematical challenges.

I sincerely thank Dr. Pierangelo Duó, Dr. Andrej Golowin, and Dr. John Schofield for hosting me at various Rolls-Royce locations in the UK and Germany. An individual thanks is due to Dr. Anders Wormsen for asking the right questions and being patient with me in finding the answers.

I would like to thank the following friends, colleagues, and staff at the Department of Engineering Science, and around the world without whom I would not have been able to complete this thesis: Dr. Luke Blades, Ms Amanda Bradbury, Mr Yifeng Chen, Ms Zoe Clark, Mr Nils Cwiekala, Mr Hisham Elamin, Dr. Elsiddig Elmukashfi, Dr. Rodolfo Fleury, Mr Simon Hills, Dr. Jhonatan Lopes, Dr. Kurien Parel, Dr. Robert Paynter, Dr. Rangarajan Ramesh, Mr Daniel Riddoch, Mr James Truelove, and Dr. Heather Wilson.

Last but not least, I would like to thank Laura, Marianne, and my friends in the UK and Germany for their love, support, and companionship throughout my doctoral studies.

Die Menschheit steckt noch in den Kinderschuhen
mit Geschmack und Niveau
sie will nicht in die Adoleszenz
denn die Pubertität, die ist nicht so.

Humanity is still in its infancy;
with taste and class;
does not want to come of age;
because puberty, is not to its liking.
— *Norbert Andresen*

Institutional

This project has received funding from the European Union's Horizon 2020 research and innovation programme under the Marie Sklodowska-Curie agreement No 721865.

Contents

1 Introduction **1**

1.1 Friction 1
1.2 Fretting Fatigue 3
1.3 Scope of the Thesis 7
1.4 Taxonomy of Contacts 9

2 Plane Elasticity and Half-Plane Contacts **15**

2.1 Airy Stress Functions and the Half-Plane 17
2.2 Inversion of Integral Equations 22
2.3 Example of a Hertzian Geometry 23
2.4 Further Examples 24
2.5 An Alternative Method for Solving Contact Problems 25
2.5.1 The Normal Problem 26
2.5.2 Re-visiting the Example of a Hertzian Geometry 29
2.5.3 Application of a Shear Force 29
2.5.4 The Effect of Bulk Tension 30
2.5.5 The Effect of a Moment 32
2.6 Inequality for Full Stick 33

3 Half Plane Partial Slip Contact Problems **36**

3.1 Asymmetrical Contact Problems 39
3.2 The Order of Load Application 42
3.2.1 Sequential Loading (Constant Normal Load) 43
3.2.2 Proportional Loading 46
3.2.3 Two-Stage Proportional Loading 48
3.2.4 Application to a Hertzian Geometry 50
3.3 The Effect of Differential Bulk Tension 52
3.3.1 Moderate Differential Bulk Tension in Partial Slip 53
3.3.2 Large Differential Bulk Tension in Partial Slip 55
3.4 Periodic Shear Loading 55
3.5 General Cyclic Proportional Loading 58
3.5.1 The Permanent Stick Zone 60

3.5.2 Mapping between the Normal and Tangential Problem . . . 63
3.5.3 Application to the Tilted Shallow Wedge 64
3.6 Conclusion 66

4 Partial Slip Solutions Based on Dislocations 68
4.1 Mathematical Framework 69
4.2 Tangential Problem under Constant Normal Load 71
4.2.1 The Adhered Condition 71
4.2.2 The Insertion of Glide Dislocations 72
4.2.3 Solution (Constant Normal Load) 73
4.2.4 Shear Force Only 75
4.2.5 Differential Tension Only 76
4.3 Cyclic Loading (Constant Normal Load) 76
4.4 Application to a Hertzian Geometry 81
4.4.1 Moderate Differential Bulk Tension 81
4.4.2 Large Differential Bulk Tension 82
4.4.3 Display of Example Problem Results 83
4.5 Cyclic Loading (Varying Normal Load) 84
4.5.1 Contact under Full Stick 85
4.5.2 Partial Slip Problem 87
4.5.3 Solution 89
4.6 Conclusion 90

5 Asymptotic Solutions for Frictional Half-Plane Contacts 91
5.1 Asymptotic Methods Applied to Normal Tractions 93
5.1.1 Mossakovskii Methods 94
5.2 Tangential Loading under Constant Normal Load 97
5.2.1 The Partial Slip Problem under Constant Normal Load . . . 98
5.3 Tangential Solution under Varying Normal Load and Moment . . . 100
5.3.1 Asymptotic Approximation of Shear Tractions 100
5.3.2 Calculation of the Steady-State Slip Zone Size 102
5.4 Example Application 103
5.4.1 Asymptotic Solution 104
5.5 Display of Results 105
5.5.1 The Cattaneo-Mindlin Problem 106
5.5.2 The Effect of a Varying Normal Load 108
5.5.3 The Effect of Differential Bulk Tension 109
5.5.4 The Effect of a Constant Angle of Tilt 111
5.5.5 A Varying Moment together with Large Differential Tension 113
5.6 Conclusion 114

6 Representation of Incomplete Contact Problems by Half-Planes 115
6.1 Proportional Loading with no Moment Developed 118
6.1.1 Demonstration of the Methodology for a Hertzian Contact . 124
6.1.2 Using Asymptotes in Step (iii) 128
6.2 Problems when a Moment is Developed 129
6.3 Dovetail Geometry Example 132
6.4 Conclusion 135

7 Fretting Fatigue Strength 137
7.1 Fatigue and Fretting 138
7.2 Experimental Set Up and Data 140
7.3 Applying Asymptotic Methods 143
7.4 Visualisation of the Fretting Fatigue Strength 145
7.4.1 Aluminium Alloys 146
7.4.2 Titanium Alloy - Ti6Al4V 149
7.5 Generalising Fretting Fatigue Testing 152

8 Summary and Future Work 154
8.1 Future Work 157

Appendices

A Appendix 161
A.1 The Tilted Three-Part Punch 161
A.1.1 Integral Evaluation 163
A.1.2 The Pressure Distribution 165
A.1.3 The Consistency Condition 165
A.1.4 The Normal Equilibrium 166
A.1.5 The Rotational Equilibrium 167
A.1.6 Case ‘A’ - The Tilted Flat but Rounded Punch with Unequal Radii 168
A.1.7 Case ‘B’ - The Rounded Punch with a Concave Central Segment 169
A.1.8 Case ‘C’ - The Tilted Punch Comprised of Two Adjoined Unequal Half-Cylinders 170
A.2 Partial Slip Problems - Sequential Loading [Andresen et al., 2020e] 171
A.3 Leading-order Asymptotic Form 173
A.4 Experimental Data 176
A.5 Range of Asymptotic Multipliers 180

Bibliography 182

1 Introduction

Contacts are present in almost all mechanical assemblies when forces are transferred from one component to another. It follows that loads which, in general terms, are diffusely carried in the majority of a component are localised where the component is in contact with other things. The scientific field concerned with the stresses arising perpendicular and tangentially to the touching interfaces is called *contact mechanics* [Johnson, 1985]. Different phenomena can be observed or are important when a contact is established including friction, wear, roughness, adhesion, heat transfer or electric conduction and it is the very first phenomenon listed here, *friction*, that is of particular interest to the contents of this thesis. While the perpendicular, or normal contact is a highly non-linear and mathematically challenging problem by itself, the tangential problem adds an additional layer of complexity when frictional behaviour is considered [Barber, 2018]. From a macroscopic perspective two contacting bodies can only be in a rolling motion, in gross relative sliding or notionally stationary.

1.1 Friction

Figure 1.1 shows an idealised two-dimensional contact problem subject to a normal load, P, and a tangential load, Q. Supposing the absence of sufficient torque to cause rolling, the answer to the question "Which combination of forces is necessary to

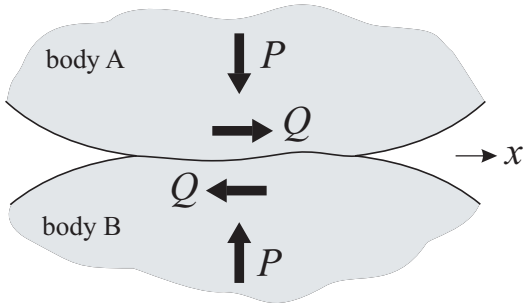


Figure 1.1: Generic two-dimensional contact subject to a normal load, P, and shear load, Q.

cause relative motion?" is found in the commonly accepted friction law by Coulomb. The law states that the frictional force in gross sliding is proportional to the applied normal load. Further, the frictional force opposes the direction of motion in each body and is independent of the contact area. These statements were first postulated and experimentally verified by Amontons [Amontons, 1699]. Coulomb added the third observation that the frictional force is also independent of the velocity of sliding [Coulomb, 1785]. The proportionality factor limiting the applied tangential force is the coefficient of friction, in this thesis denoted f, so that we can write

$$Q \leq fP. \tag{1.1}$$

For materials which obey the described friction law, i.e. metals, ceramics or wood, the coefficient of friction is considered a system property of the contacting bodies, independent of the geometry or loads present.

Suppose, now, that the tangential force is less than that necessary to cause full sliding. Knowing the nominal contact forces present at the interface, here P and Q, is insufficient to make statements about the interfacial tractions arising or the underlying stress field. The state of the contact interface, that is, the distribution of regions of stick and slip, do not depend just on the instantaneous contact forces but in which order the forces were applied. We shall see, later on, that it is quite possible to have the same set of applied forces present on a contacting pair, which in one case, the contact might be wholly adhered, whilst in others there will be significant areas of slip so that the solution becomes loading path-dependent. This

leads to inherently non-linear behaviour and makes this an interesting area of solid mechanics to study. The class of problems concerned with microscopic relative motion within a contact interface, when the tangential force is insufficient to cause full sliding, is called *partial slip*. When that is the case, parts of the interface experience relative motion while the rest of the contact remains fully adhered [Andresen and Hills, 2020]. In fact, particles on the surfaces of two components pressed together may be in one of two states; they may be stuck together, or they may be slipping. A contact where at least some of the interface is stuck cannot be in gross relative motion. When a half-plane contact (and we shall restrict ourselves to two-dimensional problems in this thesis) is in partial slip, we may apply Coulomb's friction law in a point-wise sense so that there are two sets of conditions which hold in the slip and stick regions of a contact:

- Stick region – the local shear traction, $q(x)$, must be lower in magnitude than the contact pressure, $p(x)$, here defined as positive when compressive, multiplied by the coefficient of friction, i.e. $|q(x)| \leq fp(x)$, and the relative slip displacement of pairs of contacting points is preserved at its current value, i.e. $u_{\mathrm{A}}(x) - u_{\mathrm{B}}(x)$ is constant, and the relative displacement velocity is $\Delta\dot{u}(x) = \dot{u_{\mathrm{A}}}(x) - \dot{u_{\mathrm{B}}}(x) = 0$, where $u(x)$ is the lateral displacement of surface particles.

- Slip region – the magnitude of the local shear traction is limited to the product of the coefficient of friction and the contact pressure, so that $q(x) = \pm fp(x)$ and the choice of sign must be consistent with the change in slip of surface points, so that it opposes the motion.

1.2 Fretting Fatigue

Supposing the coefficient of friction is finite and the contact is not perfectly lubricated, there are two important damage mechanisms associated with frictional contacts in engineering and which need to be addressed in the design of a new component, these are wear and fretting [Waterhouse, 1984]. The former is mostly

caused by bodies in macroscopic relative motion, i.e. $Q = fP$, and this will not be the subject of further investigation in this thesis. The latter is caused by tiny amounts of differential movement in the micrometre range, mostly when the applied tangential force is less than its limiting value, i.e. $Q < fP$ [Waterhouse, 1981]. These relative displacements are the cause of surface modifications which produce conditions ripe for the nucleation of fatigue cracks.

Furthermore, a contact itself acts as a stress concentrator that raises the local stress field in proximity to the contact interface. An important consequence of the elevated stress level is that failure of a component often begins at the interface. It seems natural to be interested in the frictional behaviour of contacts when studying fretting fatigue, which is an often overlooked failure mechanism in many structural assemblies, including aeronautical [Ruiz and Nowell, 2000]. It has been the cause of catastrophic failure of the so-called dovetail root joints between the rotor (often denoted disk) and the fan blade of a gas turbine engine, as illustrated in Figure 1.2. Other engineering examples in which fretting fatigue may affect the structural

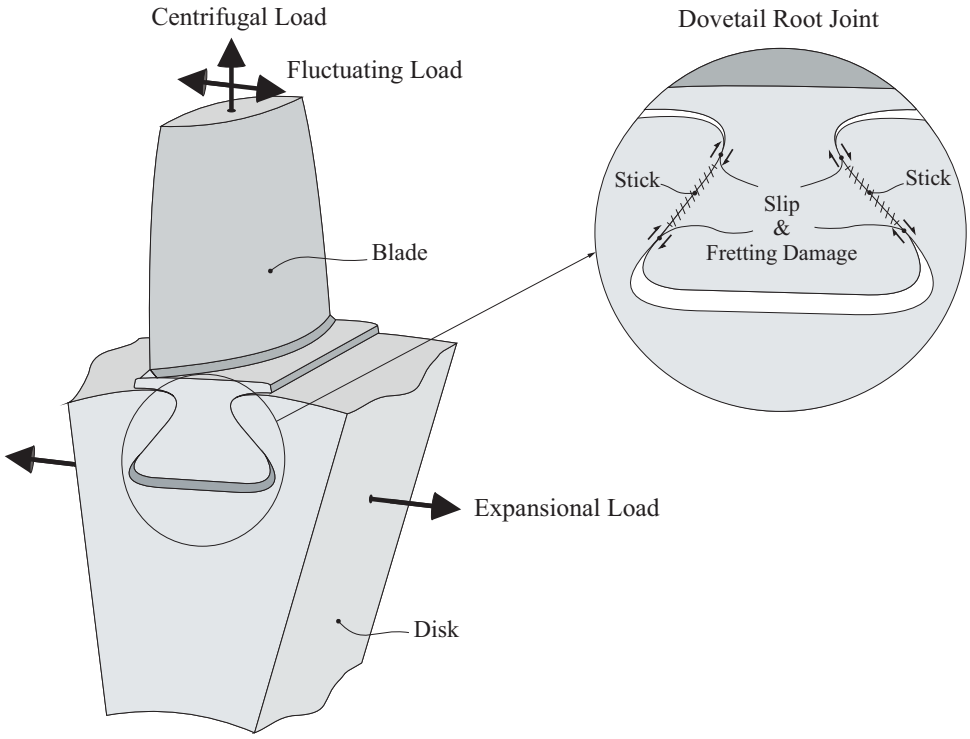


Figure 1.2: Dovetail root joint between rotor and fan blade of a gas turbine engine with areas of attendant fretting damage.

integrity of a design include swashplates of helicopter rotors or the upper end of a subsea wellhead system [Andresen et al., 2020d].

In a gas turbine engine, centrifugal forces form the contact and expand the disk. Superimposed is a fluctuating load acting on the blade, for example induced by an unsteady gas stream or the excitation of an eigenfrequency. Often, these contacts are found in a state of *partial slip* for long periods during operation, the so-called *steady-state* cycle, and fretting damage is accumulated in the regions of repetitive relative movement between blade and disk, see Figure 1.3. The external loads acting on the assembly shown in Figure 1.2 give rise to local contact loads. In its two-dimensional representation we can identify four potential contact load quantities, namely a normal load, P, a moment, M, a shear force, Q, and a differential bulk tension, $\sigma = \sigma_{\mathrm{A}} - \sigma_{\mathrm{B}}$, as indicated in the idealised half-plane contact problem shown in Figure 1.4. These quantities vary with time so that each has an oscillatory component and at least the normal load remains positive throughout the cyclic loading.

Although there are many types of contacts in an aerospace engine experiencing fretting, for example splined shafts and in minor degree bolted flanges, the dovetail root contact is the most common practical example found in the literature as fretting fatigue is known to be a dominant failure mode [Arrieta and Wackers, 2004]. A

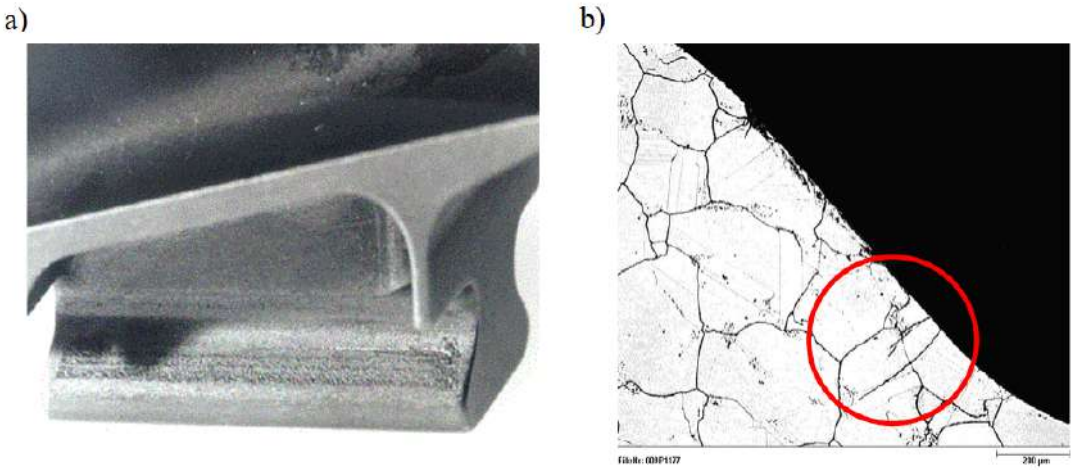


Figure 1.3: Dovetail root of a compressor blade with a) excessive fretting damage in the region of contact and b) a fretting fatigue crack adjacent to the contact edge, area circled in red [Arrieta and Wackers, 2004].

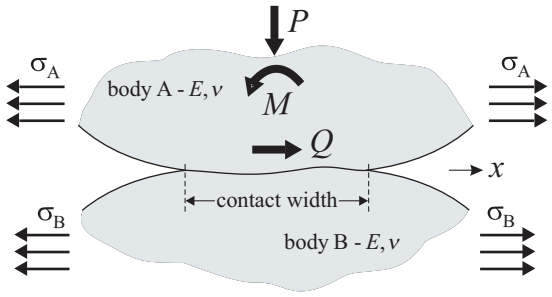


Figure 1.4: General half-plane contact subject to a normal load, P, and a moment, M, with a differential tension, $\sigma = \sigma_{\mathrm{A}} - \sigma_{\mathrm{B}}$.

tragic in-flight accident happened in April 2018 when Southwest Airlines flight 1380 experienced a failure of its left CFM International CFM56-7B turbofan engine mid-air, Figure 1.5. The engine failure occurred when one of the fan blades fractured at its dovetail root. During this fan blade off event, debris of the engine inlet and casing punctured a cabin window of the Boeing 737-7H4 aircraft which resulted in a rapid de-pressurisation of the air plane. After initiating an emergency landing, the air plane landed safely. Tragically, the incident claimed the life of one passenger and eight other passengers received minor injuries. The United States government National Transportation Safety Board (NTSB) investigated the incident and their final report states that a crack in the fan blade root initiated because of *higher-than-expected stresses* [NTSB, 2019]. Figure 1.6 shows the fractured fan



Figure 1.5: Damaged CFM56-7B engine being examined by an NTSB inspector and showing one fan blade missing, area circled in red [NTSB, 2019].

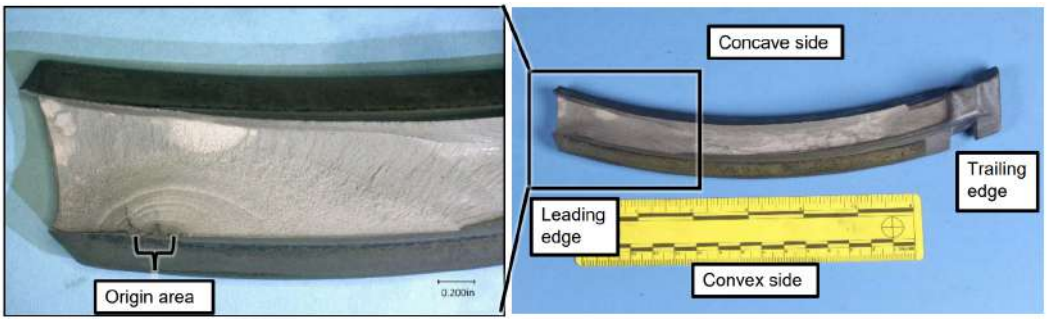


Figure 1.6: Fractured fan blade root [NTSB, 2019].

blade root with the origin area of the crack adjacent to significant fretting damage. Southwest Airlines lost $100 million in revenue as part of the accident's aftermath. The additional airworthiness directive cost across all affected CFM engines is estimated at $50 million [Southwest, 2018]. These figures do not include costs caused by the investigation itself, subsequent lawsuits, or future engine certification requirements. To this date - September 2020 - none of the safety recommendations issued by the Federal Aviation Administration in relation to the described incident include an analysis of the fretting fatigue strength of the dovetail root joint by engine manufactures. Most recommendations were concerned with improving the structural integrity of the engine's casing in order to contain fully debris in the case of a fan blade off event.

1.3 Scope of the Thesis

Engineering assemblies inevitably compose of a large number of mechanical joints. The individual components suffer degradation throughout their service lives and contact between components may be an important life-controlling factor. Despite extensive research efforts in the past decades, fretting fatigue strength prediction remains a challenge in the design process of any new mechanical assembly. Current industrial methods often require complete structural testing of the actual assembly under real loading conditions which is cost and time consuming, and often result in empirical models only, lacking generality. The consequence is either the premature

replacement of a component during overhaul, or, in the worst case scenario, the potential in-service failure of a component.

The practical motivation of this research is to understand how a number of real contact problems respond to local contact loads and which combination of loads will give rise to a state of partial slip. Following the identification of a partial slip problem the extent of the attendant fretting damage needs to be determined. This brings us to the core of this thesis, which is a family of partial slip solutions for half-plane contact problems subject to periodic loading.

This collection of partial slip solutions allows engineers and researchers alike to assess rapidly the slip-stick behaviour, namely the position and extent of the zones of potential fretting damage within a contact interface, which we will call the *slip zones*. While that, by itself, does not answer the question of whether an assembly is prone to fretting fatigue or not, it enables the user to set up simple laboratory experiments in order to determine the fretting fatigue strength of the new design under consideration.

The thesis begins with a taxonomy of the different classes of contacts that can arise in mechanical assemblies [Hills and Andresen, 2020]. In many fretting fatigue problems, we encounter one particular contact class, the so-called *incomplete contact*, which is suited for being represented by half-planes. After exploring the properties and limitations of plane elasticity and half-plane theory, we look at half-plane partial slip contact problems under different types of loading. We will make use of three different solution approaches (a) an analytical description using a superposition of full sliding shear tractions, (b) an analytical description using glide dislocations starting from a fully adhered state, and (c) an asymptotic description of the contact edge behaviour. Where suitable, the research results are applied to example geometries in order to familiarise the reader with the methodologies presented. The thesis concludes with the proposal of a generalised approach to fretting fatigue strength utilising experimental results published in the literature. The test data is reinterpreted by applying the outlined asymptotic methods in order to provide generality and comparability across different geometries and loading scenarios.

1.4 Taxonomy of Contacts

The subject of contact mechanics was initiated by Heinrich Hertz in 1881 with the publication of *"Über den Kontakt elastischer Körper"* [Hertz, 1881]. At the time, Hertz was interested in optical interference between glass lenses. He noticed that the elastic deformation of lenses brought into contact by the application of a force had a significant influence on the pattern of interference fringes [Johnson, 1985]. His observations led to the first mathematical description of the pressure distribution between contacting bodies which are elastic and have quadratic profiles. Over the past 140 years several advances have been made in the field of contact mechanics which we will examine systematically by looking at the kinds of contacts which arise. We are going to consider only contacts made from elastic (usually linear elastic) material, and capable of analysis within linear elastic theory, so that it follows that displacements are small and also that conventional first order definitions of strains apply.

Figure 1.7 shows the four main kinds of contact [Hills and Andresen, 2020]. We

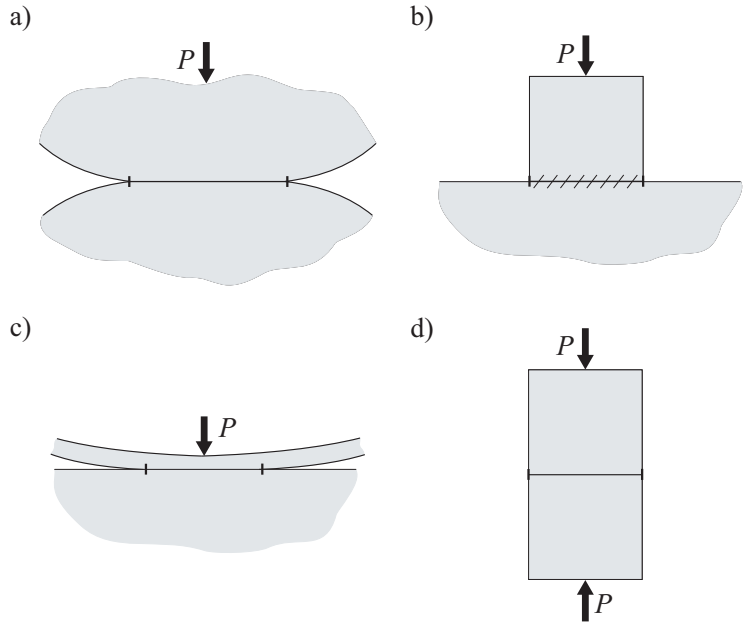


Figure 1.7: Classes of contacts (all subject to normal load, P), a) an incomplete contact formed by two cylinders pressed together, b) a complete contact formed by a square block indenting a half-plane, c) elastic strip pressed onto a half-plane forming a receding contact, d) a common-edge contact formed by two square blocks pressed together.

will restrict ourselves throughout to two-dimensional contacts, and assume that their extent perpendicular to the plane of the page is large, so that plane strain conditions obtain. One of the things we shall concentrate on is the behaviour of the contact edges. Here, even three dimensional contacts have properties which are locally 'plane'.

Incomplete contacts, Figure 1.8, are those which arise when bodies having convex front surfaces are pressed into contact. They have the properties that the contact area increases in size (or advances) as the applied load is increased, and that the contact pressure falls smoothly to zero at the edges in a locally square root bounded manner, so that $p(s) \sim \sqrt{s}$. Often, provided that the size of the contact is small compared with the extent of the body, we can approximate each to a 'half-plane'. The best known incomplete contact is that between two circular cylinders having their axes parallel, which is the plane form of the configuration famously studied by Hertz over 140 years ago [Hertz, 1881]. He made this broad simplification but as it turns out, this model is quite well satisfied by a wide range of contacts. When we come to solve the contact problem in detail we will use a formulation appropriate to a half-plane for each body. When the contact interface is a plane of symmetry and a normal load is applied, surface particles in the contact surfaces will displace laterally by the same amount if the bodies are elastically similar. No interfacial shear tractions therefore arise. Equally, if a shear force is applied so that shear tractions develop along the interface, the surface normal displacement of each body will be the same so that no change in relative surface

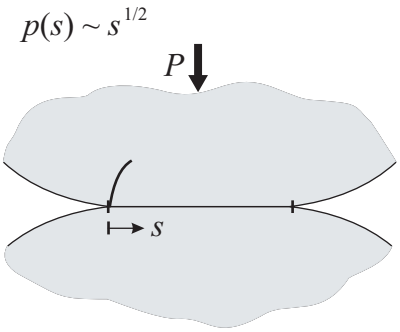


Figure 1.8: Incomplete contact formed by generally convex indenters pressed together by a normal force, P, with a square-root bounded contact pressure at the contact edge.

gradient arises. Consequently, the contact pressure distribution remains unmodified. Contacts of this kind, where the normal problem induces no shear traction and shear tractions cause no modification of the normal pressure, regardless of the value of the coefficient of friction, are said to be 'uncoupled', see §2.1.

Some contacts which are advancing in character do not permit representation of the bodies by half-planes. A good example is shown in Figure 1.9 which may be thought of as the traditional civil engineering bearing bolt. The small clearance between the pin and hole in which it is journalled ($\Delta = R_1 - R_2 > 0$ but $\Delta \ll R_2$) means that a formulation appropriate to an elastic disk and anti-disk is needed [Lau, 1964]. These contacts are also said to be 'nearly conformal'.

A wedge shaped body pressed into the surface of a second body is another example of an incomplete contact and is mentioned because surface elements of the contacting bodies will have to rotate as they pass into the contact patch under increasing normal load, with a combined rotation equal to the external wedge angle. Recall that linear elasticity requires the rotation of elements of material to be small and so solutions using this underlying theory will be valid only when the wedge is very shallow, say with an external wedge angle of no more than 10^o to 15^o [Truman et al., 1995].

We turn, now, to contacts where the front faces of the bodies have the same profile in the unloaded configuration, and so as they are placed together they *conform*, such as the square block resting on an elastically similar half-plane, Figure 1.10. In these problems the size of the contact is fixed by the points where there is

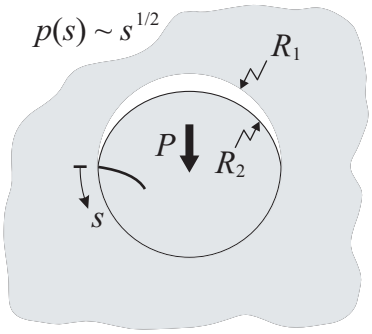


Figure 1.9: Incomplete contact which is nearly conformal with outer and inner radii, R_1 and R_2, and square-root bounded contact pressure.

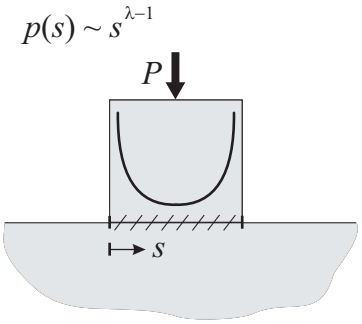


Figure 1.10: Complete contact formed by a square block indenting a half-plane with normal force, P, and a square-root singular contact pressure at the contact edge.

a discontinuity in profile gradient, and the size of the contact is independent of the applied load. A half-plane idealisation of the square block is inappropriate because the side faces of the block must be traction-free and so no general, simple, closed form formulation is possible. However, if we are mainly interested in the contact edges then one possibility is to assume that the contact interface does not slip, and hence an observation point near the edge experiences a three quarter plane domain or, more generally, if the block had inclined sides, then a wedge. The Williams analysis of these show that $p(s) \sim s^{\lambda-1}$, where $\lambda < 1$, and is therefore singular. Even if the contact edge slips it will usually be the case that the pressure takes the same form and $\lambda < 1$. There are cases [Karuppanan and Hills, 2008] where $\lambda > 1$, hence, the contact pressure is bounded.

Figure 1.11 shows an elastic strip pressed onto a half-plane. Prior to the application of a normal load the elastic strip or layer rests on the elastically similar half-plane. The contact is said to conform. When, subsequently, a distributed load is applied on the upper surface, here the finite line load, P, where the extent of the

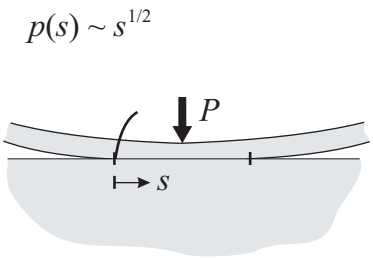


Figure 1.11: Elastic strip pressed onto a half-plane forming a receding contact with normal force, P, and a square-root bounded contact pressure at the contact edge.

loading is smaller than the thickness of the strip, the contact begins to change. The application of this finite normal load causes the contact to become much smaller, or to *recede*. In a problem of this kind where the basic geometry includes only a solitary length scale, here the strip thickness, the contact 'snaps' to its final size upon application of an infinitesimal normal load. Increasing the force merely causes the state of stress and displacements to increase in proportion, but the separation points remain the same and, in all cases, $p(s) \sim \sqrt{s}$ if the bodies are elastically similar.

It will be apparent that, in all the contacts considered so far, the contact pressure adjacent to the contact edge can take one of only two values - $p(s) \to 0$ as s$\to 0$ in the cases of advancing or receding contacts, and $p(s) \to \infty$ as $s \to 0$ in the case of most stationary, complete contacts.

The last type of contact to be considered, illustrated in Figure 1.12, is when the bodies conform over their front faces but where the length of those faces is the same in each body, terminated by an abrupt change in front face gradient. If the angle between the side faces is not 180° a local analysis would again follow the Williams' analysis for a wedge, but for the cases where the contact side faces are collinear, forming a straight line, and that are traction-free, the local contact pressure is finite ($p(s) \sim s^0$). Also, in the absence of tractions the only non-zero component of stress lies parallel with the free surface and, in the absence of out-of-plane loading but in the presence of some increasing in-plane loading, the edges must be the last point to slip. This is obvious in the case when the interface is perpendicular to the free face as the complement to the free-face shear traction lies along the contact interface. We might call problems of this kind 'common-edge'.

A general point which emerges from this taxonomy is that, in the cases of conformal contact (of whatever class - complete, receding, common edge) a possible method of investigating what happens along the interface is simply to assume that it is in intimate contact and adhered, i.e. we model the contact pair as one body - as if they form a monolith - and then we look at the tractions along the interface. If the normal (direct) traction $p(x)$ is everywhere compressive then there is no tendency to separate. If we also look at the shear tractions, $q(x)$, and form

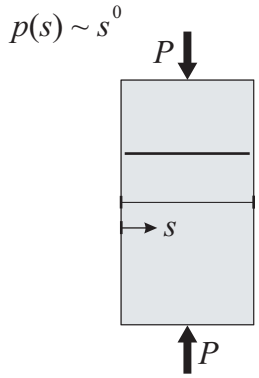


Figure 1.12: Common-edge contact formed by two square blocks pressed together by normal force P and a finite contact pressure at the contact edge.

the ratio $|q(x)/p(x)|$ then, providing that that ratio is everywhere less than the coefficient of friction, f, the interface will also be stuck and the initial assumptions justified. When the latter condition (alone) is not satisfied slip may be introduced by using an array of glide dislocations [Moore et al., 2018] and in an uncoupled contact such an array would not change the contact pressure distribution; but in others it would, and might well cause separation.

In the chapter which follows we look in more detail at the properties of half-plane theory and how contact problems and the arising tractions can be approached and solved.

2

Plane Elasticity and Half-Plane Contacts

Many practical contact problems have such complex geometries that, at first sight, the types of contacts listed in the taxonomy, see §1.4, might seem 'academic'. It is only natural that engineers, and also many researchers, turn to numerical tools, often utilising commercial finite element code, in order to solve for the tractions and underlying stresses arising within a mechanical assembly. This perceived convenience in modelling and solving of the contact problem comes at the cost of excessive computational effort. Additionally, finite element results have to be considered with caution in the following cases, (a) when singularities are present, which can arise for fully adhered or complete contacts, (b) when small changes in normal load cause abrupt changes in contact size, as observed in receding contacts, or (c) computational simplifications are used to improve convergence, such as introducing small amounts of slip between surfaces which are meant to be perfectly stuck together. In any case, classifying the type of contact problem with respect to the geometry and loading of the problem remains important for today's engineers and researchers in order to anticipate the properties of the contact solution. In some cases analytical methods will be capable of providing all the desired answers within a fraction of the time required to set up a finite element analysis.

It cannot be denied that finite element models provide realism in terms of mimicking the mechanical assembly while half-plane theory replaces the geometrical

details outside of the contact with idealised bodies. The advantage of half-plane theory lies in its rigour so that a mathematically exact solution can be obtained. As the name half-plane theory suggests, one of its major idealisation is to treat the problems as 'plane'. This means that there are no gradients of any components of stress or strain with respect to the out-of plane direction. We distinguish between the following two conditions, *plane stress* and *plane strain*. In the former, all out-of-plane stress components are assumed to vanish, $\sigma_{zi} = 0$, $i = x, y, z$. The *plane stress* assumption typically applies when the contacting bodies are 'thin' and the loads act parallel to the bodies main plane. i.e. the dimensions in the out-of-plane direction must be small compared with the smallest in-plane dimension, see Figure 2.1 a). In most contact problems, however, the contacting bodies have significant out-of-plane dimensions in order to support moments about the x-axis, see Figure 2.1 b), so that the conditions for plane stress are very unlikely to hold.

On the other hand, *plane strain* has proven to be a good assumption when one dimension is very large compared to the others. In that case the principal strain in the direction of the longest dimension is constrained and assumed to be zero, $\epsilon_z = 0$. This occurs when the contacting bodies are 'thick' in the out-of-plane direction compared with all in-plane dimensions. Even after the application of the contact loads, each cross section of the contacting bodies remains flat so that no voids or overlaps develop. Note that there might be a transition region towards the end

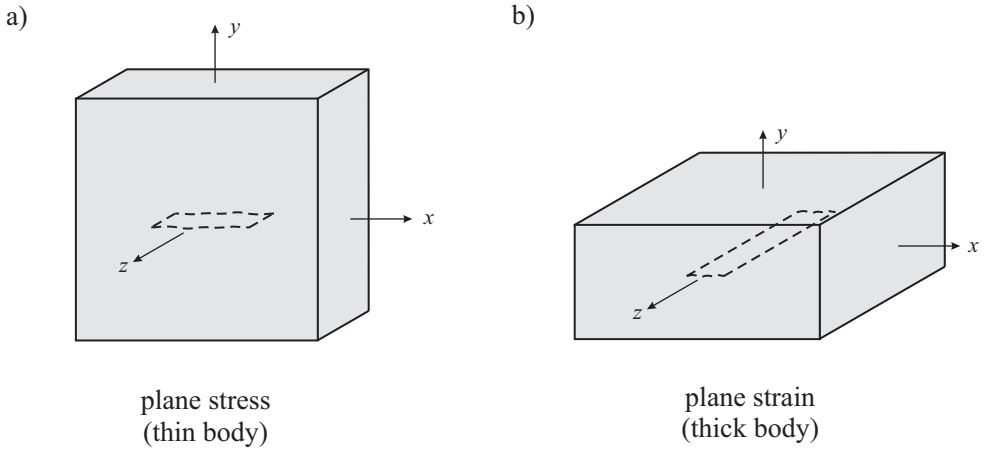


Figure 2.1: The concepts of a) plane stress and b) plane strain.

faces as a traction-free state is anticipated at the free ends. In plane elasticity most contact problems will correspond well to the plane strain assumption.

In what follows we will look at how to solve contact problems under the conditions of plane strain. The vast majority of normal contact problems solved will consist of a simple, clear algebraic expression for the contact law, i.e. the relationship between the applied normal load and contact size, and a simple description of the contact pressure distribution [Hills and Andresen, 2020]. We will also examine the effects of tangential loads or what happens when a moment is transferred through the contact interface. Lastly, we establish the load conditions under which a contact becomes fully stuck. These will be particularly helpful when we treat contact problems which are subject to complex load histories.

2.1 Airy Stress Functions and the Half-Plane

The starting point for the solution of a contact problem is Flamant's solution using an Airy stress function description of the stress state within a wedge [Barber, 2010], particularised to the case where the internal wedge angle is 180^o, Figure 2.2. If the normal load is P and the shear force Q (in each case per unit depth into the page) the appropriate Airy function is

$$\phi = -\frac{r\theta}{\pi}\left(P\sin\theta + Q\cos\theta\right) \ , \tag{2.1}$$

from which we may find the stress components by differentiation alone, using the relations

$$\sigma_{rr}\left(r,\theta\right) = \frac{1}{r}\frac{\partial\phi}{\partial r} + \frac{1}{r^2}\frac{\partial^2\phi}{\partial\theta^2} \tag{2.2}$$

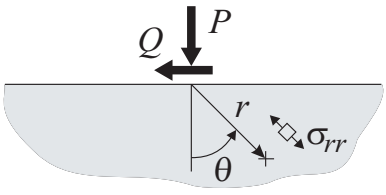


Figure 2.2: Forces acting on a half-plane.

$$\sigma_{\theta\theta}(r,\theta) = \frac{\partial^2 \phi}{\partial r^2} \tag{2.3}$$

$$\sigma_{r\theta}(r,\theta) = -\frac{\partial}{\partial r}\left(\frac{1}{r}\frac{\partial \phi}{\partial \theta}\right) , \tag{2.4}$$

giving $\sigma_{r\theta} = \sigma_{\theta\theta} = 0$ everywhere, and

$$\sigma_{rr} = -\frac{2}{\pi r}\left(P\cos\theta - Q\sin\theta\right). \tag{2.5}$$

So, the state of stress induced is very simple. There is only one non-zero component, a radial direct stress acting towards the point of application of the load. In the case of the normal load, P, this takes its maximum compressive value immediately beneath the load and falls smoothly to zero as the surface is approached. With the shear force, Q, the stress is zero beneath the load, takes its maximum compressive value at the surface ahead of the load and its maximum tensile value on the surface but 'behind' it. The state of stress in polar coordinates is very simple, but it is not a great deal of practical use. The transformation to a Cartesian set, and a shift of origin provides more utility, as we can then find the state of stress arising beneath distributed surface tractions ($p(x)$, $q(x)$) representing the contact pressure and shear traction distribution, respectively, Figure 2.3.

The state of stress is given by

$$\sigma_{xx}(x,y) = \frac{-2}{\pi y}\int_{\text{contact}} \frac{p(\xi)(x-\xi)^2 y^2 - q(\xi)(x-\xi)^3 y}{((x-\xi)^2+y^2)^2}\mathrm{d}\xi \tag{2.6}$$

$$\sigma_{yy}(x,y) = \frac{-2}{\pi y}\int_{\text{contact}} \frac{p(\xi)y^4 - q(\xi)(x-\xi)y^3}{((x-\xi)^2+y^2)^2}\mathrm{d}\xi \tag{2.7}$$

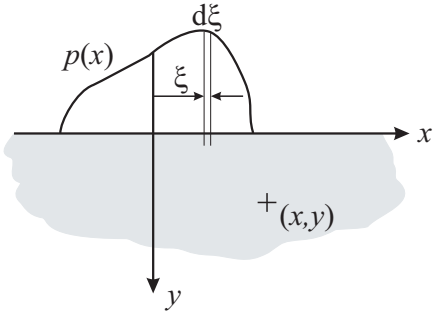


Figure 2.3: General contact pressure distribution for Flamant's solution.

$$\sigma_{xy}(x,y) = \frac{-2}{\pi y}\int_{\text{contact}} \frac{p(\xi)(x-\xi)y^3 - q(\xi)(x-\xi)^2y^2}{((x-\xi)^2+y^2)^2}\mathrm{d}\xi. \tag{2.8}$$

In practice these integrals may be quite hard to evaluate but, in principle, they may be used to find the internal stress beneath a contact. If the contact is sliding so that $q(x) = \pm fp(x)$ along the whole surface the symmetry of the results within Eqs. (2.6, 2.7, and 2.8) possesses useful properties.

But to solve the contact problem itself, we need the displacement field produced by the line forces. In order to examine this, we first find the strain field under conditions of plane strain and then integrate the strains to find the displacements. We specialise the results to the surface with the outcome

$$\begin{aligned} u(x) = &- P\left[\frac{(1-2\nu)(1+\nu)}{2E}\right]\mathrm{sgn}(x) \\ &+ Q\left[\frac{2(1-\nu)(1+\nu)}{\pi E}\right]\ln|x| + \frac{c_1(1+\nu)}{E} \end{aligned} \tag{2.9}$$

$$\begin{aligned} v(x) = &- P\left[\frac{2(1-\nu)(1+\nu)}{\pi E}\right]\ln|x| \\ &+ Q\left[\frac{(1-2\nu)(1+\nu)}{2E}\right]\mathrm{sgn}(x) + \frac{c_2(1+\nu)}{E}, \end{aligned} \tag{2.10}$$

where $v(x)$ is the surface normal displacement, $u(x)$ is the surface tangential displacement, E is Young's modulus and ν Poisson's ratio. These results merit comment; first, observe that the normal force, P, causes a logarithmically varying surface normal depression, Figure 2.4, with the depth of the depression becoming unbounded as the point of application of the load is approached. Perhaps rather less obvious is that the normal force also causes surface particles to be drawn in, parallel with the surface, towards the loaded point, and with the magnitude of the displacement independent of the position of the particle being considered. Similarly, the shear force causes surface particles to be pushed/drawn along with a magnitude varying logarithmically with position. But note, also, that ahead of the shear force material is pushed down by a constant amount whilst behind it it is raised, forming a step, Figure 2.4. Lastly, note that each equation incorporates

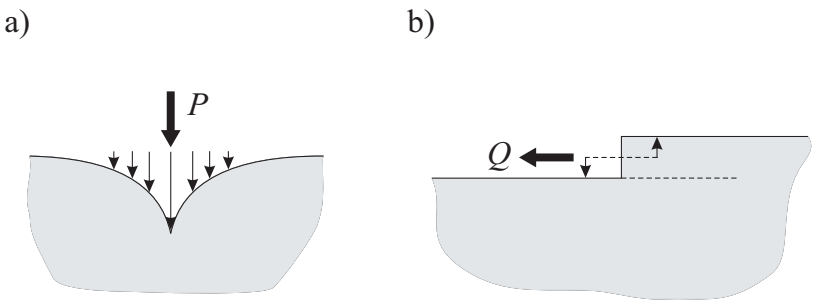


Figure 2.4: Surface displacements due to a) a normal load P b) a shear force Q acting on the surface.

an arbitrary constant so that some datum depth must be chosen at which the displacements are arbitrarily set to zero.

Partly to eliminate the need for an arbitrary datum depth, we develop a contact formulation in terms of the gradient. So, it is straightforward to find the surface slope, $\mathrm{d}v/\mathrm{d}x$, at point x due to an element of pressure, $p(\xi)\mathrm{d}\xi$ at point ξ, but the effect of the shear force needs a little more thought. If the shear force, Q, is smeared over a small length $\mathrm{d}x$ (and $Q = q(x)\,dx$), we see that the surface slope is affected only by the surface shear traction *at that point*, and not elsewhere; by contrast the contact pressure at any point influences the slope at all points. Therefore,

$$\frac{\mathrm{d}v}{\mathrm{d}x} = \frac{2\,(1-\nu)\,(1+\nu)}{\pi E}\int_{\text{contact}} \frac{p(\xi)\mathrm{d}\xi}{x-\xi} - \frac{(1-2\nu)(1+\nu)}{E}q(x). \tag{2.11}$$

Similar results follow immediately for the surface tangential displacement gradient which, we note, is also the surface strain

$$\varepsilon_{xx} = \frac{\mathrm{d}u}{\mathrm{d}x} = \frac{(1-2\nu)(1+\nu)}{E}p(x) + \frac{2\,(1-\nu)\,(1+\nu)}{\pi E}\int_{\text{contact}} \frac{q(\xi)\mathrm{d}\xi}{x-\xi}. \tag{2.12}$$

The next step is to look at the relative surface normal displacements and relative surface tangential strains when two elastic half-planes, not necessarily having the same elastic properties, are brought into contact. The contact pressure and interfacial shear traction is obviously mutual but we must work in a common coordinate set so that some signs are reversed and we can write down the relative change in surface slope as

$$\frac{E^*}{2}\frac{\mathrm{d}(v_{\mathrm{A}}-v_{\mathrm{B}})}{\mathrm{d}x} = \frac{1}{\pi}\int_{\text{contact}} \frac{p(\xi)\mathrm{d}\xi}{x-\xi} - \beta q(x), \tag{2.13}$$

where E^* is the composite plane strain modulus and is explicitly given by

$$\frac{1}{E^*} = \frac{1-\nu_{\mathrm{A}}^2}{E_{\mathrm{A}}} + \frac{1-\nu_{\mathrm{B}}^2}{E_{\mathrm{B}}}. \tag{2.14}$$

The subscripts refer to bodies A and B as shown in Figure 1.1, and β is Dundurs' constant,[1]. The last term in Eq. (2.13) is zero when both bodies have the same elastic constants or when

$$\frac{\beta}{E^*} = \frac{(1+\nu_{\mathrm{A}})(1-2\nu_{\mathrm{A}})}{E_{\mathrm{A}}} - \frac{(1+\nu_{\mathrm{B}})(1-2\nu_{\mathrm{B}})}{E_{\mathrm{B}}} \tag{2.15}$$

vanishes. Similarly, the difference in surface strains is given by

$$\frac{E^*}{2}\frac{\mathrm{d}(u_1-u_2)}{\mathrm{d}x} = \frac{1}{\pi}\int_{\text{contact}} \frac{q(\xi)\mathrm{d}\xi}{x-\xi} + \beta p(x). \tag{2.16}$$

If either (a) the two bodies are made from the same material (or certain other special combinations such that β vanishes) or (b) the contact is perfectly lubricated so that shear tractions cannot be supported, the two equations are uncoupled and take on these simpler forms

$$\frac{\mathrm{d}(v_{\mathrm{A}}-v_{\mathrm{B}})}{\mathrm{d}x} = \frac{2}{\pi E^*}\int_{\text{contact}} \frac{p(\xi)\mathrm{d}\xi}{x-\xi}, \tag{2.17}$$

$$\frac{\mathrm{d}(u_{\mathrm{A}}-u_{\mathrm{B}})}{\mathrm{d}x} = \frac{2}{\pi E^*}\int_{\text{contact}} \frac{q(\xi)\mathrm{d}\xi}{x-\xi}. \tag{2.18}$$

An example in the use of these equations is to establish the contact pressure distribution when one convex body is pressed into another, using Eq. (2.17) If the form of the contacting profile is symmetric, and we think of the relative separation when the bodies are just touching but no external load is applied as $g(x)$, contact will be made over a symmetrical interval, and we shall denote the ends of the contact by $[-a \quad a]$. We then write

$$\frac{\mathrm{d}(v_{\mathrm{A}}-v_{\mathrm{B}})}{\mathrm{d}x} = \frac{\mathrm{d}g}{\mathrm{d}x} = \frac{2}{\pi E^*}\int_{-a}^{a} \frac{p(\xi)\mathrm{d}\xi}{x-\xi} \qquad -a \le x \le a\ . \tag{2.19}$$

[1]Dundurs [Dundurs, 1969] showed that plane elastic problems composed of two bodies depend not on the obvious three dimensionless properties $\nu_{\mathrm{A}}, \nu_{\mathrm{B}}, E_{\mathrm{A}}/E_{\mathrm{B}}$ but, in fact, on only two quantities. Half-plane problems have a further reduced dependence on only the solitary quantity β.

It is important to note that the interval of integration and the interval over which the left-hand side is set to the integral is matched; this is necessary for the integral equation to be properly posed. In setting the gradient of the gap to the shape formed by the contact pressure we are, effectively, ensuring that there is intimate contact within the proposed contact region. And, we are also ensuring that, external to the putative region of contact there is no contact pressure. These constitute two of the requirements of contact embodied in the so-called Signorini conditions. The other two have to be verified *a posteriori* and are: (a) that the contact pressure is positive throughout the contact and (b) that external to the contact there is no interpenetration of the surfaces so that, for example, $\mathrm{d}v/\mathrm{d}x > \mathrm{d}g/\mathrm{d}x,\ x > a$.

2.2 Inversion of Integral Equations

We will refrain from developing, in full, the inversion procedures for the Cauchy integral equations of the type developed in the previous section. They are said to have Cauchy kernels because, when the observation point, x, approaches the integration point, ξ, a singularity arises. The inversion of the equations is, in principle, achievable through the evaluation of an integral, but first it is necessary to decide what kind of end-point behaviour is expected. So, the extent of contact is unknown *a priori*, and we seek a 'bounded both ends' solution. If we press a rigid punch having a straight front face width of width $2a$ into an elastic half plane (which we would also require to be incompressible - $\nu = 1/2$ - in order to ensure that Dundurs' second constant vanishes, the size of the contact would be known and we would require a 'singular both ends' solution. For further details of the inversion please see [Hills et al., 1993]. If the integral equation has the generic form

$$\frac{1}{\pi}\int_{-a}^{a}\frac{f(s)\mathrm{d}s}{s-x} = g(x) \qquad -a \le x \le a, \tag{2.20}$$

its solution is given by [Hills et al., 1993]

$$f(x) = -\frac{w(x)}{\pi}\int_{-a}^{a}\frac{g(s)\mathrm{d}s}{w(s)(s-x)} + Cw(x), \tag{2.21}$$

where, if we seek a 'singular both ends' solution

$$w(x) = \frac{1}{\sqrt{a^2 - x^2}} \qquad C \neq 0, \tag{2.22}$$

whereas, if we seek a 'bounded both ends' solution

$$w(x) = \sqrt{a^2 - x^2} \qquad C = 0, \tag{2.23}$$

and, in addition, we must enforce the consistency condition

$$\int_{-a}^{a} \frac{g(s)\mathrm{d}s}{w(s)} = 0. \tag{2.24}$$

When these integrals are analytically intractable, numerical integration procedures to solve these equations very efficiently are available, and the key reference is an extended paper by [Erdogan et al., 1973].

2.3 Example of a Hertzian Geometry

As an example application consider the problem of pressing together two elastically similar circular cylinders, of radii R_1, R_2, having their axes parallel, as shown in Figure 2.5. The circular profiles may be approximated by parabolae, as may be seen by applying Pythagoras' theorem and taking the first term in a binomial expansion so that

$$2Rg(x) \simeq x^2, \tag{2.25}$$

where

$$\frac{1}{R} = \frac{1}{R_1} + \frac{1}{R_2}, \tag{2.26}$$

and hence

$$\frac{\mathrm{d}g}{\mathrm{d}x} \simeq \frac{x}{R}. \tag{2.27}$$

Substitution of this geometric result into Eq. (2.20) gives

$$\frac{x}{R} = \frac{2}{\pi E^*} \int_{-a}^{a} \frac{p(\xi)\mathrm{d}\xi}{x - \xi} \qquad -a \leq x \leq a, \tag{2.28}$$

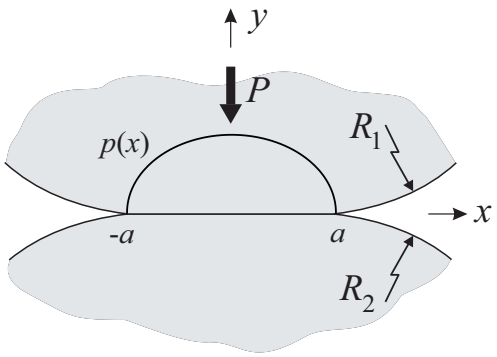


Figure 2.5: The Hertz contact problem.

and the inversion procedure gives

$$p(x) = \frac{E^*}{2\pi R}\sqrt{a^2 - x^2}\int_{-a}^{a} \frac{r\mathrm{d}r}{\sqrt{a^2 - r^2}(r - s)} = \frac{E^*\sqrt{a^2 - x^2}}{2R}. \tag{2.29}$$

At the moment this is in an unfamiliar form. But, if we write down the normal equilibrium condition, viz.

$$P = \int_{-a}^{a} p(x)\mathrm{d}x, \tag{2.30}$$

and substitute in this result we find that

$$a^2 = \frac{4PR}{\pi E^*}, \tag{2.31}$$

so that we recover [Hertz, 1881]

$$p(x) = \frac{2P}{\pi a}\sqrt{1 - (x/a)^2}. \tag{2.32}$$

2.4 Further Examples

In the case of a rigid, square-ended punch pressed onto an incompressible half-plane, we seek a 'singular both ends' solution, and, as the front face is flat, $\mathrm{d}g/\mathrm{d}x = 0$. Therefore

$$\frac{2}{\pi E^*}\int_{-a}^{a} \frac{p(r)\mathrm{d}r}{s - r} = 0 \qquad -a \le x \le a, \tag{2.33}$$

so that

$$p(x) = \frac{C}{\sqrt{a^2 - x^2}}, \tag{2.34}$$

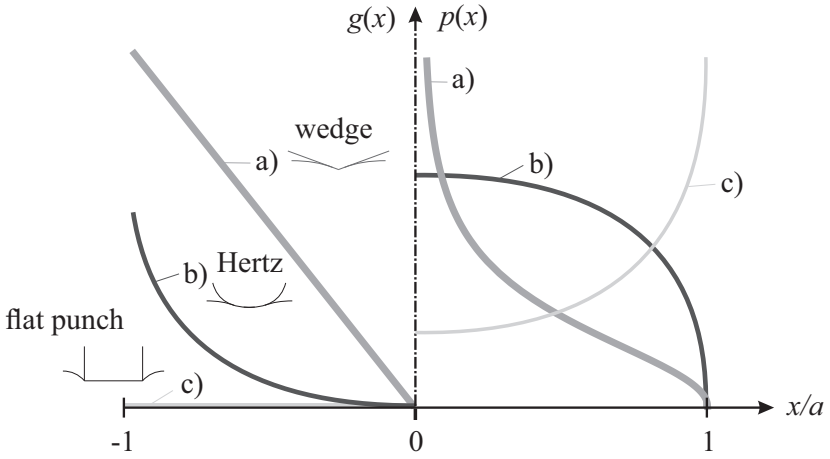


Figure 2.6: Comparison of different indenter profiles and resulting pressure distributions for (a) a wedge, (b) Hertzian contact, and (c) a complete contact [Hills and Andresen, 2020].

and the imposition of normal equilibrium gives the value of the constant, C, so that

$$p(x) = \frac{P}{\pi\sqrt{a^2 - x^2}}. \tag{2.35}$$

Figure 2.6 provides a comparison of the profiles of common indenters against the corresponding resulting pressure distribution. The qualitative results for the Hertz case and a flat punch are included, together with a shallow wedge which will be looked at in more detail in Chapter 3. Care must be taken when evaluating the integral within the interval $(-a \leq x \leq a)$ when it is Cauchy, and external to that interval, when it is regular.

Lastly, caution is urged when one of the bodies has a profile where other features, external to the contact itself, are present over a length scale not big compared with the contact half width. Examples include internal corners at, for example, firtree root corners and external corners, for example in the case of a railway line head where the line head width is only two to three times the contact size [Hills and Andresen, 2020].

2.5 An Alternative Method for Solving Contact Problems

We now want to look at a different way to solve a contact problem. The Mossakovskii-Barber procedure is based on the same fundamentals of linear elasticity as derived

above but provides a useful alternative approach compared with the usage of singular integral equations. Its main advantage will become obvious when there is a simultaneous change of normal and shear loading present at the contact interface and we shall apply these ideas in Chapter 3 when we explore partial slip problems subject to proportional loading. The basic formulation was derived by Mossakovskii in 1954 [Mossakovskii, 1954] and it was Barber who pushed these initial ideas further [Barber, 2018, Barber et al., 2011].

In addition to providing an alternative solution procedure for the normal and shear load problem, the Mossakovskii-Barber formulation remains applicable when investigating the effects of remote tensions in the contacting bodies as well the effects of a moment and how these affect the shear tractions. Lastly, these ideas will allow us to look at the loading conditions necessary to maintain a fully adhered contact interface.

2.5.1 The Normal Problem

Let us begin to develop the solution by solving the normal load problem first. The conceptual idea behind the procedure is to form the contact from a series of flat punches which mimic the profile we intend to use of the generic symmetrical incomplete contact geometry being studied, see Figure 2.7.

Consider the simple contact problem between a half-plane and a single flat punch, as shown in Figure 2.8. Without proof, we state that the application of a

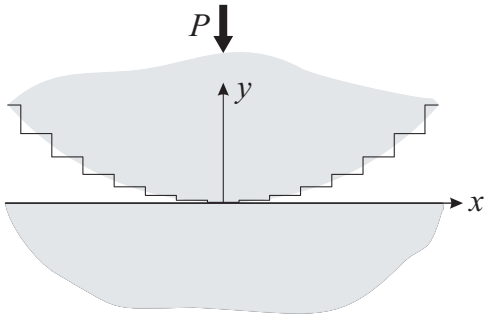


Figure 2.7: Incomplete contact formed by a contact-defining body consisting of a series of flat punches.

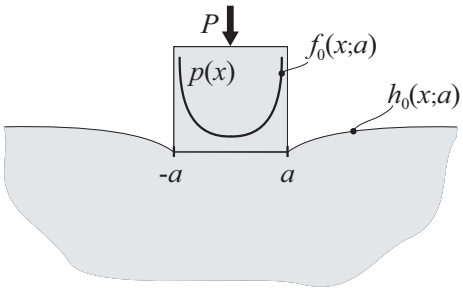


Figure 2.8: Single indentation by a flat punch over contact $[-a \quad a]$.

normal force gives rise to a normal pressure of the following form [Barber, 2018]

$$p(x) = f_0\left(x; a\right) \ , \tag{2.36}$$

where

$$f_0(x;a) = \begin{cases} {}^{1}\!/\!_{\sqrt{a^2-x^2}} & -a < x < a \\ 0 & |x| > a \end{cases} \ . \tag{2.37}$$

The sharp corners of the punch cause this square-root singular behaviour at the edges, $x = \pm a$.

Similar to our initial considerations based on Airy stress functions, the corresponding surface displacement may be found from Eq. (2.11). The surface slope is given by [Barber, 2018]

$$\frac{\mathrm{d}v}{\mathrm{d}x} = \frac{4\left(1-\nu^2\right)}{E} h_0\left(x; a\right) \ , \tag{2.38}$$

where

$$h_0\left(x; a\right) = \begin{cases} 0 & -a < x < a \\ -\mathrm{sgn}(x)/\sqrt{x^2-a^2} & |x| > a \end{cases} \ . \tag{2.39}$$

Note that we assume the conditions of plane strain to hold. Figure 2.8 illustrates the anticipated surface displacement and contact pressure. Suppose we want to achieve the shown constant surface normal displacement inside of the contact interface and we know the corresponding contact pressure, $f_0(x;a)$, then the necessary normal load is found from normal equilibrium

$$P = \int_{-a}^{a} p(x)\mathrm{d}x = \pi. \tag{2.40}$$

Now that we have established the effects of a single flat punch, let us look at how we can use these results to develop an alternative tool for solution of the normal contact problem. Imagine we have already formed a symmetrical contact between two elastically similar half-planes with generally convex contacting profiles, and we increase the normal load by an infinitesimal amount, $\mathrm{d}P$, corresponding to an infinitesimal change in contact half-width, $\mathrm{d}s$. We introduce an as of yet unknown weighting function, $F(s)$, which depends on the contact profile under consideration. When integrating Eqs. (2.36, 2.37) over the current contact length, b, we find the corresponding normal pressure distribution as

$$p(x;b) = \int_0^b F(s)\, f_0(x;s)\mathrm{d}s \;, \tag{2.41}$$

which gives rise to the surface slope

$$\frac{\mathrm{d}v}{\mathrm{d}x} = \frac{4\,(1-\nu^2)}{E} \int_0^x F(s)\, h_0\,(x;s)\,\mathrm{d}s \qquad 0 < x < b\,. \tag{2.42}$$

For a generally convex profile, the weighting function, $F(s)$, is continuous so that the singularity in the pressure distribution of a single flat punch is integrated out. In order to find the weighting function, we need to match the surface slope due to the normal indentation to the profile of the contacting bodies, $g_0(x)$. We define

$$\frac{\mathrm{d}v}{\mathrm{d}x} = -g_0'\,(x) \qquad 0 < x < b \tag{2.43}$$

so that

$$g_0'(x) = \frac{4\,(1-\nu^2)}{E} \int_0^x \frac{F(s)\,\mathrm{d}s}{\sqrt{x^2-s^2}} \qquad 0 < x < b\,. \tag{2.44}$$

This is an Abel equation which can be inverted to give

$$F(s) = \frac{E}{2\pi\,(1-\nu^2)} \frac{\mathrm{d}}{\mathrm{d}s} \int_0^s \frac{t g_0'(t)\,\mathrm{d}t}{\sqrt{s^2-t^2}}\,, \tag{2.45}$$

where details of the inversion can be found in [Barber, 1983]. In a conventional contact problem, the contact profile, $g_0(x)$, is usually an input to the problem so that by evaluating Eq. (2.45) we can find the weighting function, $F\,(s)$. Once this is done, we find the pressure distribution by evaluating

$$p(x;b) = \begin{cases} \int_{|x|}^b \frac{F(s)\mathrm{d}s}{\sqrt{s^2-x^2}} & |x| < b \\ 0 & |x| > b \end{cases}\,, \tag{2.46}$$

and the contact law is found by imposing normal equilibrium

$$P\left(b\right)=\pi\int_{0}^{b}F(s)\mathrm{d}s\ . \tag{2.47}$$

2.5.2 Re-visiting the Example of a Hertzian Geometry

While the procedure based on singular integral equations is the established framework for solving normal problems, the Mossakovskii-Barber procedure remains a perfectly applicable alternative. Here we are going to apply this new tool to re-visit the Hertzian contact problem, Figure 2.5, where $g_0'(x)=x/R$, and both bodies are elastically similar so that we find

$$F(s)=\frac{E}{2\pi\left(1-\nu^2\right)R}\frac{\mathrm{d}}{\mathrm{d}s}\int_0^s\frac{t^2\mathrm{d}t}{\sqrt{s^2-t^2}}=\frac{Es}{4\left(1-\nu^2\right)R}\ . \tag{2.48}$$

Supposing the contact interface spans $[-a \qquad a]$, the contact pressure is given by

$$p(x)=\int_{|x|}^{a}\frac{F(s)\mathrm{d}s}{\sqrt{s^2-x^2}}=\frac{E}{4\left(1-\nu^2\right)R}\int_{|x|}^{a}\frac{s\,\mathrm{d}s}{\sqrt{s^2-x^2}}=\frac{E\sqrt{a^2-x^2}}{4\left(1-\nu^2\right)R}, \tag{2.49}$$

and the contact law, $P(a)$, is found by integrating

$$P\left(a\right)=\pi\int_{0}^{a}F(s)\mathrm{d}s=\frac{\pi E}{4\left(1-\nu^2\right)R}\int_{0}^{a}s\,\mathrm{d}s=\frac{\pi Ea^2}{8\left(1-\nu^2\right)R}\ . \tag{2.50}$$

These results agree with those presented in §2.3.

2.5.3 Application of a Shear Force

Recall the analogy between the Green's functions for normal and tangential displacements, see Eqs. (2.9, 2.10). Following this equivalence, we can apply the Mossakovskii-Barber procedure developed for normal loading to solve the tangential problem due to the application of a shear force. In parallel with the normal problem, a constant tangential displacement of the surfaces is expected due to a symmetrical singular shear traction distribution. Suppose that the shear traction applied to the surface is given by

$$q(x)=f_0\left(x\right)\ . \tag{2.51}$$

In the tangential problem, the surface strain parallel with the surface, $\epsilon_{xx} = \mathrm{d}u/\mathrm{d}x$, is analogous to the surface gradient in the normal loading problem, and is given by

$$\epsilon_{xx} = \frac{4\left(1-\nu^2\right)}{E} h_0\left(x;a\right). \tag{2.52}$$

We introduce the weighting function, $G_0(s)$, replacing $F(s)$ in this tangential problem. Once the weighting function is found, the shear traction may be evaluated as

$$q(x;a) = \begin{cases} \int_{|x|}^{a} \frac{G_0(s)\mathrm{d}s}{\sqrt{s^2-x^2}} & |x| < a \\ 0 & |x| > a. \end{cases} . \tag{2.53}$$

Force equilibrium in tangential direction needs to agree with the applied shear force, so that

$$Q\left(a\right) = \pi \int_0^a G_0(s)\,\mathrm{d}s\ . \tag{2.54}$$

2.5.4 The Effect of Bulk Tension

Bulk tensions are stresses applied remotely from the contact interface in one or both contacting bodies. Consider two half-planes adhered over the interval $[-a \quad a]$. As depicted in Figure 2.9, remote tensions might be applied to bodies A and B, here denoted σ_{A} and σ_{B}. If unequal, these remote stresses result in a differential tension, $\sigma = \sigma_{\mathrm{A}} - \sigma_{\mathrm{B}}$, between the contacting bodies causing interfacial shear tractions to develop.

First think of each half-plane individually, without the contact interface, so that the strain induced by the remote tension in each body is given by

$$\epsilon_{\mathrm{A,B}} = \frac{\sigma_{\mathrm{A,B}}}{E^*}\ . \tag{2.55}$$

When the two half-planes are not separated but adhered over the interface $[-a \quad a]$, the differential strain must come to a common value in both bodies

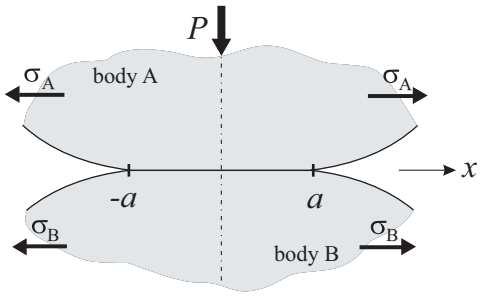


Figure 2.9: Differential tension applied to two elastically similar half-planes bonded over $[-a \quad a]$.

along the interface. This requires the presence of a zero-resultant shear traction of anti-symmetric form, say

$$q(x) = f_1(x) \tag{2.56}$$

where

$$f_1(x;a) = \begin{cases} \frac{x}{\sqrt{a^2-x^2}} & -a < x < a \\ 0 & |x| > a \end{cases} . \tag{2.57}$$

If we recall Eq. (2.12), and substitute this traction distribution, we find the surface strain as

$$\epsilon_{xx} = \frac{\mathrm{d}u}{\mathrm{d}x} = \frac{4}{E^*} h_1(x;a) \tag{2.58}$$

where

$$h_1(x;a) = \begin{cases} 1 & -a < x < a \\ -\left[\frac{|x|}{\sqrt{a^2-x^2}} - 1\right] & |x| > a \end{cases} . \tag{2.59}$$

As before, we now introduce a density function, $G_1(s)$, and together with the individual contributions from bodies A and B, Eq. (2.55), the total strain along the interface is given by

$$\epsilon_{xx}(x,a) = \frac{\sigma}{E^*} + \frac{4}{E^*} \int_0^a G_1(s) h_1(x;s)\, \mathrm{d}s \qquad 0 < x < a\,. \tag{2.60}$$

In the majority of engineering applications, a combination of shear force and differential tension will be present at the contact interface and we will look at the effects of mixed tangential loading in Chapters 3 4. It is possible to use a superposition of the shearing traction distributions

$$q(x,a) = \int_{|x|}^a \frac{G_0(s)\mathrm{d}s}{\sqrt{s^2-x^2}} + x \int_{|x|}^a \frac{G_1(s)\,\mathrm{d}s}{\sqrt{s^2-x^2}}\,. \tag{2.61}$$

Problems in which only a differential tension is applied have been studied as well, see [Moore et al., 2018] for example.

2.5.5 The Effect of a Moment

In all problems we have looked at so far the line of action of the normal load component passed the centre-line of the contact. Additionally, the indenting geometry was symmetrical about its centre-axis. However, in most problems we encounter in reality there will be a moment present, may it stem from an inherent asymmetry in the contact geometry or from an application of the normal load at an offset from the centre-line of the contact patch. It follows that the contact pressure may be considerably higher at one of the contact edges compared to the corresponding symmetrical case and making the ideas developed in this thesis applicable even when there is a moment transferred across the contact interface will prove very useful. Mossakovskii's ideas have been extended to the unsymmetrical case [Moore and Hills, 2020] and initially we will restrict ourselves to the normal problem and incorporate the effects of a moment. Later in this thesis we will show how the application of a moment affects the tangential problem as well, §3.5.2, and how certain aspects of the solution can be exploited.

Suppose, now, the contact interface currently spans $[-a \quad c]$, and instead of the symmetrical pressure distribution given in Eq. (2.36), we assume one of unsymmetrical form given by

$$f_0^U(x;a,c) = \begin{cases} \frac{1}{\sqrt{(a-x)(x+c)}} & -c < x < a \\ 0 & \text{elsewhere} \end{cases} . \tag{2.62}$$

This results in a surface displacement given by Eq. (2.39) and instead of $h_0(x;a)$, we assume an unsymmetrical form, $h_0^U(x;a)$, where

$$h_0^U(x;a) = \begin{cases} 0 & -c < x < a \\ -\frac{\operatorname{sgn}(x)}{\sqrt{(a-x)(x+c)}} & \text{elsewhere} \end{cases} . \tag{2.63}$$

The expressions for contact pressure and surface slope, Eqs. (2.41, 2.42), still apply together with the asymmetrical functions $f_0(x;a,c)$ and $h_0(x;a)$. As before, we must find the the density of punches from Eq. (2.42) first, and once

this is done, we know that the asymmetrical pressure distribution is given by [Moore and Hills, 2020]

$$p(x;a,c) = \begin{cases} \int_x^a \frac{F(s)\mathrm{d}s}{\sqrt{(s-x)(x+c(s))}} & 0 < x < a \\ \int_{c^{-1}(-x)}^a \frac{F(s)\mathrm{d}s}{\sqrt{(s-x)(x+c(s))}} & -c < x < 0 \\ 0 & \text{elsewhere} \end{cases} , \tag{2.64}$$

where $c^{-1}(\bullet)$ denotes the inverse of $c(\bullet)$. Evaluating the normal equilibrium condition requires a change in variable set which is outlined in [Moore and Hills, 2020], and which may be consulted for details of the evaluation. Note, that normal equilibrium yields only the resultant of the normal pressure distribution and in addition to the normal resultant there is a rotational component which needs to fulfil the equilibrium condition

$$M = \int_{-c}^{a} p(s)s\,\mathrm{d}s\ . \tag{2.65}$$

2.6 Inequality for Full Stick

The core of this thesis lies at solving partial slip problems, that is in the presence of tangential loads there are some parts of an interface which remain adhered and some parts that experience relative movement between the contacting surfaces. We have already learned about the conditions necessary for gross relative motion, i.e. full sliding with Coulomb's law requiring the shear force to be equal to the normal load times the coefficient of friction, $Q = fP$, and this is, of course, independent of the applied moment, M, or the applied differential tension, σ. Here, we want to look at what separates a fully adhered contact interface from one that experiences partial slip. The Mossakovskii procedure allows us to write down the necessary inequalities describing the conditions for full stick. The results we are going to develop apply to general incomplete contacts and we note that the geometry of the contact does affect the solution.

Let us begin with a symmetrical contact patch spanning $[-a \quad a]$. Now suppose, we increase the normal load by a small amount, ΔP, so that the contact

advances in size. From Eq. (2.34) we know that the contact pressure will increase *everywhere* along the interface by

$$\Delta p(x) = \frac{\Delta P}{\pi\sqrt{a^2 - x^2}} \qquad |x| < a. \tag{2.66}$$

Suppose, now, that simultaneously the shear force is changed by a small amount, ΔQ. From equivalent considerations as above we can infer that the shear traction distribution will change *everywhere* along the interface by

$$\Delta q(x) = \frac{\Delta Q}{\pi\sqrt{a^2 - x^2}} \qquad |x| < a. \tag{2.67}$$

Regardless of the state the contact was in before this change in normal and shear load occurred (i.e. whether the interface was fully stuck, in partial slip, or in full sliding), we are now able to determine the new state of the interface by evaluating the inequality

$$|\Delta Q| < f\Delta P\ . \tag{2.68}$$

The contact will become fully stuck if Coulomb's law is violated in a point-wise sense, i.e. *everywhere* along the interface if

$$\frac{|\Delta q(x)|}{\Delta p(x)} = \frac{|\Delta Q|}{\Delta P} < f\ . \tag{2.69}$$

In many practical contact problems, there is a bulk tension present in addition to a shear force. From Eqs. (2.58, 2.59) we can infer how a small change in differential tension, $\Delta\sigma$, will affect the shear tractions induced under conditions of full stick, i.e.

$$\Delta q(x) = \frac{x\Delta\sigma}{4\sqrt{a^2 - x^2}} \qquad |x| < a\ . \tag{2.70}$$

Due to this anti-symmetry, we must pay close attention to each end of the contact when determining which end of the interface might experience relative motion first in the presence of changes in normal and shear load together with bulk tension. Referring to Figure 2.9, we introduce the following sign convention. Suppose a remote tension is applied to body A alone, while the shear force in body B acts to the right, then the effects of the tension and shear force will add at the

left-hand side, $x = -a$, and will subtract at the right-hand side, $x = +a$. Using superposition, we can state the condition for full stick at the left-hand side as

$$\frac{\Delta q(-a)}{\Delta p(-a)} = \frac{4\Delta Q + \pi a \Delta\sigma}{4\Delta P} < f \ , \tag{2.71}$$

and at the right-hand side

$$\frac{\Delta q(+a)}{\Delta p(+a)} = \frac{4\Delta Q - \pi a \Delta\sigma}{4\Delta P} < f \ . \tag{2.72}$$

In order to have a complete tool set, we lastly look at what happens when a small change in moment, ΔM, occurs. We assume the change in position of the contact edge is negligible and in accordance with Figure 2.9, a counter-clockwise moment is applied to body B so that we can write the change in contact pressure associated with a small change in moment as [Sackfield et al., 2001]

$$\Delta p(x) = \frac{2x\Delta M}{\pi a^2 \sqrt{a^2 - x^2}} \qquad |x| < a \ . \tag{2.73}$$

In the spirit of the other two conditions stated above, we write the inequality for full stick in its most general form as

$$\frac{\Delta q\,(\pm a)}{\Delta p\,(\pm a)} = \frac{4a\Delta Q \pm \pi a^2 \Delta\sigma}{4a\Delta P \pm 8\Delta M} \ < f, \tag{2.74}$$

where we choose the upper sign, $+ve$, when referring to the left-hand side and *vice versa*. Note that in any case both sides of the contact need to be considered when the state of the contact is to be determined due to changes in its load components.

Note that for all stated inequalities a is the instantaneous contact half-width and the evaluation of the conditions for full stick is independent of the contact geometry or the used material, but depends, of course, on the coefficient of friction, f. Using these inequalities, we can now determine the state of a contact at every instance of a complex load cycle.

3

Half Plane Partial Slip Contact Problems

Contact mechanics is the scientific discipline concerned with the stresses arising perpendicular and *tangentially* to the contacting surfaces. Strategies to address the *normal* problem for contacts have been outlined in Chapter 2. Many engineering applications have contacts with rounded edges and it is appropriate to represent those *incomplete* contacts using half-plane theory [Barber, 2018], including dovetail roots in gas turbine fan blades, swash plate assemblies in helicopter rotor heads, or in the locking segments used to fasten risers to well heads in subsea installations. However, if the contact interface transfers tangential loading, solving the perpendicular problem is often insufficient to address the contact stresses in their entirety. In most of the given examples, complicated external loadings, which vary in time and which are applied remotely from the contact interface, are the source of local contact loads so that most real contacts inevitably transfer normal and tangential loads at the same time. The three states an incomplete contact subject to normal and tangential loading can be in, can be identified as (excluding rolling)

- gross sliding, i.e. Coulomb's law is *satisfied*, hence $|Q| = fP$,
- fully adhered, i.e. the inequality for full stick is *satisfied*,
- partial slip, i.e. when the inequality for full stick is *violated*.

Understanding the *partial slip* state, that is, which part of the contact is adhered and which part is slipping, is a crucial stage in assessing potential fretting fatigue damage. The contact itself causes a stress concentration, often particularly emphasised in the neighbourhood of the contact edges and if there is relative motion in the presence of friction, the touching surfaces might be damaged and quantifying zones of potential crack nucleation is material to designing against fretting fatigue.

Figure 3.1 shows a generic contact between two elastic half-planes subject to the four load quantities affecting the partial slip problem, the normal load, P, shear force, Q, moment, M, and the differential bulk tension, $\sigma = \sigma_{\mathrm{A}} - \sigma_{\mathrm{B}}$.

Most historic partial slip solutions are associated with a Hertzian geometry. This is not surprising as Hertz' normal contact problem between two cylinders is such a well-known and celebrated solution. The first formulation for a monotonically increasing shear force under constant normal load was found by Cattaneo [Cattaneo, 1938]. Mindlin [Mindlin, 1949] came to the same conclusions as Cattaneo and expanded the formulation to unloading and reloading problems [Mindlin et al., 1951, Mindlin and Dereiewicz, 1953]. Many years later, Hills and Nowell went on to look at the effects of differential bulk tension together with a monotonically increased shear force [Hills and Nowell, 1987]. Both, the application of a shear force and the application of a differential bulk tension induce shear tractions. If the contact does not remain fully adhered, there will be slip and the direction of this relative motion depends on the origin of tangential loading. In the presence of a shear force alone the direction of slip will be the same at

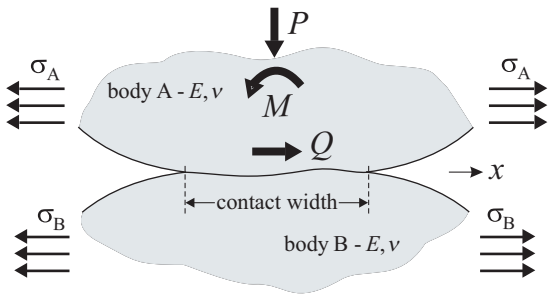


Figure 3.1: Generic half-plane contact subject to normal load, moment, shear load and differential bulk tension.

each end of the interface, while a differential bulk tension causes the direction of slip to be of opposite sign at each end. If the two are exerted simultaneously, the zones of slip will increase at one end, and become smaller at the opposite end. In some cases the differential tension is large enough to cause the direction of slip to change and becomes *dominant*[1], which complicates finding a solution significantly and which required whole new methods to be developed, see Chapters 4 and 5. The next important milestone was a very general theorem in contact mechanics discovered by Jäger in 1997 [Jäger, 1997] and, apparently unaware of this, by Ciavarella in 1998 [Ciavarella, 1998]. That is, the partial slip solution can be found from superimposing a scaled form of the full sliding traction as a 'corrective' shear traction over the stick region as long as the surfaces are generally convex and the differential tension is *moderate*.

For the development of partial slip solutions it is instructive to consider the interaction between surfaces in a point-wise sense, where x is the coordinate along the interface, see Figure 3.1. From the definition for tangential relative movement between bodies, we know that along the x-direction, surface particles will either remain stuck or be in relative motion. For the latter case, the shear tractions, $q(x)$, are found readily from the normal tractions, $p(x)$, by interpreting Coulomb's law in a point-wise notation

$$|q(x)| = fp(x) \; . \tag{3.1}$$

Although contact problems are treated as quasi-static in this thesis, we intend to investigate the zones of relative motion along an interface. If the applied contact loads were truly static, no change in surface displacements was physically possible, and hence no relative motion of particles would occur. We want the shear tractions to oppose the relative *motion* of the contacting surfaces, and that connects the sign of the time-derivative of the relative surface displacement, $h(x) = u_{\mathrm{A}}(x) - u_{\mathrm{B}}(x)$,

[1]Throughout the rest of this thesis, we refer to the case of same sign of slip direction at both ends of the contact as *moderate* differential bulk tension and to the opposite case as *large* differential bulk tension.

to the sign of the opposing shear traction by

$$\operatorname{sgn} q(x) = -\operatorname{sgn} \frac{\partial h(x)}{\partial t} \ , \tag{3.2}$$

where t is the time.

If at a certain point, x, along the interface the surface particles remain fully adhered, the shear tractions must be less than or equal to the limiting frictional value

$$|q(x)| \leq fp(x) \ . \tag{3.3}$$

A partial slip problem divides the interface into zones of slip and stick, i.e. where the shear tractions must fulfil Eqs. (3.1, 3.2) in the case of relative motion and Eq. (3.3) in the fully stuck case. These principle ideas will enable us to analyse elastic contacts where the applied tangential load is insufficient to cause full sliding.

3.1 Asymmetrical Contact Problems

It will prove very useful to solve, first, the normal load problem for asymmetrical incomplete contact problems on a general level. We can build on the procedure developed for normal load problems in §2.2 and extend the solution to the asymmetrical case. This will enable us to employ a very useful and compact analogy between normal and tangential solution later on, resulting in a succinct mapping procedure, see §3.5.2. In order to avoid any repetition, we assume that the idea of relating the surface gradient and contact pressure using basic integral equations is a known concept to the reader. A full derivation and additional comments can be found in Chapter 2.

We will further assume that the normal and tangential problems are uncoupled. More specifically, this means normal tractions do not introduce tangential tractions and *vice versa*. This is either the case when the interface is frictionless, which is infeasible in this chapter as we intend to investigate frictional contact problems, or by setting by setting Dunudrs' constant $\beta = 0$, see §2.1. In all engineering problems investigated in this thesis and also in most real world problems affected by fretting, the contacting bodies will be elastically similar, and hence $\beta = 0$. This gives some

reassurance that the uncoupled assumption is a realistic one. An additional benefit of the uncoupled assumption is that there is no load history dependence in the normal load problem. Knowing the instantaneous values of the normal load and moment, P and M, suffices to determine the normal tractions, $p(x)$.

The interest in asymmetrical contacts is sparked by the fact that in most engineering applications the normal force will not pass through the centre-line of the contact patch, but at an offset from the centre-line, thereby inducing a moment which needs to be transferred to the contacting body. An additional potential origin of a moment is an inherent asymmetry in the contacting geometry. Let us begin by considering an asymmetrical half-plane contact under plane strain conditions, Figure 3.2. The contact is established in the presence of a normal load, P, and moment, M. The relative slope of the half-plane surfaces, $\mathrm{d}v/\mathrm{d}x$, is given by

$$\frac{\mathrm{d}v}{\mathrm{d}x} = \frac{2}{\pi E^*} \int_{-a}^{c} \frac{p(\xi)\,\mathrm{d}\xi}{x-\xi}, \tag{3.4}$$

where $E^* = {}^{E}/_{2(1-\nu^2)}$ is the composite modulus, E being Young's modulus and ν being Poisson's ratio. The interface spans $-a < x < c$ as depicted in Figure 3.2. The application of a moment will cause the indenter to tilt through some small angle, here denoted α. This angle will vary with the applied moment. Supposing that the relative surface profile of the contacting bodies is $g(x)$, the relative surface slope, ${}^{\mathrm{d}v}/_{\mathrm{d}x}$, can be expressed as

$$\frac{\mathrm{d}v}{\mathrm{d}x} = \frac{\mathrm{d}g}{\mathrm{d}x} + \alpha = \frac{2}{\pi E^*} \int_{-a}^{c} \frac{p(\xi)\,\mathrm{d}\xi}{x-\xi}, \quad -a < x < c\,, \tag{3.5}$$

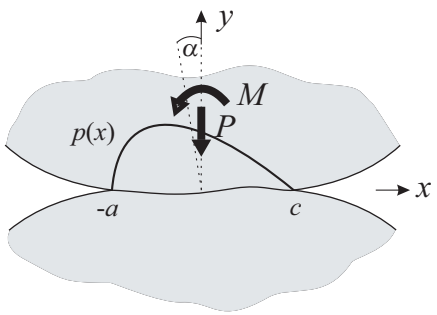


Figure 3.2: Tilted half-plane contact subject to a normal load, P and a moment, M, with a corresponding pressure distribution, $p(x)$.

yielding an integral equation with the inversion [Hills et al., 1993]

$$p(x) = \frac{w(x,a,c)}{2\pi} E^* \int_{-a}^{c} \frac{(\mathrm{d}g/\mathrm{d}\xi + \alpha)\,\mathrm{d}\xi}{w(\xi,a,c)(x-\xi)}\ , \quad -a \le x \le c\ , \tag{3.6}$$

where $w(x,a,c) = \sqrt{(x+a)(c-x)}$ and $w(\xi,a,c) = \sqrt{(\xi+a)(c-\xi)}$. Note that Eq. (3.6) is subject to the following consistency condition

$$\int_{-a}^{c} \frac{(\mathrm{d}g/\mathrm{d}\xi + \alpha)\,\mathrm{d}\xi}{w(\xi,a,c)} = 0\ , \tag{3.7}$$

and using the identity $\int_{-a}^{c} \frac{\mathrm{d}\xi}{w(\xi,a,c)} = \pi$, we conclude that

$$\int_{-a}^{c} \frac{\mathrm{d}g/\mathrm{d}\xi}{w(\xi,a,c)} \mathrm{d}\xi = -\pi\alpha\ . \tag{3.8}$$

Further, the identity

$$\int_{-a}^{c} \frac{\mathrm{d}\xi}{w(\xi,a,c)(x-\xi)} = 0, \quad -a \le x \le c \tag{3.9}$$

simplifies the inverted integral equation as the angle of tilt, α, does not affect the normal pressure explicitly

$$p(x) = \frac{w(x,a,c)}{2\pi} E^* \int_{-a}^{c} \frac{\mathrm{d}g/\mathrm{d}\xi}{w(\xi,a,c)(x-\xi)} \mathrm{d}\xi\ , \quad -a \le x \le c\ . \tag{3.10}$$

Note, however, that the angle of tilt has an effect on the integration limits, $[-a, \quad c]$, and the consistency condition is to be evaluated depending on the gradient of the relative surface profile, $\mathrm{d}g/\mathrm{d}x$, see Eq. (3.8).

In addition to normal equilibrium, the rotational equilibrium condition needs to be fulfilled by setting

$$P = \int_{-a}^{c} p(x)\,\mathrm{d}x, \tag{3.11}$$

$$M = \int_{-a}^{c} p(x)\,x\,\mathrm{d}x. \tag{3.12}$$

Closed-form solutions that have been attached to a particular geometry include the tilted wedge [Moore and Hills, 2020] or the tilted flat and rounded punch [Andresen et al., 2019b]. Those are the two commonly used example geometries which support a moment, contrary to the Hertzian geometry which only yields symmetrical pressure distributions. In Appendix A.1 we demonstrate how closed-form solutions can be found for Eqs. (3.8, 3.10, 3.11, 3.12), despite being algebraically taxing.

3.2 The Order of Load Application

The order in which contact loads are applied affects the tangential problem. The first partial slip solutions, including the well-known solutions by [Cattaneo, 1938] and [Mindlin, 1949], treated a sequential order of load application. This means that the contact is first established by the application of a normal load and subsequently the tangential loading is added. In most real world problem, however, the application of normal and tangential loads is not separable but loads come on simultaneously. Despite the normal and tangential problem being uncoupled in the sense that the application of a normal load does not introduce shear tractions and vice versa, the load path taken has a significant effect on the shear tractions arising.

For this reason it is important to highlight three common load trajectories and how these are to be treated, Figure 3.3. We will restrict ourselves to PQ-problems to begin with. In all of the scenarios considered in this chapter, the shear load, Q, never reaches the full sliding condition, hence $|Q| < fP$. Note also that the order of load application can take possibly any form as long as the limit condition $|Q| = fP$ is not exceeded.

The first scenario, Figure 3.3 a), considers a sequential loading sequence. In a case like that the normal load is applied first and then held constant. Given the coefficient of friction, f, is finite, the subsequent application of a tangential load will cause some form of relative motion to ensue. If, on the other hand, Figure 3.3 b), the loading sequence is proportional, so that $^{\mathrm{d}Q}/_{\mathrm{d}P} < f$, a fully adhered interface is anticipated, despite the final load point, 2, being the same in all three scenarios. The

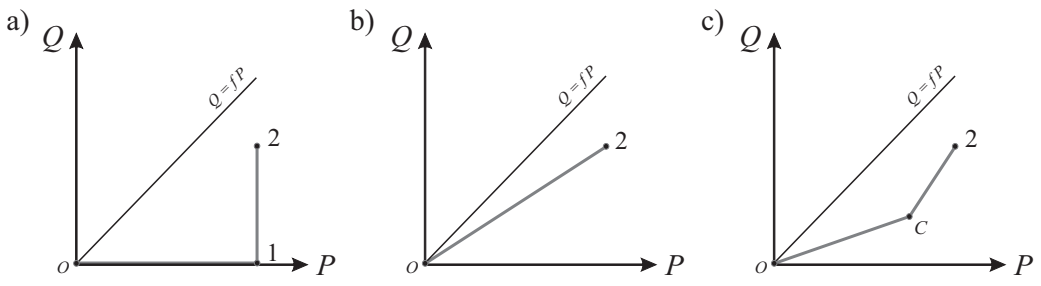


Figure 3.3: PQ-space with three different loading trajectories; a) tangential loading from O – 1 – 2, under constant normal load b) proportional loading directly from O – 2, and c) two-stage proportional loading from O – C – 2.

final case, Figure 3.3 c), considers a two-staged proportional loading scenario. The first leg of the loading trajectory is very similar to that depicted in Figure 3.3 b) and full stick is anticipated. After the intermediate change in gradient at point C the proportionality between shear and normal load is such that $^{\mathrm{d}Q}/_{\mathrm{d}P} > f$. This causes some form of slip stick pattern to develop along the interface from this point onwards.

3.2.1 Sequential Loading (Constant Normal Load)

We begin by looking at a half-plane contact spanning $[-a \quad a]$, where a is the instantaneous contact half-width. The contact size advances until the normal load reaches point 1, Fig. 3.3 a). We assume the two half-planes to be elastically similar and plane strain conditions to apply. The slope of the contact profile, $\mathrm{d}g/\mathrm{d}x$, can be connected to the normal pressure, $p(x)$, using the integral equation formulated in Chapter 2, so that

$$\frac{\mathrm{d}g}{\mathrm{d}x} = \frac{2}{\pi E^*} \int_{-a}^{a} \frac{p(\xi)\mathrm{d}\xi}{x-\xi}. \tag{3.13}$$

The inversion of Eq. (3.13) follows the procedure outlined in §2.2 and yields a similar result to that given in Eq. (3.10) for the normal pressure, taking the limit $c \to a$. Full details on the inversion are given in [Barber, 2010] or [Hills et al., 1993]. Normal equilibrium needs to be fulfilled by integrating the normal pressure over the contact interface

$$P = \int_{-a}^{a} p(x)\,\mathrm{d}x, \tag{3.14}$$

so that the contact law is given by $a(P)$. The normal load is then held constant at its instantaneous value so that $P = P_1 = P_2$, and hence $p(x) = p_1(x) = p_2(x)$. Supposing the coefficient of friction is finite, we subsequently apply a shear force, $|Q| < fP$, from load point 1 to load point 2. If we consider the inequality for full stick, Eq. (2.69), we notice that $\mathrm{d}P \to 0$, since we keep the normal load constant. It follow that

$$\frac{\mathrm{d}Q}{\mathrm{d}P} > f, \tag{3.15}$$

and some form of slip is anticipated to develop along the contact interface and it is natural to ask where these zones of slip will be positioned along the interface. The point-wise definition of Coulomb's law, $|q(x)| \leq fp(x)$, is the first step in finding an answer. We also know that in incomplete contacts, the normal pressure falls smoothly to zero at both ends of the contact, see §1.4. This means that the shear tractions will reach the limit condition at the edges of the contact first

$$|q(x)| = fp(x) \qquad x \in \text{slip} \; . \tag{3.16}$$

Since we have restricted ourselves, here, to a symmetrical contact interface in the absence of a moment, a pressure distribution symmetrical about its centre axis is expected. If a shear force is subsequently applied, the the slip zones will start to grow from both ends of the contact and the slip stick boundary will be positioned equidistantly from the centre axis of the contact. In the regions of stick, $-b \leq x \leq b$, the no relative movement of surface particles occurs and the relative surface strain must vanish

$$\Delta\varepsilon_{xx} = 0 \quad -b \leq x \leq b. \tag{3.17}$$

In order to find the exact location of the slip stick boundary, b, let us try to relate the information we have about the the shear tractions in the slip region, Eq. (3.16), and relative strains in the stick region, Eq. (3.17). The equivalence between normal and tangential displacements, see Eqs. (2.9, 2.10), allows us to relate the relative surface strains, $\Delta\varepsilon_{xx}$, to the shear tractions, $q(x)$, similarly to the integral equation used to solve the normal load problem in §2.2, so that

$$\Delta\varepsilon_{xx} = \frac{2}{\pi E^*} \int_{-a}^{a} \frac{q(\xi)d\xi}{x-\xi} \quad -a \leq x \leq a. \tag{3.18}$$

Jäger [Jäger, 1997] and Ciavarella [Ciavarella, 1998], apparently unaware of Jäger's findings, almost simultaneously discovered that the relative surface strain can be expressed as a superposition of strains induced by the full sliding shear traction, $|q(x)| = f(p(x)$, and a yet unknown second traction, $q'(x)$, which corrects the strains in the stick region, giving

$$\Delta\varepsilon_{xx} = \frac{2}{\pi E^*} \left[\int_{-a}^{a} \frac{fp(\xi)\mathrm{d}\xi}{x-\xi} + \int_{-b}^{b} \frac{q'(\xi)\mathrm{d}\xi}{x-\xi} \right] \qquad -a \leq x \leq a. \tag{3.19}$$

If we exploit the information that the relative surface strains in the stick region must vanish, $\Delta\varepsilon_{xx} = 0$, we can write

$$0 = \frac{2}{\pi E^*}\left[\int_{-a}^{a} \frac{fp(\xi)d\xi}{x-\xi} + \int_{-b}^{b} \frac{q'(\xi)d\xi}{x-\xi}\right] \qquad -b \le x \le b. \tag{3.20}$$

The first part of the bracket term is very similar to that arising in the integral equation for the normal problem, given in Eq. (3.13), only differing by the factor f, so that Eq. (3.20) can be re-written as

$$-f\,\frac{\mathrm{d}g}{\mathrm{d}x} = \frac{2}{\pi E^*}\int_{-b}^{b} \frac{q'(\xi)\mathrm{d}\xi}{x-\xi} \qquad -b \le x \le b. \tag{3.21}$$

Above equation reveals that the corrective traction is simply a scaled form of the full sliding traction, $fp(x)$, and this is the very powerful result found by Jäger [Jäger, 1997] and Ciavarella [Ciavarella, 1998] at the end of the last century, today known as the Jäger-Ciavarella theorem. As we shall see, this superposition principle is applicable to a wide range of partial slip problems, independent of the geometry of the indenter, as long as the contact profile gives rise to an incomplete contact. However, the scaling found does not answer our initial question as to where the slip stick boundary must be positioned along the interface, $-a < b \le x \le b < a$. Tangential equilibrium is the condition we have not yet exploited. The corrective shear traction must correspond to a lower load, Q', than the full sliding shear load, fP, and the applied shear force together with the corrective load must be equal to $Q = fP - Q'$. In terms of traction resultants this gives

$$Q = fP - Q' = \int_{-a}^{a} fp(x)\,\mathrm{d}x - \int_{-b}^{b} q'(x)\,\mathrm{d}x\ . \tag{3.22}$$

The shear tractions at any point along the trajectory 1–2 can be expressed as a piecewise function

$$q(x) = \begin{cases} fp(x) - q'(x) & |x| < b \\ fp(x) & b < |x| < a \end{cases}\ . \tag{3.23}$$

Barber et al. [Barber et al., 2011] introduced a contracted notation which enables us to visualise the superposition principle in PQ-space very easily. He denotes the contact pressure distribution for any incomplete contact problem as

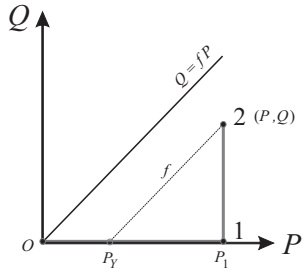


Figure 3.4: PQ-space with sequential loading trajectory and the visual construction to find the corrective force P_Y.

$p(x, P)$, where P is the applied normal load. Now, recall that the corrective traction is simply a scaled form of the full sliding tractions. Applying this new notation to the shear tractions in partial slip, Eq. (3.23) gives

$$q(x) = \begin{cases} f\,[p(x,P) - p(x,P_Y)] & |x| < b \\ fp(x,P) & b < |x| < a \end{cases} . \tag{3.24}$$

where $P_Y = Q'/f$. Furthermore, this simplified notation allows to visualise the construction of the corrective load, P_Y, see Figure 3.4. Note that for the PQ problem under consideration, P_Y lies on the P-axis and is connected to load point 2 by a line of gradient f, so that

$$P_Y = \frac{fP - Q}{f} . \tag{3.25}$$

Finally, the stick zone half-width, b, is given by evaluating the contact law $b = a(P_Y)$.

As we shall find out, the Jäger-Ciavarella theorem applies not only to all incomplete geometries, but it is applicable to a wide range of complicated loading problems, including those that are subject to a moment or moderate differential bulk tension.

3.2.2 Proportional Loading

The loading scenario depicted in Figure 3.1 b) shows how most contact loads are imposed in engineering applications. Often there is an external force acting on the assembly giving rise to local contact loads which then grow in proportion so that we can write

$$\frac{\mathrm{d}P}{P} = \frac{\mathrm{d}Q}{Q} . \tag{3.26}$$

Let us denote the gradient of the load path shown in Figure 3.1 b) as λ. If the gradient is less than the coefficient of friction, f, the inequality for full stick, Eq. (2.74), is satisfied and we can write

$$\lambda = \frac{\Delta Q}{\Delta P} = \frac{Q_2 - Q_O}{P_2 - P_O} < f \ . \tag{3.27}$$

From the previous section we know that along a fully adhered interface there is no relative movement of surface particles. This means the relative direct strains along the entire contact interface must vanish

$$\Delta\varepsilon_{xx} = 0 \qquad -a \leq x \leq a \ , \tag{3.28}$$

and no zones of slip are to be developed. Now, what do the shear tractions look like in this case? From §2.5.1 we know that small changes in normal load, $\mathrm{d}P$, give rise to a singular change in normal pressure [Hills et al., 2011]

$$\mathrm{d}p(x) = \frac{\mathrm{d}P}{\pi\sqrt{a^2 - x^2}} \ . \tag{3.29}$$

If summed up over finite changes in normal load, the normal pressure is given by

$$p(x) = \frac{1}{\pi}\int_0^P \frac{\mathrm{d}P}{\sqrt{a^2 - x^2}} \ . \tag{3.30}$$

An Infinitesimal change in shear loading, $\mathrm{d}Q$ - applied at the same time as a small change in normal load - generates a singular change in shear tractions, given by [Hills et al., 2011]

$$\mathrm{d}q(x) = \frac{\mathrm{d}Q}{\pi\sqrt{a^2 - x^2}} \ . \tag{3.31}$$

In the example under consideration, the gradient of simultaneous load changes in PQ-space is constant such that

$$\lambda = \frac{\mathrm{d}Q}{\mathrm{d}P} < f \ . \tag{3.32}$$

From combining Eqs. (3.31) and (3.32), we find

$$\mathrm{d}q(x) = \lambda\,\frac{\mathrm{d}P}{\pi\sqrt{a^2 - x^2}} \ , \tag{3.33}$$

so that we can give the developing shear tractions across the interface under proportional loading where the gradient is smaller than the coefficient of friction as

$$q(x) = \frac{\lambda}{\pi} \int_0^P \frac{\mathrm{d}P}{\sqrt{a^2 - x^2}} = \lambda\, p(x, P) \; . \tag{3.34}$$

In summary, we find that for PQ problems the shear tractions are a scaled form of the normal pressure if the loading is proportional and the loading trajectory is such that the inequality for stick, Eq. (2.74), is satisfied. As a consequence the interface will remain fully adhered despite the application of a tangential load. What happens, when the loading trajectory is such that this inequality is violated, will be the topic of the remaining loading scenario, see Figure 3.3 c).

3.2.3 Two-Stage Proportional Loading

The third loading scenario under consideration is illustrated in Figure 3.3 c). Similarly to the previous scenario, the contact is formed under proportional loading. The gradient of the load path, however, changes at the intermediate point C from λ_{I} to λ_{II}, Figure 3.5. The objective of this exercise is to demonstrate the effect a change in gradient has on the resulting shear tractions at load point II. From the previous example for proportional loading, §3.2.2, we know the shear tractions until load point C is reached, given by

$$q(x) = \lambda_{\mathrm{I}}\, p(x, P) \; . \tag{3.35}$$

Beyond load point C, the loading path violates the inequality for a fully adhered interface

$$\lambda_{\mathrm{II}} = \frac{Q_2 - Q_{\mathrm{C}}}{P_2 - P_{\mathrm{C}}} = \frac{\Delta Q}{\Delta P} > f \; , \tag{3.36}$$

so that slip is expected to develop somewhere along the interface. The onset of slip will begin from the contact edges as this is where the contact pressure falls smoothly to zero and the conditions for slip will be fulfilled first, $|q(x)| = f(p(x))$. We also anticipate the size of the slip zones to be smaller compared with the loading scenario depicted in Figure 3.3 a), since $|\Delta Q| < Q_2$, and hence less shear loading

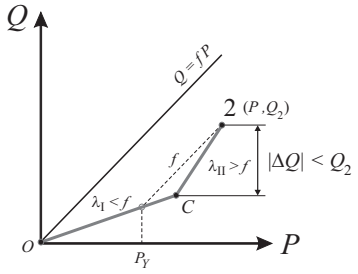


Figure 3.5: PQ-space with a two-stage proportional loading trajectory and the visual construction to find the corrective force P_Y.

can cause relative movement. A corrective shear traction is needed and it will be associated with a lower load, $fp(x, P_Y)$. Figure 3.5 shows that the corrective load, P_Y, is found at the intersection of a line of gradient f with the previous load path, O – C. However, during the fully adhered loading, shear tractions have been locked-in and it is those that need to be added to ensure tangential equilibrium, $Q_2 = \int_{-a}^{a} q(x)\,\mathrm{d}x$, using an extended version of the superposition principle found by Jäger and Ciavarella [Barber et al., 2011]. The shear tractions during the loading along the trajectory, C – 2, will be given by

$$q(x) = \begin{cases} fp(x,P) - fp(x,P_Y) + \lambda_{\mathrm{I}}\, p(x,P_Y) & |x| < b \\ fp(x,P) & b < |x| < a \end{cases} . \tag{3.37}$$

For a PQ problem, a visual construction is possible, Figure 3.5, and the corrective load, P_Y, is found to be

$$P_Y = \frac{fP - Q}{f - \lambda_{\mathrm{I}}} . \tag{3.38}$$

Note the similarities between Eqs. (3.25 and 3.37), yielding an almost identical result for the corrective load, P_Y. The difference is due to the additional term associated with the locked-in shear tractions, $\lambda_{\mathrm{I}}\, p(x, P_Y)$. There is a different way of looking at this difference. In §3.2.1 the first leg of the loading trajectory has no contribution from a shear load, hence the gradient of the loading path is naught until load point 1 is reached, hence there are not locked-in shear tractions. On the other hand, in this section, the corrective load, P_Y, is larger, ensuring the remaining stick zone, $b = a(P_Y)$, to be larger as well, compared with sequential loading.

3.2.4 Application to a Hertzian Geometry

In this example we wish to apply the three solutions developed above to the celebrated Hertzian problem. We hope this guides the reader in gaining complementary insight into the three scenarios explored in §3.2.1, §3.2.2, §3.2.3.

We begin by recalling the problem of a plane Hertzian contact, as depicted in Figure 3.6. The contact is established between two elastically similar half-planes, where the contacting profiles have the equivalent curvature $1/R = 1/R_1 + 1/R_2$. The application of a normal force, P, induces the well-known elliptical normal pressure distribution [Hertz, 1881]

$$p(x, P) = p_0\sqrt{1 - \frac{x^2}{a^2}} \quad \text{where} \quad p_0 = \frac{2P}{\pi a} , \tag{3.39}$$

where the contact spans $[-a \qquad a]$. The contact law is given by

$$a(P) = \sqrt{\frac{4PR}{\pi E^*}} , \tag{3.40}$$

where E^* is the composite modulus.

We wish to emphasise that in all three examples presented, the final load point 2, has been the same, i.e. tangential equilibrium, $Q_2 = \int_{-a}^{a} q(x)\,\mathrm{d}x$, has to provide the same answer in all three scenarios. The resulting shear tractions, however, will differ considerably and this is shown in Figure 3.7.

Following the solution for the first loading scenario, see §3.2.1, we first establish an interface by application of a normal load, P, until load point 1 is reached. From here on the normal load is kept constant while a shear force is increased

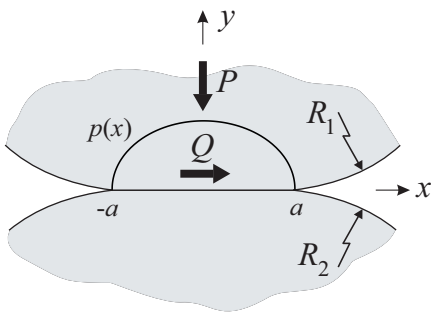


Figure 3.6: Two contacting Hertzian cylinders with respective radii R_1 and R_2 subject to normal and shear loading.

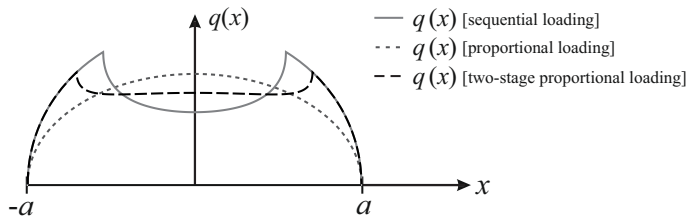


Figure 3.7: Comparison of shear tractions for linear, bi-linear proportional and sequential loading to the same point in PQ-space.

monotonically until load point 2 is reached, see Figure 3.3 a). We expect regions of slip to develop, given the coefficient of friction is finite and the condition for full stick to be violated. Since the Hertzian contact and pressure distribution are symmetrical about the centre-axis of the contact, we expect the stick zone to be positioned centrally, $-a < -b < x < b < a <$. Employing the notation developed by Barber [Barber et al., 2011], the shear tractions for this partial slip problem are simply given as

$$q(x) = \begin{cases} f\left[p(x,P) - p(x,P_Y)\right] & |x| < b \\ fp(x,P) & b < |x| < a \end{cases} , \tag{3.41}$$

where the corrective load is $P_Y = {}^{fP-Q}/_{f}$. The stick zone half-width is given conveniently by the contact law, $a(P)$, associated with the value of P_Y

$$b = a(P_Y) = \sqrt{\frac{4P_Y R}{\pi E^*}} . \tag{3.42}$$

Figure 3.8 illustrates the superposition of the full sliding shear tractions, $fp(x,P)$, and a scaled form of it, $fp(x,P_Y)$. The resulting relative strains induced cancel in the stick region, effectively ensuring an adhered interface, $[-b \quad b]$.

We now turn to the case of proportional loading, shown in Figure 3.3 b). The loading trajectory is such that ${}^{\mathrm{d}P}/_{P} = {}^{\mathrm{d}Q}/_{Q}$. Suppose now, the gradient of the loading path is

$$\lambda = \frac{Q_2}{P_2} < f . \tag{3.43}$$

As outlined in §3.2.2, Eq. (3.43) fulfils the condition for full stick and no relative movement of surface particles is expected along the interface. We further

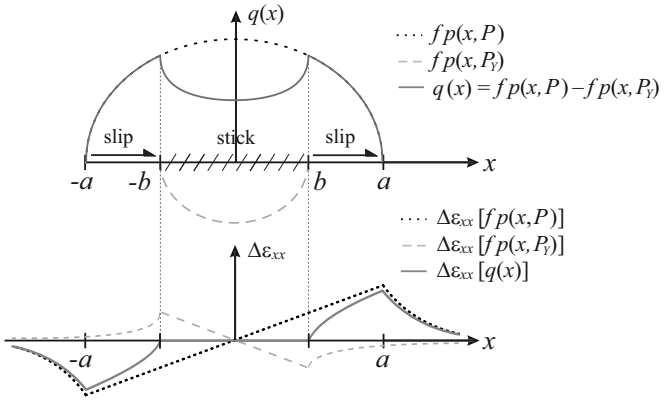


Figure 3.8: Illustration of shear tractions and relative surface strains for a Hertzian contact subject to a monotonically increasing shear force with constant normal load.

demonstrated that the shear tractions during a fully adhered proportional loading condition will be scaled with the gradient of the load path taken, giving

$$q(x) = \lambda\, p(x, P)\ . \tag{3.44}$$

The final case we wish to illustrate here considers two-stage proportional loading. That is, the gradient of the loading trajectory starts off ensuring a fully adhered interface and changes at an intermediate point C, from where on regions of slip are expected to develop, see Figure 3.3 c). It is possible to employ a slightly modified superposition of scaled forms of the full sliding traction to describe the partial slip tractions between load point C and 2, giving

$$q(x) = \begin{cases} fp(x,P) - fp(x,P_Y) + \lambda_{\mathrm{I}}\, p(x,P_Y) & |x| < b \\ fp(x,P) & b < |x| < a \end{cases}\ , \tag{3.45}$$

where $P_Y = {}^{fP-Q}/_{f-\lambda_{\mathrm{I}}}$.

3.3 The Effect of Differential Bulk Tension

Interfacial shear tractions may arise from either the application of a shear load, or due to the presence of a differential tension. That is, bulk stresses are applied remotely to one or both half-planes. The differential tension is caused my a mismatch

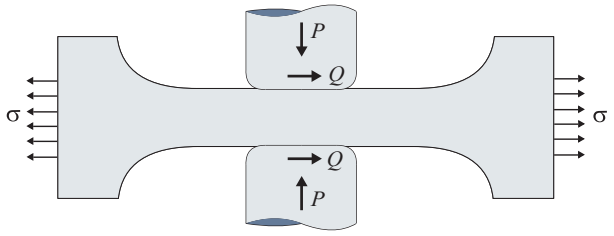


Figure 3.9: Typical set up for a fretting fatigue experiment.

in strains parallel with the interface. In order to represent this additional relative strain, we add a constant term to Eq. (3.18), giving

$$\Delta\varepsilon_{xx} = \frac{2}{\pi E^*}\int_{-a}^{a}\frac{q(\xi)d\xi}{x-\xi} + \frac{\sigma}{2E^*} \qquad -a \le x \le a\ , \tag{3.46}$$

where $\sigma = \sigma_{\mathrm{A}} - \sigma_{\mathrm{B}}$ is the differential bulk tension, as indicated in Figure 3.1.

Conditions of fretting can arise from the presence of a normal and oscillating shear load alone. Once a crack is nucleated in the zones of slip, the presence of an alternating stress field is required to propel the crack until fatigue failure occurs. Figure 3.9 shows a typical experimental fretting fatigue set up. Two pads, often flat and rounded punches, are clamped onto a dogbone specimen, effectively establishing the normal contact. The alternating tangential load is commonly applied to the dogbone as a combination of shear load and bulk tension, and for describing the partial slip problem it is important to distinguish between two cases. One in which the differential bulk tension is *moderate* and the Jäger-Ciavarella theorem is applicable and the other in which the differential bulk tension is *large* enough to reverse the direction of slip at one end of the contact [Hills and Nowell, 1987] and alternative methods are required.

3.3.1 Moderate Differential Bulk Tension in Partial Slip

In contact problems, differential tension alone causes a skew-symmetric shear traction to arise. This means tangential equilibrium is not affected by a differential tension. However, when applied under conditions of partial slip, together with a shear force, the effect of the differential tension will cause the stick zone to be no longer centrally positioned, but at an offset from the centre-axis, spanning

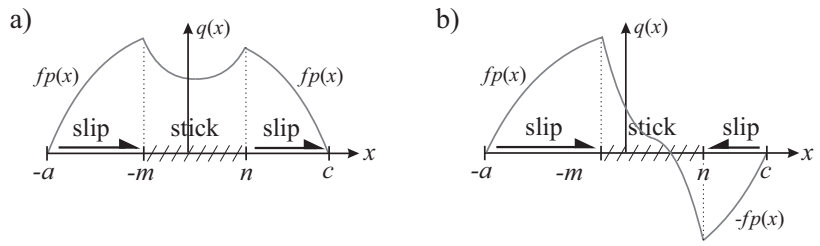


Figure 3.10: Shear tractions for mixed-loading for a) *moderate* differential bulk tension and b) *large* differential bulk tension.

$[-m \quad n]$. In mixed shear loading, the effect of the differential tension will add to the size of the slip zones at one end of the contact and subtract from the other, see Figure 3.10. In case a), i.e. when the differential tension is *moderate*, the direction of slip is the same at both ends of the interface and a superposition of a full sliding shear traction together with an appropriate corrective term will yield the correct answer. Suppose now, we add a further complication and investigate an asymmetrical interface, spanning $[-a \quad c]$, subject to mixed tangential loading with a *moderate* bulk tension. Following a similar line of reasoning as in §3.2.1, we find the integral equation

$$-f\left(\frac{\mathrm{d}g}{\mathrm{d}x}+\alpha\right)-\frac{\sigma}{2E^*}=\frac{2}{\pi E^*}\int_{-m}^{n}\frac{q'(\xi)\mathrm{d}\xi}{x-\xi} \qquad -m\le x\le n\,, \tag{3.47}$$

where the relative profile has slope $^{\mathrm{d}g}/_{\mathrm{d}x}$, tilted through a small angle, α. Note that from Eq. (3.47) we infer that the integral equation for the corrective shear traction, $q'(x)$, is of the same form as the one for the normal traction, Eq. (3.5), including an additional term due to the differential tension. Once Eq. (3.47) is inverted, the corresponding consistency condition is

$$\int_{-m}^{n}\frac{^{\mathrm{d}g}/_{\mathrm{d}\xi}\,\mathrm{d}\xi}{w(\xi,m,n)}=-\pi\alpha+\frac{\pi\sigma}{2fE^*}\,, \tag{3.48}$$

where $w(\xi,m,n)=\sqrt{(\xi+m)(n-\xi)}$ and together with tangential equilibrium these two equations will suffice to determine the position and extent of the stick zone. Note that the angle of tilt, α, affects the normal and tangential solution. Obviously, the tangential solution developed is also applicable to symmetrical contact problems, in which the angle of tilt $\alpha \to 0$.

3.3.2 Large Differential Bulk Tension in Partial Slip

As the differential tension, σ, increases, the stick zone position will eventually reach one end of the contact. If the differential tension is increased any further, the differential tension becomes dominant and the direction of slip reverses at the respective end of the contact, rendering the Jäger-Ciavarella principle inapplicable, see Figure 3.10 b). The superposition of a full sliding shear tractions requires the shear tractions in the slip zones to be of the same sign, $fp(x)$. The threshold between *moderate* and *large* bulk tension is geometry-dependent and we will look at the threshold expressions for the cases of a Hertzian and shallow wedge geometry later in this thesis, see Eq. (4.46) and Eq. (5.43). Partial slip solutions in the presence of *large* differential tension can be treated using the mathematical concept of dislocations. Instead of hinging the solution on the superposition of shear tractions and correcting for the strains in the stick zone, the dislocation method corrects for the strains in the slip zones, independent of the direction of slip, for details see Chapter 4.

3.4 Periodic Shear Loading

The reciprocal relative motion of surface particles in the presence of a stress concentration produces the conditions ripe for crack nucleation. Fatigue is a phenomenon associated with the oscillation of a stress field and in order to assess fretting damage, it is necessary to look at partial slip due to periodic shear loading. Mindlin and Deresiewicz were the first who studied partial slip problems due to an oscillating shear force [Mindlin and Dereiewicz, 1953]. They looked at a PQ problem in which the symmetrical contact is first established through the application of a normal load, which is then held constant while the shear force starts to oscillate between a maximum, Q_2, and minimum load point, Q_1. Figure 3.11 a) depicts a marching-in-time plot of the periodic loading, where $|Q_1| = Q_2$. We assume the load changes to occur in a quasi-static manner so that inertia effects can be neglected. In Figure 3.11 b) the cyclic loading history is translated to PQ-space. This enables the visualisation of some of the solutions presented in the following.

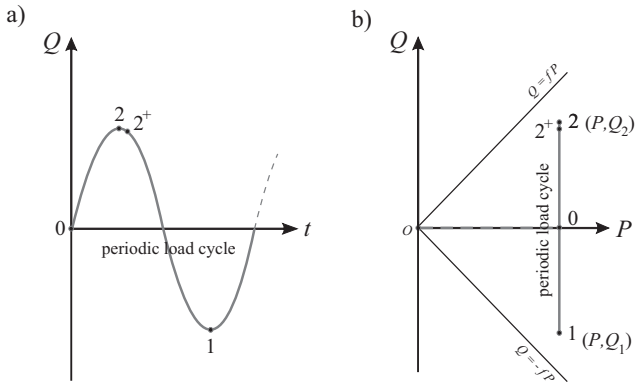


Figure 3.11: Periodic Loading of a shear force in a) a time-history plot and b) in PQ-space.

In §3.2.1 we treated the partial slip problem up to load point 2. Recall Eq. (3.24) and the slip stick pattern during the sequential application of a monotonically increasing shear force. Applied to a Hertzian geometry, we can expect the shear traction distribution at load point 2 to be of the form as the one illustrated in Figure 3.12 a). Once the shear load starts to reverse from its maximum, Q_2, to a point close to 2, say 2^+, the shear tractions and corresponding tangential displacement reduce infinitesimally. The rate of change of relative displacement has now changed sign and does not fulfil the necessary requirement for shear tractions to oppose relative motion, see Eqs. (3.1, 3.2). As a consequence, the entire interface becomes instantaneously stuck at the point of load reversal, Figure 3.12 b).

When the shear force is reduced further, particles begin to move back into their original position and slip in the *reverse* direction to allow for the conservation of material. The new slip zone size is denoted $b' < |x| < a$ and in order for particles to move in the *reverse* direction, the slipping traction will change from $q(x) = fp(x, P)$ to $q(x) = -fp(x, P)$, see Figure 3.12 c). Suppose we wish to find the new slip stick boundary, b', and corresponding shear traction distribution, we take the solution developed for the slip stick pattern when load point 2 was reached for the first time and superimpose an additional corrective traction over the new stick region, $|x| < b'$. Overall tangential equilibrium during shear load reversal, $2 \to 1$, is given by

$$Q = Q_2 - \Delta Q = \int_{-a}^{a} q(x)\,\mathrm{d}x = Q_2 - 2fP + 2fP_C\,. \tag{3.49}$$

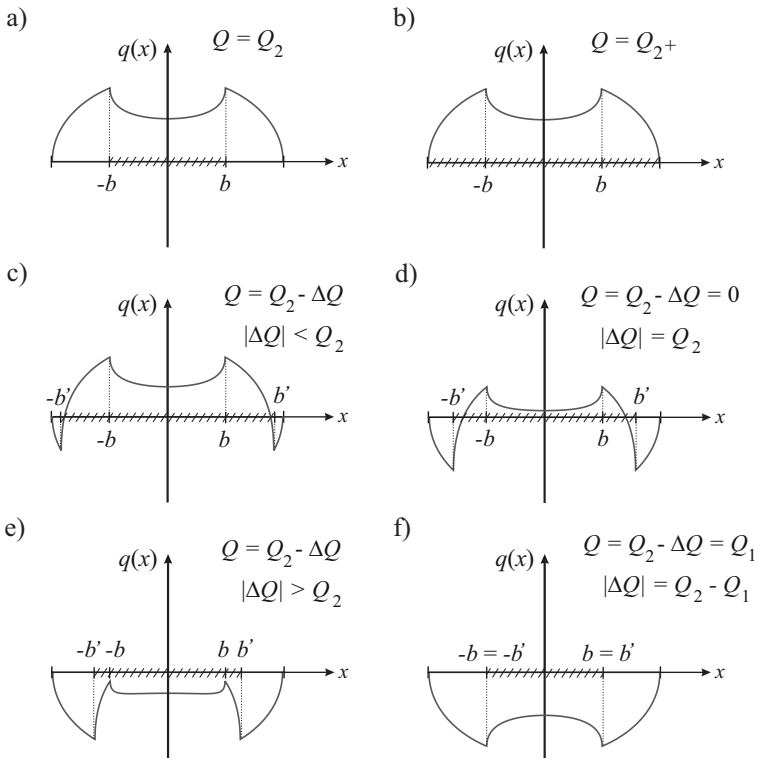


Figure 3.12: The evolution of shear tractions occurring during the loading cycle shown in Figure 3.11 for a Hertzian example geometry.

The new corrective force, P_C, is then given as

$$P_C = \frac{2fP - \Delta Q}{2f} \,, \tag{3.50}$$

and the visual construction is illustrated in Figure 3.13. Once the value of P_C is known, the half-width of the new stick zone, b', is given by evaluating the contact law $b' = a(P_C)$.

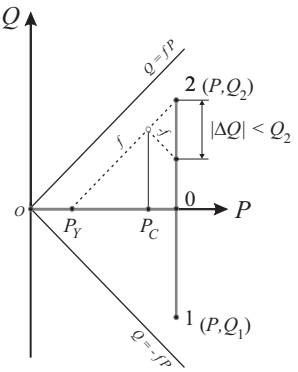


Figure 3.13: The visual construction to find the corrective force P_C in PQ-space foe periodic loading.

Comparing Eqs. (3.25 and 3.50), the factor of 2 ensures that the corrective term cancels the relative slip displacement that has already occurred. The shear traction distribution for any point during load reversal, $2 \rightarrow 1$, is given by

$$q(x) = \begin{cases} f\left[-p(x,P) + 2p(x,P_C) - p(x,P_Y)\right] & |x| < b \\ f\left[-p(x,P) + 2p(x,P_C)\right] & b < |x| < b' \\ -fp(x,P) & b' < |x| < a \end{cases} . \tag{3.51}$$

When the instantaneous applied shear force reaches zero, $Q = \int_{-a}^{a} q(x)\,\mathrm{d}x = 0$, during load reversal, it is important to note the residual shear tractions along the interface, see Figure 3.12 d). Once, the net shear force becomes negative, $Q_1 < Q = \int_{-a}^{a} q(x)\,\mathrm{d}x < 0$, we expect to observe a shear traction distribution as illustrated in Figure 3.12 e). At the minimum load point, $Q = Q_1$, all particles have been reversed fully so that $b' = b$, Figure 3.12 f).

Problems which involve a varying normal load, moment, shear load, and tension are treated in the next section.

3.5 General Cyclic Proportional Loading

In this section we are going to treat problems which involve a proportional variation of all loads possibly present at an interface, so that

$$\frac{\mathrm{d}P}{P} = \frac{\mathrm{d}M}{M} = \frac{\mathrm{d}Q}{Q} = \frac{\mathrm{d}\sigma_{\mathrm{A}}}{\sigma_{\mathrm{A}}} = \frac{\mathrm{d}\sigma_{\mathrm{B}}}{\sigma_{\mathrm{B}}} , \tag{3.52}$$

where $\sigma = \sigma_{\mathrm{A}} - \sigma_{\mathrm{B}}$.

In engineering applications, there is often a major external load acting on the assembly which takes all five local contact loads stated above to a mean value in load space during the transient phase. In the case of a gas turbine, the dovetail root contact, Figure 3.14, experiences a rapid increase in centrifugal loading, here denoted F_C and T, in the transient phase which is then held constant during steady-state operation. The steady-state variation of local contact loads is then induced by a minor external load varying. In the gas turbine for example, an unsteady air stream can cause an additional vibrational load, F_V. Since the minor external loading is a solitary load, the local contact loads change in phase (or proportionally), Eq. (3.52),

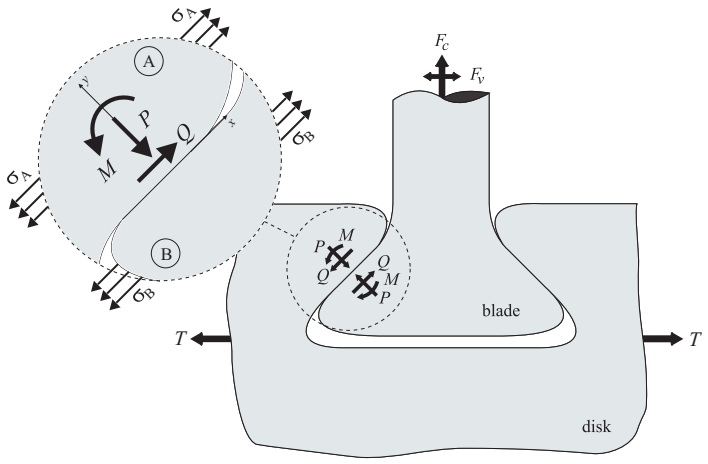


Figure 3.14: Illustration of a dovetail root contact with the resulting contact loads.

and thousands of cycles of load change per major cycle can clock up quickly. The proportionality of load variation collapses the steady-state cycle to a straight line in load space, as depicted in Figure 3.15. We denote the mean point of the cycle as 0, and 1 and 2 mark the minimum and the maximum points of the cycle. A partial slip problem arises if the changes in contact loads (ΔP, ΔQ, ΔM, $\Delta\sigma$) together with the instantaneous contact size violate the condition for full stick, Eq. (2.74). If we stick to the gas turbine example, it is evident that during operation the number of cycles accumulated in the steady-state is orders of magnitude larger compared with transient load cycles. This is also true for most other engineering applications which operate in a steady-state cycle. It is therefore our ambition to find a succinct solution to the steady-state partial slip problem. The solution we seek enables us to determine the contact size and the position and extent of the portion of the contact that does not experience any slip during the steady-state, therefore effectively

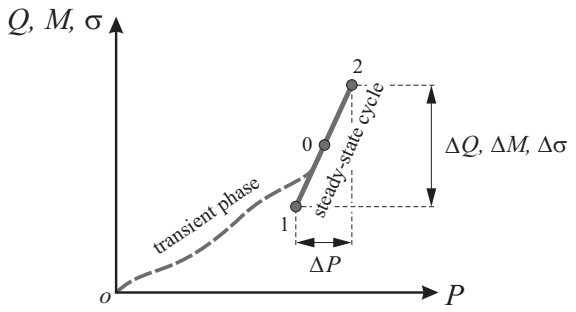


Figure 3.15: Illustration of a steady-state cycle in load space for variations of normal load, P, shear load, Q, moment, M, and differential bulk tension, σ, [Andresen et al., 2020a].

determining the size of the zones of relative motion along the interface. As we shall see, none of the coordinates we seek depend on the transient problem or how the steady-state cycle was entered, rendering a marching-in-time solution unnecessary.

3.5.1 The Permanent Stick Zone

Barber et al. [Barber et al., 2011] have shown that in a partial slip PQ problem some part of the contact interface experiences no relative movement during steady-state operation. In this section we expand the complexity of the problem by looking at loading scenarios involving all loads varying, including a moment and differential bulk tension and seek a solution for the so-called permanent stick zone.

Let us consider a contact interface capable of supporting a moment. The application of a moment will cause the pressure distribution and contact patch to be asymmetrical about its centre axis, say $[-a \quad c]$, see §3.1. The load history will not affect the solution to the normal problem, given Dundurs' constant is $\beta = 0$. However, in §3.3.1 we showed that an asymmetry in the normal problem affects the tangential solution directly and this is something we wish to pay close attention to in the steps we make in the following.

In addition to the normal and shear loading transferred through the interface, each half-plane might be subject to a bulk stress applied remotely from the interface, denoted σ_{A} and σ_{B}, as shown in Figure 3.1. The resulting differential tension, $\sigma = \sigma_{\mathrm{A}} - \sigma_{\mathrm{B}}$, causes a strain mismatch along the interface, hence differential tensions are an additional source of shear tractions. For the solution we intend to develop in this section we shall assume the differential tension to be *moderate*. Therefore, the slip direction is the same at both ends of the contact and the surface particles are displaced in one direction when going from point 1 to point 2 of the steady-state cycle and in reverse direction when going from point 2 to point 1.

Figure 3.16 illustrates the evolution the contact size and stick slip pattern during a steady-state cycle for a general incomplete contact. Note that due to the varying normal load the contact edge moves throughout the steady-state cycle, causing the contact patch to expand when going from point 1 to 2 and contract when

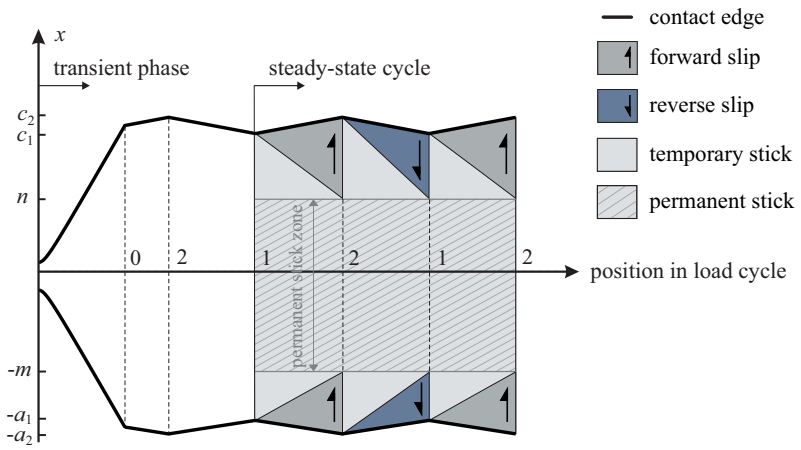


Figure 3.16: Illustration of a evolving steady-state cycle in a marching-in-time sense with the outer parts of the contact experiencing reciprocating slip and stick and the inner part being permanently stuck.

the contact loads reverse. Particles that have moved outwards, slip backwards in order ensure the continuity of material. It is important to note that the maximum extent of the slip zones is reached just before the end points of the steady-state are approached, reducing the stick zone to its minimum and permanent extent, spanning $[-m \quad n]$, and this is quantity what we seek.

We jump straight to the steady-state and begin developing the solution by writing down the change in relative surface strains at load point 1, (P_1, M_1, Q_1, σ_1), over the whole interface, $[-a_1 \quad c_1]$. We use the Jäger-Ciavarella superposition principle and state

$$\Delta\varepsilon_{xx,1} = \frac{2}{\pi E^*}\left[-\int_{-a_1}^{c_1}\frac{fp_1(\xi)\mathrm{d}\xi}{\xi - x} + \int_{-m}^{n}\frac{q_1^*(\xi)\mathrm{d}\xi}{\xi - x} + \frac{\pi}{4}\sigma_1\right] , \tag{3.53}$$

where the corrective term, $q_1^*(x)$, over the permanent stick region $[-m \quad n]$, is unknown yet. Almost the same can be done at load point 2, (P_2, M_2, Q_2, σ_2), only that during load reversal the slipping tractions are of opposite sign and we state

$$\Delta\varepsilon_{xx,2} = \frac{2}{\pi E^*}\left[\int_{-a_2}^{c_2}\frac{fp_2(\xi)\mathrm{d}\xi}{\xi - x} + \int_{-m}^{n}\frac{q_2^*(\xi)\mathrm{d}\xi}{\xi - x} + \frac{\pi}{4}\sigma_2\right] , \tag{3.54}$$

where $q_2^*(x)$ is the corrective term at the other end of the load cycle, corresponding to the new full sliding traction, $fp_2(x)$. An important physical observation is that the change in relative strains in the permanent stick region must be the same at

both ends of the cycle, as no slip occurs, hence

$$\Delta\varepsilon_{xx,1} = \Delta\varepsilon_{xx,2}\ . \ -m < x < n \tag{3.55}$$

This allows us to subtract Eq. (3.53) from Eq. 3.54) over the permanent stick region, $-m < x < n$. Rearranging the terms yields

$$-\int_{-a_1}^{c_1} \frac{fp_1(\xi)\mathrm{d}\xi}{\xi - x} - \int_{-a_2}^{c_2} \frac{fp_2(\xi)\mathrm{d}\xi}{\xi - x} - \frac{\pi}{4}(\sigma_2 - \sigma_1) = \int_{-m}^{n} \frac{[q_2^* - q_1^*]\,\mathrm{d}\xi}{\xi - x}\ , \tag{3.56}$$

where $x \in (-m, n)$. Note that the left-hand side of Eq. (3.56) can be stated in terms of the profile gradient and angle of tilt. Using the simple result obtained in Eq. (3.47) and knowing that $-a_2 < -a_1 < -m < x < n < c_1 < c_2$, we rewrite Eq. (3.56) in the form

$$fE^*\frac{\mathrm{d}g}{\mathrm{d}x} + fE^*\alpha_0 - \frac{\Delta\sigma}{4} = \frac{1}{\pi}\int_{-m}^{n} \frac{[q_2^* - q_1^*]\,(\xi)\mathrm{d}\xi}{\xi - x}, \ \ -m < x < n, \tag{3.57}$$

where

$$\alpha_0 = \frac{\alpha_1 + \alpha_2}{2} \qquad \text{and} \qquad \Delta\sigma = \sigma_2 - \sigma_1 \tag{3.58}$$

are, respectively, the average angle of tilt and the range of differential bulk tension between the minimum and maximum load points. Note that the left-hand side of Eq. (3.57) leaves us with a term for the gradient of the surface profile, $^{\mathrm{d}g}/_{\mathrm{d}x}$, and a constant term, $\alpha_0 - {}^{\Delta\sigma}/_{4fE^*}$. This emphasises a striking similarity between the arguments made in §3.1 and the inversion of Eq. (3.57), which is given by [Andresen et al., 2020b]

$$[q_2^* - q_1^*](x) = \frac{fE^*}{\pi} w(x,m,n) \int_{-m}^{n} \frac{\left[{}^{\mathrm{d}g}/_{\mathrm{d}\xi} + \alpha_0 - \frac{\Delta\sigma}{4fE^*}\right]\mathrm{d}\xi}{w(\xi,m,n)(\xi - x)}\ , \tag{3.59}$$

where $w(\xi,m,n) = \sqrt{(\xi+m)(n-\xi)}$ and $w(x,m,n) = \sqrt{(x+m)(n-x)}$. Eq. (3.59) is subject to the consistency condition

$$\int_{-m}^{n} \frac{{}^{\mathrm{d}g}/_{\mathrm{d}\xi}\ \mathrm{d}\xi}{w(\xi,m,n)} = -\pi\alpha_0 + \frac{\pi\Delta\sigma}{4fE^*}\ , \tag{3.60}$$

and using the identity $\int_{-m}^{n} \frac{\mathrm{d}\xi}{w(\xi,m,n)(\xi-x)} = 0$, simplifies Eq. (3.59) to

$$[q_2^* - q_1^*](x) = \frac{fE^*}{\pi} w(x,m,n) \int_{-m}^{n} \frac{{}^{\mathrm{d}g}/_{\mathrm{d}\xi}\ \mathrm{d}\xi}{w(\xi,m,n)(\xi - x)}\ , \ \ -m \le x \le n\ . \tag{3.61}$$

In order to have a complete set of equations enabling the determination of the size of the permanent stick zone, we impose tangential equilibrium at each end of the loading cycle as

$$Q_1 = -fP_1 + Q_1^* \,, \tag{3.62}$$

$$Q_2 = fP_2 + Q_2^* \,, \tag{3.63}$$

where

$$Q_i^* = \int q_i^*(x)\mathrm{d}x \;; \quad i = 1, 2 \,, \tag{3.64}$$

is the resultant *corrective* shear force.

Subtracting Eq. (3.62) from Eq. (3.63) defines the range of the shear force as

$$\Delta Q = Q_2 - Q_1 = 2fP_0 + \Delta Q^*, \tag{3.65}$$

where

$$P_0 = \frac{P_1 + P_2}{2}$$

is the mean normal load and

$$\Delta Q^* = \int_{-m}^{n} [q_2^* - q_1^*](x)\mathrm{d}x \,. \tag{3.66}$$

Eqs. (3.60, 3.65) are sufficient to determine the extent and position of the permanent stick zone, $[-m \quad n]$, for frictional half-plane contacts in partial slip in the steady-state. We refer to the original publications [Andresen et al., 2019a, Andresen et al., 2020b] for full details of the procedure described.

3.5.2 Mapping between the Normal and Tangential Problem

Not in all cases it is necessary to evaluate the equations associated with the tangential problem. It is possible to formulate a succinct mapping between the normal problem for asymmetrical contacts and the tangential problem, exploiting

striking parallels in the problem formulation. Comparing the expressions stated in §3.1 and §3.5.1, gives the mapping [Andresen et al., 2020b]

$$\begin{aligned} [-a \quad c] &\rightarrow [-m \quad n] \\ p(x) &\rightarrow -\frac{1}{2f}\,[q_2^* - q_1^*](x) \\ P &\rightarrow P_0 - \frac{\Delta Q}{2f} \\ \alpha &\rightarrow \alpha_0 - \frac{\Delta\sigma}{4fE^*} \end{aligned} \quad . \tag{3.67}$$

If a closed-form solution to a normal contact problem for an indenter capable of supporting a moment is tractable, the complete solution to the steady-state partial slip problem can be found readily. All that is needed to connect, or map, the normal and tangential solution are explicit or implicit expressions for the contact coordinates $[-a \quad c]$ and the normal traction, $p(x)$, for chosen values of P and α. It is not always desired to define the problem in terms of the angle of tilt, α, but instead the external moment, M, is used as an input to the problem. This will require to evaluate of the corresponding tilt angles, α_i, at both ends of the steady-state cycle in order to find the average angle of tilt, α_0. The mapping is illustrated in the following example.

3.5.3 Application to the Tilted Shallow Wedge

The tilted shallow wedge under consideration has apex angle $(\pi - 2\phi)$ where $0 < \phi \ll 1$ and is tilted through a small angle $0 < \alpha \ll 1$, Figure 3.17. We assume the internal wedge angle to be large enough for the half-plane assumption to hold. The contact is established by applying a normal force, P, and moment, M.

To carry out the mapping procedure, we need a closed-form solution for the *normal* contact problem. For the titlted shallow wedge this was first published by Sackfield et al. [Sackfield et al., 2005]. The pressure distribution is given by

$$p(x) = \frac{E^*\phi}{\pi} \log \left| \frac{\sqrt{\gamma} + \sqrt{(\gamma a - x)/(x + a)}}{\sqrt{\gamma} - \sqrt{(a\gamma - x)/(x + a)}} \right| , \tag{3.68}$$

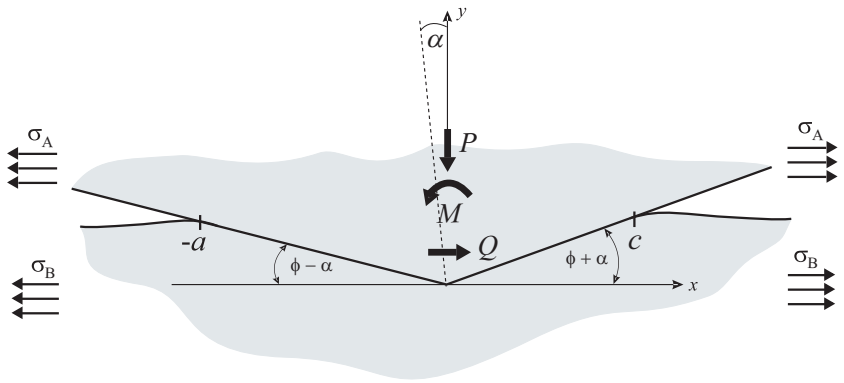


Figure 3.17: A tilted wedge contact subject to a normal load, moment, shear load with remote bulk tensions arising in each half-plane.

where γ is given by [Moore and Hills, 2020]

$$\gamma = \left(1 - \sin\left(\frac{\pi\alpha}{2\phi}\right)\right)\left(1 + \sin\left(\frac{\pi\alpha}{2\phi}\right)\right)^{-1} . \tag{3.69}$$

The angle of tilt, α, can be expressed in terms of the normal load, P, and moment, M, [Moore and Hills, 2020]

$$\alpha = -\frac{2\phi}{\pi}\arcsin\left(\frac{2E^*\phi M}{\sqrt{4(E^*\phi M)^2 + P^4}}\right) . \tag{3.70}$$

The symmetry of the wedge geometry connects the contact coordinates, so that

$$c = \gamma a \, , \tag{3.71}$$

where the contact spans $[-a \quad c]$ and the contact half-width a is found from imposing normal equilibrium

$$P = \int_{-a}^{c} p(x)\,\mathrm{d}x = E^*\phi\sqrt{\gamma a^2} \, , \tag{3.72}$$

yielding the following explicit expression

$$a = \frac{P}{E^*\phi}\sqrt{\frac{1}{\gamma}} \, ; \qquad c = \frac{P}{E^*\phi}\sqrt{\gamma} \, . \tag{3.73}$$

Rotational equilibrium is imposed by

$$M = \int_{-a}^{c} p(x)x\,\mathrm{d}x = \frac{E^*\phi}{4}\sqrt{\gamma}(1-\gamma)a^2 \, . \tag{3.74}$$

With this set of equations the mapping outlined in §3.5.2 allows us to solve the steady-state partial slip problem by carrying out a the following substitutions. We begin by replacing $\alpha \to \alpha_0 - \frac{\Delta\sigma}{4fE^*}$, as given in the Eq. (3.67), so that

$$\gamma_t = \left(1 - \sin\left(\frac{\pi\left(\alpha_0 - \frac{\Delta\sigma}{4fE^*}\right)}{2\phi}\right)\right)\left(1 + \sin\left(\frac{\pi\left(\alpha_0 - \frac{\Delta\sigma}{4fE^*}\right)}{2\phi}\right)\right)^{-1}, \qquad (3.75)$$

where α_0 is the average angle of tilt and $\Delta\sigma$ is the range of differential bulk tension during the steady-state, see Eq. (3.58). Since the tilted shallow wedge yields explicit expressions for the contact coordinates $[-a \quad c]$, the permanent stick zone is found readily by substituting the mapping, Eq. (3.67), into Eq. (3.73), giving

$$m = \frac{1}{E^*\phi}\left(P_0 - \frac{\Delta Q}{2f}\right)\sqrt{\frac{1}{\gamma_t}}\,; \qquad n = \frac{1}{E^*\phi}\left(P_0 - \frac{\Delta Q}{2f}\right)\sqrt{\gamma_t}\,, \qquad (3.76)$$

where P_0 is the mean normal load and ΔQ defines the range of the shear load during the steady-state. Note that the extent and position of the permanent stick zone depend only on P_0, $\alpha_0(M_0, P_0)$, ΔQ, and $\Delta\sigma$, but do *not* depend on the range of the normal load and moment, ΔP and ΔM. However, the latter two affect the contact size, $[-a \quad c]$.

The final substitution $p(x) \to -1/2f[q_2^* - q_1^*](x)$ gives the change in corrective shear tractions

$$[q_2^* - q_1^*](x) = -\frac{2fE^*\phi}{\pi}\ln\left|\frac{\sqrt{1/\gamma_t} - \sqrt{(a-x)/(x+\gamma_t a)}}{\sqrt{1/\gamma_t} + \sqrt{(a-x)/(x+\gamma_t a)}}\right|, \qquad (3.77)$$

but the result is not needed to determine the permanent stick zone.

3.6 Conclusion

In this Chapter we treated the classical approach to partial slip problems, exploiting the well-known Jäger-Ciavarella theorem. That is, finding the slip stick boundary through the superposition of scaled forms of the normal traction associated with the contact under consideration. We showed that problems of different complexity can be solved using this simple principle, including mixed tangential loading problems in the presence of alternating shear forces and differential tension. We extended

these ideas to partial slip problems subject to a varying normal load and moment. Where applicable, the closed-form solutions developed have been attached to either a Hertzian problem or the geometry of a shallow wedge. A limitation to the method is encountered when the differential tension is large enough to reverse the direction of slip at one end of the contact and a new approach has to be taken, see Chapter 4

4

Partial Slip Solutions Based on Dislocations

In Chapter 3 we approached the partial slip problem starting from a shear traction distribution in full sliding and superposed a corrective traction over the sticking region to maintain the relative direct strain during load changes. The Jäger-Ciavarella principle [Jäger, 1997, Ciavarella, 1998] revealed that this corrective traction is a scaled form of the full sliding traction and we have shown that the method is applicable to a number of loading scenarios, including those with a sequential order of load application as well as those subject to periodic loading. We extended the principle to the effects of a varying normal load and *moderate* differential tension, as well as to the effects of asymmetry in the contact patch, possibly induced by an externally applied moment or an inherent asymmetry of the indenter. However, the superposition principle is by no means the only possibility of solving a partial slip problem.

In this chapter we will use strains to induce a consistent shear traction distribution instead of using a superposition of scaled forms of the full sliding shear traction. Dislocations induce strains and although the concept of dislocations is commonly used to describe crystalline defects [Weertman and Weertman, 1993, Hull and Bacon, 2011, Anderson et al., 2016], their mathematical interpretation

is equally applicable to solve problems occurring in fracture and contact mechanics, see [Hills et al., 1996]. When Comninou and Dundurs [Comninou, 1976, Dundurs, 1969] pioneered this approach, they used it for problems where the interface was surrounded by continuous material. Recently, Lopes and Hills [Lopes and Hills, 2019] extended the application of dislocation arrays to receding contact problems, where there is separation of material at infinitely remote points outside the interface, by introducing climb dislocations in those regions where the contact is open. These same ideas can be applied to half-plane problems, to solve both the normal problem through the introduction of climb dislocations [Moore and Hills, 2018] and the tangential problem using glide dislocations in regions where the contacting surfaces are moving relative to each other [Moore et al., 2018].

4.1 Mathematical Framework

In order to develop a robust mathematical framework we begin by looking at the stresses resulting from inserting a single edge dislocation at a certain point, $x-\xi$, along an interface spanning $[-a \quad c]$ similar to that illustrated in Figure 4.1, where the ξ-axis is parallel with the x-axis. The domain may be viewed either as two half-planes bonded over the interval $[-a \quad c]$ or an infinite plane with two semi-infinite cracks reaching from $-\infty$ to $-a$ and c to ∞ along the x-axis. The Burger's vector, $b_i(\xi)$ (where $i = x, y$), associated with the dislocation will cause a non-zero traction, which is given by [Moore and Hills, 2018]

$$\sigma_{iy}(x) = \frac{E^* b_i(\xi)}{2\pi(\xi - x)} \sqrt{\frac{(a+x)(c-x)}{(a+\xi)(c-\xi)}} \qquad i = x, y, \tag{4.1}$$

where E^* is the composite plane strain modulus and is explicitly given by

$$\frac{1}{E^*} = \frac{1-\nu_{\mathrm{A}}^2}{E_{\mathrm{A}}} + \frac{1-\nu_{\mathrm{B}}^2}{E_{\mathrm{B}}}\,, \tag{4.2}$$

$E_{\mathrm{A,B}}$ being Young's modulus and $\nu_{\mathrm{A,B}}$ being Poisson's ratio for the respective bodies. The effect of the two kinds of dislocations are uncoupled. A dislocation density

is then defined as [Moore and Hills, 2018]

$$B_i(\xi) = \frac{\mathrm{d}b_i}{\mathrm{d}\xi}. \tag{4.3}$$

In Chapter 2 we connected the gradient of the profile, $\mathrm{d}g/\mathrm{d}x$, to the pressure distribution using Flamant's solution resulting in an integral equation, Eq. (2.19), which can be inverted to solve for the contact pressure. Here, the dislocation array will be chosen as to mimic the profile gradient $B_y(x) = \mathrm{d}y/\mathrm{d}x$ so that the contact pressure, $p(x) = -\sigma_{yy}$, can be given as

$$p(x) = -\frac{E^*\sqrt{(c-x)(a+x)}}{2\pi}\int_{-a}^{c}\frac{B_y(\xi)\,\mathrm{d}\xi}{(\xi-x)\sqrt{(c-\xi)(a+\xi)}}\,. \tag{4.4}$$

In the case of an asymmetrical contact patch, the dislocation density needs to fulfil the following side condition [Moore and Hills, 2018]

$$\int_{-a}^{c}\frac{B_y(\xi)\,\mathrm{d}\xi}{\sqrt{(c-\xi)(a+\xi)}} = 0\,. \tag{4.5}$$

As an example, suppose now, the dislocation density $B_y(x) = -\mathrm{d}g/\mathrm{d}x = -x/R$, is such that the profile gradient for a Hertzian geometry is matched, where $1/R$ is the relative curvature of the two cylinders pressed together, and hence

$$p(x) = \frac{E^*\sqrt{a^2-x^2}}{2\pi R}\int_{-a}^{a}\frac{\xi\mathrm{d}\xi}{(\xi-x)\sqrt{a^2-\xi^2}} = \frac{E^*\sqrt{a^2-x^2}}{2R}\,. \tag{4.6}$$

In what follows we will focus on how best to solve partial slip contact problems which can be modelled using half-plane theory. The problems we look at will be for symmetrical contact interfaces subject to tangential loading under constant

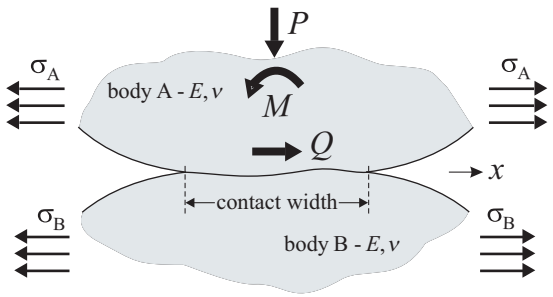


Figure 4.1: Generic half-plane contact subject to normal load, moment, shear load and differential bulk tension.

and varying normal load. While the methods presented can be modified to include the effects of a constant moment, we refrain from adding this further complication here for clarity. The effects of a varying moment, however, cannot be treated using glide dislocations[1]. and we will use an asymptotic description to tackle the problem in Chapter 5 for cases when the differential tension is large to obviate the problem encountered. Interfacial shear tensions may be excited by one of two ways - either by the action of an external shear force, Q, or by the development of differential tensions between the two bodies, $\sigma = \sigma_{\mathrm{A}} - \sigma_{\mathrm{B}}$. This new method will not only provide an alternative solution to those presented in Chapter 3 but will allow us to look also at partial slip problems for which the superposition principle reaches its limits, i.e. when the differential tension is *large* enough to reverse the direction of slip at one end of the contact.

4.2 Tangential Problem under Constant Normal Load

Let us begin by looking at the simplest loading case for an uncoupled partial slip problem, that is a symmetrical contact over the interval $[-a \quad a]$ has been formed by the application of a normal load, P, which is then held constant. The normal and tangential problem are assumed to be uncoupled, meaning neither does the normal problem induce shear tractions, nor does the size of the contact nor the normal traction distribution change upon the application of tangential loads, i.e. Dundurs' constant is set to $\beta = 0$. In any incomplete contact problem, see §1.4, the normal traction falls smoothly to zero at the edges. It follows that the edges are the first points to slip when subjected to a tangential loading.

4.2.1 The Adhered Condition

We start by modelling the contacting half-planes as a monolith over the contact area spanning $[-a \quad a]$, i.e. the interface will be fully adhered at first and no

[1] We have been unable to find the change in shear traction distribution under full stick, as will be shown in §6.2

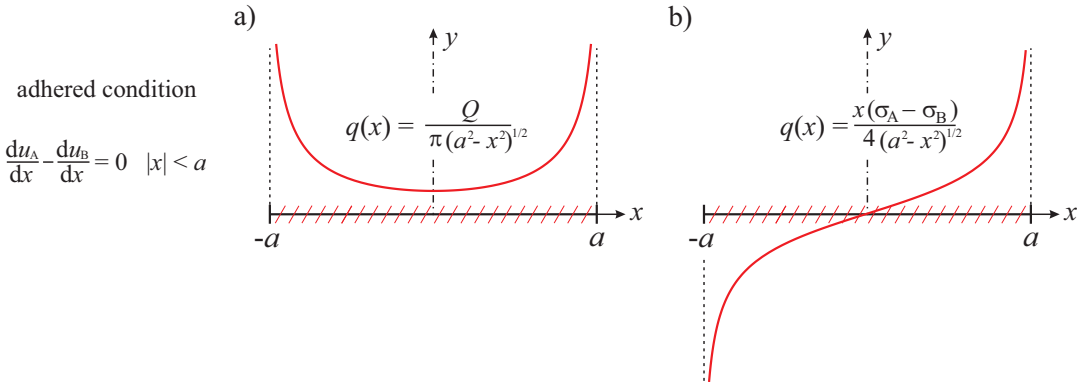


Figure 4.2: Shear tractions in the fully adhered state due to a) shear force only and b) bulk tension only.

relative motion is allowed. If the coefficient of friction, f, was indefinitely high, all slip would be prevented when a shear force, Q, was subsequently applied. Therefore, the difference in strains parallel with the surface between the two bodies will be zero, i.e. $\frac{du_A}{dx} - \frac{du_B}{dx} = 0\,, |x| < a$, and the shear traction is as shown in Figure 4.2 a). On the other hand, if unequal tensions, σ_A, σ_B, are developed in each body as shown in Figure 4.1, the shear tractions arising will be as shown in Figure 4.2 b).

We note that, if the coefficient of friction, f, were high enough to prevent all slip, the fully stuck shear traction, $q(x)$, when a shear force, Q, and a differential bulk tension, σ, are imposed, is given by

$$q(x) = \frac{Q}{\pi\sqrt{a^2 - x^2}} + \frac{x\sigma}{4\sqrt{a^2 - x^2}}\,. \tag{4.7}$$

4.2.2 The Insertion of Glide Dislocations

In Chapter 2 we derived the relationship between the relative tangential surface displacement, $u(x) = u_A - u_B$, and shear traction distribution, $q(x)$, when two half-planes are bonded over the interval $[-a, \quad a]$, see Eq. (2.18). We repeat this here for the reader's convenience

$$\frac{du}{dx} = \frac{2}{\pi E^*} \int_a^a \frac{q(\xi) d\xi}{x - \xi}\,. \tag{4.8}$$

The inversion of Eq. (4.8), when a solution for singular tractions as given in Eq. (4.7) is sought, is given by

$$q(x) = \frac{1}{\pi\sqrt{a^2 - x^2}} \left[C + \frac{E^*}{2} \int_{-a}^{a} \frac{\sqrt{a^2 - \xi^2}\, u'(\xi)\, d\xi}{\xi - x} \right] \quad |x| < a\,, \tag{4.9}$$

where $u' = \frac{\mathrm{d}u}{\mathrm{d}x}$ and C is the term associated with rigid body motion. Suppose, now, the surfaces remain fully adhered everywhere except for one point, t, where we can observe a jump in displacement, b_x, the surface displacement slope is given by

$$\frac{\mathrm{d}u}{\mathrm{d}x} = b_x\,(t)\,\delta(x-t) \quad |x| < a, \tag{4.10}$$

so that we can re-write Eq. (4.1) as

$$q(x) = \frac{E^* b_x\,(t)}{2\pi\sqrt{a^2-x^2}}\frac{\sqrt{a^2-t^2}}{t-x} \quad |x| < a\ . \tag{4.11}$$

As we intend to solve a partial slip problem, the rigid body term, C, in Eq. (4.9) vanishes. As stated earlier, for incomplete contact problems zones of slip will develop starting from the contact edge. If a distribution of glide dislocations is supposed to extend to the edges of the contact in regions where we expect slip, and that distribution is of density $B_x\,(x) = {}^{\mathrm{d}b_x}/_{\mathrm{d}x}$, we can write the shear traction induced as

$$q(x) = \frac{E^*}{2\pi\sqrt{a^2-x^2}}\int_{-a}^{a}\frac{\sqrt{a^2-\xi^2}B_x\,(\xi)\,\mathrm{d}\xi}{\xi-x} \quad |x| < a. \tag{4.12}$$

4.2.3 Solution (Constant Normal Load)

We noted earlier that the method's starting point is a fully adhered contact interface, where the coefficient of friction, f, is assumed to be infinitely high so as to inhibit all slip. The application of a tangential load will give rise to singular shear tractions, as illustrated in Figure 4.2. A partial slip problem, however, requires the coefficient of friction to be finite, enabling regions of slip to develop where the slipping shear traction distribution is of the form $q_{\mathrm{sl}}(x) = fp(x)\ \forall\ x \in$ slip zones, where $fp(x)$ is a scaled form of the normal traction. This means that by introducing a yet unknown distribution of dislocations in the slip zones, we *induce* a corrective traction, $q_{\mathrm{c}}(x)$, which balances the fully stuck shear traction distribution, $q_{\mathrm{st}}(x)$, to the desired value of $fp(x)$ in slip zones but does not alter the fully adhered condition, ${}^{\mathrm{d}u}/_{\mathrm{d}x} = 0$ in the stick region

$$q_{\mathrm{sl}}(x) = fp(x) = q_{\mathrm{c}}(x) + q_{\mathrm{st}}(x) \qquad \forall x\ \in \text{slip zones}\ . \tag{4.13}$$

We anticipate two regions of slip to ensue, one at each end of the contact, so that an output of the procedure we develop will be the position of the slip stick boundaries, denoted m and n, where $-a < -m < n < a$. Depending on the type of tangential loading, the slip zone directions will either be the same at both ends of the contact, see Figure 4.3 a), or oppose each other, see Figure 4.3 b). If the source of tangential loading is wholly applied shear or wholly applied differential tension, the slip stick boundaries will be symmetrical, i.e. $m = n$.

Inserting a distribution of glide dislocations of density $B_x(x)$ along the interface will induce a corrective strain. Note that the dislocation density is the same as the relative direct surface strain resulting in a traction, q_c. Using Eq. (4.12), we can write down the integral equation as

$$q_c(x) = \frac{E^*}{2\pi\sqrt{a^2-x^2}}\left[\int_{-a}^{-m}\frac{\sqrt{a^2-\xi^2}B_x(\xi)}{\xi-x}\mathrm{d}\xi + \int_{n}^{a}\frac{\sqrt{a^2-\xi^2}B_x(\xi)}{\xi-x}\mathrm{d}\xi\right], \quad (4.14)$$

where $x \in$ slip soznes and the dislocation density, $B_x(x)$, is the remaining unknown function. We can invert the above integral equation to find

$$B_x(x) = \pm\frac{2}{E^*\pi}\sqrt{(x-n)(x+m)}\left[-\int_{-a}^{-m}\frac{q_c(\xi)\,\mathrm{d}\xi}{\sqrt{(\xi-n)(\xi+m)}(\xi-x)} + \right.$$
$$\left. + \int_{n}^{a}\frac{q_c(\xi)\,\mathrm{d}\xi}{\sqrt{(\xi-n)(\xi+m)}(\xi-x)}\right], \quad (4.15)$$

where the upper sign must be chosen when $-a < x < -m$ and the lower sign when $n < x < a$. For details on the inversion of the integral equation please

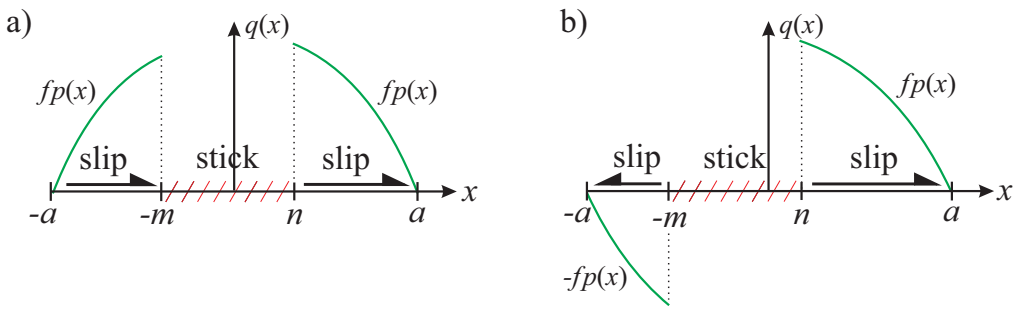


Figure 4.3: Shear tractions for; a) the moderate tension case, b) the large tension case in partial slip.

see [Moore et al., 2018]. The inversion is subject to the following two consistency conditions, effectively determining the slip stick boundaries, m and n,

$$\int_{-a}^{-m} \frac{q_{\mathrm{c}}(s)\,\mathrm{d}s}{\sqrt{(s-n)(s+m)}} - \int_{n}^{a} \frac{q_{\mathrm{c}}(s)\,\mathrm{d}s}{\sqrt{(s-n)(s+m)}} = 0\,, \tag{4.16}$$

$$\int_{-a}^{-m} \frac{q_{\mathrm{c}}(s)\ s\,\mathrm{d}s}{\sqrt{(s-n)(s+m)}} - \int_{n}^{a} \frac{q_{\mathrm{c}}(s)\ s\,\mathrm{d}s}{\sqrt{(s-n)(s+m)}} = 0\,. \tag{4.17}$$

For problems where the normal load is held constant, we can readily find the contact pressure, $p(x)$, from methods outlined in Chapter 2. For the subsequent application of a tangential load, either by a shear force or differential tension alone, or in a mixed loading condition, we know the fully stuck tractions, see Eq. (4.7). When substituted into the integrals in Eq. (4.15) the dislocation density or displacement gradient can be found and details of this are given in [Moore et al., 2018]. We are interested in the side conditions, Eqs. (4.16, 4.17), as they reveal the slip-stick boundaries, and which give [Moore et al., 2018]

$$\int_{-a}^{-m} \frac{\pm f p(s)\,\mathrm{d}s}{\sqrt{(s-n)(s+m)}} + \int_{n}^{a} \frac{\mp f p(s)\,\mathrm{d}s}{\sqrt{(s-n)(s+m)}} = \pi\frac{\sigma}{4}\,, \tag{4.18}$$

$$\int_{-a}^{-m} \frac{\pm f p(s)\ s\,\mathrm{d}s}{\sqrt{(s-n)(s+m)}} + \int_{n}^{a} \frac{\mp f p(s)\ s\,\mathrm{d}s}{\sqrt{(s-n)(s+m)}} = \pi\frac{\sigma(n-m)}{8} - Q\,. \tag{4.19}$$

4.2.4 Shear Force Only

Very commonly, a solution to a mixed form of tangential loading is desired. However, in the absence of any bulk tension, we can make a number of simplifications. One simplifying property is that the slip zones at either end of the contact will be of the same size and the direction of slip is the same and we can state $n = m$. The fully adhered traction due to the application of a shear force only is given by, see Eq. (4.7)

$$q_{\mathrm{st}}(x) = \frac{Q}{\pi\sqrt{a^2 - x^2}} \qquad |x| \le a\,. \tag{4.20}$$

The slip displacements are an even function of x so that the dislocation density is odd, and therefore $B_x(x) = -B_x(-x)$, giving [Moore et al., 2018]

$$B_x(x) = \frac{4f}{E^*\pi}\sqrt{x^2 - n^2}\int_{n}^{a} \frac{\xi p(\xi)\,\mathrm{d}\xi}{\sqrt{\xi^2 - n^2}(\xi^2 - x^2)}\,, \tag{4.21}$$

and the first side condition, Eq. (4.18) is automatically satisfied, while the remaining side condition may be written as

$$\int_n^a \frac{p\,(s)\;s\,\mathrm{d}s}{\sqrt{s^2-n^2}} = \frac{Q}{2f}\;\;. \tag{4.22}$$

4.2.5 Differential Tension Only

Now, we turn to the effects of a differential tension only, as this is a case that cannot be treated using superposition of slipping traction distributions. Similarly to the example above, we can make a few simplifications in the absence of a shear force. The slip zone sizes will be symmetrical about the centre-axis of the contact, i.e. $n = m$, and the slipping traction will be of opposite sign at either end of the contact, giving the corrective traction as

$$q_{\mathrm{c}}(x) = \mathrm{sgn}(x) f p(x) - \frac{x\sigma}{4\sqrt{a^2-x^2}} \qquad n \le |x| \le a\;. \tag{4.23}$$

The slip displacements are an odd function of x so that the dislocation density is even, and therefore $B_x(x) = B_x(-x)$, giving [Moore et al., 2018]

$$B_x(x) = \frac{4f}{E^*\pi}\sqrt{x^2-n^2}\int_n^a \frac{x p(\xi)\,\mathrm{d}\xi}{\sqrt{\xi^2-n^2}(\xi^2-x^2)}\;. \tag{4.24}$$

Opposite to the shear force case, the first side condition, Eq. (4.18), is no longer automatically satisfied, giving

$$\int_n^a \frac{p\,(s)\;\mathrm{d}s}{\sqrt{(s^2-n^2}} = \frac{\sigma\pi}{8f}\;\;, \tag{4.25}$$

while the second side condition, Eq. (4.19), is now automatically satisfied.

4.3 Cyclic Loading (Constant Normal Load)

In most practical problems the loads at the contact are excited by a solitary varying remote force which does not change orientation. This means that there is no phase shift between the loads excited at the contact, and a commonly arising problem is when the normal force, P, is held constant and the shear force oscillates

between two values (Q_1, Q_2), and, at the same time, the bulk tension fluctuates between two values (σ_1, σ_2), Figure 4.4.

Although problems of this kind can be solved by marching-in-time type methods it is very helpful for the user of these results if the solution can be obtained quickly and in as near closed-form as possible. In §3.3.1 we demonstrated a very simple solution to the problem posed, and where the solution is appropriate when only a shear force is applied or the applied tension is moderate, so that the slip zones at each edge of the contact are of the same sign. The solution, which was originally developed in [Andresen et al., 2019a], is a variant of the Jäger-Ciavarella principle, developed further by Barber et al [Barber et al., 2011], in which the fundamental form of the shear traction distribution is taken as the sum of a sliding shear traction together with a corrective term applied over the stick region $[-m \quad n]$, where $m, n > 0$, to restore stick there, Figure 4.1. This method has stood the test of time well but it is extremely difficult to adapt it to problems where the slip zones are of opposite sign, at any rate in a way which can be solved in closed-form.

The object here, and what was originally treated in [Andresen et al., 2020c], is to extend the solutions in [Andresen et al., 2019a] to those for a steady-state response, and in particular to the case where the bulk tension may be large. At the same time the normal load will be kept constant as this permits the integral equations to be developed in a particularly simple form.

As before, we start from a fully adhered condition. Note that we now look at a cyclic problem so that the change in shear traction, $\Delta q(x)$, when a change in

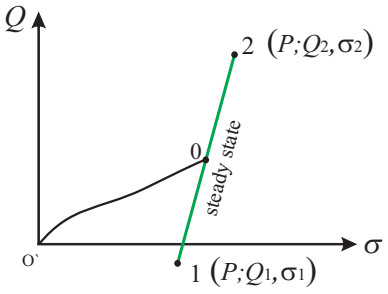


Figure 4.4: The steady-state cycle in σ-Q-space under a constant normal load P.

shear force, ΔQ, and change in bulk tension, $\Delta\sigma$, are imposed, when moving from load state 1 to load state 2, Figure 4.4, is given by

$$\Delta q(x) = \frac{\Delta Q}{\pi\sqrt{a^2 - x^2}} + \frac{x\Delta\sigma}{4\sqrt{a^2 - x^2}}. \tag{4.26}$$

In this problem the change in shear load is

$$\Delta Q = Q_2 - Q_1, \tag{4.27}$$

and change in bulk tension is

$$\Delta\sigma = \sigma_2 - \sigma_1, \tag{4.28}$$

where σ_1 and σ_2 represent the difference in bulk tension[2] between the two bodies at the ends of the load cycle, respectively. If both ΔQ and $\Delta\sigma$, are positive, we see that at the right hand edge of the contact their effects will sum (as $x \to a^-$) whilst at the left hand edge (as $x \to -a^+$) their effects tend to cancel, see Figure 4.2.

Suppose we are near load state 1 and the increment of loading has changed sign and is now increasing, locking in $q_1^+(x)$. As we approach point 2 the shear traction is now given by

$$\begin{aligned} q_2^-(x) = q_1^+(x) + \frac{\Delta Q}{\pi\sqrt{a^2 - x^2}} + \frac{x\Delta\sigma}{4\sqrt{a^2 - x^2}} + \\ \frac{E^*}{2\pi\sqrt{a^2 - x^2}} \left[\int_{-a}^{-m} \frac{\sqrt{a^2 - \xi^2} B_x^L(\xi)}{\xi - x} \mathrm{d}\xi + \int_n^a \frac{\sqrt{a^2 - \xi^2} B_x^L(\xi)}{\xi - x} \mathrm{d}\xi \right], \end{aligned} \tag{4.29}$$

where $x \in (-a, a)$ and $B_x^L(x)$ is the density of dislocations arising during the loading phase. When we 'move around the corner' at point 2 this shear traction, in turn, becomes locked-in and as we approach point 1 we can write

$$\begin{aligned} q_1^-(x) = q_2^+(x) - \frac{\Delta Q}{\pi\sqrt{a^2 - x^2}} - \frac{x\Delta\sigma}{4\sqrt{a^2 - x^2}} + \\ \frac{E^*}{2\pi\sqrt{a^2 - x^2}} \left[\int_{-a}^{-m} \frac{\sqrt{a^2 - \xi^2} B_x^U(\xi)}{\xi - x} \mathrm{d}\xi + \int_n^a \frac{\sqrt{a^2 - \xi^2} B_x^U(\xi)}{\xi - x} \mathrm{d}\xi \right], \end{aligned} \tag{4.30}$$

where $x \in (-a, a)$ and $B_x^U(x)$ is the density of dislocations arising during the unloading phase. In each equation, the glide dislocation distributions over the slip

[2] In general, bulk stresses may arise in each body. When this is the case, providing they are synchronous, we define $\sigma_i = \sigma_{\mathrm{A},i} - \sigma_{\mathrm{B},i}$. for $i = 1, 2$ representing two load points in the steady-state (see Figure 4.4).

intervals physically represent the slip displacements there, and the shear tractions vanish outside the intervals stated.

If we subtract integral (4.30) from integral (4.29) we arrive at the following integral

$$q_2^-(x) - q_1^-(x) = q_1^+(x) - q_2^+(x) + \frac{2\Delta Q}{\pi\sqrt{a^2-x^2}} + \frac{2x\Delta\sigma}{4\sqrt{a^2-x^2}} + \frac{E^*}{2\pi\sqrt{a^2-x^2}}\left[\int_{-a}^{-m}\frac{\sqrt{a^2-\xi^2}B_x^L(\xi)}{\xi-x}\mathrm{d}\xi + \int_n^a \frac{\sqrt{a^2-\xi^2}B_x^L(\xi)}{\xi-x}\mathrm{d}\xi - \int_{-a}^{-m}\frac{\sqrt{a^2-\xi^2}B_x^U(\xi)}{\xi-x}\mathrm{d}\xi - \int_n^a \frac{\sqrt{a^2-\xi^2}B_x^U(\xi)}{\xi-x}\mathrm{d}\xi\right], \quad (4.31)$$

where $x \in (-a, a)$. We know that, in the slip regions, the shear tractions are equal to their limiting value, i.e.

$$q_2^-(x) = q_2^+(x) = fp(x)\,\mathrm{sgn}(x) \quad -a \le x \le -m \quad \text{and} \quad n \le x \le a \quad (4.32)$$

and

$$q_1^-(x) = q_1^+(x) = -fp(x)\,\mathrm{sgn}(x) \quad -a \le x \le -m \quad \text{and} \quad n \le x \le a, \quad (4.33)$$

where we should *omit* the sgn(•) functions when we are considering the moderate tension case, Figure 4.3 a), and *include* them when we are considering the large tension case, Figure 4.3 b). We have already used the principle of conservation of material in assuming that the maximum extent of slip penetration in the steady-state loading cycle is the same at points $1^-, 2^-$, but we can also say that the change in the slip displacement of all opposing particles within the slip zones during the loading and unloading phases is equal in magnitude and opposite in sign. For example, in the right-hand slip region we see that the slip displacement at point x, $u^L(x)$, during loading is given by

$$u^L(x) = \int_n^x B_x^L(\xi)\,d\xi \qquad n < x < a. \quad (4.34)$$

We know that during unloading we will recover the slip displacement, i.e. $u^L(x) + u^U(x) = 0$ within the slip zones. Hence, we infer that

$$B_x^U(x) = -B_x^L(x) \qquad -a \le x \le -m \qquad \text{and} \qquad n \le x \le a. \quad (4.35)$$

If we make use of these results and restate Eq. (4.31) for the slip zones only, we arrive at the following integral equation, in terms of the dislocation density $B_x^L(x)$

$$\begin{aligned} 2fp(x)\,\mathrm{sgn}(x) - \left(\frac{\Delta Q}{\pi\sqrt{a^2-x^2}} + \frac{x\Delta\sigma}{4\sqrt{a^2-x^2}}\right) = \\ = \frac{E^*}{2\pi\sqrt{a^2-x^2}}\left[\int_{-a}^{-m}\frac{\sqrt{a^2-\xi^2}B_x^L(\xi)}{\xi-x}\mathrm{d}\xi + \int_n^a \frac{\sqrt{a^2-\xi^2}B_x^L(\xi)}{\xi-x}\mathrm{d}\xi\right], \end{aligned} \tag{4.36}$$

where $x \in (-a,-m)\cup(n,a)$.

The formulation works equally well with the same or opposite signs of slip, so we start by making some progress towards a general solution. We note that the left-hand side of Eq. (4.36) may be interpreted as the difference between the fully stuck and slipping shear traction distributions within the slip region, which we will denote by $q_{\mathrm{c}}(x)$, and hence we may write

$$\begin{aligned} q_{\mathrm{c}}(x) = -\frac{\Delta Q}{\pi\sqrt{a^2-x^2}} - \frac{\Delta\sigma x}{4\sqrt{a^2-x^2}} + 2fp(x)\,\mathrm{sgn}(x) = \\ = \frac{E^*}{2\pi\sqrt{a^2-x^2}}\left[\int_{-a}^{-m}\frac{\sqrt{a^2-\xi^2}B_x^L(\xi)}{\xi-x}\,\mathrm{d}\xi + \int_n^a \frac{\sqrt{a^2-\xi^2}B_x^L(\xi)}{\xi-x}\,\mathrm{d}\xi\right], \end{aligned} \tag{4.37}$$

where $x \in (-a,-m)\cup(n,a)$. A bounded-both-ends solution for Eq. (4.37) is sought, and inverting this equation in the standard way leads to the two consistency conditions [Moore et al., 2018]

$$0 = \int_{-a}^{-m}\frac{q_{\mathrm{c}}(\xi)\xi^k}{\sqrt{(\xi-n)(\xi+m)}}\,\mathrm{d}\xi - \int_n^a \frac{q_{\mathrm{c}}(\xi)\xi^k}{\sqrt{(\xi-n)(\xi+m)}}\,\mathrm{d}\xi, \tag{4.38}$$

where $k = 0, 1$. Making use of the knowledge that [Andresen et al., 2020c]

$$\begin{aligned} \int_{-a}^{-m}\frac{\xi^k}{\sqrt{a^2-\xi^2}\sqrt{(\xi-n)(\xi+m)}}\,\mathrm{d}\xi - \int_n^a \frac{\xi^k}{\sqrt{a^2-\xi^2}\sqrt{(\xi-n)(\xi+m)}}\,\mathrm{d}\xi = \\ = \begin{cases} 0 & \text{for } k=0\,, \\ -\pi & \text{for } k=1\,, \\ \dfrac{(m-n)\pi}{2} & \text{for } k=2\,, \end{cases} \end{aligned} \tag{4.39}$$

we can reduce the consistency conditions to the following pair of equations for m, n

$$\frac{\Delta\sigma\pi}{8} = -\int_{-a}^{-m}\frac{fp(\xi)\,\mathrm{sgn}(\xi)\,\mathrm{d}\xi}{\sqrt{(\xi-n)(\xi+m)}} + \int_n^a \frac{fp(\xi)\,\mathrm{sgn}(\xi)\,\mathrm{d}\xi}{\sqrt{(\xi-n)(\xi+m)}}, \tag{4.40}$$

$$\frac{\Delta Q}{2} + \frac{(n-m)\Delta\sigma\pi}{16} = -\int_{-a}^{-m}\frac{\xi fp(\xi)\,\mathrm{sgn}(\xi)\,\mathrm{d}\xi}{\sqrt{(\xi-n)(\xi+m)}} + \int_n^a \frac{\xi fp(\xi)\,\mathrm{sgn}(\xi)\,\mathrm{d}\xi}{\sqrt{(\xi-n)(\xi+m)}}. \tag{4.41}$$

The left-hand side of Eq. (4.40) is constant and independent of the contact geometry. The right-hand side is specific to the geometry and applies whether moderate or large tension is being considered, i.e sgn (•) is *included* or *omitted*. Similarly, the left-hand side of Eq. (4.41) is geometry-independent, whereas the right-hand side is geometry and tension case-dependent.

4.4 Application to a Hertzian Geometry

The motivation behind this example section is to illustrate the application of the method developed for the steady-state problem outlined in §4.3. We will recover the results for the case of *moderate* differential tension, which were first acquired using the Jäger-Ciavarella principle [Andresen et al., 2019b]. Once we have observed agreement, we go on to look at the case of *large* differential tension and how to obtain a solution in closed-form. An illustration of both branches of the steady-state solution will display the transition between *moderate* and *large* tension.

4.4.1 Moderate Differential Bulk Tension

We start by re-evaluating the 'moderate tension' case, for which a solution already exists based on the Jäger-Ciavarella principle [Andresen et al., 2019a]. As the slip direction will be the same at both ends of the contact, Figure 4.3 (a), the sgn (•) function is *omitted* from equations (4.40) and (4.41). Consider a Hertzian contact, where the pressure distribution is semi-elliptical in form, and may be written as

$$p(x) = \frac{E^*}{2R}\sqrt{a^2 - x^2}, \qquad |x| \leq a. \tag{4.42}$$

So, by making use of the following standard results [Moore et al., 2018]

$$\begin{aligned} &\int_{-a}^{-m} \frac{\xi^k\sqrt{a^2-\xi^2}}{\sqrt{(\xi-n)(\xi+m)}}\,\mathrm{d}\xi - \int_{n}^{m} \frac{\xi^k\sqrt{a^2-\xi^2}}{\sqrt{(\xi-n)(\xi+m)}}\,\mathrm{d}\xi \\ &= \begin{cases} \dfrac{(n-m)\pi}{2} & \text{for } k=0\ , \\ \left(\dfrac{(n-m)^2}{4} + \dfrac{(n+m)^2}{8} - \dfrac{a^2}{2}\right)\pi & \text{for } k=1\ . \end{cases} \end{aligned} \tag{4.43}$$

the first consistency condition, Eq. (4.40), provides the result that

$$\frac{(n-m)}{2} = -\frac{R\Delta\sigma}{4E^* f}, \tag{4.44}$$

and after a little manipulation, the second consistency condition, Eq. (4.41), gives

$$\left(\frac{(n+m)}{2}\right)^2 = a^2 - \frac{2R\Delta \mathrm{Q}}{\pi E^* f}. \tag{4.45}$$

These are the same results as those obtained by [Andresen et al., 2019a]. Provided ΔQ and $\Delta\sigma$ are positive, the same sign slip direction is maintained as long as the change in bulk stress satisfies

$$\Delta\sigma \leq \frac{4E^* f}{R}\left(a - \sqrt{a^2 - \frac{2R\Delta \mathrm{Q}}{\pi E^* f}}\right) = \Delta\sigma_{\text{threshold}} \ . \tag{4.46}$$

4.4.2 Large Differential Bulk Tension

Suppose now, that the change in tension is large enough for inequality (4.46) to be violated so that the slip directions are of opposite sign as shown in Figure 4.3(b). The sgn (•) function is therefore now *included* in equations (4.40) and (4.41). In a Hertzian example, where Eq. (4.42) again applies, we use the following results to evaluate the consistency conditions [Moore et al., 2018]

$$\begin{aligned}\int_{-a}^{-m} \frac{s^{j-1}\sqrt{a^2-s^2}}{\sqrt{(s-n)(s+m)}}\,\mathrm{d}s + \int_{n}^{a} \frac{s^{j-1}\sqrt{a^2-s^2}}{\sqrt{(s-n)(s+m)}}\,\mathrm{d}s = \\ = \alpha_j \mathrm{E}(\chi) + \beta_j \mathrm{K}(\chi) + \gamma_j \Pi\left(\frac{m-a}{m+a}, \chi\right) + \delta_j \Pi\left(\frac{a-n}{a+m}, \chi\right),\end{aligned} \tag{4.47}$$

for $j = 1, 2$ and where $\mathrm{K}(\chi)$, $\mathrm{E}(\chi)$, and $\Pi(t, \chi)$ are complete elliptic integrals of the first[3], second and third kind, and

$$\alpha_1 = -2\sqrt{(a+m)(a+n)}, \quad \alpha_2 = \frac{3(m-n)}{2}\sqrt{(a+m)(a+n)},$$
$$\beta_1 = (n-m+4a)\sqrt{\frac{a+m}{a+n}}, \quad \beta_2 = \frac{-3}{2}\sqrt{\frac{a+m}{a+n}}\left(\left(\frac{n}{3}+2a\right)m - \frac{m^2+n^2}{2} - \frac{2a}{3}(a+n)\right),$$
$$\gamma_1 = \frac{2a(n-m)}{\sqrt{(a+m)(a+n)}}, \qquad \gamma_2 = \frac{3a}{2\sqrt{(a+m)(a+n)}}\left(n^2 - \frac{2mn}{3} + m^2 - \frac{4a^2}{3}\right),$$
$$\delta_1 = \frac{m^2-n^2}{\sqrt{(a+m)(a+n)}}, \qquad \delta_2 = \frac{-3(m+n)}{4\sqrt{(a+m)(a+n)}}\left(n^2 - \frac{2mn}{3} + m^2 - \frac{4a^2}{3}\right), \text{ and}$$
$$\chi = \frac{\sqrt{(a^2-m^2)(a^2-n^2)}}{(a+m)(a+n)}\,.$$

Therefore, m and n must satisfy the following non-linear equations

$$\frac{\Delta\sigma\pi}{8} = \frac{fE^*}{2R}\left[\alpha_1\mathrm{E}(\chi) + \beta_1\mathrm{K}(\chi) + \gamma_1\Pi(\phi,\chi) + \delta_1\Pi(\omega,\chi)\right]\,, \tag{4.48}$$

$$\frac{\Delta Q}{2} + \frac{(n-m)\Delta\sigma\pi}{16} = \frac{fE^*}{2R}\left[\alpha_2\mathrm{E}(\chi) + \beta_2\mathrm{K}(\chi) + \gamma_2\Pi(\phi,\chi) + \delta_2\Pi(\omega,\chi)\right]\,, \tag{4.49}$$

where $\phi = \frac{m-a}{m+a}$ and $\omega = \frac{a-n}{a+m}$. Eqs. (4.48) and (4.49) are sufficient to define the size of the stick zone for given numerical values of ΔQ and $\Delta\sigma$.

4.4.3 Display of Example Problem Results

The results presented in the above sections show that the solution behaviour of a Hertzian contact is fundamentally different for moderate and large tension. In the case of moderate tension, we arrive at a set of two uncoupled explicit equations, Eqs. (4.44, 4.45). This is a unique result as the former equation determines the position while the latter equation determines the extent of the permanent stick zone. In terms of tangential load, the *extent* of the permanent stick zone is solely dependent on the change in shear force, ΔQ. Its *position*, or eccentricity, on the other hand, is solely dependent on the change in bulk stress, $\Delta\sigma$. In the case of

[3]The elliptic integral of the first kind is sometimes defined in terms of $\psi = \chi^2$ rather than χ. For example, the algebraic manipulator Mathematica uses this alternative notation and caution needs to be exercised when implementing the solution [Barber, 2018].

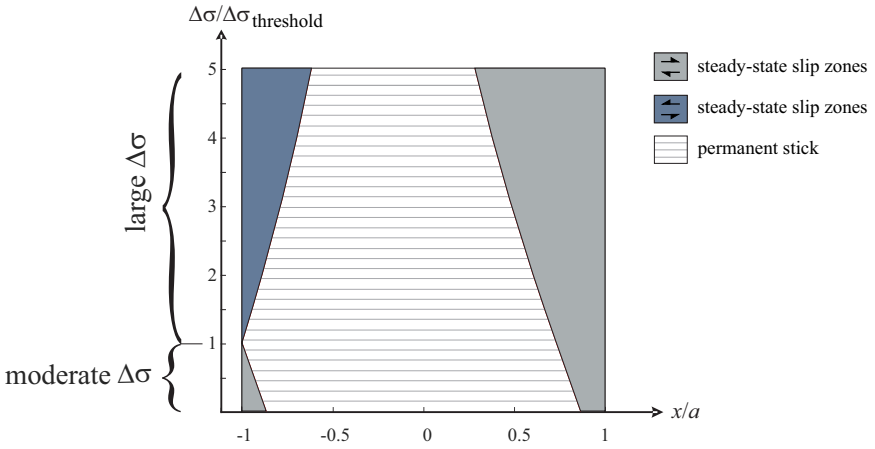


Figure 4.5: Steady-state solutions of maximum slip and permanent stick zone extents for different values of a change in bulk stress, $\Delta\sigma$.

large tension, the two consistency conditions, Eqs. (4.48, 4.49), are non-linearly coupled, and they must be treated numerically in order to determine the extent and position of the permanent stick zone.

Figure 4.5 displays *steady-state* solutions, i.e. the permanent stick zone and maximum extent of the slip zones, for a Hertzian geometry. The contact is subject to a constant normal load, P. The shear load fluctuation, ΔQ, is also kept constant. The permanent stick zone, spanning $[-m \quad n]$, is then given for different values of $\Delta\sigma\, a/\Delta Q$. Here, we distinguish between the moderate and large tension case. We see that, as the change in bulk stress is increased, the extent of the permanent stick zone is indeed constant and its position shifts linearly towards the left-hand contact edge and the direction of slip is the same at both ends of the contact. When the change in bulk stress is high enough so that inequality (4.46) is violated, the other branch of the solution becomes valid. From this point onwards the behaviour of the solution is non-linear. The extent and position of the permanent stick zone are coupled and the directions of slip oppose at either end of the contact.

4.5 Cyclic Loading (Varying Normal Load)

Here, we extend the dislocation method developed above to cases where the normal load is also varying with time, and in doing so a number of extra principles will be adduced. We will assume that the contact is symmetrical, and this precludes the

inclusion of an applied moment. Problems including a (varying) moment can be treated exactly under conditions of *moderate* tension, see Chapter 3, and will be treated using an asymptotic approach for the case of *large* tension in Chapter 5.

4.5.1 Contact under Full Stick

It is essential for the solution to know the tractions locked in as the contact is formed, under conditions of full stick, and the ideas of Mossakovskii, as developed by Barber [Barber, 2010, Hills et al., 2011], are used. If the current contact half-width is a, the change in contact pressure, $\Delta p(x)$, when a small change in normal load, ΔP, is applied, which imposes a constant normal displacement over the interval $[-a \quad a]$, is given by

$$\Delta p(x) = \frac{\Delta P}{\pi\sqrt{a^2 - x^2}} \, . \tag{4.50}$$

The change in shear traction, $\Delta q(x)$, when, simultaneously, a change in shear force, ΔQ, and a change in bulk tension, $\Delta\sigma$, are imposed, when there is a constant tangential displacement over the same interval, is given by §2.6

$$\Delta q(x) = \frac{\Delta Q}{\pi\sqrt{a^2 - x^2}} + \frac{x\Delta\sigma}{4\sqrt{a^2 - x^2}} \, . \tag{4.51}$$

So, first we see that if full stick is to be maintained during a positive load increment the minimum coefficient of friction, f, needed is given by

$$\frac{|\Delta Q|}{\Delta P} + \frac{\pi}{4}\frac{a\,|\Delta\sigma|}{\Delta P} < f \, . \tag{4.52}$$

Secondly, we wish to find the change in interfacial shear traction moving linearly from state 1$[P_1, Q_1, \sigma_1]$ to state 2 $[P_2, Q_2, \sigma_2]$, $(P_2 > P_1)$, Figure 4.6, when this

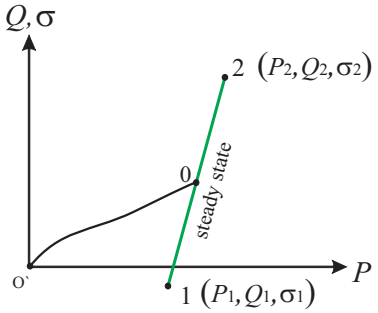


Figure 4.6: Two-dimensional illustration of a P-Q-σ load space.

inequality is satisfied. The change in normal pressure, $\Delta p(x)$, moving from state $1 \rightarrow 2$ is given by (notation introduced in [Barber et al., 2011]) $p(x, P_i)$

$$\Delta p(x) = p(x, P_2) - p(x, P_1) \; . \tag{4.53}$$

The overall change in contact pressure could be found by considering a sequence of punches each producing the pressure change given by Eq. (4.50)

$$\Delta p(x) = \frac{1}{\pi} \int_{P_1}^{P_2} \frac{\mathrm{d}P}{\sqrt{a^2 - x^2}} \; , \tag{4.54}$$

and denoting the contact law by $a = g(P)$, i.e.

$$\frac{\mathrm{d}a}{\mathrm{d}P} = g^{'}(P) \; , \tag{4.55}$$

we see that

$$\Delta p(x) = \frac{1}{\pi} \int_{a_1}^{a_2} \frac{1}{g^{'}(P)} \frac{\mathrm{d}a}{\sqrt{a^2 - x^2}} \; . \tag{4.56}$$

The shear traction locked-in may be found from the Green's functions just introduced. We assume that the changes in shear force and tension vary linearly over the steps $1 \rightarrow 2$ and $2 \rightarrow 1$ so that

$$\frac{\Delta Q}{\Delta P} = \lambda = \frac{Q_2 - Q_1}{P_2 - P_1} \; , \tag{4.57}$$

and

$$\frac{\Delta \sigma}{\Delta P} = \frac{2\eta}{(a_2 + a_1)} \; , \tag{4.58}$$

where

$$\eta = \frac{(a_2 + a_1)\,(\sigma_2 - \sigma_1)}{2\,(P_2 - P_1)} \; . \tag{4.59}$$

Therefore the incremental change in shear traction is given by

$$\Delta q(x) = \frac{\lambda \Delta P}{\pi \sqrt{a^2 - x^2}} + \frac{x \eta \Delta P}{2\,(a_2 + a_1)\sqrt{a^2 - x^2}} \; , \tag{4.60}$$

and hence the finite shear loading change may be found by a sequence analogous to that represented by Eqs. (4.54, 4.56), and we see that

$$q_2(x) - q_1(x) = [p(x, P_2) - p(x, P_1)] \left[\lambda + \frac{\eta x \pi}{2\,(a_2 + a_1)} \right] \; . \tag{4.61}$$

4.5.2 Partial Slip Problem

A distribution of glide dislocations, of density $B_x(x)$, present over an interval $[-h \quad k]$ will give rise to a shear traction distribution, $q(x)$, given by [Moore et al., 2018]

$$q(x) = \frac{E^*}{2\pi\sqrt{a^2 - x^2}} \int_{-h}^{k} \frac{\sqrt{a^2 - \xi^2} B_x(\xi)}{\xi - x} \mathrm{d}\xi \, . \tag{4.62}$$

Without loss of generality we assume that $P_2 > P_1$, and hence $a_2 > a_1$, and we wish to find the steady-state solution. In particular, we wish to find the extent of the steady-state or 'permanent' stick zone, which spans the interval $[-m \quad n]$ because, when once that is known the slip displacements and other important quantities may be easily found.

Suppose that we are in the steady-state and have unloaded the contact ($P_2 \to P_1$) and reached load state 1, Figure 4.6. The changes in load are now reversed and, as the increments in slip displacement have changed sign, full stick ensues, locking in $q_1(x)$. Because the normal and shear forces are changing in proportion to each other we expect to find a bounded change in shear traction, and as we approach point 2 the shear traction is now given by

$$\begin{aligned} q_2(x) =& q_1(x) + [p(x, P_2) - p(x, P_1)] \left[\lambda + \frac{\eta x \pi}{2(a_2 + a_1)} \right] + \\ & \frac{E^*}{2\pi\sqrt{a_2^2 - x^2}} \left[\int_{-a_2}^{-m} \frac{\sqrt{a_2^2 - \xi^2} B_x^L(\xi)}{\xi - x} \mathrm{d}\xi + \int_{n}^{a_2} \frac{\sqrt{a_2^2 - \xi^2} B_x^L(\xi)}{\xi - x} \mathrm{d}\xi \right] , \end{aligned} \tag{4.63}$$

where $-a_2 < x < a_2$ and $B_x^L(x)$ is the density of dislocations to be distributed over the slip regions during this loading phase. When we attain the maximum load at point 2, and start to move back towards point 1 full stick again ensues (Figure 4.6) and, in turn, this shear traction becomes locked-in. As we approach point 1 we can write

$$\begin{aligned} q_1(x) =& q_2(x) - [p(x, P_2) - p(x, P_1)] \left[\lambda + \frac{\eta x \pi}{2(a_2 + a_1)} \right] + \\ & \frac{E^*}{2\pi\sqrt{a_1^2 - x^2}} \left[\int_{-a_2}^{-m} \frac{\sqrt{a_1^2 - \xi^2} B_x^U(\xi)}{\xi - x} \mathrm{d}\xi + \int_{n}^{a_2} \frac{\sqrt{a_1^2 - \xi^2} B_x^U(\xi)}{\xi - x} \mathrm{d}\xi \right] , \end{aligned} \tag{4.64}$$

where $-a_2 < x < a_2$ and $B_x^U(x)$ is the *change* in density of dislocations to be distributed over the slip regions during this unloading phase. The glide dislocation distributions over the slip intervals physically represent the slip displacements there, and the shear tractions ratio remains constant outside the intervals stated.

We know that, in the slip regions, the shear tractions are equal to their limiting value, i.e.

$$q_1(x) = fp(x, P_1)\,\mathrm{sgn}(x) \qquad -a_1 \le x \le -m \qquad n \le x \le a_1 \tag{4.65}$$

where the $sgn\,(\bullet)$ is omitted where the slip zones are of the same sign and included when they are of opposite sign. The shear stress vanishes when $a_1 < |x|$. Also

$$q_2(x) = -fp(x, P_1)\,\mathrm{sgn}(x) \qquad -a_2 \le x \le -m \qquad n \le x \le a_2\ , \tag{4.66}$$

and again the $\mathrm{sgn}\,(\bullet)$ is omitted where the slip zones are of the same sign and included when they are of opposite sign. Again, the shear stress vanishes when $a_2 < |x|$. We have used the principle of conservation of material already when we assert that the maximum extent of slip penetration is the same at points $1^-, 2^-$, i.e. that the end points of the stick zone $[-m \quad n]$ are the same at each end of the loading cycle. But, we can also say that the change in the slip displacement of all particles within any part of the contact which slips during the loading and unloading phases is equal and opposite. For example, in the right hand slip region we see that the slip displacement at point x, $u(x)$, during unloading is given by

$$u(x) = \int_n^x B_x^U\,(\xi)\,\mathrm{d}\xi \qquad n < x < a_2\ , \tag{4.67}$$

and points must return to their original positions after a loading cycle, so that

$$B_x^U(x) = -B_x^L(x) \qquad -a_2 \le x \le -m \qquad \text{and} \qquad n \le x \le a_2\ . \tag{4.68}$$

Physically, in the intervals $[-a_1 < x < -m]$ and $[n < x < a_1]$, $u(x)$ represents the slip displacement while in the ranges $[-a_2 < x < a_1]$ and $[a_1 < x < a_2]$ it continues to represent the tangential displacement of particles, this time in the region which separates but, in any event, during the sequence $1 \to 2 \to 1$ all surface particles must return to their same positions.

4.5.3 Solution

We may therefore write, as *either* end 2 or end 1 of the load range is approached

$$p(x,P_2)\left[f\,\mathrm{sgn}(x)+\lambda+\frac{\eta x\pi}{2\,(a_2+a_1)}\right]+p(x,P_1)\left[f\,\mathrm{sgn}(x)-\lambda-\frac{\eta x\pi}{2\,(a_2+a_1)}\right]=$$
$$\frac{E^*}{2\pi\sqrt{a_2^2-x^2}}\left[\int_{-a_2}^{-m}\frac{\sqrt{a_2^2-\xi^2}B_x^L\,(\xi)}{\xi-x}\mathrm{d}\xi+\int_n^{a_2}\frac{\sqrt{a_2^2-\xi^2}B_x^L\,(\xi)}{\xi-x}\mathrm{d}\xi\right]$$
$$-a_2<x<-m\qquad\text{and}\qquad n\le x\le a_2. \tag{4.69}$$

This is a singular integral equation over the intervals $[-a_1 \quad -m]$ and $[n \qquad a_1]$. The left-hand side consists of terms which are the contact pressure distributions together with products of those distributions and x. Input parameters are: the contact geometry implying the contact law, and contact pressure distributions $a(P), p(x,P)$, the coefficient of friction, f, and gradients of the trajectory in load space, λ, η, together with the range of normal load $[P_1, P_2]$. The output variables are the size of the permanent stick zone, $-m, n$, together with the slip dislocation density $B_x^L(x)$.

Although the primary unknown quantity in Eq. (4.69) is the dislocation density and, indeed, this is needed if the slip displacements are to be found, there are side conditions on it which must be enforced and it is these which reveal the extent of the permanent stick zone.

A bounded-both-ends solution for Eq. (4.69) is sought, and inverting this equation in the standard way leads to the two consistency conditions

$$0=\int_{-a_1}^{-m}\frac{q_c(\xi)\xi^k}{\sqrt{(\xi-n)(\xi+m)}}\,\mathrm{d}\xi-\int_n^{a_1}\frac{q_c(\xi)\xi^k}{\sqrt{(\xi-n)(\xi+m)}}\,\mathrm{d}\xi\,, \tag{4.70}$$

where $k=0,1$. The corrective traction, $q_c(x)$, is given by the left-hand side of Eq. (4.69) which depends on terms associated with the normal tractions, $p(x,P_1)$ and $p(x,P_2)$, both scaled by the coefficient of friction, f, and parameters describing the steady-state loading, λ and η. The concepts given have not been attached to a particular geometry as a numerical implementation of Eq. (4.70) is the only way forward.

4.6 Conclusion

On one hand it was the ambition behind employing the concept of dislocations to demonstrate a different approach to solving partial slip problems compared to the well-known superposition of full sliding tractions, see Chapter 3. On the other hand it was also the aim to find a solution in loading scenarios involving *large* differential tension. This has been successful for problems subject to constant and varying normal load. We have been unsuccessful to apply the procedure to problems which involve a varying moment and this will make an asymptotic description not only a useful alternative, but also a necessity to tackle the whole range of possible loading scenarios occurring in reality.

5

Asymptotic Solutions for Frictional Half-Plane Contacts

In Chapters (2, 3, 4) we analysed *finite* contacts using various methods, all of which rendered a mathematically exact description of the contact problem within half-plane elasticity. For many of the problems considered we were able to obtain closed-form solutions. While some of the solutions are quite elegant and easy-to-apply, see §3.5.2 and §4.4.1, one thing they have in common is their dependence on a finite contact and a large number of geometry and loading-dependent parameters. These all influence the solution we seek, i.e. the size of slip zones during the steady-state. The case-specific information gained from this rigorous type of contact analysis can be used to match very accurately the partial slip behaviour between a prototype and an experimental set up. A comparison between different designs becomes tedious with such a high number of parameters involved. For this reason we will establish an alternative representation of the contact problem.

An asymptotic framework for contact analysis focuses on one end of the interface [Andresen et al., 2019a]. Commonly, we would look at the severely stressed edge of the contact, which is likely to be the origin of a fretting fatigue crack. A major advantage of this approach is that we will simplify the contact problem and collapse the multi-parameter space of all solutions previously presented into a

two-parameter space. This becomes possible by exploiting certain aspects of the contact tractions found for *incomplete* contacts, such as the square root bounded nature of normal tractions.

Although we exchange the mathematically exact description of the partial slip state for an approximation, we gain the ability to compare experimental and prototypical results for fretting fatigue problems across different designs and loading scenarios [Andresen et al., 2020d]. An additional advantage is that the asymptotic description of the problem enables us to find answers when other comprehensive methods reach their limits, particularly in those problems where the contact patch is asymmetric and the applied differential tension is large enough to reverse the direction of slip at one end of the contact, so that analysing the contact edges separately, using asymptotes, becomes favourable [Andresen et al., 2020a].

Recall the contact problem presented in §1.4 of a rectangular block resting on an elastic half-plane, see Figure 5.1. Contacts of this type can be found in spline connections between split shafts, and, because of the abrupt change in surface gradient at the contact edge, a stress singularity arises which makes the contact edge prone to failure. Another way of looking at the problem is to *zoom in* on one end of the finite contact and to model the problem as a three-quarter plane and this is where the usage of asymptotic methods finds its origin [Williams, 1952]. The motivation is to obtain the local stress distribution for a semi-infinite wedge, or in the given example, for a three-quarter plane with internal wedge angle $^{3\pi}/_{2}$ rad, Figure 5.1. Suppose we centre the coordinate system at the wedge apex, Figure 5.1, then the normal tractions, $p(s)$, along the assumed interface can be found to vary

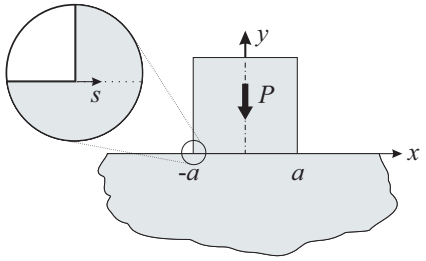


Figure 5.1: Elastic block resting on an elastically similar half-plane with spreading at the edges.

in the form of $p(s) \sim s^{\lambda-1}$, where λ depends on the internal wedge angle and where we will find $\lambda < 1$ for the problem presented in Figure 5.1, which therefore gives a singular stress at the corner, as anticipated [Williams, 1952, Hills et al., 1996].

The idea to use the asymptotic approach to study partial slip was sparked in 2002 when Mugadu et al. [Mugadu et al., 2002] looked at the relative motion along an interface of a complete contact subject to fretting fatigue. The asymptotic approach to incomplete contacts was first introduced in [Sackfield et al., 2003] and later extended to the tangential contact problem in [Dini and Hills, 2004, Dini et al., 2005], using the Jäger-Ciavarella theorem [Jäger, 1997, Ciavarella, 1998]. Asymptotic approaches have since been used for different contact problems, such as flat and rounded punches [Fleury et al., 2016a, Fleury et al., 2016b], and incomplete problems with constant normal but varying shear and bulk loading. More recently, the asymptotic approach was extended to the varying normal load case [Fleury et al., 2017, Andresen et al., 2020a], as an asymptotic version of the work in [Barber et al., 2011].

5.1 Asymptotic Methods Applied to Normal Tractions

Let us begin by assuming that the half-plane problem we wish to study is uncoupled, meaning that the application of a normal load does not induce shear tractions and *vice versa*, i.e. Dundurs' constant is $\beta = 0$. This allows us to study the form of the contact pressure separately from the tangential problem, regardless of the loading scenario under consideration. From §1.4 we know that when an incomplete contact is formed the contact pressure distribution adjacent to the contact edge is square root bounded [Barber, 2010]. Consider a Hertzian contact spanning $[-a \quad a]$, Figure 5.2, to which we know the standard result for the pressure distribution [Hertz, 1881]

$$p(x) = \frac{E^* a}{2R}\sqrt{1 - \frac{x^2}{a}}\,, \tag{5.1}$$

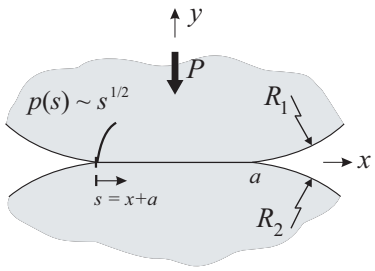


Figure 5.2: Elastic block resting on an elastically similar half-plane with spreading at the edges.

where $E^* = E/(2(1-\nu^2))$ is the composite Young's modulus of the contacting bodies[1] and $1/R = 1/R_1 + 1/R_2$ is the relative curvature of the contacting cylinders. If we move the origin of the coordinate system from the centre of the interface to the left-hand edge, $x = s - a$, and expand the resulting expression by the binomial theorem, we can write [Dini and Hills, 2004] (taking the first term only)

$$p(s) \approx \frac{E^* a}{2R}\sqrt{2\frac{s}{a}}, \quad 0 \leq s/a \ll 1 \,. \tag{5.2}$$

This suggest that the contact pressure in proximity to the contact edge might be written in the form

$$p(s) \approx K_N \sqrt{s} \,, \tag{5.3}$$

where s is the local coordinate measured positively inwards from the contact edge and K_N is the asymptotic multiplier for the normal tractions, here for the Hertzian example given as

$$K_N = \frac{E^* a}{2R}\sqrt{\frac{2}{a}} \,. \tag{5.4}$$

5.1.1 Mossakovskii Methods

Before approaching the tangential problem, let us develop a more rigorous way of arriving at the calibration for K_N, since the form of K_N is always geometry dependent, and there are several approaches we could take to isolate it. However, recent work [Moore and Hills, 2020] using the Mossakovskii-Barber method [Mossakovskii, 1953]

[1]Note that we assume the contacting bodies to be elastically similar, i.e. $(E, \nu) = (E_A, \nu_A) = (E_B, \nu_B)$, in order to uncouple the normal and tangential problem [Dundurs, 1969]

lends itself particularly well to finding K_N for general geometries including the effects of both an applied normal force and an applied moment.

We consider the contact of an indenter with body profile given by $y = g(x)$, where (x, y) are Euclidean coordinates centred at the minimum of the body. Under an applied normal force, P, and an applied moment, M, the indenter presses into an elastically-similar half space, with the contact extending across $[-a \quad c]$, where $a, c > 0$. The standard manner of treating this contact is then to invert a singular integral equation relating the contact pressure $p(x)$ to the body geometry gradient, see [Barber, 2010] for details. In doing so, one finds that a consistency condition must be satisfied for the contact pressure to be bounded

$$0 = \int_{-a}^{c} \frac{g'(s)}{\sqrt{(a-s)(s+c)}} \, \mathrm{d}s. \tag{5.5}$$

The main drawback of this approach is the difficulty in dealing with the Cauchy principal value integrals that arise, since they have singular kernels within the contact. The Mossakovskii method aims to circumvent this problem by converting the singular integral form to a regular — albeit nonsymmetric — Abel integral equation.

The central idea of the Mossakovskii method is depicted in Figure 5.3. The aim is to approximate the geometry of the indenter by an infinite series of flat punches. In order to do this, [Moore and Hills, 2020] formulate the problem in such a way that Eq. (5.5) is used as an equation to isolate the left-hand contact point as a

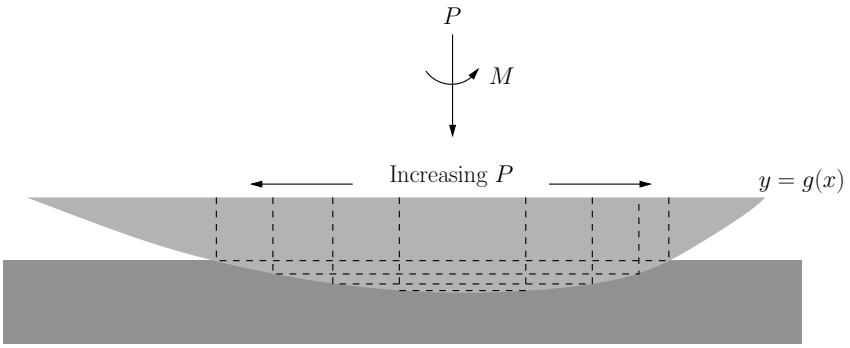


Figure 5.3: A large, almost flat body $y = g(x)$ is pressed into an elastically-similar half-space with an applied normal force, P, and an applied moment, M. The Mossakovskii idea approximates the geometry of the indenter by a series of flat punches, whose widths increase as the contact pressure increases [Andresen et al., 2020a].

function of the right-hand contact point, i.e. giving $a(c)$. The contact pressure, $p(x,c)$, is then given through a superposition of these of the form

$$p(x,c) = \int_0^c F(s)h(x,s)\,\mathrm{d}s, \tag{5.6}$$

where $h(x,a)$ is the contact pressure corresponding to the *complete* contact of a flat punch, that is

$$h(x,c) = \begin{cases} \dfrac{1}{\sqrt{(a(c)+x)(c-x)}} & \text{for } -a(c) < x < c \\ 0 & \text{otherwise} \end{cases}. \tag{5.7}$$

The unknown function $F(\cdot)$ in Eq. (5.6) can then be shown to satisfy the non-symmetric Abel equation

$$\frac{E^* g'(x)\pi}{2} = \int_0^x \frac{F(s)}{\sqrt{(x-s)(x+a(s))}}\,\mathrm{d}s \text{ for } 0 < x < c\,, \tag{5.8}$$

where $E^* = E/(2(1-\nu^2))$ is the composite Young's modulus of the contacting bodies. One key point noted in [Moore and Hills, 2020] is that in order for the Mossakovskii approach to work, the minimum of the indenter must be fixed as P increases, which precludes a change in M as P varies. To get around this, [Moore and Hills, 2020] assume that the geometry is known *a priori* and then find the required M necessary to sustain the contact for a given P. This is equivalent to choosing a particular path in the (P,M) load space. But, as is well-known, the contact pressure — and hence, the K_N coefficients — at load state (P,M) is history-independent, so that this requirement is not overly-restrictive.

To find the K_N coefficients, it transpires that we do not even need to solve Eq. (5.8) for $F(\cdot)$. Vertical equilibrium demands that

$$P = \int_{-a(c)}^c p(s,c)\,\mathrm{d}s, \tag{5.9}$$

which can be manipulated to show that

$$F(c) = \frac{1}{\pi}\frac{\mathrm{d}P}{\mathrm{d}c}. \tag{5.10}$$

Then, [Moore and Hills, 2020] expand Eq. (5.6) close to the edges of the contact and show that

$$p \approx \frac{2}{\pi}\frac{P'(c)}{\sqrt{c+a(c)}}\sqrt{c-x} \text{ as } c-x \to 0, \text{ so that } K_{N,c} = \frac{2}{\pi}\frac{P'(c)}{\sqrt{c+a(c)}}, \tag{5.11}$$

while

$$p \approx \frac{2}{\pi}\frac{P'(c)}{a'(c)\sqrt{c+a(c)}}\sqrt{a(c)+x} \text{ as } a(c)+x \to 0\ , \tag{5.12}$$

so that

$$K_{N,a} = \frac{2}{\pi}\frac{P'(c)}{a'(c)\sqrt{c+a(c)}}. \tag{5.13}$$

5.2 Tangential Loading under Constant Normal Load

Suppose after forming a symmetrical incomplete contact, $[-a \quad a]$, the normal force is held constant and subsequently a mixed tangential load[2] is applied, which increases monotonically to a value that is less than that necessary to cause full sliding. From §4.2.1 we can state that the shear tractions, $q(x)$, developed will be singular at the edges if the interface remains fully adhered, giving

$$q(x) = \frac{Q}{\pi a\sqrt{1-{}^{x}\!/_{a}{}^{2}}} + \frac{x\sigma}{4a\sqrt{1-{}^{x}\!/_{a}{}^{2}}}\ . \tag{5.14}$$

As before, if we shift the origin of the coordinate system from the centre of the contact patch to the left-hand edge, $x = s - a$, and expand the resulting expression by the binomial theorem, we can express the singular shear tractions as

$$q(s) \approx \left[\frac{Q}{\pi\sqrt{2a}} \pm \frac{\sigma}{4}\sqrt{\frac{a}{2}}\right]\frac{1}{\sqrt{s}} = \frac{K_T}{\sqrt{s}}\ , \qquad s \ll a \tag{5.15}$$

where we pick the upper sign when we look at the right-hand edge of the contact and the lower sign when the left-hand side is under consideration. Further we can state, that the asymptotic multiplier of the shear tractions under conditions of full stick is given as

$$K_T = \frac{Q}{\pi\sqrt{2a}} \pm \frac{\sigma}{4}\sqrt{\frac{a}{2}}\ . \tag{5.16}$$

[2]In the asymptotic approach any possible combination of shear load and differential tension is easily treatable as only one edge of contact is under consideration.

We note that this result is independent of the geometry under consideration and only the half-width of the contact, a, and the applied tangential loading affect the value of K_T.

5.2.1 The Partial Slip Problem under Constant Normal Load

From Chapter 3 we know that for a finite coefficient of friction, f, zones of slip are expected to develop. If we assume a scenario where the slip zones are small compared with overall size of the contact, we can pursue the following asymptotic description of the slip stick boundaries. In the zones of slip the shear tractions, $q(s)$, are going to take the form

$$q(s) = \pm fp(s) \approx \pm fK_N\sqrt{s}\,, \qquad 0 < s < d\,, \tag{5.17}$$

where d is the size of the slip zone at the end of the contact under consideration and the sign depends on the direction of slip[3]. Everywhere else along the interface no relative motion is expected. Let us recall that the Jäger-Ciavarella principle from Chapter 3 made use of a corrective traction superimposed on the full sliding shear traction to bring down the relative strain in the regions of stick. In the spirit of that idea we approximate the tractions in the stick zone in the neighbourhood of the contact edge as

$$q(s) \approx fK_N\sqrt{s} - fK_N^c\sqrt{s-d} \qquad d < s \ll a\,, \tag{5.18}$$

where K_N^c is the asymptotic multiplier on the corrective shear traction. When the observation point is shifted closer to the centre of the contact, the effect of slip zones on the shear tractions in the stick region wears off and the shear tractions take the form of a fully adhered interface, see Eq. (5.15)

$$q(s) \approx \frac{K_T}{\sqrt{s}} \qquad d \ll s < a\,. \tag{5.19}$$

These asymptotes are illustrated in Figure 5.4 alongside sketches of the exact forms of $p(s)$ and $q(s)$. If we now move the observation point for Eq. (5.18) to a

[3]We will omit the $\pm$ symbol on the slipping tractions from here on. The sign should be chosen with care, though, depending on whether the differential tension is *moderate* or *large*.

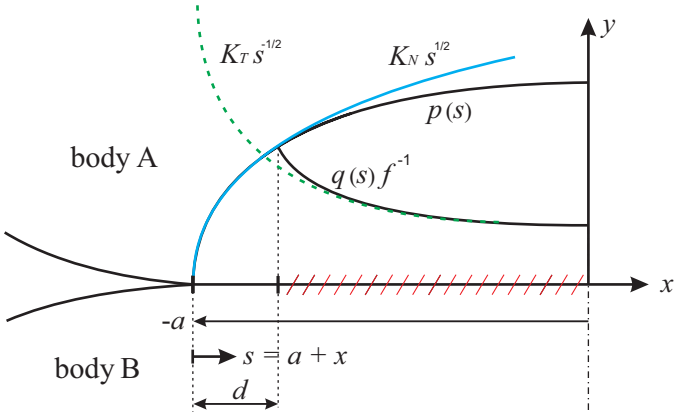


Figure 5.4: Normal and tangential asymptotes at the edge of an incomplete contact [Andresen et al., 2020a].

point where $d \ll s < a$, we may re-write the equation as

$$\begin{aligned} q(s) &\approx f K_N \sqrt{s} \left[1 - \frac{K_N^c}{K_N} \sqrt{1 - \frac{d}{s}} \right] \\ &\approx f K_N \sqrt{s} \left[1 - \frac{K_N^c}{K_N} \left(1 - \frac{d}{2s} + ... \right) \right] \qquad d \ll s < a \, . \end{aligned} \tag{5.20}$$

As stated, we assume the slip zone size to be small compared with the overall size of the contact so that $K_N^c / K_N \approx 1$, simplifying Eq. (5.20) to

$$q(s) \approx \frac{f K_N d}{2\sqrt{s}} \qquad d \ll s < a \, . \tag{5.21}$$

Now, we equate Eqs. (5.19) and (5.21), yielding an expression for the size of the slip zone in asymptotic form as

$$d = \frac{2K_T}{f K_N} \qquad d \ll a \, . \tag{5.22}$$

In many problems the tangential loading cycles between two points in Q-σ load space so that an approximation of the steady-state slip zones size is of particular interest, for instance when a fretting fatigue experiment is to be calibrated. Dini et al. [Dini et al., 2005] showed that for partial slip problems under constant normal loading it is the range of the asymptotic shear traction multiplier, which controls the size of the *steady-state* slip zone size

$$d = \frac{\Delta K_T}{f K_N} \, , \tag{5.23}$$

where

$$\Delta K_T = \frac{\Delta Q}{\pi\sqrt{2a}} \pm \frac{\Delta\sigma}{4}\sqrt{\frac{a}{2}}\,, \tag{5.24}$$

and the Δ terms indicate the range between maximum and minimum load points of the cycle. As shown in §3.4, the difference in a factor of two between Eq. (5.22) and Eq. (5.23) is because the corrective term for the shear tractions must cancel the relative displacement occurring when the slip zone tractions are fully reversed from maximum to minimum during the cycle, see §3.4.

5.3 Tangential Solution under Varying Normal Load and Moment

In Chapters 3 and 4 we showed that the analytical solution for slip zone size can be obtained in closed-form for some specific contact geometries under varying normal, moment, shear and differential bulk tension loading. However, for problems subject to large tension and a varying moment, as explained in Chapter 4, the use of an asymptotic approach, which focuses on one contact edge and its surroundings only, must be adopted. Even for cases where an analytical solution exists, it might be of interest to have a succinct and easy-to-apply method at hand and this is what we shall establish here [Andresen et al., 2020a].

5.3.1 Asymptotic Approximation of Shear Tractions

The shear traction at the maximum shear load during a generic steady-state loading cycle, as depicted by point 2 in Figure 5.5, can be expressed as a scaled superposition[4] of the contact pressure at different load pressures throughout the loading path, i.e. using the Jäger-Ciavarella theorem, as [Barber et al., 2011]

$$\begin{aligned} q_1(x) = &+ \int_0^{P_Z} \frac{\partial p(x,P,M)}{\partial P}\frac{\mathrm{d}P}{\mathrm{d}Q}\mathrm{d}P \\ &+ fp(x,P,M) - 2fp(x,P_S,M_S) + fp(x,P_Z,M_Z)\,, \end{aligned} \tag{5.25}$$

[4] We assume moderate differential tension for the initial formulation of the approach, which once written down in asymptotic form, is applicable to both, *moderate* and *large* differential tension.

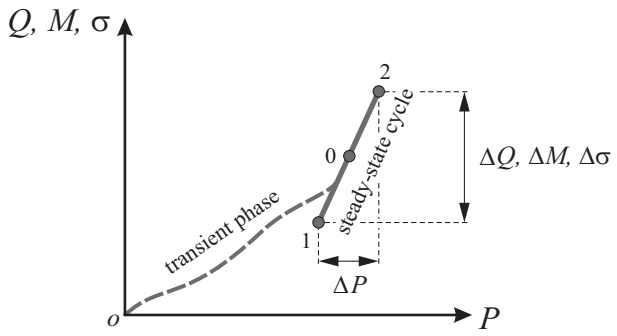


Figure 5.5: Cyclic loading with in phase changes in all load components [Andresen et al., 2020a].

where P_S and P_Z are previous loads in the load history defining the current size of the stick zone, $a(P_S, M_S)$, and the permanent stick zone, $a(P_Z, M_Z)$, respectively. These may be obtained by enforcing tangential equilibrium, see [Barber et al., 2011]. The integral in Eq. (5.25) represents the accumulated shear traction in the stick zone during the transient loading, as described in detail in [Barber et al., 2011]. Although calculating the size of the stick zone, current and permanent, when the loading is purely due to P and Q is straightforward as demonstrated in [Barber et al., 2011, Fleury et al., 2017], it is not so if a moment, M, and a differential tension, σ, are also present.

By expanding the shear traction in a series expansion and taking only the leading-order terms, the asymptotic approximation of the shear traction at the left edge of the contact and at the minimum load point of the steady-state in Figure 5.5 may be obtained by a superposition of the normal bounded asymptote [Fleury et al., 2017] as

$$\begin{aligned} q_1^{(asy)}(x) =& K_{Q1}\sqrt{x + a_1 - d_1} + fK_{N1}\sqrt{x + a_1} - 2fK_{N1}\sqrt{x_1 + a_1 - d_1} + \\ & fK_{N1}\sqrt{x + a_2 - d_2}; \end{aligned} \tag{5.26}$$

where d_1 and a_1 are the slip zone size and contact size at the minimum load point, and d_2 and a_2 are the slip zone size and contact size at the maximum steady-state loading point. The coefficients K_N, here, may be obtained as in §2 and K_Q is scaled from K_N during the transient (and proportional) loading, i.e. when the loading did not cause slip.

At the maximum load point of the steady-state the shear traction is given by

$$q_2(x) = \int_0^{P_Z, M_Z} \frac{\partial p(x,P,M)}{\partial P} \frac{\mathrm{d}P}{\mathrm{d}Q} \mathrm{d}P - fp(x,P,M) + fp(x,P_Z,M_Z), \tag{5.27}$$

and its analogous asymptotic approximation is

$$q_2^{(asy)}(x) = K_{Q2}\sqrt{x+a_2-d_2} - fK_{N2}\sqrt{x+a_2} + fK_{N2}\sqrt{x+a_2-d_2}. \tag{5.28}$$

5.3.2 Calculation of the Steady-State Slip Zone Size

In order to calculate the size of the slip zone at the maximum and minimum points in the steady-state loading, the change in shear traction from the maximum to minimum loading points, Δq, is compared with the change of traction in the absence of slip [Dini et al., 2005]. One assumption we make here is that the change in K_N and K_Q between the two ends of the steady-state loading can be neglected, which is valid only for moderate loading. The change in shear loading at the left hand side edge of the contact, see Figure 5.4, from the maximum to minimum loading may thus be written as

$$\begin{aligned}\Delta q(x) &= q_1^{(asy)}(x) - q_2^{(asy)}(x) \qquad (5.29)\\ &= K_{Q1}\sqrt{x+a_1-d_1} + fK_{N1}\sqrt{x+a_1} \\ &\quad - 2fK_{N1}\sqrt{x+a_1-d_1} + fK_{N1}\sqrt{x+a_2-d_2} \\ &\quad - \left(K_{Q2}\sqrt{x+a_2-d_2} - fK_{N2}\sqrt{x+a_2} + fK_{N2}\sqrt{x+a_2-d_2}\right). \qquad (5.30)\end{aligned}$$

Now, let us take the limit $(K_{N1}, K_{N2}) \to K_N$. This simplifies the difference in shear tractions to

$$\begin{aligned}\Delta q(x) \simeq & fK_N \left(\sqrt{x+a_1} - 2\sqrt{x+a_1-d_1}\right. \\ & \left. + \sqrt{x+a_2-d_2} + \sqrt{x+a_2} - \sqrt{x+a_2-d_2}\right). \end{aligned} \tag{5.31}$$

We further expand the expression at $(x+a_1) \to \infty$. By doing so the effects of the slip zones on the shear tractions are distant enough to justify the use of

a singular traction multiplier, which yields

$$\Delta q(x) \simeq f K_N \left(2 \left(\frac{d_2}{2\sqrt{x+a_1}} + ... \right) + \frac{\Delta a}{2\sqrt{x+a_1}} \right) \tag{5.32}$$

$$= \frac{\Delta K_T}{\sqrt{x+a_1}} \, , \tag{5.33}$$

where $\Delta a = |a_2 - a_1|$ is the change in contact size over one half loading cycle at the end of the contact under consideration and where $0 \leq \Delta a << a_2 + a_1$.

We now have means of expressing the size of the slip zone at either end of the load cycle, so that by combining Eqs. (5.33 and 5.32), the steady-state slip zone size is given in asymptotic form as

$$d_1 = \frac{\Delta K_T}{f K_N} - \frac{\Delta a}{2} \qquad \text{and} \qquad d_2 = \frac{\Delta K_T}{f K_N} + \frac{\Delta a}{2} \, . \tag{5.34}$$

We can go one step further and approximate the instantaneous size of the slip zones at every point of the steady-state load cycle. Now, the value of the asymptotic shear traction multiplier, ΔK_T, must be evaluated based on the the finite changes in tangential loading, $\Delta Q = Q_2 - Q_i$ and $\Delta \sigma = \sigma_2 - \sigma_i$, where i represents the instantaneous value of the respective load component. The normal traction multiplier, K_N, depends on the instantaneous value of the normal loading, see §5.1.1. The change in contact size is then defined as $\Delta a = |a_2 - a_i|$, where a_i is the instantaneous contact size.

5.4 Example Application

In this section we wish to draw an instructive comparison between the mathematically exact solution presented in §3.5.3 and its asymptotic expressions for the example of a shallow wedge subject to a cyclically varying normal load, moment, shear load and initially *moderate* differential bulk tension, see Figure 5.6. An example illustration of a steady-state load cycle between the minimum and maximum load points, 1 and 2 respectively, is given in Figure 5.5. Analytical methods reach the limit of what they are able to treat when we look at problems which involve a varying moment and the differential bulk tension becomes *large* enough to reverse

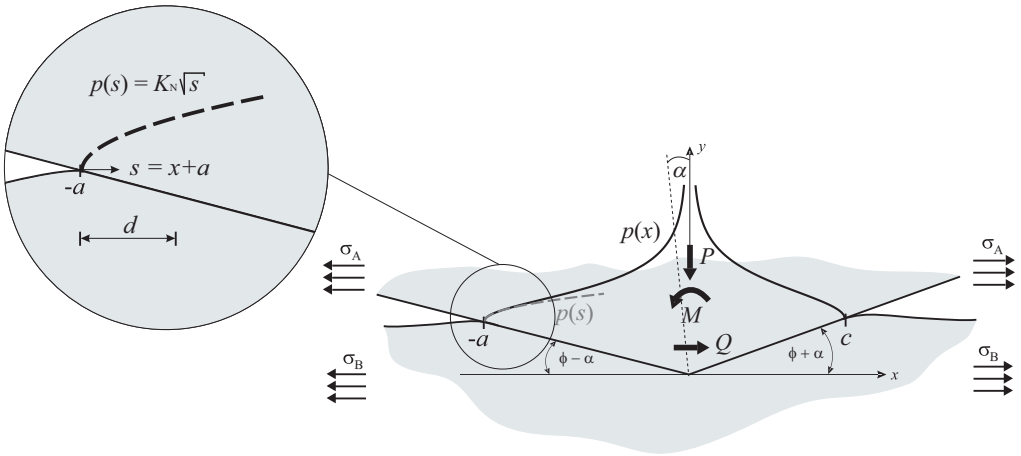


Figure 5.6: A tilted wedge contact subject to a normal load, moment, shear load with remote bulk tensions arising in each half-plane and a zoom-in on the left-hand contact edge.

the direction of slip at one end of the contact. The asymptotic description allows us to go beyond this limitation and, here, we present the results.

5.4.1 Asymptotic Solution

As the contact law and the permanent stick zone during the steady-state cycle are known in closed-form, see §3.5.3, the mathematically exact maximum extent of the slip zones is given as[5]

$$d^{\mathrm{LHS}} = a - m \ , \tag{5.35}$$

at the left-hand end of the contact and

$$d^{\mathrm{RHS}} = c - n \ , \tag{5.36}$$

at the right-hand end of the contact. Here, we wish to find equivalent explicit statements using the asymptotic description outlined in §5.3.2. In its most general form the maximum slip zone extent is given as in Eq. (5.34). The values for ΔK_T and K_N will be different at each end of the load cycle and can be found by two different means. Either we use numerical results from, say, a finite element analysis [Andresen et al., 2020e, Fleury et al., 2016a, Fleury et al., 2016b], or we

[5]Note, we again omit the suffix indicating the ends of the load cycle, $i = 1, 2$, for clarity.

apply the explicit expressions given in §5.1.1 for K_N and write the range of the asymptotic shear traction multiplier as

$$\Delta K_T = \frac{\Delta Q}{\pi\sqrt{2a}} \pm \frac{\Delta\sigma}{4}\sqrt{\frac{a}{2}}\,, \tag{5.37}$$

where we choose the upper sign when looking at the left-hand side and the lower when looking at the right-hand side. Note that the respective contact half-width (a, c) should be used for the contact edge under consideration. While ΔK_T is independent of the geometry, i.e. only the range of the tangential loads and the instantaneous contact half-width matter, the asymptotic multiplier for the normal tractions is dependent on the geometry and material of the contacting bodies. For an explicit expression, we need to know the instantaneous contact law, $P'(a)$, so that for the left-hand side of the tilted wedge we can write Eq. (5.13) in explicit form by differentiating Eq. (3.72) with respect to a, yielding

$$K_N^{\mathrm{LHS}} = \frac{2E^*\phi}{\pi}\sqrt{\frac{\gamma}{a\,(1+\gamma)}}\,, \tag{5.38}$$

which can be readily connected to the other end of the contact by

$$K_N^{\mathrm{RHS}} = \frac{K_N^{\mathrm{LHS}}}{\gamma}\,. \tag{5.39}$$

5.5 Display of Results

The example section of this chapter is certainly the most comprehensive one in the thesis and we will use the solution developed above to display several results for a wedge geometry. There are five example loading scenarios we wish to look at in detail. In §5.5.1 we wish to recover the classical Cattaneo-Mindlin solution using a wedge geometry in order to gain confidence in the asymptotic approach. We then go on to look at how this solution is affected by a varying normal load. The effects of a differential bulk tension, which may be *moderate* or *large*, are studied in the subsequent example. That is of particular interest because of the case when the sign of slip reverses due to *large* differential tension. Note that for the asymptotic approach it is irrelevant whether the differential tension is moderate

or large, as we only look at one end at a time. In §5.5.4 we investigate the effect of an asymmetry in the contact patch and how that affects the partial slip behaviour. From §3.5.2 we know that it is the mean angle of tilt, α_0, that enters the partial slip solution. Lastly, we look at the effects of a varying moment in combination with large differential tension. That is, the case in which only the asymptotic approach can provide an answer, see §5.5.5.

5.5.1 The Cattaneo-Mindlin Problem

It will be instructive to restrict ourselves, first, to the problem described in §5.2 where a contact is established by a normal force, P, which is then held constant while a shear load, Q varies between a minimum load point, 1, and a maximum load point, 2, over the range ΔQ. This type of loading sequence was first solved for a Hertzian contact subject to a monotonically increasing tangential load [Cattaneo, 1938] and later extended to periodically varying tangential forces [Mindlin et al., 1951]. The Jäger-Ciavarella theorem allows us to apply these ideas to any kind of incomplete geometry, including the shallow wedge. The established contact is symmetrical and, given the coefficient of friction, f, is finite, slip zones of equal extent will ensue so that the maximum slip zone extent is found using Eqs. (3.73), (3.76)

$$d = a - m = \frac{1}{E^* \phi} \left(\frac{\Delta Q}{2f} \right) . \tag{5.40}$$

The asymptotic description yields the exact same result using Eqs. (5.23), (5.37), and (5.38)

$$d = \frac{\Delta K_T}{f K_N} = \frac{1}{E^* \phi} \left(\frac{\Delta Q}{2f} \right) . \tag{5.41}$$

The reason for this is the proportionality between applied normal load and contact size of the wedge solution, see Eq. (3.73). For a different geometry, a relative error between the exact and asymptotic solutions is expected, which will depend on the nature of the contact law. Figure 5.7 a) shows the linearity of the steady-state solution associated with this problem for values of $0 < {}^{\Delta Q}/_{fP} < 2$. For each value of ${}^{\Delta Q}/_{fP}$ a stand-alone maximum slip zone size extent can be obtained.

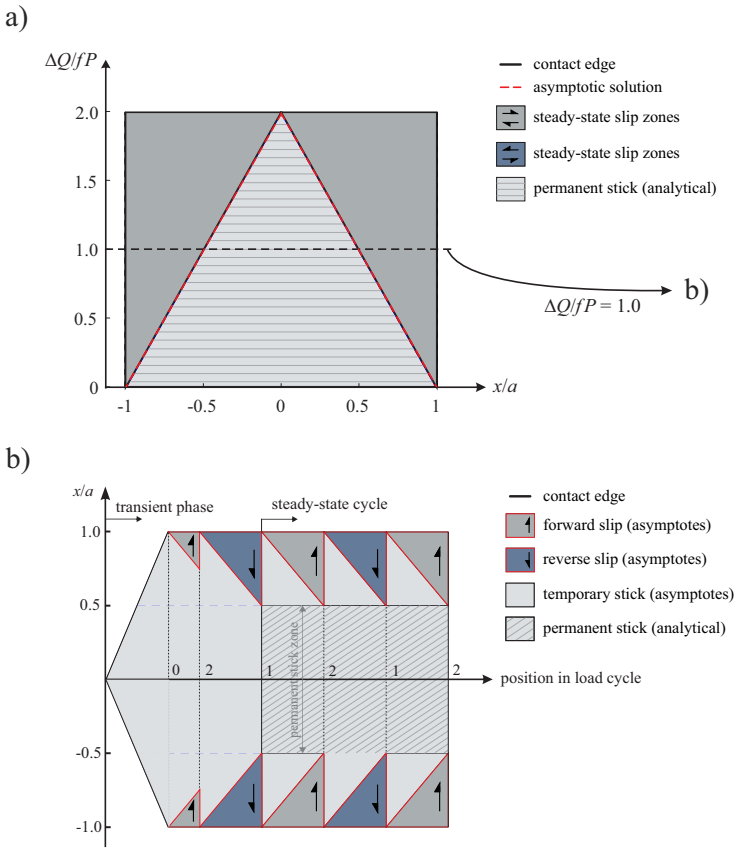


Figure 5.7: a) Stand-alone steady-state solutions under constant normal load showing the contact size and maximum slip zone extent for $0 < {}^{\Delta Q}/_{fP} < 2$, b) the marching-in-time solution for ${}^{\Delta Q}/_{fP} = 1.0$ with zones of forward and reverse slip [Andresen et al., 2020a].

In Figure 5.7 b) the steady-state solution for ${}^{\Delta Q}/_{fP} = 1.0$ is plotted in a marching-in-time sense. After a transient phase - note, the path taken to reach the steady-state only affects the locked-in tractions in the permanent stick zone, but not the steady-state slip-stick pattern - the steady-state cycle is established and we see zones of reciprocating slip emerge at both ends of the contact. As said before, since we have chosen the wedge geometry, the Cattaneo-Mindlin problem yields the exact same solution as the asymptotic and analytical approach for the maximum extent of the slip zones, see Eqs. (5.40 and 5.41). Note that the explicit solution, Eq. (5.40), will allow us to find the maximum extents of the steady-state slip zones only, while the asymptotic solution makes it possible to *march* through the steady-state load cycle and find the slip-stick boundary at every point in time. For the sake of comparability, we will adopt this style of presenting the results for the other

loading scenarios considered in this example section.

5.5.2 The Effect of a Varying Normal Load

From Eqs. (3.76 and 3.75) we see that the position and extent of the permanent stick zone is independent of variations in normal load, ΔP. The slip zone size will vary, of course, due to the variation in size of the contact. The asymptotic description of the slip zone size, Eq. (5.34), depends on the instantaneous values of the asymptotic multipliers, ΔK_T and K_N, as well as the overall change in contact size, Δa, throughout a cycle. This means there is no explicit dependence on the normal load variation, ΔP. Implicitly, however, all three of the stated parameters are affected by changes in normal load. It is therefore of interest to employ the asymptotic framework developed to a varying normal load problem and demonstrate its applicability. In order to simplify comparability, we will use the same parameters as used in the example above, i.e. ${}^{\Delta Q}/_{fP} = 1.0$ and add a varying normal load of ${}^{\Delta P}/_{P} = 0.15$ to the problem. Figure 5.8 shows a marching-in-time solution for the problem described. We notice that the size and position of the permanent stick zone remains unchanged compared with Figure 5.7 b). The overall contact size, however, increases and decreases throughout the cycle, therefore effectively changing the size of the slip zones not only due to a variation in shear load, but also due to movement of the contact edge. The asymptotic framework tends to underestimate the slip zone

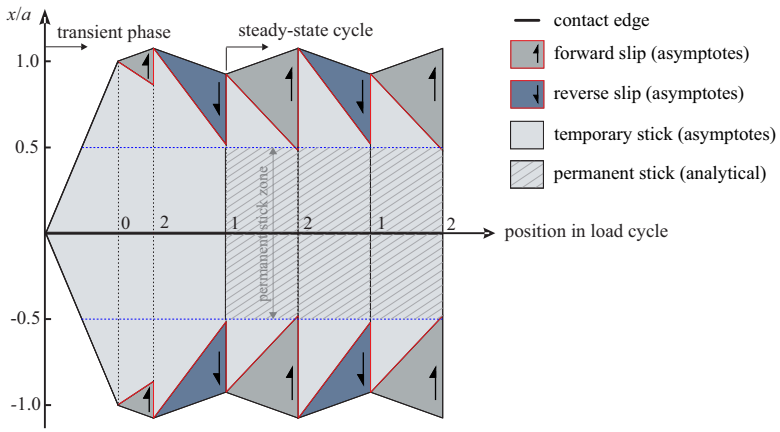


Figure 5.8: Marching-in-time solution for a varying normal load problem, ${}^{\Delta P}/_{P} = 0.15$, while the tangential load variation is ${}^{\Delta Q}/_{fP} = 1.0$ [Andresen et al., 2020a].

size at the minimum load point of the cycle and to overestimate it at the maximum load point of the cycle. While it is not possible to make a general statement regarding the relative error, we regard the results obtained for this example case as acceptable, since the error between the values for the exact and approximated size of the slip zones is certainly less than 5%. Encouraged by this comparison, in the examples which follow, we will refrain from adding the effect of a varying normal load, in order to concentrate on the effects of the loading under consideration.

5.5.3 The Effect of Differential Bulk Tension

Let us now look at what happens to the steady-state solution when in addition to a varying shear force, ΔQ, a varying differential tension, $\Delta\sigma$ is present. We will use the results presented in §5.2 to compare the closed-form solution for moderate differential tension to the asymptotic description. The solution given in Eq. (3.76) is valid as long as the same sign slip direction is maintained at both ends of the contact. That is the range of differential tension, $\Delta\sigma$, is smaller than or equal to its transition value to the onset of reverse slip, $\Delta\sigma_{th}$

$$\Delta\sigma \leq \Delta\sigma_{th} \ , \tag{5.42}$$

where

$$\Delta\sigma_{th} = \frac{4E^* f}{\pi}\left[\pi\alpha_0 - 2\phi\sin^{-1}\left(\frac{8f^2P^2}{\Delta Q\gamma(\Delta Q - 4fP) + (1+\gamma)4f^2P^2} - 1\right)\right] . \tag{5.43}$$

Suppose, now, that the range of differential tension is *large* enough for inequality (5.42) to be violated, $\Delta\sigma > \Delta\sigma_{th}$, so that the slip directions are of opposite sign. In order to have a mathematically exact point of comparison against the asymptotic solution, we use the following consistency conditions for constant normal load problems subject to varying *large* differential tension and shear load from Andresen et al. [Andresen et al., 2020c] and evaluate for m and n numerically

$$\frac{\Delta\sigma\pi}{8} = -\int_{-a}^{-m}\frac{fp(\xi)\,\mathrm{sgn}(\xi)\,\mathrm{d}\xi}{\sqrt{(\xi-n)(\xi+m)}} + \int_{n}^{a}\frac{fp(\xi)\,\mathrm{sgn}(\xi)\,\mathrm{d}\xi}{\sqrt{(\xi-n)(\xi+m)}}, \tag{5.44}$$

$$\frac{\Delta Q}{2} + \frac{(n-m)\Delta\sigma\pi}{16} = -\int_{-a}^{-m}\frac{\xi fp(\xi)\,\mathrm{sgn}(\xi)\,\mathrm{d}\xi}{\sqrt{(\xi-n)(\xi+m)}} + \int_{n}^{a}\frac{\xi fp(\xi)\,\mathrm{sgn}(\xi)\,\mathrm{d}\xi}{\sqrt{(\xi-n)(\xi+m)}}. \tag{5.45}$$

A closed-form solution can be obtained for the Hertzian geometry, and we provide this in §4.4. In the example we examine in this section, the contact is established by the normal load, P, until the contact half-width reaches a. The shear force is then varied with range $\Delta Q = 0.3fP$ and we see the effect of a change in differential bulk tension over $0 \leq \Delta\sigma/\Delta\sigma_{th} < 3$ for the asymptotic and analytical solutions, Figure 5.9 a). Note that the $\Delta\sigma$ is normalised to its transition value, $\Delta\sigma_{th}$, see Eq. (5.42). When the transition value is reached, $\Delta\sigma/\Delta\sigma_{th} = 1$, we observe that the direction of slip changes at one end of the contact and the underlying analytical approach switches from the explicit branch of its solution for moderate differential tension, Eq. (3.76), to the numerical branch, Eqs. (5.44, 5.45) for large differential tension. The larger the slip zones become relative to the overall contact size, the less accurate the asymptotic description becomes. We will

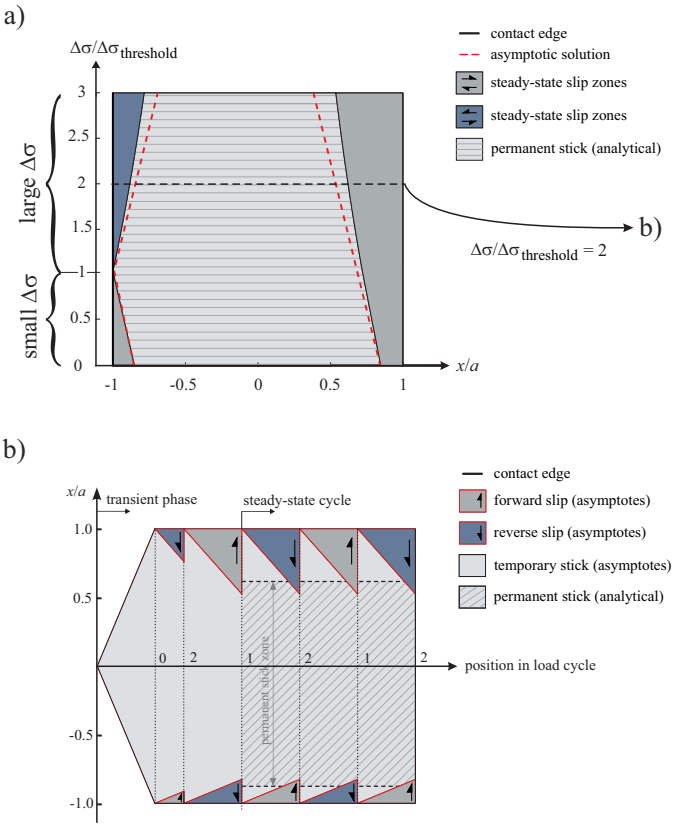


Figure 5.9: a) Stand-alone steady-state solutions under constant normal load showing the contact size and maximum slip zone extent for $\Delta\sigma/\Delta\sigma_{th} < 3$, b) the marching-in-time solution for $\Delta\sigma/\Delta\sigma_{th} = 2$ with opposing zones of slip at both ends of the contact [Andresen et al., 2020a].

refrain from further assessing the relative error between analytical and asymptotic approach as the number of input parameters is too large to make any general statements beyond the one we have just made. It is the responsibility of the user to acknowledge this trade-off between the mathematically exact analytical approach and the very convenient asymptotic description.

Figure 5.9 b) on the other hand shows the steady-state slip-stick pattern in a marching-in-time sense for large differential tension, $\Delta\sigma/\Delta\sigma_{th} = 2$. Note that the direction of slip is of opposite sign at each end of the contact and that the asymptotic description overestimates the maximum extent of the slip zones at both ends of the contact.

5.5.4 The Effect of a Constant Angle of Tilt

In most engineering applications, there is a moment transmitted through the interface causing the bodies to tilt relative to each other. We continue to use the wedge geometry as an example. From §3.5.2 we know that the coordinates for the permanent stick zone $[-m(\alpha_0) \quad n(\alpha_0)]$ change with the average angle of tilt, α_0, unaffected by the a change in moment, ΔM, over the course of a cycle. Consider Figure 5.10 a) and note that each value of α_0 represents a stand-alone steady-state solution for a contact subject to a constant normal load, P_0, and angle of tilt, α_0, giving the mean contact size spanning $[-a_0 \quad c_0]$. Throughout the example, we maintain the shear load fluctuation at the level of $\Delta Q = 0.3fP_0$. From these inputs we can infer size of the permanent stick zone $[-m \quad n]$ and plot this for different values of α_0/ϕ.

The fluctuation in bulk stress, $\Delta\sigma$, is kept zero as the intention is to demonstrate the effects of tilt exclusively. We see that increasing the average angle of tilt influences not only the extent and position of the contact, but also the extent and position of the permanent stick zone within the contact. The example reflects the solution behaviour indicated by Eq. (3.76). We note that it is the mean normal load, P_0, and the average angle of tilt, α_0, which affect the tangential solution, together with the tangential load inputs, $\Delta\sigma$ and ΔQ, although we have not looked

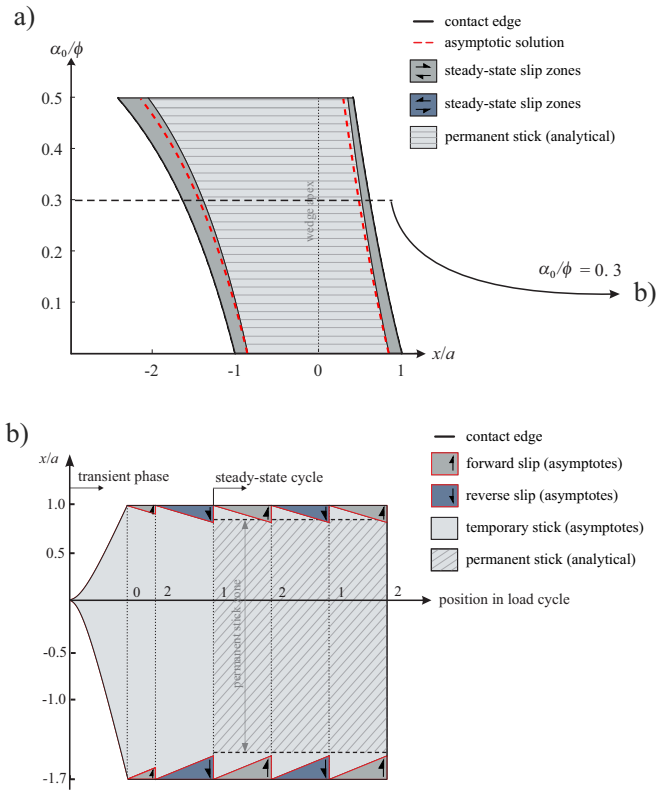


Figure 5.10: Wedge geometry a) stand-alone steady-state solutions under constant normal load showing the contact size and maximum slip zone extent for $0 < \alpha_0/\phi < 0.5$ subject to a varying shear force, $\Delta Q/fP0 = 0.3$, b) the marching-in-time solution for $\alpha_0/\phi = 0.3$ with zones of forward and reverse slip [Andresen et al., 2020a].

at the effects of the latter two. The solution developed above will remain valid as long as a shear-dominant behaviour is expected, i.e. the change in differential bulk tension is *moderate* such that the direction of slip is the same at both ends of the contact during each half-cycle.

Figure 5.10 b) shows the marching-in-time steady-state solution with the expected asymmetrical slip-stick behaviour across the interface. Note that if the average angle of tilt, α_0, becomes zero, a symmetrical slip-stick pattern, qualitatively equal to that presented in Figure 5.7, would be recovered. The asymptotic solution underestimates the size of the steady-state slip zone at one end, while overestimating it at the other end. In summary, however, we see good agreement between the two different approaches for all depicted values of α_0/ϕ.

5.5.5 A Varying Moment together with Large Differential Tension

In all loading scenarios examined so far in this example section there has always been a mathematically exact solution for the maximum extent of the steady-state slip zones with which to compare their asymptotic description. As explained in the earlier, the analytical approach reaches its limitation once we consider a *large* varying bulk tension in the presence of a varying moment, or angle of tilt. Now that we have gained confidence in the applicability of the asymptotic description, we fill in this remaining puzzle piece by revisiting the case of Figure 5.10 b). Now the normalised angle of tilt, α/ϕ, is going to vary between 0.28 and 0.32, as opposed to being kept constant at 0.3. This is going to cause a repetitive movement of the contact edge throughout the cycle. In addition to a varying shear force, $\Delta Q/fP_0 = 0.3$, we apply a large differential tension, $\Delta\sigma/\Delta\sigma_{th} = 2$, so that the direction of slip is not the same at both ends of the contact.

Figure 5.11 shows the marching-in-time slip-stick pattern throughout the cycle. Note that while the slip zones at one end are small compared with the overall contact half-width, they advance quite significantly into the inner part of the contact at the other end of the contact. From the experience gained with previous examples we know that the smaller the slip zones compared with the overall contact size, the higher the quality of approximation.

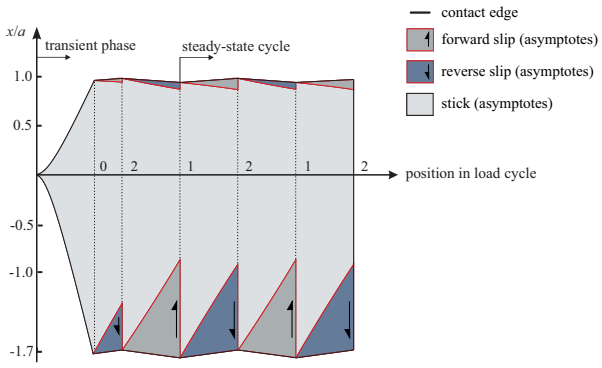


Figure 5.11: The marching-in-time solution for a shallow wedge with a normalised angle of tilt, α/ϕ, varying between 0.28 and 0.32 while being subject to mixed shear loading of $\Delta Q/fP_0 = 0.3$ and large differential tension, $\Delta\sigma/\Delta\sigma_{th} = 2$ with zones of forward and reverse slip using the asymptotic description [Andresen et al., 2020a].

5.6 Conclusion

In this Chapter we have outlined recipes for obtaining the slip-stick behaviour for incomplete contacts under constant and varying normal load and moment, together with oscillatory tangential loading, using an asymptotic approach. The motivation for the latter stems from the limitations of the analytical description, that is, the lack of a mathematically exact solution to the steady-state slip stick behaviour in the presence of a varying moment and a differential bulk tension large enough to reverse the direction of slip at one end of the contact. A comparison is drawn between the asymptotes and the analytical solution for a shallow wedge geometry for different loading scenarios in order to gain confidence in the asymptotic approach. The chapter concludes with the application of the asymptotic description to a case where no analytical approach can provide an answer. Overcoming the limitations of the analytical approach provides us with an answer using the easy-to-apply asymptotic description in convenient manner.

In Chapter 7 we will use the asymptotic description for oscillating tangential loads under constant normal loading to reinterpret experimental data from the literature and present a generalised approach to determining the fretting fatigue strength experimentally. The asymptotic approach collapses the multi-parameter space of the experimental data to a two-parameter space (K_N and ΔK_T). This makes it possible to compare easily different loading scenarios and experimental set ups for a specific material.

6

Representation of Incomplete Contact Problems by Half-Planes

In cyclic problems, it is the extent of the slip zones near the contact edge we wish to determine, as this is where the surface damage is accumulated and cracks may nucleate. It is this damage zone that needs matching between the real thing and any laboratory fretting fatigue experiment in order to mimic crack nucleation life together with the underlying cyclic stress responsible for crack propagation. The contact problem therefore has two aspects: first, there is a normal component, where the contact extent and normal traction are dictated by the normal load and moment, and secondly a tangential component in which the shear tractions are controlled by a combination of shear load and differential bulk tension.

Generally, two different approaches can be taken to solve the normal and tangential contact problem. First, if the contacting bodies can be idealised as half-planes, a closed-form solution may be found, or existing solutions may be used. While the analytical approach is very good at handling frictional slip, the half-plane idealisation is a step removed from a real profile geometry. The other available approach is a numerical one. The contact problem may be solved by means of a finite element analysis. Commercial tools are attractive because of their versatility and the model will be very good at representing the finite geometry of the problem.

However, it will be computationally expensive to model the end-of-contact slip zones with the required fidelity. Notwithstanding this reservation, an initial finite element analysis of any prototypical connector profile is essential in identifying the local contact loads present in each contact flank.

Figure 6.1 a) shows a typical two-dimensional contact problem arising in the fan blade root dovetail of gas turbine engines due to the application of a centrifugal load, F_C, vibrational load F_V, and expansion load T. In its 'core' we can identify five quantities which are relevant to the local contact problem, all of which may be functions of time, and four of which control the partial slip problem. These are: the normal load, P, moment, M, shear force, Q, and the differential tension, σ, developing between bodies A and B, where $\sigma = \sigma_{\mathrm{A}} - \sigma_{\mathrm{B}}$, Figure 6.1.

The normal contact problem is defined by the front face geometry (profile) together with the applied normal force, P, and applied moment, M. It is trivial to deduce these from the finite element output by evaluating

$$P = \int_{-a}^{b} p(x)\mathrm{d}x \ , \tag{6.1}$$

$$M = \int_{-a}^{b} p(x)x\mathrm{d}x \ , \tag{6.2}$$

where $p(x)$ is the contact pressure. Shear tractions, which tend to induce slip, are actually excited by two forms of loading. One is by the application of an

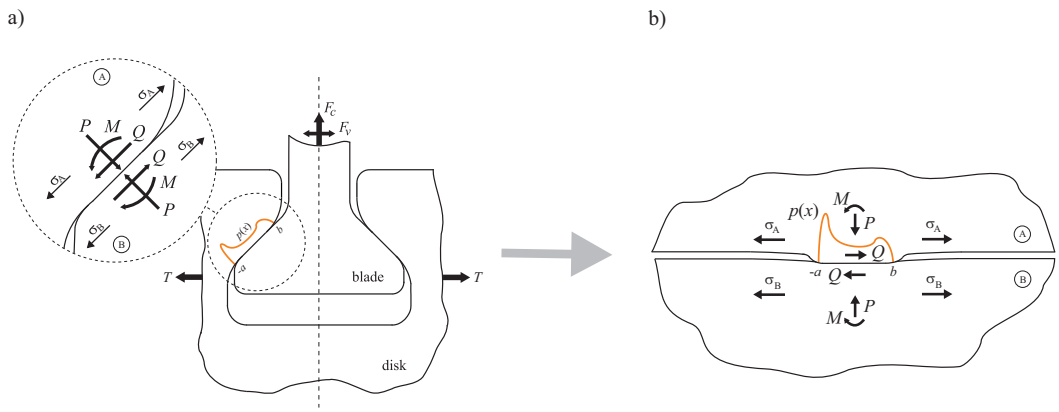


Figure 6.1: The fan blade dovetail root contact shown in a) is analysed using the half-plane representation shown in b) [Andresen et al., 2020e].

external shear force, Q, which again is straightforward to deduce as a traction resultant by evaluating

$$Q = \int_{-a}^{b} q(x)\mathrm{d}x \ , \tag{6.3}$$

where $q(x)$ is the shear traction within the contact.

However, there is also a second form of excitation of shear tractions which is clear in the half-plane model, Figure 6.1 b), namely the effect of the bulk tensions exerted remotely parallel with the surface which, if unequal, produce an (approximately) antisymmetric interfacial shear traction distribution in the half-plane contact. These remote forms of loading are very easy to visualise in the half-plane problem, but when we consider finite problems such as that shown in Figure 6.1 a), and where the geometry of individual components looks very different from a half-plane, their 'equivalent' is very much harder to interpret. It is the primary function of this section to show how we may best interpret the output of the finite element analysis of a problem such as that shown in Figure 6.1 a) to enable finding the optimal choices for the remote stresses applied to the half-plane contact problem shown in Figure 6.1 b).

In a structural engineering sense, the prototypical problem shown in Figure 6.1 a) is redundant, because the two contact flanks mean that the loads carried on each individual contact cannot be determined by considerations of equilibrium alone, and we would therefore normally begin our analysis by forming a finite element model of the problem using a commercial code. This code outputs the local contact pressure, $p(x)$, and shear tractions, $q(x)$. These outputs, along with the geometry of the structure together with the coefficient of friction, provide a connection between the external loads and the local response acting on the contact interface

$$\left\{ \begin{array}{c} P \\ Q \\ M \\ \sigma_{\mathrm{A}} \\ \sigma_{\mathrm{B}} \end{array} \right\} = \left[\begin{array}{ccc} e_{11} & e_{12} & e_{13} \\ e_{21} & e_{22} & e_{23} \\ e_{31} & e_{32} & e_{33} \\ e_{41} & e_{42} & e_{43} \\ e_{51} & e_{52} & e_{53} \end{array} \right] \left\{ \begin{array}{c} F_C \\ F_V \\ T \end{array} \right\} \ . \tag{6.4}$$

Since the loads P, Q, M, σ_A and σ_B are the necessary inputs to any half-plane analysis, Figure 6.1 b), it is the intention of this section to provide means

of determining this connection, here indicated by the matrix entries e_{ij}, for $i = 1, 2, 3, 4, 5$ and $j = 1, 2, 3$. While the first nine matrix entries (e_{1j}, e_{2j}, e_{3j}) manifest themselves in evaluating Eqs. (6.1, 6.2, 6.3), determining the remaining entries (e_{4j}, e_{5j}) is far more complicated. But good estimates of σ_{A} and σ_{B} are needed in order to construct, firstly, an analytical model of the individual contact using a model based on half-plane domains, where the shape of the contacting surfaces is the same as the corresponding function for the prototypical contact. The half-plane analysis becomes advantageous because the computationally justifiable resolution of the finite element model is too poor to investigate thoroughly the partial slip problem in full detail [Banerjee et al., 2009]. Secondly, by knowing the individual remote stresses present in each body, a far more accurate representation of the propagation stresses for potentially initiated cracks in the prototype can be applied when a simpler laboratory set up is used in an experimental investigation.

Once the values for all five contact loads, P, Q, M, σ_{A} and σ_{B} are found, the whole of the family of solutions for partial-slip analysis becomes available, for example the pioneering solutions of Cattaneo and Mindlin [Cattaneo, 1938], [Mindlin, 1949] and more recent developments [Andresen et al., 2020b], including dislocation-based formulations [Moore et al., 2018], [Moore and Hills, 2018]. We wish to emphasise that, for reasons which will become clear, the finite problem is investigated under fully adhered conditions. This simply allows us to exploit specific properties of the tractions arising during loading which are relevant in identifying the tension components. However, this does not imply that any subsequent analysis must be carried out with this assumption. We will develop the problem in stages.

6.1 Proportional Loading with no Moment Developed

Figure 6.2 shows two very common loading sequences for a P, Q, σ-problem neglecting the effect of a moment. In red we see a sequential order of load application and in green we see proportional loading from one load point to another. The sequence in which the loads are applied greatly affects the procedure we wish to

develop. In real problems the external loads may not be applied separately, in the sense of forming the contact first, and then applying the forces which excite shear but, since it is of interest academically, we discuss details of sequential loading in detail in Appendix A.2.

Usually, the external loads applied have the effect of exerting all local loads proportionally, so that

$$\frac{\mathrm{d}P}{P} = \frac{\mathrm{d}M}{M} = \frac{\mathrm{d}Q}{Q} = \frac{\mathrm{d}\sigma_{\mathrm{A}}}{\sigma_{\mathrm{A}}} = \frac{\mathrm{d}\sigma_{\mathrm{B}}}{\sigma_{\mathrm{B}}} \,. \tag{6.5}$$

The problem becomes significantly more complicated when there is a moment present, and it is not possible to treat the problem as comprehensively (see §6.2) so here we will begin by looking in some detail at problems where the moment may be neglected. Consider the problem shown in Figure 6.1 a) and b), and suppose that the contacting bodies are elastically similar. In our analysis we will neglect the shear tractions induced by the application of the normal load as they will be much smaller in magnitude than the contact pressure when the bodies are elastically similar and arise only because the contacting bodies usually have different domain shapes. While the remarks about deducing the values of normal load and shear force (P, Q) as traction resultants still apply, we now need a means of finding the individual remote tensions ($\sigma_{\mathrm{A}}, \sigma_{\mathrm{B}}$). To simplify even further, we will look at the reduced case of a contact in which the indenter is also symmetric, so that in the half-plane formulation of Figure 6.1 b), $b = a$. Moreover, this also implies that we neglect the presence of the vibrational external load, F_V, which somewhat simplifies the matrix system Eq. (6.4).

We shall begin by describing a methodology for finding the bulk tension difference, $\sigma = \sigma_A - \sigma_B$. Suppose that we have a contact whose current half-width is a, and we make a small change, ΔP, in normal load. The corresponding change in contact pressure is given by [Hills et al., 2011]

$$\Delta p(x) = \frac{\Delta P}{\pi\sqrt{a^2 - x^2}} \,. \tag{6.6}$$

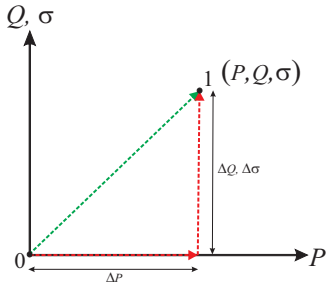


Figure 6.2: Sequential loading (red) and proportional loading (green) for a P, Q, σ-problem [Andresen et al., 2020e].

If at the same time there are small changes in shear force, ΔQ, and differential bulk tension, $\Delta\sigma$, the change in shear traction, $\Delta q(x)$, generated is given by [Hills et al., 2011]

$$\Delta q(x) = \frac{\Delta Q}{\pi\sqrt{a^2 - x^2}} + \frac{\Delta\sigma x}{4\sqrt{a^2 - x^2}} \, . \tag{6.7}$$

If full stick is to be maintained during a positive load increment we require that [Hills et al., 2011]

$$\frac{|\Delta Q|}{\Delta P} + \frac{\pi}{4}\frac{a\Delta\sigma}{\Delta P} < f \, . \tag{6.8}$$

We wish to find the change in interfacial shear traction moving linearly from an unloaded state 0 to state 1 $[P_1, Q_1, \sigma_1]$[1], see Figure 6.2, under conditions which ensure full stick, i.e. inequality (6.8) is satisfied. Suppose we also know, from the contact geometry, the contact law, $a = g(P)$, and we denote the contact pressure distribution at normal load P by $p(x, P)$. The contact pressure at state 1 is given by integrating Eq. (6.6),

$$p(x) = \frac{1}{\pi}\int_{P_x}^{P} \frac{\mathrm{d}\tilde{P}}{\sqrt{a^2 - x^2}} \, , \tag{6.9}$$

where $g(P_x) = x$. We make the change of variable $\tilde{a} = g(\tilde{P})$ in the integrand, which gives

$$p(x) = \frac{1}{\pi}\int_{x}^{a} \frac{1}{g'(\tilde{P})}\frac{\mathrm{d}\tilde{a}}{\sqrt{\tilde{a}^2 - x^2}} \, , \tag{6.10}$$

where a prime indicates differentiation with respect to the argument.

[1]For simplicity, we will omit the subscript for the load state from here on.

Now we consider the developing shear tractions and study first, for simplicity, the effect of a simultaneously exerted shear force alone. Then, from Eq. (6.8), we require the change in normal and shear load to be

$$\frac{\Delta Q}{\Delta P} = \frac{Q}{P} = \lambda < f \ , \tag{6.11}$$

where the Δ terms indicate the change in load from state 0 and 1. Hence

$$\Delta q(x) = \frac{\lambda \Delta P}{\pi\sqrt{a^2 - x^2}} \ , \tag{6.12}$$

so that, if we apply a shear force only,

$$q(x, P) = \lambda p(x, P) \ . \tag{6.13}$$

If we introduce a differential bulk tension as well, so that both develop concurrently (satisfying the 'proportional loading' property), and set

$$\eta = \frac{a\Delta\sigma}{\Delta P} = \frac{a\sigma}{P} \ , \tag{6.14}$$

($\Delta\sigma \equiv \sigma$ and $\Delta P \equiv P$ as we start from an unloaded state), we see that Eq. (6.12) is now replaced by

$$\Delta q(x) = \frac{\lambda \Delta P}{\pi\sqrt{a^2 - x^2}} + \frac{x\eta\Delta P}{4a\sqrt{a^2 - x^2}} \ . \tag{6.15}$$

Thus after integrating Eq. 6.15 with respect to P, we find that

$$\begin{aligned} q(x, P) &= \int_{P_x}^{P} \left[\frac{\lambda}{\pi\sqrt{a^2 - x^2}} + \frac{x\eta}{4a\sqrt{a^2 - x^2}} \right] \mathrm{d}\tilde{P} \\ &= \left[\lambda + \frac{\eta\pi}{4a} x \right] \frac{1}{\pi} \int_{P_x}^{P} \frac{\mathrm{d}\tilde{P}}{\sqrt{a^2 - x^2}} \ , \end{aligned} \tag{6.16}$$

and, by comparison with Eq. (6.6), we find the traction ratio as

$$\frac{q(x, P)}{p(x, P)} = \lambda + \frac{\eta\pi}{4a} x \ , \tag{6.17}$$

which clearly reduces to Eq. (6.13) in the case that the bulk tension difference is negligible.

As expected, the shear traction is related to a scaled form of the contact pressure. Thus, given output data for $p(x)$ and $q(x)$ from a finite element simulation

or otherwise, we are able to find the implied values of $\Delta\sigma$ and ΔQ, or σ and Q by considering the traction ratio across the contact interface, Eq. (6.17). We shall illustrate this in detail in the upcoming examples.

We now turn our attention to finding the *sum* of the bulk stresses, $\sigma_{\mathrm{A}} + \sigma_{\mathrm{B}}$, and start by writing down the total surface strains arising along the contact interface in the presence of a normal load, P, a shear force, Q, differential tension, $\sigma = \sigma_{\mathrm{A}} - \sigma_{\mathrm{B}}$, and the *average* remote bulk loads, ${}^{\sigma_{\mathrm{A}}+\sigma_{\mathrm{B}}}/_{2}$,

$$\varepsilon_{xx}(x) = \varepsilon_{xx}^{P}(x) + \varepsilon_{xx}^{Q}(x) + \varepsilon_{xx}^{\sigma} + \varepsilon_{xx}^{\sigma_{\mathrm{A}}+\sigma_{\mathrm{B}}}(x) \ , \ -a < x < a. \tag{6.18}$$

The contribution to the total direct strain from a normal force, P, can be written as

$$\varepsilon_{xx}^{P}(x) = \frac{(1-2\nu)}{(1-\nu)\,\tilde{E}}\, p(x) \ , -a < x < a \ , \tag{6.19}$$

where $\tilde{E} = E/\left(1-\nu^2\right)$, E is Young's modulus and ν is Poisson's ratio. As we have found a solution under no-slip conditions, we can also find the implied surface strains resulting from the effects of an applied shear force, Q, and the shear tractions arising from differential bulk tension, σ, which gives

$$\varepsilon_{xx}^{Q}(x) = -\frac{2}{\pi\tilde{E}}\,\lambda \int_{-a}^{a} \frac{p\left(\xi\right)}{x-\xi}\mathrm{d}\xi \ , -a < x < a \ , \tag{6.20}$$

and

$$\varepsilon_{xx}^{\sigma}(x) = -\frac{2}{\pi\tilde{E}}\,\frac{\eta\pi}{4a} \int_{-a}^{a} \frac{p\left(\xi\right)\,\xi}{x-\xi}\,\mathrm{d}\xi \ , -a < x < a \ . \tag{6.21}$$

The total strain distribution within the fully stuck contact will therefore have four contributions, *viz.* the three just derived $\varepsilon_{xx}^{P}(x), \varepsilon_{xx}^{Q}(x), \varepsilon_{xx}^{\sigma}(x)$ together with the effect of the *average* remote bulk loads, i.e.

$$\varepsilon_{xx}^{\sigma_{\mathrm{A}}+\sigma_{\mathrm{B}}}\left(x\right) = \frac{\sigma_{\mathrm{A}} + \sigma_{\mathrm{B}}}{2\tilde{E}} \ . \tag{6.22}$$

Hence, given data for the contact pressure, $p(x)$, from finite element results or otherwise, we can now calculate the individual strain contributions given by Eqs. (6.19, 6.20, 6.21). A comment is appropriate in relation to the evaluation of the integral. We will require the surface strains within the contact ($-a \leq x \leq a$) so that

the integral is interpreted in the Cauchy principal value sense. It will therefore be appropriate to use a numerical integration scheme to evaluate Eqs. (6.20, 6.21), such as Gauss-Chebyshev [Hills et al., 1996]. In order to implement this the integrand should be evaluated at the prescribed integration points. Therefore either the mesh used in the finite element analysis should be chosen so that the nodes lie at the desired coordinates or an appropriate interpolation scheme might be used, such as a variant of that developed by Krenk [Krenk, 1975]. As we have seen, the total direct surface strain is a combination of the strains arising from the tractions and those emanating directly from the sum of the bulk stresses, and so the latter may be found as

$$\sigma_{\mathrm{A}} + \sigma_{\mathrm{B}} = 2\tilde{E}\left[\varepsilon_{xx}(x) - \varepsilon^{P}_{xx}(x) - \varepsilon^{Q}_{xx}(x) - \varepsilon^{\sigma}_{xx}\right]. \tag{6.23}$$

In summary, the following steps are needed in order to find the values of P, Q, σ_{A} and σ_{B} under proportional loading of a symmetric indenter in the absence of a moment:

(i) Find values for the contact tractions $p(x)$, $q(x)$, and $\varepsilon_{xx}(x)$ from finite element simulations or otherwise.

(ii) The contact resultants, P and Q, are found from integrating the tractions using Eqs. (6.1, 6.3).

(iii) The gradient of the linear function ${}^{q(x,P)}/_{p(x,P)} = \lambda + \frac{\eta\pi}{4a}x$ reveals the value of $\sigma = \sigma_{\mathrm{A}} - \sigma_{\mathrm{B}}$, using Eq. (6.14).

(iv) Evaluate the individual contributions to the direct strain, $\varepsilon_{xx}(x)$, using Eqs. (6.19, 6.20, 6.21) and subtract those from the numerical output for the total strain to determine the sum of the bulk stresses using Eq. (6.23).

(v) Finally, output $\sigma_{\mathrm{A}} = {}^{\sigma}/_{2} + {}^{\sigma_{\mathrm{A}}+\sigma_{\mathrm{B}}}/_{2}$ and $\sigma_{\mathrm{B}} = {}^{\sigma_{\mathrm{A}}+\sigma_{\mathrm{B}}}/_{2} - {}^{\sigma}/_{2}$.

We thus have all the required information in the matrix system Eq. (6.4): given inputs F_C, F_V, and T, we output $p(x)$ and $q(x)$ and are then able to follow (i)-(v) to recover the loads necessary for an equivalent half-plane analysis.

One of the advantages of considering the simplified case in which we neglect a moment and any geometrical asymmetry is that it is often possible to find closed-form solutions for the equivalent half-plane model, so we are able to illustrate this methodology for cases in which we already know the relationships in Eq. (6.4), which we shall pursue in §6.1.1. We shall then conclude our discussion of the symmetric problem by discussing an alternative to step (iii) in the methodology that will be of great value to our extension to problems involving a moment or asymmetry in §6.2.

6.1.1 Demonstration of the Methodology for a Hertzian Contact

The motivation behind developing this method is to be able to find the remote stresses applied, which in many real problems such as that shown in Figure 6.1 a) are difficult to interpret. However, in order to illustrate the methodology described by the steps (i)-(v), we shall, as a first example, forgo the wider geometry that leads to the contact as illustrated in Figure 6.1 a) and consider the well-known example of a Hertzian contact of two elastically-similar cylinders. We perform finite element simulations of the configuration illustrated in Figure 6.3 to output the contact tractions $p(x)$ and $q(x)$. Obviously, this is a contrived problem where we actually know the desired values P, Q, σ_A and σ_B, but we will recover the remote stresses from the finite element output for the tractions, $p(x)$ and $q(x)$, and the direct surface strain, ε_{xx}, alone, *as if* σ_A *and* σ_B *were unknowns*, i.e. we shall follow steps (iii)-(v) algorithmically to recover the correct values of the bulk stresses. Generally, the finite element output alone, together with an appropriate numerical scheme, suffices to solve the problem, and the closed-form results, if tractable, serve as a point of comparison and simplifies the calculation.

Figure 6.3 shows the input configuration for our finite element simulations. We consider two half-planes connected by a Hertzian-type geometry with radius, R, over a contact patch spanning $[-a \quad a]$. Body B is constrained in the vertical direction such that the normal load is supported and shear loading in the lateral direction is balanced between the two bodies. We thereby acknowledge that the half-planes are

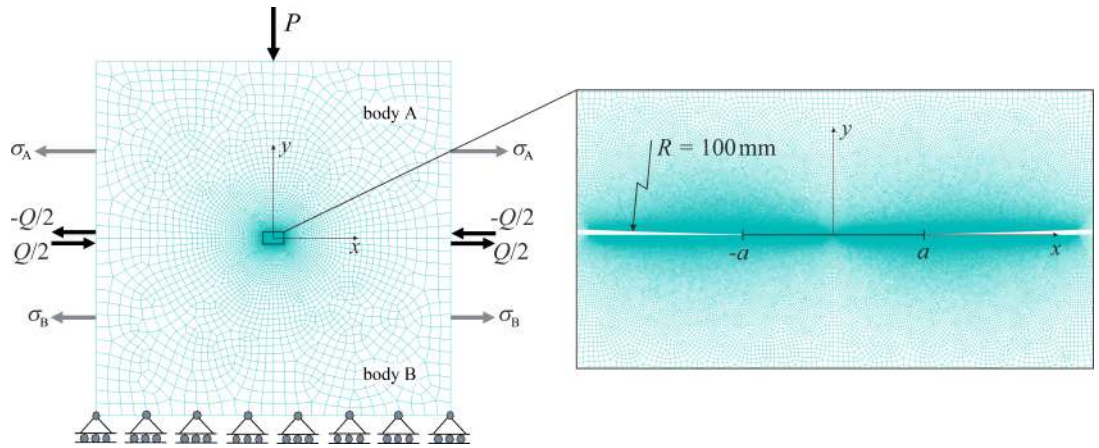


Figure 6.3: FE-Model of two half-planes connected by a Hertzian-type geometry subject to loads P, Q, σ_{A}, and σ_{B} [Andresen et al., 2020e].

only approximated as each body is finite in size, where the proportion of contact half-width to width or height of the two bodies is less than 1/100. The four loads, P, Q, σ_{A}, and σ_{B} are applied in proportion from an unloaded state under fully adhered conditions until they reach the desired load state, as shown in Figure 6.2.

We use the commercial finite element solver Abaqus to solve the contact problem with quadratic quadrilateral and triangular elements under plane strain conditions with a mesh refinement towards the contact interface so that the element size to contact size ratio is less than 1/1000. The contact interface is meshed such that nodes are coincidental. The contact is modelled as a surface-to-surface interaction with default properties for normal and tangential behaviour suppressing relative lateral motion of the two bodies.

The contact tractions extracted from the finite element simulation are shown in Figure 6.4, where the input values of P, Q are such that $\lambda = 0.347$. The input for the remote tensions is and $\sigma_{\mathrm{A}} = 80^{\mathrm{N}}/_{\mathrm{mm}^2}$ and $\sigma_{\mathrm{B}} = 180^{\mathrm{N}}/_{\mathrm{mm}^2}$ giving $\eta = -0.08$. Thus, our aim is now to reproduce these by following step (iii).

Given P, the contact law $a = g(P)$ for a Hertzian geometry is given by [Hertz, 1881]

$$a = \left(\frac{8PR}{\pi\tilde{E}}\right)^{\frac{1}{2}}. \tag{6.24}$$

Thus, for the input value of P and with $R = 100\mathrm{mm}, \tilde{E} = 225\ 10^{3\mathrm{N}}/_{\mathrm{mm}^2}$, the contact size at state 1 as defined in Figure 6.2 is $a = 1.4\mathrm{mm}$. We now plot the ratio

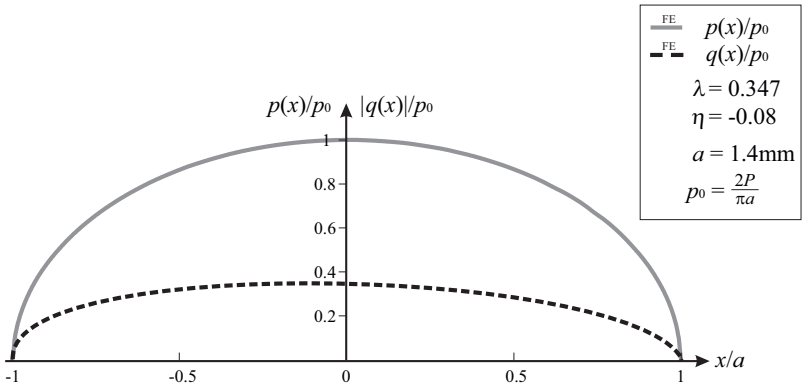


Figure 6.4: Normal and shear tractions for a Hertzian geometry under proportional loading in fully adhered conditions [Andresen et al., 2020e].

$q(x)/p(x)$ in Figure 6.5 and find a linear fit, which referring back to (iii) finds that

$$\lambda = 0.35 \quad \text{and} \quad \frac{\eta\pi}{4a} = -0.05\text{mm}^{-1} \Rightarrow \eta = -0.09 \Rightarrow \sigma \approx -111^{\text{N}}/_{\text{mm}^2}. \tag{6.25}$$

As is evident, we are reliably extracting plausible values of λ and η from step (iii). To recover the sum of the bulk stresses, we follow step (iv) and consider the direct strain in the contact interface. We can output the total strain $\varepsilon_{xx}(x)$ directly from the finite element simulations. To evaluate $\sigma_A + \sigma_B$, we also need the individual contributions $\varepsilon^P_{xx}(x), \varepsilon^Q_{xx}(x), \varepsilon^\sigma_{xx}(x)$. While these can be calculated numerically from the given data for $p(x)$, we note that, for this simple example, we can in fact evaluate them in closed form. By integrating Eq. (6.10), the pressure distribution is given by

$$p(x) = \frac{\tilde{E}}{4R}\int_x^a \frac{\tilde{a}\,\mathrm{d}\tilde{a}}{\sqrt{\tilde{a}^2 - x^2}} = \frac{\tilde{E}}{4R}\sqrt{a^2 - x^2}\,, \tag{6.26}$$

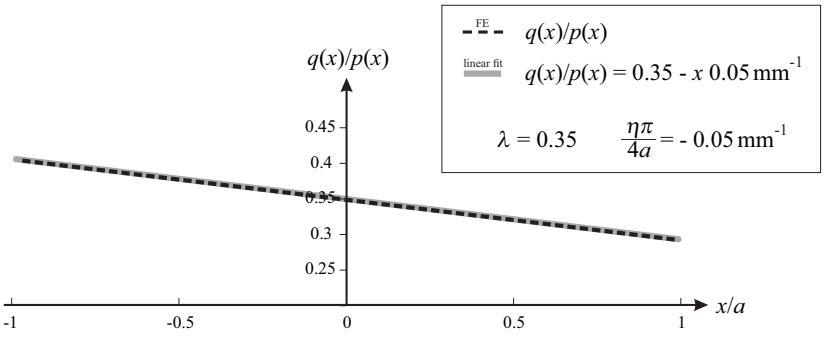


Figure 6.5: Traction ratio between shear and normal tractions for a Hertzian geometry under proportional loading in fully adhered conditions [Andresen et al., 2020e].

so that directly evaluating Eq. (6.19) yields

$$\varepsilon_{xx}^{P}(x) = \frac{(1-2\nu)}{(1-\nu)\,\tilde{E}}\,p(x) = \frac{(1-2\nu)}{4R\,(1-\nu)}\,\sqrt{a^2-x^2}\;, \tag{6.27}$$

while Eq. (6.20) gives

$$\varepsilon_{xx}^{Q}(x) = -\frac{2}{\pi\tilde{E}}\,\lambda\int_{-a}^{a}\frac{p\,(\xi)}{x-\xi}\mathrm{d}\xi = -\frac{1}{2R}\frac{Q}{P}\,x\;, \tag{6.28}$$

and Eq. (6.21) gives

$$\varepsilon_{xx}^{\sigma}(x) = -\frac{2}{\pi\tilde{E}}\,\frac{\eta\pi}{4a}\int_{-a}^{a}\frac{p\,(\xi)}{x-\xi}\,\xi\,\mathrm{d}\xi = -\frac{1}{16R}\frac{\sigma}{P}\left(a^2-2x^2\right)\;. \tag{6.29}$$

Thus, we find that

$$\frac{\sigma_{\mathrm{A}}+\sigma_{\mathrm{B}}}{2\tilde{E}} = \varepsilon_{xx}(x) + \frac{1}{2R}\frac{Q}{P}\,x + \frac{1}{16R}\frac{\sigma}{P}\left(a^2-2x^2\right) - \frac{(1-2\nu)}{4R\,(1-\nu)}\,\sqrt{a^2-x^2}\;, \tag{6.30}$$

where $|x| < a$. Figure 6.6 illustrates that Eq. (6.30) yields a constant value using the analytical description and an almost constant value of $\sigma_{\mathrm{A}}+\sigma_{\mathrm{B}} \approx 260\,{}^{\mathrm{N}}/_{\mathrm{mm}^2}$ using the finite element output for the direct strain. The slight curvature in the numerical result might stem from the half-plane approximation in the finite element model, see Figure 6.3.

Therefore, combining our values for η and $\sigma_{\mathrm{A}}+\sigma_{\mathrm{B}}$, we finally back out the values

$$\sigma_{\mathrm{A}} \approx 74\,{}^{\mathrm{N}}/_{\mathrm{mm}^2} \text{ and } \sigma_{\mathrm{B}} \approx 186\,{}^{\mathrm{N}}/_{\mathrm{mm}^2} \tag{6.31}$$

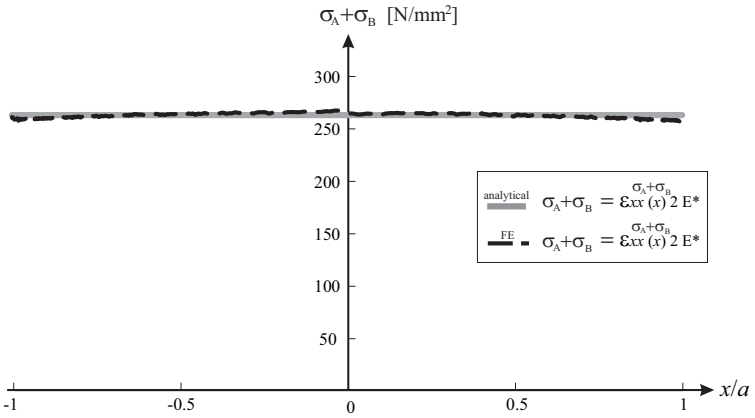


Figure 6.6: Sum of the bulk stresses, $\sigma_{\mathrm{A}}+\sigma_{\mathrm{B}}$, obtained using Eq. (6.30) and finite element output for the direct strain, $\varepsilon_{xx}(x)$, [Andresen et al., 2020e].

from step (v), which again shows good agreement with the (for this example known) inputs.

With this example, we demonstrated that it is possible to recover all external load inputs, P, Q, σ_{A}, and σ_{B}, from the tractions and direct strains within the contact interface alone. In §6.2, we will show how this methodology may be adapted to find answers to the same questions in more complicated problems, for instance when a moment is present or for redundant systems such as the dovetail geometry for gas turbine fan blade joints.

6.1.2 Using Asymptotes in Step (iii)

In most real problems, we will not know the contact geometry in a simple form, but the steps (i)-(v) can still be employed. We conclude by reconsidering step (iii). Given numerical results for $p(x)$ and $q(x)$, there are basically two routes which may be followed. The most obvious method is to plot the ratio $q(x)/p(x)$ across the length of the contact from the finite element results directly, as we did in §6.1.1. This ratio should be linear in x and have an intercept giving the value of λ and the gradient $\eta\pi/4a$. This is the preferred method as it applies averaging of the given numerical results.

An alternative method, whose extension to the asymmetric case will be exploited in the subsequent section, is to look in detail at the traction-ratio towards the ends of the contact, where the contact edge values are given by

$$\frac{q(a^-)}{p(a^-)} = \lambda + \frac{\eta\pi}{4} = \frac{Q}{P} + \frac{\pi a\sigma}{4P} \,, \tag{6.32}$$

and

$$\frac{q(-a^+)}{p(-a^+)} = \lambda - \frac{\eta\pi}{4} = \frac{Q}{P} - \frac{\pi a\sigma}{4P} \,. \tag{6.33}$$

If we move the origin to the contact edge and set $s = a + x$, $t = a - x$, we can express the normal and shear tractions near the contact edges in asymptotic form as [Fleury et al., 2017]

$$p(s) \approx K_P^- \sqrt{s} \,, \qquad p(t) \approx K_P^+ \sqrt{t} \,, \tag{6.34}$$

$$q(s) \approx K_Q^- \sqrt{s} \,, \qquad q(t) \approx K_Q^+ \sqrt{t} \,, \tag{6.35}$$

and as $s, t \to 0$, the ratio is given as

$$\frac{q(-a^+)}{p(-a^+)} = \frac{K_Q^-}{K_P^-} \,, \tag{6.36}$$

$$\frac{q(a^-)}{p(a^-)} = \frac{K_Q^+}{K_P^+} \,. \tag{6.37}$$

Thus, we intend to find the multipliers $(K_P^-, K_P^+, K_Q^-, K_Q^+)$ from the finite element analysis output by plotting the ratios $p(s)/\sqrt{s}, q(s)/\sqrt{s}$ and taking the limit $s \to 0$, and similarly at the other end point. We can then find (Q, σ) from equations (6.32) and (6.33), fulfilling step (iii). The other steps can be pursued as discussed previously.

6.2 Problems when a Moment is Developed

We now turn to problems which involve the effects of asymmetry, which may stem from an externally applied moment or an inherent asymmetry of the contacting geometry. As we shall see, it is not possible to write down a closed-form expression for the traction ratio as we did for the symmetric case in Eq. (6.17) and we will need to make use of an asymptotic description of the ratio near the contact edges similar to that outlined in §6.1.2 in order to find the differential tension, $\sigma = \sigma_{\mathrm{A}} - \sigma_{\mathrm{B}}$. The other steps, however, translate directly into the asymmetric regime.

Suppose that we have a contact spanning [-a b], and we make a small change, ΔP in normal load together with a small change in applied moment, ΔM. The corresponding change in contact pressure is given by [Sackfield et al., 2001]

$$\Delta p(x) = \frac{\Delta P}{\pi\sqrt{(a+x)\,(b-x)}} + \frac{4\Delta M\,(2x+a-b)}{\pi\,(a+b)^2\sqrt{(a+x)\,(b-x)}} \,. \tag{6.38}$$

If, at the same time, there are small changes in shear force, ΔQ, and differential bulk tension, $\Delta\sigma$, the change in shear traction, $\Delta q(x)$, generated is given by

$$\Delta q(x) = \frac{\Delta Q}{\pi\sqrt{(a+x)\,(b-x)}} + \frac{\Delta\sigma\,(2x+a-b)}{8\sqrt{(a+x)\,(b-x)}} \,. \tag{6.39}$$

The contact law is now given by $a = a(P, M)$ and $b = b(P, M)$. Therefore

$$\mathrm{d}a = \frac{\partial a}{\partial P}\mathrm{d}P + \frac{\partial a}{\partial M}\mathrm{d}M, \quad \mathrm{d}b = \frac{\partial b}{\partial P}\mathrm{d}P + \frac{\partial b}{\partial M}\mathrm{d}M. \tag{6.40}$$

We demand a proportional load path (Eq. (6.5)), i.e. $\mathrm{d}M/M = \mathrm{d}P/P$, so that

$$\mathrm{d}a = \left[\frac{\partial a}{\partial P} + \frac{\partial a}{\partial M}\frac{\mathrm{d}M}{\mathrm{d}P}\right]\mathrm{d}P = \left[\frac{\partial a}{\partial P} + \frac{\partial a}{\partial M}\left(\frac{M}{P}\right)\right]\mathrm{d}P\,, \tag{6.41}$$

$$\mathrm{d}b = \left[\frac{\partial b}{\partial P} + \frac{\partial b}{\partial M}\frac{\mathrm{d}M}{\mathrm{d}P}\right]\mathrm{d}P = \left[\frac{\partial b}{\partial P} + \frac{\partial b}{\partial M}\left(\frac{M}{P}\right)\right]\mathrm{d}P\,, \tag{6.42}$$

and hence, in place of equation (6.9), we now have

$$p(x) = \frac{1}{\pi}\int_{P_x}^{P}\left[\frac{1}{\sqrt{(a+x)(b-x)}} + \frac{4(2x+a-b)}{(a+b)^2\sqrt{(a+x)(b-x)}}\frac{\mathrm{d}M}{\mathrm{d}\tilde{P}}\right]\mathrm{d}\tilde{P}\,, \tag{6.43}$$

and proportional loading also requires that $\mathrm{d}P/P = \mathrm{d}Q/Q = \mathrm{d}\sigma/\sigma$ giving

$$q(x) = \int_{P_x}^{P}\left[\frac{1}{\pi\sqrt{(a+x)(b-x)}}\frac{\mathrm{d}Q}{\mathrm{d}\tilde{P}} + \frac{(2x+a-b)}{8\sqrt{(a+x)(b-x)}}\frac{\mathrm{d}\sigma}{\mathrm{d}\tilde{P}}\right]\mathrm{d}\tilde{P}\,. \tag{6.44}$$

Following the symmetric case from §6.1, we would like to reveal the ratio

$$\frac{q(x)}{p(x)} = \frac{\displaystyle\int_{P_x}^{P}\left[\frac{1}{\sqrt{(a+x)(b-x)}}\frac{\mathrm{d}Q}{\mathrm{d}\tilde{P}} + \frac{\pi(2x+a-b)}{8\sqrt{(a+x)(b-x)}}\frac{\mathrm{d}\sigma}{\mathrm{d}\tilde{P}}\right]\mathrm{d}\tilde{P}}{\displaystyle\int_{P_x}^{P}\left[\frac{1}{\sqrt{(a+x)(b-x)}} + \frac{4(2x+a-b)}{(a+b)^2\sqrt{(a+x)(b-x)}}\frac{\mathrm{d}M}{\mathrm{d}\tilde{P}}\right]\mathrm{d}\tilde{P}}\,, \tag{6.45}$$

but it is difficult to proceed with the integrals on the right-hand side. In a real problem we will know both $p(x)$ and $q(x)$ together with

$$\frac{Q}{P} = \lambda, \quad \frac{M}{aP} = \gamma\,, \tag{6.46}$$

from the force resultants Eq. (6.1, 6.2, 6.3), where a has been chosen arbitrarily as means of normalisation. It is the quantity

$$\frac{a\,\sigma}{P} = \eta\,, \tag{6.47}$$

and hence σ, that we seek. Although we cannot evaluate Eq. (6.45) for a general point in closed-form, we are able to find the limits of the traction ratio at each end of the contact, where η is the only remaining unknown. The results, which are generalisations of those found in §6.1.2, are

$$\frac{q(-a^+)}{p(-a^+)} = \frac{1}{8}\frac{\left(1+\left(\frac{b}{a}\right)\right)^2\left[8\lambda - \pi\eta\left(1+\frac{b}{a}\right)\right]}{\left(1+\left(\frac{b}{a}\right)\right)^2 - 4\gamma\left(1+\frac{b}{a}\right)}\,, \tag{6.48}$$

$$\frac{q(b^-)}{p(b^-)} = \frac{1}{8}\frac{\left(1+\left(\frac{b}{a}\right)\right)^2\left[8\lambda+\pi\eta\left(1+\frac{b}{a}\right)\right]}{\left(1+\left(\frac{b}{a}\right)\right)^2+4\gamma\left(1+\frac{b}{a}\right)}\,, \tag{6.49}$$

where details of finding the limits can be found in the Appendix A.3. We note that we actually only need one of Eq. (6.48) and Eq. (6.49) to determine η and hence σ. In practice, however, the second equation serves as a excellent check on the accuracy of the results.

All that remains is to find the sum of the bulk stresses, $\sigma_{\rm A}+\sigma_{\rm B}$, which can be evaluated by considering the direct strain in the contact interface, as previously. The only small change is somewhat notational, since the presence of a moment means that we replace the term $\varepsilon_{xx}^{P}(x)$ in Eq. (6.19) by $\varepsilon_{xx}^{P,M}(x)$.

Therefore, in summary, when there is asymmetry in the problem, the steps necessary to find the values of P, M, Q, $\sigma_{\rm A}$ and $\sigma_{\rm B}$ in the presence of a moment can be summarised as follows.

(I) Find values for the contact tractions $p(x)$, $q(x)$, and $\varepsilon_{xx}(x)$ from finite element simulations or otherwise.

(II) The contact resultants for P, M, and Q are found from integrating the tractions, using Eqs. (6.1, 6.2, 6.3).

(III) Obtain the near edge multipliers $(K_P^-, K_P^+, K_Q^-, K_Q^+)$ from the finite element output by plotting the ratios $p(s)/\sqrt{s}, q(s)/\sqrt{s}$ and taking the limit $s \to 0$, and similarly at the other end point.

(IV) Use the ratios of the asymptotic multipliers in order to obtain the left-hand sides of Eq. (6.48) and (6.49), and, hence, a way of determining the value of η and thus $\sigma = \sigma_{\rm A} - \sigma_{\rm B}$.

(V) Evaluate the individual contributions to the direct strain, $\varepsilon_{xx}(x)$, using Eqs. (6.19, 6.20, 6.21) and subtract those from the numerical output for the total strain to determine the sum of the bulk stresses using Eq. (6.23).

(VI) Finally, output $\sigma_{\rm A} = \sigma/2 + \sigma_{\rm A}+\sigma_{\rm B}/2$ and $\sigma_{\rm B} = \sigma_{\rm A}+\sigma_{\rm B}/2 - \sigma/2$.

This algorithm gives the values of the loads necessary to formulate an equivalent half-plane representation of the full contact problem (Figure 6.1). We shall now present an example that illustrates the effectiveness of this methodology.

6.3 Dovetail Geometry Example

We return to the example of a fan blade dovetail root contact displayed in Figure 6.1 a), and examine the implementation of a numerical analysis in the complex scenario of this prototype problem. The joint is commonly used to connect fan blades to the rotor disk in jet engines. As the engine starts spinning, centrifugal and expansion forces, F_{C} and T, will act on the blade and disk, respectively. Note that, here, we consider a symmetrical configuration for the sake of simplicity (i.e. $F_V = 0$), while in reality a vibrational component may act on the blade thereby inducing an asymmetry about the centre-axis of the blade and a *steady-state* variation of the local load components we are interested in.

The system, as depicted in Figure 6.7, is statically indeterminate. The equilibrium equations are insufficient to determine the local forces and reactions. As explained in the introduction, the finite element analysis of the structure allows us to connect the external loads to the local response where a matrix with complicated, yet unknown entries, makes this connection, see Eq. (6.4). Our algorithm (I)-(VI) allows us to determine these local forces.

The finite element model consists of a disk and a blade-representation with symmetry conditions exploited about the vertical centre-axis and the disk supports forces in the vertical direction. As required by the method presented, the external loads, F_{C} and T, are applied proportionally from an unloaded state under fully adhered conditions until they reach the desired load state. The structure is meshed with a gradual mesh refinement towards the contact interface and all other properties are the same as in the model used in §6.1.1.

For comparison, and in order to verify that the same contact behaviour is found in a half-plane representation of the dovetail root contact, we use the local loads found above to initiate an interface between two half-planes connected by a flat and

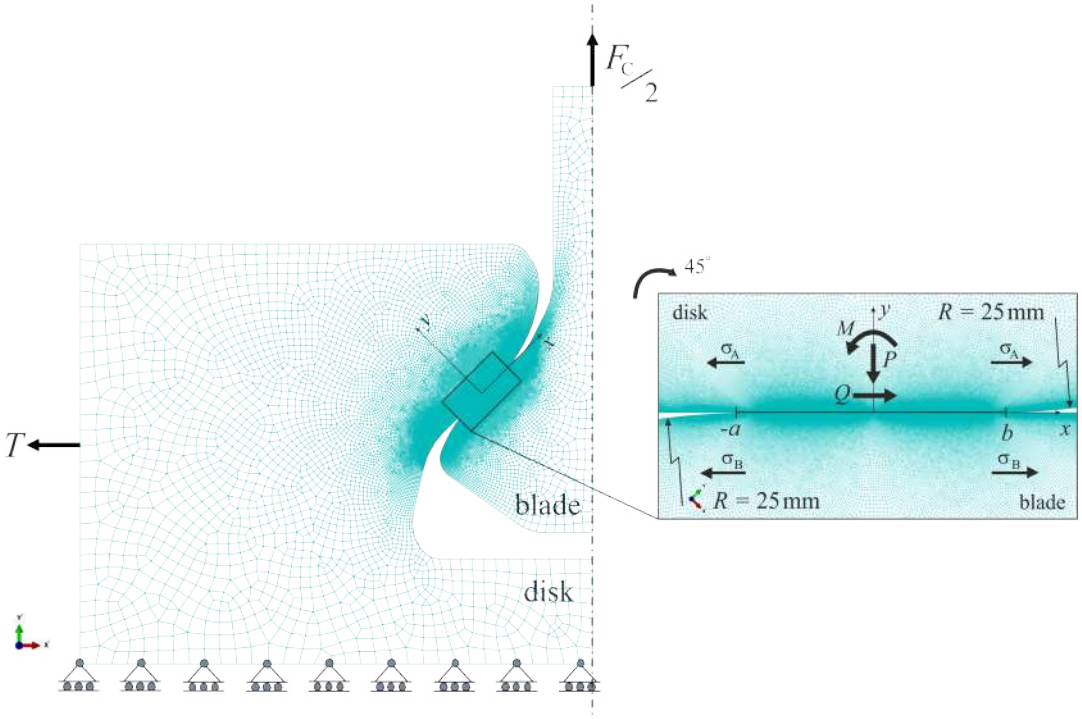


Figure 6.7: Finite element model of a dovetail prototype subject to external loads F_C and T and the local response [Andresen et al., 2020e].

rounded punch where the contacting shape is the same as the corresponding function for the dovetail root contact, see Figure 6.8. In the half-plane representation, we expect to observe the same contact behaviour, up to a reasonable degree of accuracy, as in the prototype example. This means the normal and shear tractions, as well as the direct strain in the contact interface, ought to match between the two problems.

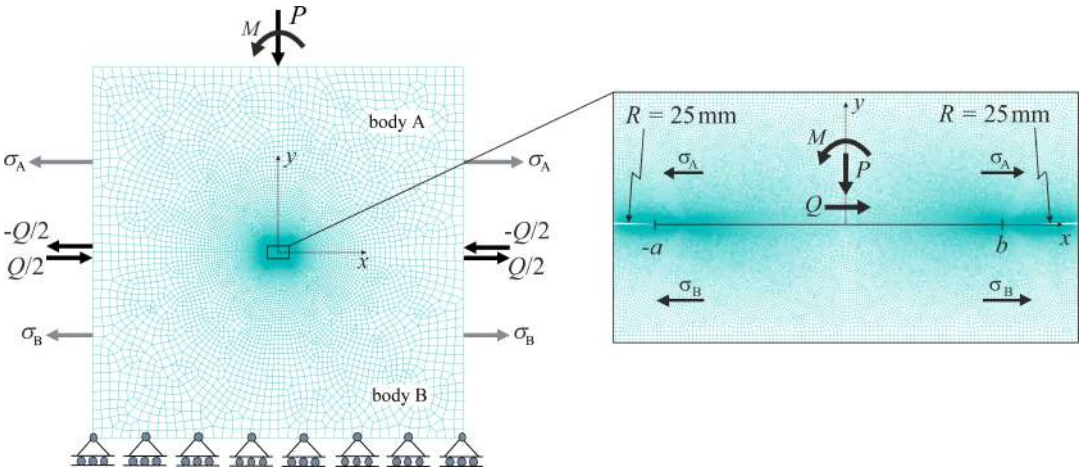


Figure 6.8: Finite element model of two half-planes connected by a flat and rounded geometry subject to loads P, M, Q, σ_A, and σ_B, [Andresen et al., 2020e].

The contact pressure and shear tractions calculated using the two finite element models are displayed in Figures 6.9 a) and b) as the black lines. It is trivial to use these to find the resultants P, M and Q using Eqs. (6.1)–(6.3). To determine σ_{A} and σ_{B}, since $M \neq 0$, we follow (III)-(VI) in using the edge asymptotes introduced in §6.2 to find the difference in bulk tensions, σ, and then use the direct strain, ε_{xx}, within the contact interface to reveal the sum of the bulk stresses, see Figure 6.9 c).

The prototype and half-plane representation differ from one another in terms of contact initialisation and mesh refinement. This may cause a slight difference in the quality of numerical results between the two. Notwithstanding, the normal tractions and contact extent shown in Figure 6.9 match up very well between prototype and half-plane. This indicates that the normal load, P, and moment, M, have been found accurately from the prototype.

The shear tractions are affected by the four load components, normal load, moment, shear load, and differential bulk tension. The comparison of shear tractions shown in Figure 6.9 b) and the direct strain in Figure 6.9 c) gives reassurance

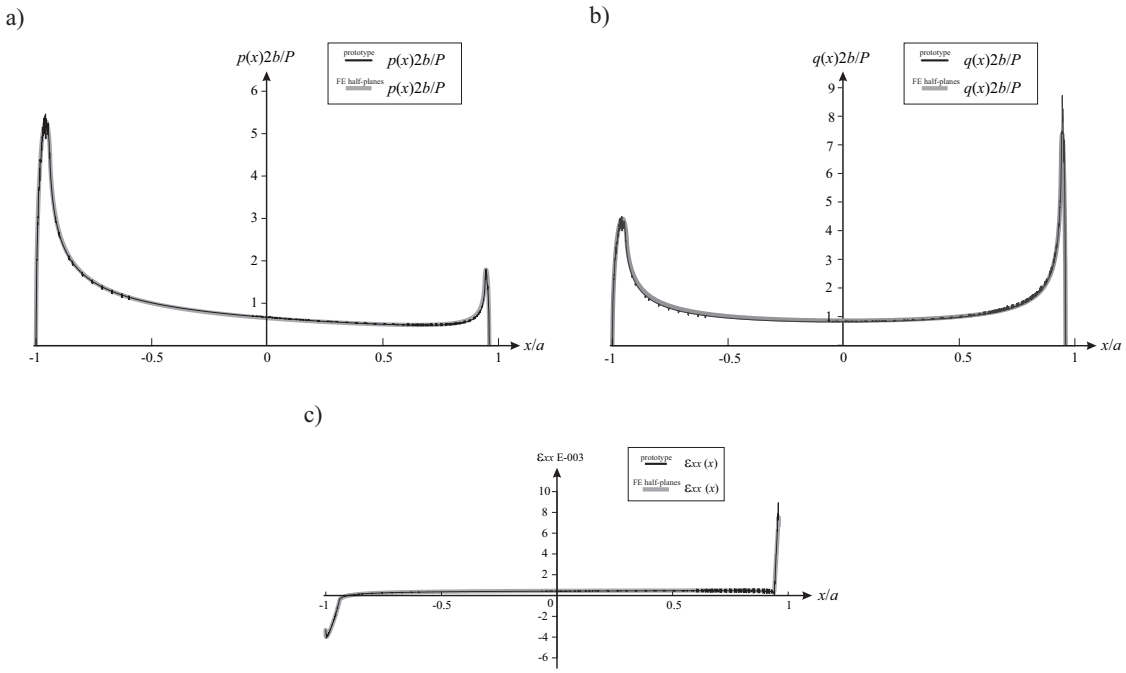


Figure 6.9: Comparison between finite element outputs for prototype, Figure 6.7, and the half-plane representation, Figure 6.8, for a) the normal pressure distribution, $p(x)$, b) the shear traction distribution, $q(x)$, and c) the direct strain, $\varepsilon_{xx}(x)$, along the interface [Andresen et al., 2020e].

that the values derived for Q, σ_{A} and σ_{B} agree very well indeed between prototype and half-plane representation.

6.4 Conclusion

In this Chapter we have developed an algorithm which enables practical contact problems that are analysed, usually, by a finite element procedure using commercial code, to be matched to half-plane idealisations. We set ourselves the task of finding the best choices for the contact loads present in a prototype, that is the normal force P, shear force Q, moment M, and bulk stresses $\sigma_{\mathrm{A}}, \sigma_{\mathrm{B}}$. While exploiting equilibrium conditions to find the traction resultants P, Q, and M is trivial, of particular note is the problem in devising the best-match for the bulk stresses acting parallel with the surface of the contact, σ_{A} and σ_{B}, whose difference is material in modifying the slip pattern, but which are separately responsible for propelling cracks. We were able to extract these values by considering the traction ratio within the contact as well as the direct strains, which gave us two expressions for the difference and sum of the bulk stresses respectively. With the extracted values to hand, we are then able to formulate a half-plane problem to approximate the full prototype behaviour.

We considered two specific examples to illustrate the methodology. The first neglected all asymmetry (thus precluding a moment) and looked at the slightly academic set-up of a Hertzian prototype, in which the results are generally obtainable in closed form by other means. However, we were able to show that the algorithm was robust, finding excellent agreement with the expected values of P, Q, σ_{A} and σ_{B}. The second example considered a prototype dovetail root geometry, in which there is a moment and formulating an equivalent half-plane problem is non-trivial. We used the algorithm to derive the contact loads, and were able to demonstrate that the methodology is again robust.

Thus, given the results of commercial code, we are able to devise an equivalent problem using half-plane theory with suitable loads applied that can be used to analyse finer details of the contact problem that are poorly resolved by the finite element analysis, for example the regions of slip at the contact edges. These results

can then be used to set up a much simpler laboratory fretting fatigue test mimicking the prototype contact behaviour with the highest fidelity possible. While setting up a finite element model of the prototypical problem is a necessary first step in most contact analysis procedures, the finite element analysis also offers the benefit that secondary complications can be added to the problem at any stage and which are usually rather difficult to tackle by the analytical methods developed. For example, the effects of surface coatings can be investigated to a realistic degree by means of a finite element model when an additional elastic layer is added to the interface, thereby modelling the inhomogeneity in material near the interface, as well as the influence of an altered coefficient of friction. In summary, the holistic contact analysis of a prototypical problem remains to be an iterative process in which analytical and numerical methods complement each other.

Note that the contents of this Chapter have been published in [Andresen et al., 2020e].

7
Fretting Fatigue Strength

In the literature encountered, little has been published towards generalising the testing for the fretting fatigue strength of a certain material. In engineering practice, due to the sheer number of parameters possibly affecting crack nucleation and propagation, the fretting fatigue strength is determined as a component-specific property under the given external loading. This results in cost- and time-intensive testing during the design process of a new component and, perhaps even more importantly, lacks generality.

During the design of a highly loaded mechanical assembly, the specific geometry, the contact flanks, and the proximity to a geometric stress concentration may all need to be considered. The intention here is to propose a generalised approach to fretting fatigue testing when frictional slip is dominant and any plasticity is at such a scale that the plastic state is buried well within the slip zones. We will outline these ideas by determining the partial slip behaviour of severely stressed contact edges using asymptotic methods. This enables us to reduce the parameter space responsible for crack nucleation significantly and reveal the fretting fatigue strength in terms of two asymptotic quantities. The method is very simple to apply. We may infer results from a simple laboratory test and which are transferable between a wide range of prototypical geometries. Lastly, we apply the asymptotic

framework to experimental results published in the literature and reinterpret the fretting fatigue strength as the two-parameter specific property.

7.1 Fatigue and Fretting

It is the aspiration of a good mechanical design approach to avoid the occurrence of a sudden failure of a component. Most engineering applications are subject to some form of cyclic loading and therefore fatigue has to be considered as a potential failure mode. While many materials seem to show fatigue-related failures, including composites, plastics, and ceramics, metal fatigue has motivated most of the research on understanding crack initialisation and growth, and in the following we will restrict ourselves to metal components. The first systematic study of fatigue was carried out by Wöhler in the 1860's when he investigated the occurrence of fractures of railway axles [Wöhler, 1870]. He found that components can fail after a certain time of cyclic loading, even when operated within nominally elastic limits, and it is the cyclic stress range rather than the peak stresses which controls the fatigue life [Timoshenko, 1983]. His efforts resulted in the definition of an endurance limit for metal materials below which a high number of loading cycles can be undergone without causing fatigue failure (usually 10^7 or 10^8 cycles are considered *infinite* life in an engineering sense) [Hibbeler, 2016]. On the basis of Wöhler's experimental data Basquin suggested a relationship between stress range and the number of cycles to failure, today well-known known as S-N curves, or sometimes Wöhler curves [Basquin, 1910].

The *total life* of a specimen is commonly measured as the number of cycles it takes from the onset of cyclic loading (start of the test) until the sudden failure by fracture (supposing the run out limit for infinite life is not reached first). In plain fatigue testing, however, this approach often results in a significant spread in the test data as the number of cycles it takes for a crack to initiate may differ from specimen to specimen, depending on tiny interior and surface flaws in the metal structure. This led to a more refined definition of a specimen's life which distinguishes between *nucleation* and *propagation* life. Fracture mechanics provides the tools needed to

investigate the crack growth by using an asymptotic description of the stress state near the crack tip, encapsulated in the stress intensity factor. The commonly accepted crack propagation law by Paris and Erdogan [Paris, 1963] correlates the range of the stress intensity factor to the crack growth rate enabling the separation and quantification of the nucleation and propagation stages of a crack.

Most critical components in today's engineering landscape are designed as to minimise stress raisers in the geometry, by avoiding anything that resembles a notch-like defect. The surface finish is generally manufactured to a standard which removes any pre-existing defects along the surface, keeping the flow of stress as uniform as possible. However, when two components are in contact under conditions of small oscillatory displacements an additional form of crack nucleation at surface level is possibly introduced, namely fretting, and this can weaken the fatigue strength of a component significantly.

An initial investigation of the phenomenon of fretting began in 1927 when Tomlinson carried out a number of experiments designed to study the surface damage and corrosion associated with fretting [Tomlinson, 1927]. He concluded that the relative motion is one parameter affecting fretting damage. The first connection between fretting damage and a reduced fatigue strength was observed by Warlow-Davies in 1941 [Warlow-Davies, 1941] when he carried out a fatigue test after fretting damage had been accumulated on a specimen. A decade later McDowell [McDowell, 1953] combined this two stage test in a single experiment and found an even more detrimental effect on the fatigue strength. A few years later, Fenner and Field observed accelerated crack initiation in areas with fretting damage [Fenner and Field, 1958, Fenner and Field, 1960]. In the last couple of decades a small number of books have been published on the subject including those by Waterhouse [Waterhouse, 1972, Waterhouse, 1981] and by Hills [Hills and Nowell, 1994].

It seems natural that researchers have been trying to understand the contact behaviour that governs the fretting damage, i.e. a mathematically exact quantification of the expected slip-stick pattern which is controlled by a number of parameters and where the known solutions have been discussed in Chapters 3 and 4. The idea

behind those solutions is to quantify the fretting fatigue strength of a new design through an experiment which reproduces the expected fretting damage and therefore reveals the fretting fatigue strength. Bramhall postulated that the local stress field induced by the contact itself indeed controls the nucleation of cracks in the zones of fretting [Bramhall, 1973]. If sufficient to propagate the crack to a critical length, further crack growth would happen in a plain fatigue manner under the cyclic tension applied to the specimen alone [Bramhall, 1973]. Two further observations have been made in fretting fatigue testing; a) the propagation stage takes up only $10\% - 15\%$ of the total life [Szolwinski and Farris, 1998] and b) the repeatability of fretting fatigue tests is significantly improved compared with plain fatigue tests in which cracks initiate freely without notching the specimen [Nowell, 1988]. Those two statements are the reason why in the following we will focus on the total life instead of a separation of nucleation and propagation stage.

7.2 Experimental Set Up and Data

To aid in predicting the fatigue strength of a component, experimental tests are usually carried out using specimens to measure the fatigue strength by applying constant amplitude cyclic loading and establishing contact with a different component, most often two pads are clamped on either side of the specimen, Figure 7.1. Fretting damage is expected to ensue in regions of slip along the interface possibly resulting in cracks sufficiently long to grow under the applied cyclic bulk stress until failure.

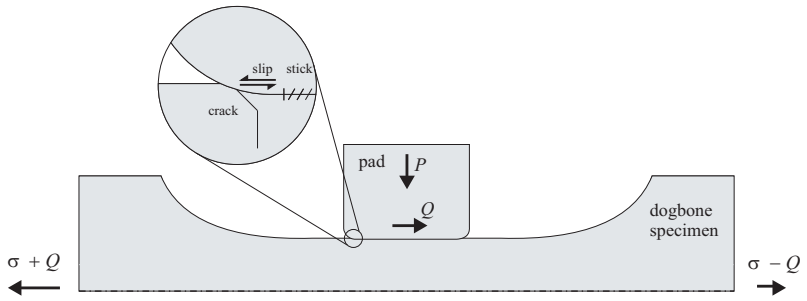


Figure 7.1: Schematic of a common fretting fatigue experimental set up using a flat and rounded pad on a dogbone specimen.

Common geometries for pads are the Hertzian-type cylinders and, because of their relevance to industrial problems, flat and rounded punches. A number of data sets have been published for different materials and different attempts have been made to quantify the fretting fatigue strength. We will refrain from going into the details of these different attempts as that is beyond the scope of this thesis. What they all have in common is a dependence on a large number of parameters and this is what we will try to remedy. In what follows we will examine four data sets from the literature for fretting fatigue strength testing for metal to metal contacts, three for Aluminium alloys and one for a Titanium alloy.

The first set of fretting fatigue data under consideration was conducted by Nowell in the late 1980's [Nowell, 1988] using the Aluminium alloy HE15-TF, see Table 7.1. He confirmed that the fretting fatigue strength varies with contact size and concluded that larger slip amplitudes are the reason for a higher amount of fretting damage increasing the likelihood of crack initiation. All of his tests were carried out under closely controlled conditions of partial slip under constant normal load using cylindrical pads. A schematic of his choice of apparatus is shown in Figure 7.2.

The second data set comes from Szolwinski and Ferris [Szolwinski and Farris, 1998] who attempted to predict the fretting fatigue strength using multiaxial fatigue analysis. The results were coupled with strain-life theory and values of uni-axial fatigue constants from the literature to predict fretting fatigue crack nucleation. They also used an Aluminium alloy, AL 2024-T351, and performed all tests using cylindrical pads.

The third data set stems from Hojati-Talemi et al. [Hojjati-Talemi et al., 2014]. The main aim of their work was to estimate crack nucleation and propagation

Material		Young's Modulus, E [GPa]	Poisson's Ratio, υ [-]	Yield Stress, σ_Y [MPa]	Coefficient of Friciton, f [-]
Aluminium Alloy	AL2024-T3	72	0.33	383	0.7
	AL2024-T351	74	0.33	310	0.7
	HE15-TF	74	0.33	400	0.7
Titanium Alloy	Ti6Al4V	123	0.33	880	0.7

Table 7.1: Material parameters for the Aluminium and Titanium alloys under consideration, including the coefficient of friction.

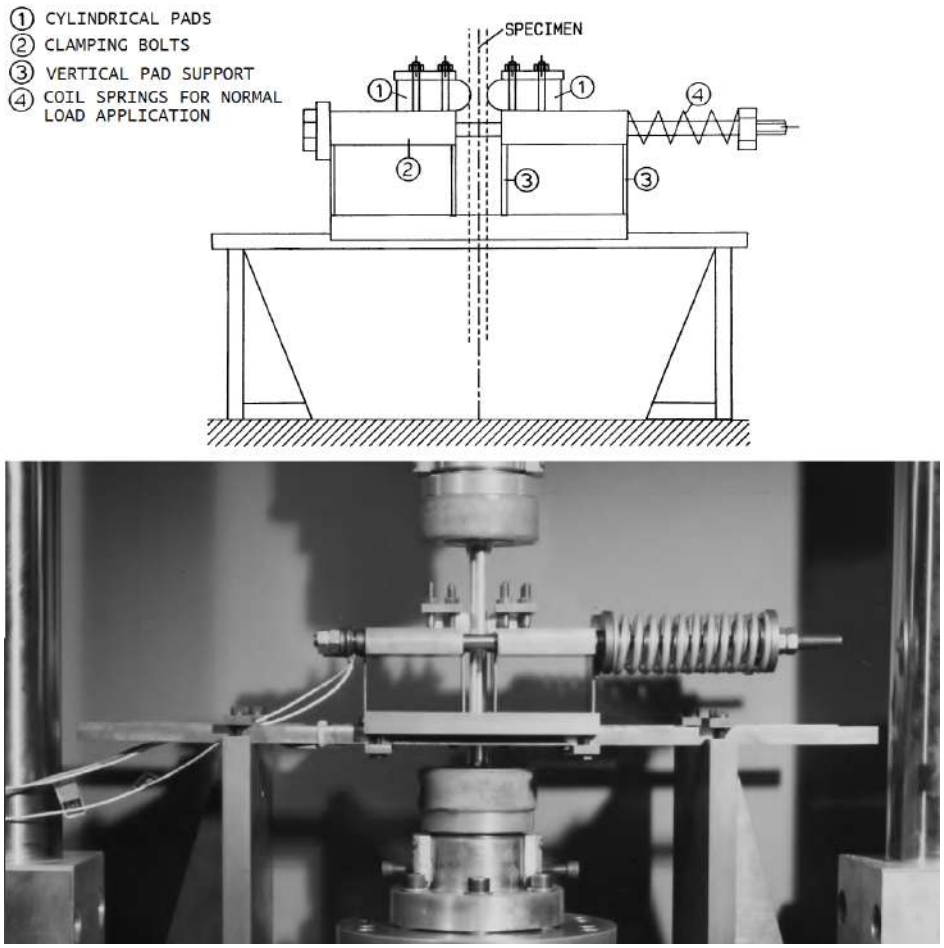


Figure 7.2: Diagram and picture of the fretting fatigue apparatus used by Nowell [Nowell, 1988].

life under conditions of fretting. For the crack nucleation stage they used a numerical approach utilising an uncoupled damage model based on a thermodynamic potential function, and classic fracture mechanics under mixed-mode loading for the propagation stage. The material used was AL2024-T3 and once more the geometry of choice were Hertzian cylinders pressed onto a specimen under constant normal load and in partial slip.

The last data set we will reinterpret is for a different type of alloy, a Titanium Ti6Al4V alloy [Dini, 2003]. The tests were carried out using different flat and rounded geometries. While the radii of the symmetrical pads were varied, the flat portion was kept constant at $2b = 8$mm throughout. These tests were meant to determine the fretting fatigue strength of engineering applications by mimicking the

geometry and loading conditions of the prototype subject to alternating tangential loading under constant normal load.

A summary of all loads and geometry specific parameters for each data set can be found in Appendix A.4. Regardless of the original intent behind those data sets, we will employ the asymptotic ideas outlined in Chapter 5 in order to collapse the multi-parameter space into a two-parameter space and reveal the fretting fatigue strength of the Aluminium and Titanium alloys in a compact and comprehensible manner. We assume the behaviour under conditions of fretting to be comparable for the three data sets on Aluminium so that those comprise 82 data points for Aluminium and the data set on Titanium comprises 67 data points. Note that all experiments have been conducted under nominally fully elastic conditions.

7.3 Applying Asymptotic Methods

In Chapter 5 we developed the asymptotic framework necessary to collapse a vast parameter space - as evident by the experimental data shown in Tables A.2 - A.5 in Appendix A.4 - into a two-parameter space, comprising an asymptotic multiplier for the normal tractions, K_{N}, and one for the alternating shear tractions, ΔK_{T}.

Since closed-form solutions are available for the geometries under consideration all that is needed to find the asymptotic multiplier on the normal tractions is the instantaneous contact law, $^{\mathrm{d}P}/_{\mathrm{d}a}$, for a Hetzian contact and a symmetrical flat and rounded punch. Those can be found from the normal equilibrium condition, so if we recall the contact law for a Hertzian contact of relative curvature $^{1}/_{R}$

$$P_{\mathrm{Hertz}}(a) = \frac{\pi a^2 E}{8\,(1-\nu^2)\,R}\,, \tag{7.1}$$

the instantaneous contact law is given as

$$\frac{\mathrm{d}P_{\mathrm{Hertz}}}{\mathrm{d}a} = \frac{\pi a E}{4\,(1-\nu^2)\,R}\,, \tag{7.2}$$

where E is Young's modulus and ν is Poisson' ratio. The instantaneous contact size is a.

The contact law for a symmetrical flat and rounded punch, F+R, can be found by considering the solution given in Appendix A.1.4 and taking the limits $c \to a$ and $(R_1, R_2) \to R$ so that the vertical equilibrium condition becomes

$$P_{\mathrm{F+R}}(a) = \frac{E}{4(1-\nu^2)R}\left[b\sqrt{a^2-b^2} - a^2 \arccos\left(\frac{b}{a}\right)\right] , \tag{7.3}$$

where b is the half-width of the flat portion and R is the radius at either end of the punch. The instantaneous contact law for a symmetrical flat and rounded punch is given as

$$\frac{\mathrm{d}P_{\mathrm{F+R}}}{\mathrm{d}a} = \frac{E}{4(1-\nu^2)R}\left[\frac{b}{\sqrt{1-(b/a)^2}} - \frac{ab}{\sqrt{a^2-b^2}} + 2a \arccos\left(\frac{b}{a}\right)\right] . \tag{7.4}$$

In §5.1.1 we demonstrated how the asymptotic multiplier for the normal tractions can be expressed in a general form using Mossakovskii methods so that in the symmetrical case Eq. (5.13) becomes

$$K_{\mathrm{N}} = \frac{1}{\pi}\sqrt{\frac{2}{a}}\frac{\mathrm{d}P}{\mathrm{d}a} . \tag{7.5}$$

Since all experimental data were collected for partial slip problems under constant normal load, we know from §5.2.1 that the size of the slip zone, d, can be approximated as

$$d \approx \frac{\Delta K_{\mathrm{T}}}{f K_{\mathrm{N}}} , \tag{7.6}$$

where f is the coefficient of friction and

$$\Delta K_{\mathrm{T}} = \frac{\Delta Q}{\pi\sqrt{2a}} \pm \frac{\Delta\sigma}{4}\sqrt{\frac{a}{2}} , \tag{7.7}$$

where ΔQ and $\Delta\sigma$ follow the sign convention of previous chapters and the upper sign is chosen when the left-hand side of the contact is considered and lower sign when the right-hand side is considered. ΔQ and $\Delta\sigma$ are the range of the shear force and applied tension, respectively. The calculated values for K_{N}, ΔK_{T} and the approximated slip zone size, d, can be found along with the other parameters in Appendix A.4.

7.4 Visualisation of the Fretting Fatigue Strength

The stress concentration close to the edges of an interface is relieved by frictional slip and, as outlined above, this might accelerate crack nucleation compared to conditions of plain fatigue. The zones of frictional slip are the areas where the nucleation of a crack takes place. We argue that capturing the zones of fretting damage is a necessary step in determining the fretting fatigue strength experimentally. As indicated by Eq. (7.6), the slip zone size is a result of the ratio between tangential and normal stress contributions, assuming the coefficient of friction is a finite and constant system property. Parallels can be drawn between a frictional contact interface and a notch-type problem in which the tangential loading is equivalent to a mode II loading along the interface. The normal load, when kept constant, induces a constant mode I loading, which in combination with the oscillation of tangential loads gives rise to the reciprocating movement of surface particles in the slip zones, see Figure 7.3. Using this analogy, we hypothesis that the resulting slip zone size lends itself particularly well as a guiding parameter in the visualisation of the fretting fatigue strength. We note that the majority of a component's total life is dictated by the nucleation phase [Nowell, 1988, Szolwinski and Farris, 1998], so that we will refrain from assessing the propagation stage which can be examined by classical fracture mechanics. We hypothesise, however, that it is not the slip zone size alone which determines the fretting fatigue strength, but both normal and tangential stress components play a role and the slip zone size is merely a consequence of the presence of the two. It is the intention of this section to demonstrate that the

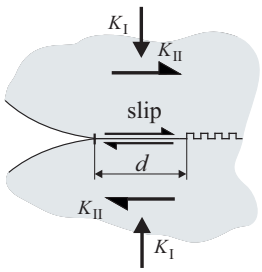


Figure 7.3: Contact edge under a combination of mode I and II loading, giving rise to the slip zone d.

usage of a K_N-ΔK_T parameter space is sufficient to characterise the fretting fatigue strength of a material, independent of geometrical factors.

7.4.1 Aluminium Alloys

Let us begin to visualise the two-parameter space by looking at the effects of the values of K_N for the pooled data set for Aluminium alloys, Figure 7.4. We observe a wide range of K_N values that is available to us. For reasons which will become clear we divide the data set into three groups of equal size, High K_N ranging from 743 $^{MPa}/_{mm^{1/2}}$ – 352 $^{MPa}/_{mm^{1/2}}$, Middle K_N ranging from 311 $^{MPa}/_{mm^{1/2}}$ – 229 $^{MPa}/_{mm^{1/2}}$, and Low K_N ranging from 223 $^{MPa}/_{mm^{1/2}}$ – 169 $^{MPa}/_{mm^{1/2}}$. Figure 7.5 shows the corresponding values for ΔK_T. It would have been ideal if we had had the same band-width of ΔK_T values for each group of K_N. However, we see sufficient similarity between the groups for Low and Middle K_N. The lower range in ΔK_T values for high values of K_N could, on one hand, be owed to the nature of the data set. On the other hand it prompts the question whether K_N has a significant effect on the fatigue strength and limits the achievable life that is still acceptable for engineering purposes to, say $< 10^4$ cycles. In Appendix A.5 we added a diagram showing ΔK_T over K_N with run outs ($> 10^7$ cycles) indicated in order to support the claim that both parameters, K_N and ΔK_T, affect the fretting fatigue strength.

While Eq. (7.6) suggests that an infinite number of combinations of ΔK_T and K_N values can give rise to the same slip zone size, it will become evident that not

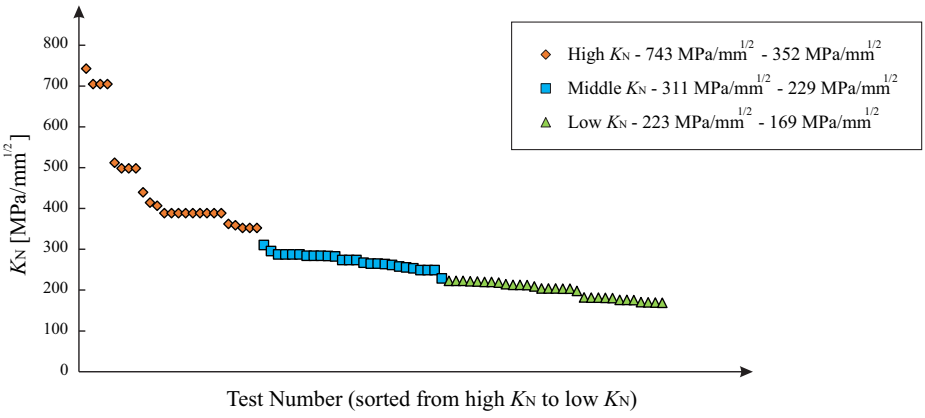


Figure 7.4: Available range of K_N values for the pooled data set of Aluminium alloys.

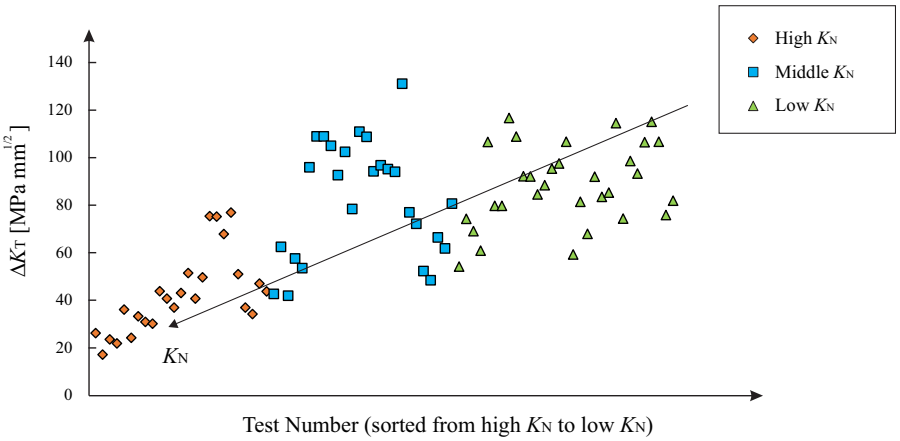


Figure 7.5: Corresponding range of ΔK_T values for the pooled data set of Aluminium alloys.

every combination that gives rise to the same slip zone size has the same total life. In order to support this claim let us plot the slip zone size for each group of K_N against the achieved total life (on a logarithmic scale), Figure 7.6. The first salient impression is the decreased total life that comes with an increased slip zone size for each K_N group. Obviously the value of K_N varies slightly within the respective K_N group, however, if we ignore this slight variation and note that the coefficient of friction is assumed to be same for all tests, $f = 0.7$, it is the increase in ΔK_T which explains the shortened total life. Figure 7.6 shows a logarithmic

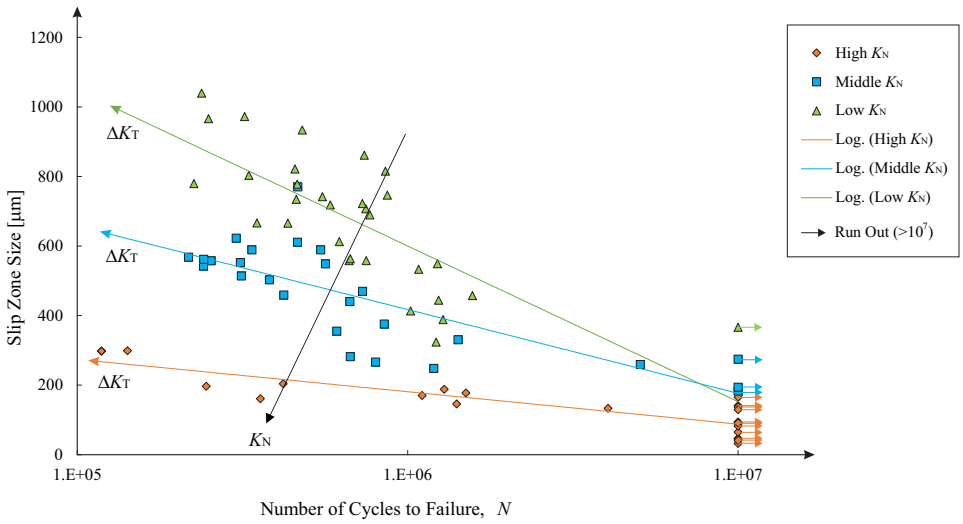


Figure 7.6: Total life of Aluminium alloy experiments plotted against the slip zone size, data grouped in terms of K_N to show dependence on both, the tangential asymptotic multiplier, ΔK_T, and the normal traction multiplier, K_N.

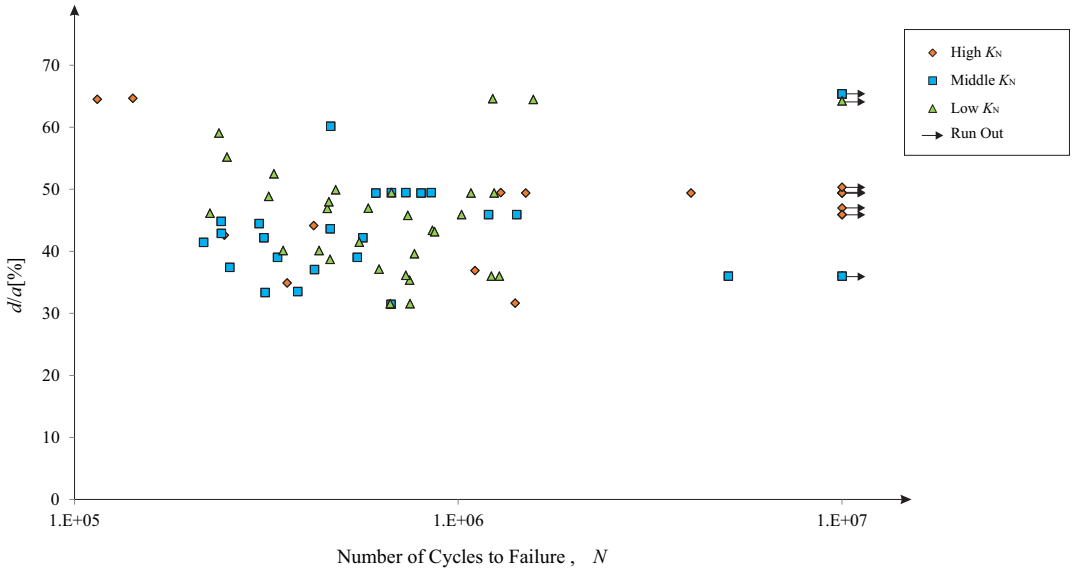


Figure 7.7: Total life of Aluminium alloy experiments plotted against the slip zone size as a percentage of the contact half-width, a, where the data is grouped in terms of K_{N}.

fit for each group of K_{N}. We note that with higher K_{N} values the slope of the logarithmic fit becomes shallower, confirming that slight changes in ΔK_{T} have a more prevalent effect on total life the higher the value of K_{N}.

For very high values of K_{N} the sensitivity to even slight increases in ΔK_{T} might have a catastrophic effect, potentially reducing the total life to a value that is not acceptable for engineering purposes. While these observations show that the slip zone size is not the only parameter controlling the fretting fatigue strength, the dependence on ΔK_{T} raises the question whether there is some form of an endurance limit, $\Delta K_{\mathrm{T}}^{\mathrm{th}}$?

While the slip zone size is a very sensible choice for the representation and correlation of the fretting fatigue strength, it has dimensions of length, and a dimensionless formulation of the problem might collapse the three different lifing curves (one for each K_N value) shown Figure 7.6. The asymptotic multiplier K_N is directly related to the instantaneous contact law, see Eq. (7.5), so that the contact half-width, a, is an appropriate parameter for a normalisation. The normalised data is shown in Figure 7.7. As expected, the normalisation removes the distinction between the three groups of K_N values we observed so clearly in Figure 7.6. This makes it very difficult to notice any trends such has the detrimental

effect a higher value of ΔK_T has on the fretting fatigue strength. However, the normalisation adds one additional insight, namely Figure 7.7 indicates that the fretting fatigue strength appears to be unaffected by the size of the slip zones with respect to the overall contact half-width.

In order to strengthen the case for this two-parameter space approach to fretting fatigue strength, we wish to apply the same ideas outlined above to the Titanium alloy, Ti6Al4V, that, in addition to the obviously different chemical metal composition, displays generally different fatigue properties compared with Aluminium alloys.

7.4.2 Titanium Alloy - Ti6Al4V

The data set at hand utilises flat and rounded geometries which were varied by changing the size of the radius at the edges of the nominally 8 mm flat portion of the punch [Dini, 2003]. As before, we begin by grouping the data set into three equally sized groups based on the calculated values for K_{N}. The range of values of K_{N} shows a more discrete range than before which should help in emphasising the dependence of the total life on ΔK_{T} within the respective group of K_{N} values. Figure 7.8 shows the distribution of K_{N} values, wherein the group of High K_{N} is constant at $3050\,{}^{\mathrm{MPa}}/_{\mathrm{mm}^{1/2}}$, Middle K_{N} ranges from $2355,{}^{\mathrm{MPa}}/_{\mathrm{mm}^{1/2}} - 2263\,{}^{\mathrm{MPa}}/_{\mathrm{mm}^{1/2}}$, and the Low K_{N} group ranges from $2163\,{}^{\mathrm{MPa}}/_{\mathrm{mm}^{1/2}} - 1500\,{}^{\mathrm{MPa}}/_{\mathrm{mm}^{1/2}}$.

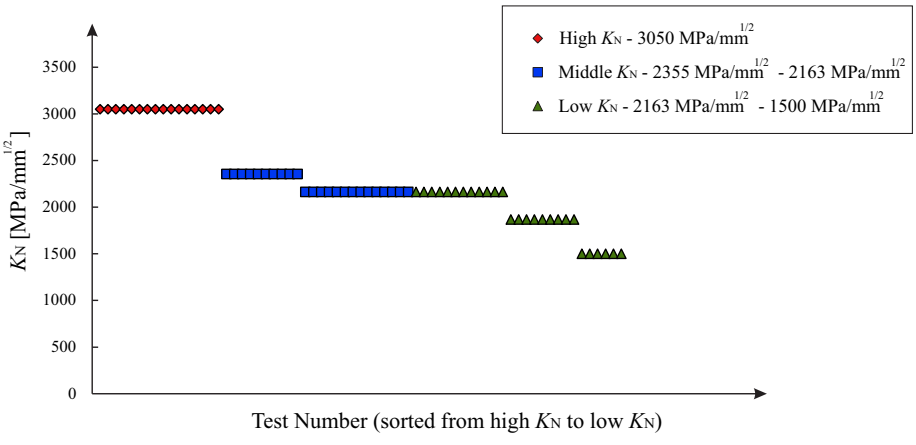


Figure 7.8: Available range of K_{N} values for the data set for Ti6Al4V.

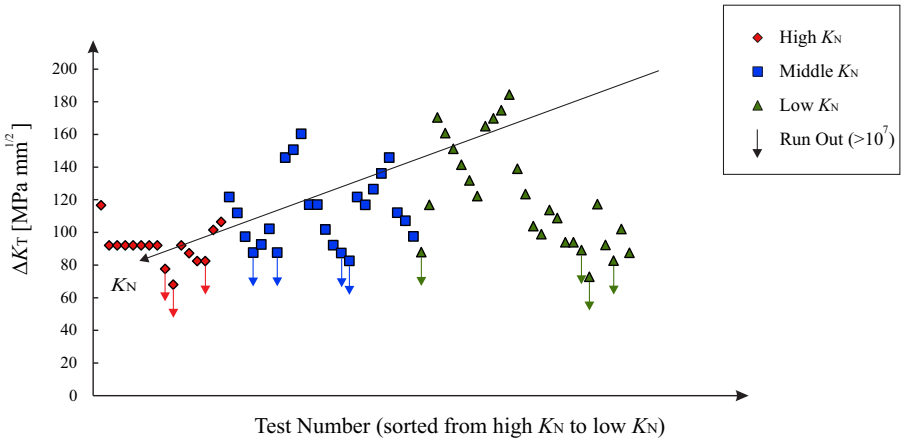


Figure 7.9: Corresponding range of ΔK_{T} values for the data set for Ti6Al4V with run out tests indicated.

The corresponding vales for ΔK_{T} are shown in Figure 7.9. As before, we note the reduction in range for the highest value of K_{N}, which again might be due to the nature of the experimental data or is a result of a significant reduction in achievable life for slight increases in ΔK_{T}. Additionally, we use this graph to demonstrate the potential for the definition of a $\Delta K_{\mathrm{T}}^{\mathrm{th}}$ threshold by indicating those values of ΔK_{T} that have led to run outs. Note that all of them lie at the bottom end of the range. In Appendix A.5 a K_N vs ΔK_T diagram (with run outs indicated by arrows) supports our choice of parameters.

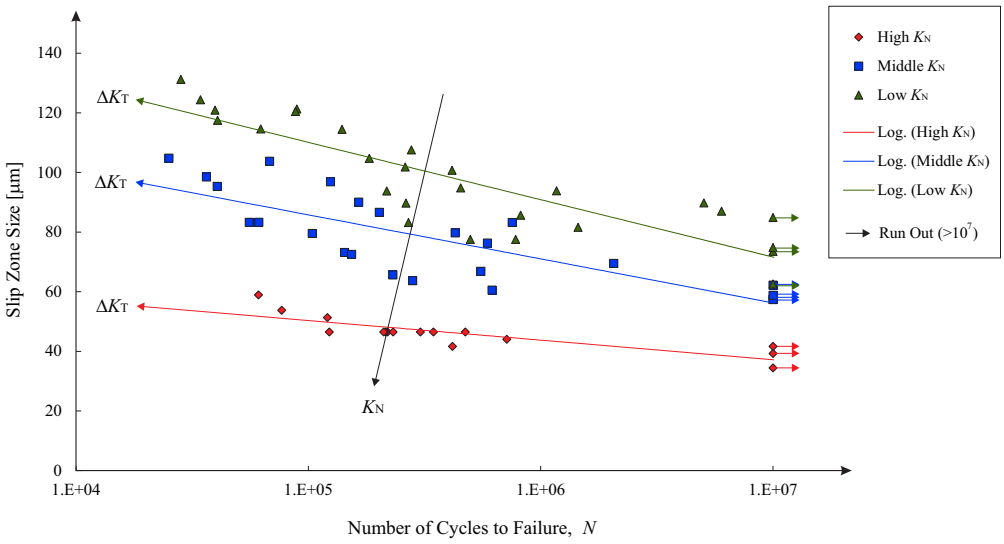


Figure 7.10: Total life of Titanium alloy experiments plotted against the slip zone size, data grouped in terms of K_{N} to show dependence on both, the tangential asymptotic multiplier, ΔK_{T}, and the normal traction multiplier, K_{N}.

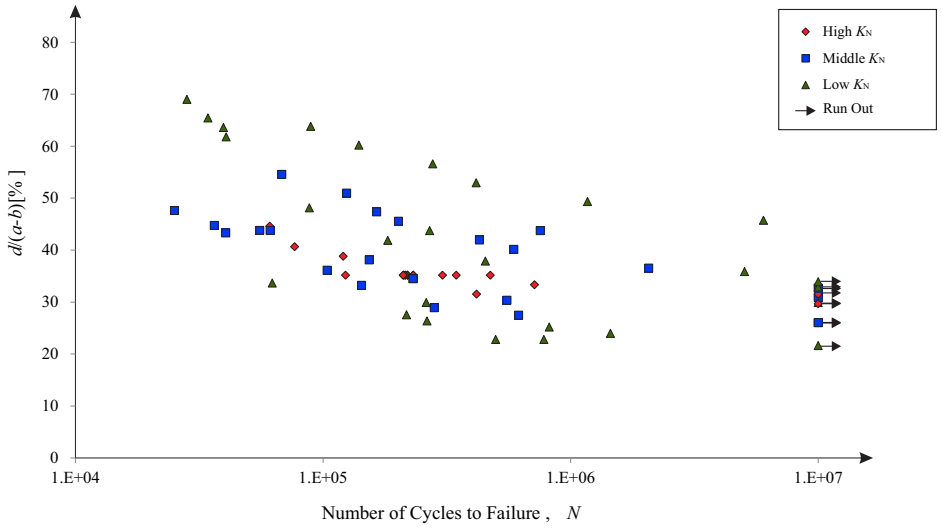


Figure 7.11: Total life of Titanium alloy experiments plotted against the slip zone size as a percentage of the contact half-width, a, where the data is grouped in terms of K_{N}.

Plotting the slip zone size against the total life (as before on a logarithmic scale) shows a similar kind of qualitative behaviour as before, compare Figures 7.6 and 7.10. As differences we note that the absolute size of the slip zones is only about $1/10$ of those calculated for the Aluminium alloys. Note also that the slope of the logarithmic fits is very similar between the three groups for K_{N}, indicating that the effect of K_{N} on the total life is weaker here compared with Aluminium alloys.

Additionally, Figure 7.11 shows the Titanium alloy experiments plotted against the slip zone size as a percentage of rounded part that is contact. Subtracting the flat portion, b, from the contact half-width, a, is necessary to make observable the normalisation as, in the data given, the flat portion takes up the majority of the contact half-width. Similar to the normalisation shown in Figure 7.7 for the Aluminium data, the dependence on K_N is lost due to the normalisation. However, it remains evident that the fretting fatigue strength is independent of the fraction of the rounded part taken by the slip zone size.

In summary it is reassuring to observe a similar kind of behaviour in a different type of alloy. Finally, we wish to outline the advantages this two-parameter approach offers when it comes to fretting fatigue testing and what is needed to gain further confidence in the method.

7.5 Generalising Fretting Fatigue Testing

In this chapter, we here introduced a new concept of fretting fatigue data interpretation. The analysis presented is based on four types of experimental data sets, conducted by four different researchers, using a number of different geometries. In order to reveal the fretting fatigue strength in a simple way, we applied an asymptotic description of the stress state adjacent to the severely stressed contact edge, collapsing the vast parameter space associated with frictional slip into two simple parameters. In addition to the simplicity the two-parameter space of K_{N} and ΔK_{T} provides, it remedies the dependence on the geometry used in the experiment. This paves the way towards a generalised approach to fretting fatigue. Instead of testing the component-specific fretting fatigue strength individually a standardised apparatus could test a matrix of desired combinations of K_{N} and ΔK_{T} so that engineers could use graphs like the ones shown in Figures 7.6 and 7.10 as some

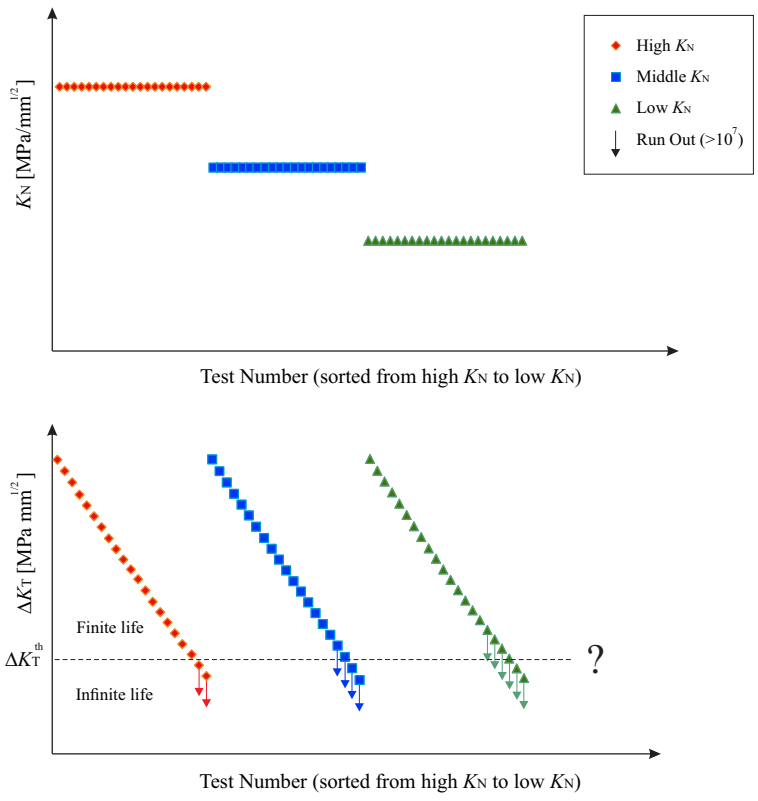


Figure 7.12: Potential test matrix for K_{N} and ΔK_{T} values with potential run out tests indicated in order to reveal the threshold value for $\Delta K_{\mathrm{T}}^{\mathrm{th}}$.

form of look-up table for the fretting fatigue strength of a material, similar to the usage of S-N curves in plain fatigue today. Figure 7.12 shows a potential systematic test matrix that could be employed to populate the lifing graph as well as to reveal the threshold value, $\Delta K_{\mathrm{T}}^{\mathrm{th}}$, for the material under consideration.

In summary, more experimental testing is needed to build up a case for a standardised approach to fretting fatigue in terms of K_{N} and ΔK_{T} and these ideas will remain valid only, if frictional slip is the dominant damage mechanism. As soon as plastic slip becomes an additional concern, a new approach to testing must be taken.

8

Summary and Future Work

In order to obtain an overview of the current state of understanding of half-plane contact problems, the thesis began with a taxonomy of contact problems, §1.4. This was followed by a review of methods available to solve contact problems, Chapter 2. In the beginning of this project in 2017 there was a practical need for a closed-form solution for asymmetrical incomplete contact problems, such as the one depicted in Figure 1.4. In most practical applications the contact will be subject to a normal load and moment, either due to an external load or due to an inherent asymmetry of the indenter. The solution found for the normal contact problem [Andresen et al., 2019b] is applicable to the flat and rounded geometry which may represent a dovetail root contact, Figure 1.2. This type of punch is also a common pad geometry in fretting fatigue experiments. Fretting fatigue experiments conducted in the Department of Engineering Science at the time motivated further research on partial slip solutions to guide experiments.

The partial slip solutions published in the literature - starting from the solution for shear loading under constant normal load revealed by Cattaneo over eighty years ago [Cattaneo, 1938] towards problems involving varying normal and shear loads, which were first solved by Barber et al. in 2011 [Barber et al., 2011] - were not sufficient to tackle problems in which all load components vary in a cyclic manner, i.e. normal force, P, moment, M, shear force, Q, and differential tension, σ. The

first necessary step in solving partial slip problems in the steady-state is identifying whether the cyclic loading present is going to lead to a slip stick pattern or whether the contact is going to remain fully adhered. The conditions for full stick were explored in §2.6. If inequality (2.74) becomes violated some part of the contact is going to experience slip and a partial slip solution is needed.

The solutions presented in the thesis distinguish clearly between the transient and steady-state response. While the former requires to track out the problem in a marching-in-time sense, the latter often makes it simpler to obtain results for the steady-state stick zone size and position for half-plane contacts, avoiding the complication of the marching-in-time procedure. Where useful and possible, we applied the results found to example geometries, such as Hertzian, wedge and flat and rounded geometries, in order to familiarise the reader with the concepts of the solution under consideration. The partial slip solutions obtained throughout the course of this project have been published in scientific journals [Andresen and Hills, 2020, Andresen et al., 2020e, Andresen et al., 2019a, Andresen et al., 2020b, Andresen et al., 2020c].

Table 8.1 gives a quick overview of the family of partial slip solutions developed in this thesis. The classical approach to solve a partial slip problem has been to use a superposition of the full sliding tractions together with a scaled form of the former as the corrective term, with the goal of bringing down the relative strains to zero in the stick region. This type of approach has been utilised and explored in Chapter 3

loading scenario	moderate bulk tension $\Delta Q + \Delta\sigma$	large bulk tension $\Delta\sigma + \Delta Q$
P const	Traction Superposition, see §3.3 & §3.4	Dislocations Method, see §4.3
ΔP	Traction Superposition, see §3.5	Dislocations Method, see §4.5
P const, M const	Traction Superposition, see §3.5	Asymptotic Method, see §5.3
ΔP, ΔM	Traction Superposition, see §3.5	Asymptotic Method, see §5.3

Table 8.1: Family of solutions for partial slip problems in the steady-state under complex loading histories.

to solve partial slip problems involving a varying normal load and varying moment. The traction superposition principle is applicable to problems in which there is only a shear force present or the mixed tangential loading is such that the differential tension is *moderate*, i.e. the direction of slip is the same at both ends of the contact.

If, on the other hand, the differential tension is *large*, a different route has to be taken. We employed a method in which, instead of correcting the tractions to allow for stick, we started off from a fully adhered state and corrected the strains by inserting dislocations in the regions of slip. This remedied the constraint of the same-sign direction of slip at both ends of the contact, and made the procedure applicable to both, *moderate* and *large* bulk tension problems, see §4.5. However, the dislocation method reached its limitation in the presence of a (varying) moment and made it necessary to utilise an asymptotic description of the partial slip problem to go forward. In this approach, we zoomed in on one end of the contact, rendering the considerations regarding the direction of slip obsolete, Chapter 5. The usage of asymptotic multipliers allowed us to express the tractions near the contact edge in asymptotic form and to approximate the slip zone size for all cases of proportional cyclic loading, even those in which closed-form solutions remain intractable, §5.3.

In Chapter 6, we explored what is needed to extract the local contact loads present in a prototype. Finding the load resultants for normal force, moment, and shear force from considerations of equilibrium is trivial. The more complicated question is "What is the best choice for the individual contributions to the differential bulk tension?", denoted σ_{A} and σ_{B} for the respective contacting bodies. By exploiting information embodied in the shear tractions and the direct strains parallel with the interface, we were able to reveal the value of the individual bulk stresses. We showed that by applying the extracted contact loads to a half-plane idealisation finite element model the same tractions and strains as those found in the prototype can be recreated.

In the final Chapter 7, we looked at what is needed to generalise fretting fatigue strength testing. We made use of the asymptotic concept developed in §5.2 to make comparable a number of experimental results from the literature

obtained for Aluminium and Titanium alloys, across different geometries and loading scenarios. We further introduced the concept of a lifing curve dependent on the asymptotic multipliers for normal and shear tractions and hypothesised that there might be a critical threshold for the shear traction multiplier below which the fretting fatigue life is infinite. These concepts need more experimental backing up in the future, which brings us to the final section outlining what work remains to be interesting for future research.

8.1 Future Work

The family of partial slip solutions developed in this thesis is only one small contribution in a bigger scheme of research efforts toward understanding the frictional behaviour between contacting bodies. The next natural steps that will fit in nicely with the theme of this thesis concern the frictional damping properties of incomplete contacts in partial slip. It is certain to assume that in regions that remain adhered the frictional damping is zero, so that all frictional energy is dissipated in the regions of slip. Knowing the amount and position of peak energy dissipation might help in assessing the localisation of surface damage. The solutions developed in Chapter 4 allow us to determine the slip displacement, $u(x)$, by integrating the dislocation density, $B_x(x)$, giving

$$u(x) = \int_n^x B_x(\xi)\mathrm{d}\xi \ , \tag{8.1}$$

where the slip zone spans $n < x < a$. The irreversible work done by the external tangential loading over the slip region per unit length is then given as

$$W(x) = f \int_n^x p(\xi)u(\xi)\mathrm{d}\xi \ , \tag{8.2}$$

where $fp(x)$ is the shear traction in the slip regions. This reveals how the frictional work varies with position and might indicate where cracks nucleate from along the slip region.

Once that is known, a fracture mechanics approach could be employed to investigate the growth of a freshly nucleated crack in the neighbourhood of the

stress field induced by the surface tractions, potentially encapsulated in the asymptotic multipliers, K_{N} and ΔK_{T}. Once the crack reaches a critical length, the underlying bulk tension will become the dominant driver of further crack propagation. Establishing a connection between the frictional stress field responsible for crack nucleation and the point at which the underlying stress field takes over to propagate the crack is a promising approach for additional investigations.

A further detail that is currently missing in the literature - but which may be of significant importance - is a varying coefficient of friction. Many engineering components have surface coatings, which are meant to improve several frictional surface properties. One effect is a generally lower coefficient of friction than the one associated with bare material. As the assembly undergoes load cycles the coating can wear off at the edges of a contact. This could result in an uncoated-uncoated contact in the slip zones and a coated-coated in the stick zone. Hypothetically, the coefficient of friction may vary by a finite amount between the slip and stick zones. It is possible that the effect of wear in the slip zone could change the entire geometry and previously unforeseen contact properties could come into play. These effects have not been investigated thoroughly but are important types of potential wear mechanisms.

An interesting aspect of contact problems is how a varying normal load affects the fretting fatigue strength of a component. While the analytical description of the contact behaviour has pushed forward and is able to quantify the stress field and partial slip pattern associated with varying normal loads (see §3.5, §4.5, §5.3), the phenomenon has not received much attention from the experimental side. This is also the reason why the observations made in Chapter 7 have been limited to constant normal load problems. Until experimental evidence exists one can only speculate as to how crack nucleation is affected by a change in contact size during periodic loading. In any partial slip problem the requirement for a conservation of material during steady-state loading needs to be fulfilled. Particles which have moved in one direction by a certain amount over the course of a half-cycle need to move back into their original position in the other half of the loading cycle. When the normal load is varying in a contact problem, the contact edge will advance with

an increase in normal load. At the point of load reversal, however, the contact starts to decrease in size, leaving particles that have experienced frictional relative motion during *uploading*, to move back into their original position without any frictional dissipation during *downloading*. Does this suggest that damage accumulation is less severe in the part of the contact that is changing and what does that imply for the fretting fatigue strength of a component? Only experimental evidence will shed further light onto this issue.

Finally, all findings presented in this thesis have been restricted to fully elastic problems. In real frictional contact problems, the stresses associated with a contact can exceed the yield stress of a material quickly causing the material to deform plastically. When this is the case there are two competing damage mechanisms at work, frictional and plastic slip, and it is important to assess how both interact and which one of them is dominant.

Appendices

A
Appendix

A.1 The Tilted Three-Part Punch

The tilted three-part punch, Figure A.1, is formulated as a linear-elastic body within half-plane theory indenting a linear-elastic half-plane. The solution to be developed is mathematically exact only if the contact is perfectly lubricated or the materials considered are elastically similar so that the normal indentation does not induce tangential tractions. This means the problem is uncoupled and the solutions for the normal and shear tractions may be obtained independently.

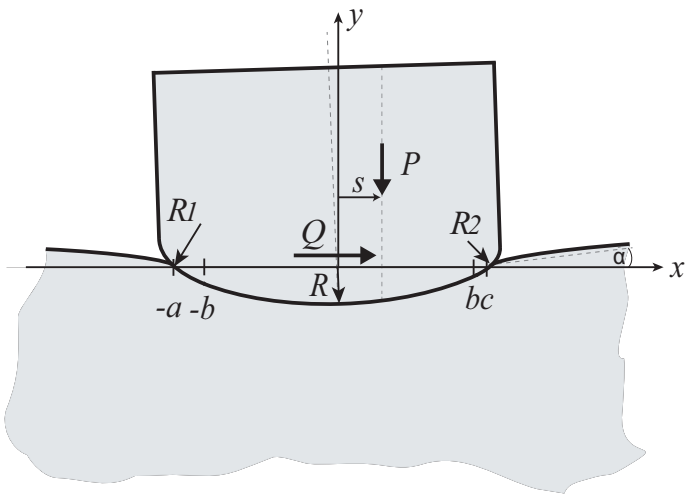


Figure A.1: Illustration of the tilted punch comprised of three different rounded segments.

The profile of the indenting punch is represented by the usual Hertz parabolic approximation to a circle with radius R_1 from $-a$ to $-b$, radius R from $-b$ to b and radius R_2 from b to c. The relative surface normal displacement, $v(x)$, and its gradient, $v'(x)$, can be expressed as piecewise functions

$$v(x) = \begin{cases} \Delta + \alpha x + \frac{x^2 + 2bk_1 x + b^2 k_1}{2R_1} & -a < x < -b \\ \Delta + \alpha x + \dfrac{x^2}{2R} & -b < x < b \\ \Delta + \alpha x + \frac{x^2 - 2bk_2 x + b^2 k_2}{2R_2} & b \leq x \leq c \end{cases} \tag{A.1}$$

$$v'(x) = \begin{cases} \alpha + (x + bk_1)/R_1 & -a < x < -b \\ \alpha + x/R & -b \leq x \leq b \\ \alpha + (x - bk_2)/R_2 & b < x < c \end{cases}, \tag{A.2}$$

where $k_i = 1 - R_i/R$ for $i = 1, 2$. The absolute indentation is the constant Δ. The inclination of the punch, α, must be sufficiently small for small strain conventional elasticity to apply. The normal traction distribution, $p(x)$, along the contact interface $[-a, c]$ can be found through inverting the following integral equation

$$v'(x) = \frac{2}{\pi E^*} \int_{-a}^{c} \frac{p(t)\,\mathrm{d}t}{(x - t)} \,. \tag{A.3}$$

Once the normal problem has been solved for this most general case, as shown in Figure A.1, we look at three different derivations of the original problem statement, as shown in Figure A.2. Case A shows the tilted flat and rounded punch, which is an important geometry for the dovetail root contact idealisation. Case B shows the rounded punch with a concave central segment and case C is the tilted punch comprised of two adjoined unequal half-cylinders.

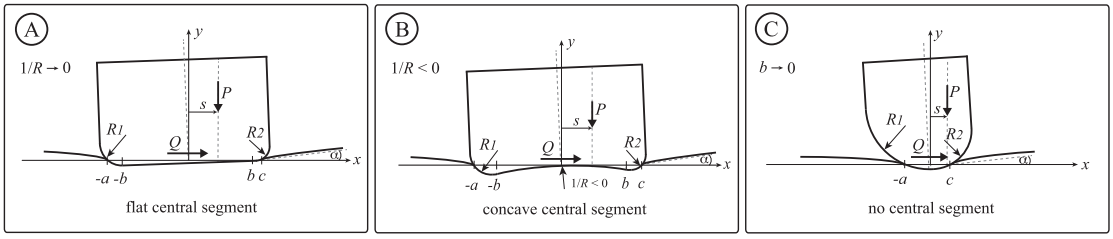


Figure A.2: Three derivations from the original problem statement; case A the tilted flat and rounded punch, case B the rounded punch with a concave central segment, and case C the tilted punch comprised of two adjoined unequal half-cylinders.

A.1.1 Integral Evaluation

As the punch's profile, $v(x)$, (and also its derivative, $v'(x)$) is a piecewise function, the normal surface stress can also be expressed as a piecewise function. Hence, the normal pressure can be written as

$$p\left(x\right) = \frac{w(x)E^*}{2\pi} \ldots \tag{A.4}$$

$$\begin{cases} -\frac{1}{R_1}\left[\int_{-a}^{-b} \frac{(\alpha R_1 + t + bk_1)\ \mathrm{d}t}{w(t)\,(t-x)}\right]^{\mathrm{CPV}} - \frac{1}{R}\int_{-b}^{b} \frac{(\alpha R + t)\,\mathrm{d}t}{w(t)\,(t-x)} - \frac{1}{R_2}\int_{b}^{c} \frac{(\alpha R_2 + t - bk_2)\ \mathrm{d}t}{w(t)\,(t-x)}, \\ -\frac{1}{R_1}\int_{-a}^{-b} \frac{(\alpha R_1 + t + bk_1)\ \mathrm{d}t}{w(t)\,(t-x)} - \frac{1}{R}\left[\int_{-b}^{b} \frac{(\alpha R + t)\,\mathrm{d}t}{w(t)\,(t-x)}\right]^{\mathrm{CPV}} - \frac{1}{R_2}\int_{b}^{c} \frac{(\alpha R_2 + t - bk_2)\ \mathrm{d}t}{w(t)\,(t-x)}, \\ -\frac{1}{R_1}\int_{-a}^{-b} \frac{(\alpha R_1 + t + bk_1)\ \mathrm{d}t}{w(t)\,(t-x)} - \frac{1}{R}\int_{-b}^{b} \frac{(\alpha R + t)\,\mathrm{d}t}{w(t)\,(t-x)} - \frac{1}{R_2}\left[\int_{b}^{c} \frac{(\alpha R_2 + t - bk_2)\ \mathrm{d}t}{w(t)\,(t-x)}\right]^{\mathrm{CPV}}, \end{cases}$$

where $w(x) = \sqrt{(x+a)(c-x)}$ and $w(t) = \sqrt{(t+a)(c-t)}$, such that the the first piece can be evaluated over the range $-a < x < -b$, the second over $-b < x < b$, and the third over $b < x < c$. The integrals marked with CPV are singular and must be evaluated as Cauchy principal values (CPV).

First, a partial decomposition on the integrands is performed so that

$$\frac{(\alpha R_1 + t + bk_1)}{(t-x)} = 1 + \frac{\alpha R_1 + bk_1 + x}{t-x}\ , \tag{A.5}$$

$$\frac{(\alpha R + t)}{(t-x)} = 1 + \frac{\alpha R + x}{t-x}\ , \text{ and} \tag{A.6}$$

$$\frac{(\alpha R_2 + t - bk_2)}{(t-x)} = 1 - \frac{-\alpha R_2 + bk_2 - x}{t-x}\ . \tag{A.7}$$

The integrals that are regular and independent of x can be evaluated as follows

$$\int_{-a}^{-b} \frac{1\,\mathrm{d}t}{w\left(t\right)} = \arccos\left[\frac{2b-(a-c)}{a+c}\right]\ , \tag{A.8}$$

$$\int_{-b}^{b} \frac{1\,\mathrm{d}t}{w\left(t\right)} = \arccos\left[\frac{2b-(a-c)}{a+c}\right] + \arccos\left[\frac{(a-c)+2b}{a+c}\right] - \pi\ , \text{ and} \tag{A.9}$$

$$\int_{b}^{c} \frac{1\,\mathrm{d}t}{w\left(t\right)} = \arccos\left[\frac{(a-c)+2b}{a+c}\right]\ . \tag{A.10}$$

The contribution of these integrals to the normal pressure is

$$F_0 = \frac{k_1}{R_1}\arccos\left[\frac{2b-(a-c)}{a+c}\right] + \frac{k_2}{R_2}\arccos\left[\frac{(a-c)+2b}{a+c}\right] + \frac{\pi}{R}\ . \tag{A.11}$$

The results for integrals affected by the CPV are the following

$$\begin{aligned}
&\mathrm{CPV}\int_{-a}^{-b}\frac{1}{w\left(t\right)\left(t-x\right)}\mathrm{d}t=\\
&\quad+\frac{\ln\left(-\frac{(b+x)(c+a)}{2\sqrt{(c-x)(a+x)(a-b)(c+b)}+2(ac+bx)+(a-c)(b-x)}\right)}{\sqrt{\left(c-x\right)\left(a+x\right)}},\ x\in[-a,-b]\ , \qquad \text{(A.12)}\\
&\int_{-a}^{-b}\frac{1}{w\left(t\right)\left(t-x\right)}\mathrm{d}t=\\
&\quad+\frac{\ln\left(\frac{(b+x)(c+a)}{2\sqrt{(c-x)(a+x)(a-b)(c+b)}+2(ac+bx)+(a-c)(b-x)}\right)}{\sqrt{\left(c-x\right)\left(a+x\right)}},\ x\notin[-a,-b]\ , \qquad \text{(A.13)}\\
&\mathrm{CPV}\int_{-b}^{b}\frac{1}{w\left(t\right)\left(t-x\right)}\mathrm{d}t=\\
&\quad+\frac{\ln\left(\frac{\left(2\sqrt{(c-x)(a+x)(a-b)(c+b)}+2(ac+bx)+(a-c)(b-x)\right)(b-x)}{\left(2\sqrt{(c-x)(a+x)(a+b)(c-b)}+2(ac-bx)-(a-c)(b+x)\right)(b+x)}\right)}{\sqrt{\left(c-x\right)\left(a+x\right)}},\ x\in[-b,b]\ , \qquad \text{(A.14)}\\
&\int_{-b}^{b}\frac{1}{w\left(t\right)\left(t-x\right)}\mathrm{d}t=\\
&\quad+\frac{\ln\left(-\frac{\left(2\sqrt{(c-x)(a+x)(a-b)(c+b)}+2(ac+bx)+(a-c)(b-x)\right)(b-x)}{\left(2\sqrt{(c-x)(a+x)(a+b)(c-b)}+2(ac-bx)-(a-c)(b+x)\right)(b+x)}\right)}{\sqrt{\left(c-x\right)\left(a+x\right)}},\ x\notin[-b,b]\ , \qquad \text{(A.15)}\\
&\mathrm{CPV}\int_{b}^{c}\frac{1}{w\left(t\right)\left(t-x\right)}\mathrm{d}t=\\
&\quad-\frac{\ln\left(-\frac{(b-x)(c+a)}{2\sqrt{(c-x)(a+x)(a+b)(c-b)}+2(ac-bx)-(a-c)(b+x)}\right)}{\sqrt{\left(c-x\right)\left(a+x\right)}},\ x\in[b,c]\ ,\text{ and} \qquad \text{(A.16)}\\
&\int_{b}^{c}\frac{1}{w\left(t\right)\left(t-x\right)}\mathrm{d}t=\\
&\quad-\frac{\ln\left(\frac{(b-x)(c+a)}{2\sqrt{(c-x)(a+x)(a+b)(c-b)}+2(ac-bx)-(a-c)(b+x)}\right)}{\sqrt{\left(c-x\right)\left(a+x\right)}},\ x\notin[b,c]\ . \qquad \text{(A.17)}
\end{aligned}$$

Therefore, regardless whether they are CPV or not, they can be written as

$$\int_{-a}^{-b} \frac{1}{w\,(t)\,(t-x)}\mathrm{d}t = \\ + \frac{\ln\left(\left|\frac{(b+x)(c+a)}{2\sqrt{(c-x)(a+x)(a-b)(c+b)}+2(ac+bx)+(a-c)(b-x)}\right|\right)}{\sqrt{(c-x)\,(a+x)}} = \frac{F_1(x)}{w(x)}\ , \tag{A.18}$$

$$\int_{-b}^{b} \frac{1}{w\,(t)\,(t-x)}\mathrm{d}t = \\ + \frac{\ln\left(\left|\frac{\left(2\sqrt{(c-x)(a+x)(a-b)(c+b)}+2(ac+bx)+(a-c)(b-x)\right)(b-x)}{\left(2\sqrt{(c-x)(a+x)(a+b)(c-b)}+2(ac-bx)-(a-c)(b+x)\right)(b+x)}\right|\right)}{\sqrt{(c-x)\,(a+x)}} = \frac{F_2(x)}{w(x)}\ \text{, and} \tag{A.19}$$

$$\int_{b}^{c} \frac{1}{w\,(t)\,(t-x)}\mathrm{d}t = \\ - \frac{\ln\left(\left|\frac{(b-x)(c+a)}{2\sqrt{(c-x)(a+x)(a+b)(c-b)}+2(ac-bx)-(a-c)(b+x)}\right|\right)}{\sqrt{(c-x)\,(a+x)}} = \frac{F_3(x)}{w(x)}\ . \tag{A.20}$$

A.1.2 The Pressure Distribution

Carrying out the integration, the pressure distribution is obtained as

$$p\,(x) = -\frac{w(x)E^*}{2\pi}\left(F_0 + \frac{\alpha R_1 + bk_1 + x}{R_1\,w(x)}\,F_1(x) + \frac{\alpha R + x}{R\,w(x)}\,F_2(x) - \right. \\ \left. - \frac{-\alpha R_2 + bk_2 - x}{R_2\,w(x)}\,F_3(x)\right)\ , \tag{A.21}$$

where the expression F_0 and the functions $w(x)$ and $F_j(x)$, for $j = 1, 2, 3$ are given in A.1.1.

A.1.3 The Consistency Condition

The consistency condition can be evaluated as follows

$$\begin{aligned} 0 =& \int_{-a}^{c} \frac{v'(t)\,\mathrm{d}t}{\sqrt{(t+a)(c-t)}} \\ =& \frac{1}{R_1}\int_{-a}^{-b} \frac{(\alpha R_1 + (x + bk_1))\ \mathrm{d}t}{\sqrt{(t+a)(c-t)}} + \frac{1}{R}\int_{-b}^{b} \frac{(\alpha R + x)\ \mathrm{d}t}{\sqrt{(t+a)(c-t)}} + \\ & \frac{1}{R_2}\int_{b}^{c} \frac{(\alpha R_2 + (x - bk_2))\ \mathrm{d}t}{\sqrt{(t+a)(c-t)}}\ . \end{aligned} \tag{A.22}$$

Evaluating the integrals in equation (A.22) and solving the resulting equation for α gives the algebraic expression

$$\begin{aligned}\alpha = \frac{1}{2\pi}\Bigg(&+ \frac{k_1}{R_1}(a-2b-c)\,\arccos\left[\frac{-a+2b+c}{a+c}\right] + \\ &+ \frac{k_2}{R_2}(a+2b-c)\,\arccos\left[\frac{a+2b-c}{a+c}\right] + \frac{\pi\,(a-c)}{R} \\ &+ \frac{\pi\,(a-c)}{R} + \frac{k_1}{R_1}\,2\sqrt{(a-b)(b+c)} - \frac{k_2}{R_2}\,2\sqrt{(a+b)(c-b)}\Bigg)\ . \end{aligned} \tag{A.23}$$

A.1.4 The Normal Equilibrium

Normal equilibrium must be satisfied so that

$$\begin{aligned} P &= -\int_{-a}^{c} p(x)\,\mathrm{d}x \\ &= -\int_{-a}^{c}\left[-\frac{w(x)E^*}{2\pi}\int_{-a}^{c}\frac{v'(t)\mathrm{d}t}{w(t)(t-x)}\right]\mathrm{d}x \\ &= +\frac{E^*}{2\pi}\int_{-a}^{c}\left[\frac{v'(t)}{w(t)}\int_{-a}^{c}\frac{w(x)\mathrm{d}x}{(t-x)}\right]\mathrm{d}t \\ &= +\frac{E^*}{2\pi}\int_{-a}^{c}\left[\frac{v'(t)}{w(t)}\left(\frac{1}{2}\pi(a-c+2t)\right)\right]\mathrm{d}t \\ &= +\frac{E^*}{4}\int_{-a}^{c}\left[\frac{(a-c+2t)}{w(t)}v'(t)\right]\mathrm{d}t\ . \end{aligned} \tag{A.24}$$

Integration by parts (where $f'(t) = \frac{(a-c+2t)}{w(t)}$ and $g(t) = v'(t)$) gives

$$\begin{aligned} P &= +\frac{E^*}{4}\left[\left[f(t)g(t)\Big|_{-a}^{c}\right] - \int_{-a}^{c} f(t)g'(t)\mathrm{d}t\right] \\ &= +\frac{E^*}{4}\Bigg[+\left(\left[f(t)g(t)\Big|_{-a}^{-b}\right] - \int_{-a}^{-b} f(t)g'(t)\mathrm{d}t\right) + \\ &\qquad +\left(\left[f(t)g(t)\Big|_{-b}^{b}\right] - \int_{-b}^{b} f(t)g'(t)\mathrm{d}t\right) + \\ &\qquad +\left(\left[f(t)g(t)\Big|_{b}^{c}\right] - \int_{b}^{c} f(t)g'(t)\mathrm{d}t\right)\Bigg]\ . \end{aligned} \tag{A.25}$$

The indefinite integral of $f'(t)$ is

$$f(t) = \int f'(t)\mathrm{d}t = \int\frac{(a-c+2t)}{w(t)}\mathrm{d}t = -2\sqrt{(a+t)(c-t)} + C_1\ , \tag{A.26}$$

where C_1 is a constant.

The derivative of $g(t) = v'(t)$ gives the piecewise function

$$g'(t) = v''(t) = \begin{cases} 1/R_1 & , -a < t < -b \\ 1/R & , -b < t < b \\ 1/R_2 & , b < t < c \end{cases} . \tag{A.27}$$

Now normal equilibrium is

$$\begin{aligned} P = & \frac{E^*}{16} \left((a+c)^2 \left(-\frac{k_1}{R_1} \arccos\left[\frac{-a+2b+c}{a+c}\right] - \frac{k_2}{R_2} \arccos\left[\frac{a+2b-c}{a+c}\right] - \frac{\pi}{R} \right) - \right. \\ & \left. - \frac{k_1}{R_1} 2\,(a-2b-c)\sqrt{(a-b)(b+c)} + \frac{k_2}{R_2} 2\,(a+2b-c)\sqrt{(a+b)(c-b)} \right) . \end{aligned} \tag{A.28}$$

A.1.5 The Rotational Equilibrium

For rotational equilibrium the same procedure as for normal equilibrium applies

$$\begin{aligned} Ps &= \int_{-a}^{c} p(x)\, x \, \mathrm{d}x \\ &= \int_{-a}^{c} \left[-\frac{E^*}{2\pi} w(x)\, x \int_{-a}^{c} \frac{v'(t)\mathrm{d}t}{w(t)(t-x)} \right] \mathrm{d}x \\ &= -\frac{E^*}{2\pi} \int_{-a}^{c} \left[\frac{v'(t)}{w(t)} \int_{-a}^{c} \frac{w(x)\, x \, \mathrm{d}x}{(t-x)} \right] \mathrm{d}t \\ &= -\frac{E^*}{2\pi} \int_{-a}^{c} \left[\frac{v'(t)}{w(t)} \left(\frac{1}{8}\pi \left(4t(a-c) - (a+c)^2 + 8t^2 \right) \right) \right] \mathrm{d}t \\ &= -\frac{E^*}{16} \int_{-a}^{c} \left[\frac{(4t(a-c) - (a+c)^2 + 8t^2)}{w(t)} v'(t) \right] \mathrm{d}t \, . \end{aligned} \tag{A.29}$$

Integration by parts (where $f'(t) = \frac{\left(4t(a-c)-(a+c)^2+8t^2\right)}{w(t)}$ and $g(t) = v'(t)$) gives

$$\begin{aligned} Ps = & -\frac{E^*}{16} \left[\left[f(t)g(t) \Big|_{-a}^{c} \right] - \int_{-a}^{c} f(t)g'(t)\mathrm{d}t \right] \\ = & -\frac{E^*}{16} \left[+ \left(\left[f(t)g(t) \Big|_{-a}^{-b} \right] - \int_{-a}^{-b} f(t)g'(t)\mathrm{d}t \right) + \right. \\ & + \left(\left[f(t)g(t) \Big|_{-b}^{b} \right] - \int_{-b}^{b} f(t)g'(t)\mathrm{d}t \right) + \\ & \left. + \left(\left[f(t)g(t) \Big|_{b}^{c} \right] - \int_{b}^{c} f(t)g'(t)\mathrm{d}t \right) \right] . \end{aligned} \tag{A.30}$$

The indefinite integral of $f'(t)$ is

$$\begin{aligned} f(t) = \int f'(t)\mathrm{d}t = & \int \frac{(4t(a-c) - (a+c)^2 + 8t^2)}{w(t)}\mathrm{d}t \\ = & -2\sqrt{(a+t)(c-t)}(-a+c+2t) + C_2 \ , \end{aligned} \tag{A.31}$$

where C_2 is a constant.

The derivative of $g(t) = v'(t)$ gives the piecewise function

$$g'(t) = v''(t) = \begin{cases} 1/R_1 & , -a < t < -b \\ 1/R & , -b < t < b \\ 1/R_2 & , b < t < c \end{cases} \ . \tag{A.32}$$

The rotational equilibrium condition gives $Ps = M$ so that

$$\begin{aligned} M = & \frac{E^*(a-c)}{96}\left(3(a+c)^2\left(\frac{k_1}{R_1}\arccos\left[\frac{-a+2b+c}{a+c}\right] + \right.\right. \\ & + \frac{k_2}{R_2}\arccos\left[\frac{a+2b-c}{a+c}\right] + \frac{\pi}{R}\Bigg) + \\ & + \frac{k_1}{R_1}4\left(\frac{a^2-2b^2+c^2}{a-c} + \frac{1}{2}(a-2b-c)\right)\sqrt{(a-b)(b+c)} - \\ & \left. - \frac{k_2}{R_2}4\left(\frac{a^2-2b^2+c^2}{a-c} + \frac{1}{2}(a+2b-c)\right)\sqrt{(a+b)(c-b)}\right) \ . \end{aligned} \tag{A.33}$$

A.1.6 Case 'A' - The Tilted Flat but Rounded Punch with Unequal Radii

Case 'A' considers what happens when the curvature of the middle segment, $1/R$, goes to 0. Ans said before, an indenter like this is often referred to as the flat but rounded punch. The symmetrical case has been studied thoroughly in the literature [Vazquez et al., 2010, Ciavarella et al., 1998]. Here, asymmetry is introduced to the problem in the sense that the radii can be unequal and the normal load is applied at an offset, s. The problem is of high interest to the aerospace industries since this kind of punch can be used to represent a dovetail flank contact. A closed-form solution is found by taking the limit $R \to \infty$ for equation (A.21) and the respective side conditions, i.e. equations (A.23), (A.28), and (A.33).

It follows that $k_1 \to 1$ and $k_2 \to 1$, so that the pressure distribution is given in compact and closed form by

$$p\,(x) = -\frac{w(x)E^*}{\pi 2}\left(F_0 + \frac{\alpha R_1 + b + x}{R_1\,w(x)}\,F_1(x) + \frac{\alpha}{w(x)}F_2(x) - \right. \\ \left. - \frac{-\alpha R_2 + b - x}{R_2\,w(x)}\,F_3(x)\right)\,, \tag{A.34}$$

where the expression F_0 and the functions $w(x)$ and $F_j(x)$, for $j = 1, 2, 3$ are given in A.1.1. The consistency condition is given by

$$\alpha = \frac{1}{\pi}\left(+\frac{\sqrt{(a-b)(b+c)}}{R_1} + \frac{a-2b-c}{2R_1}\arccos\left[\frac{-a+2b+c}{a+c}\right] + \right. \\ \left. - \frac{\sqrt{(a+b)(c-b)}}{R_2} + \frac{a+2b-c}{2R_2}\arccos\left[\frac{a+2b-c}{a+c}\right]\right)\,. \tag{A.35}$$

Imposing normal and rotational equilibrium, the two side conditions are

$$P = \frac{E^*\,(a+c)^2}{8}\left[-\frac{\arccos\left[\frac{-a+2b+c}{a+c}\right]}{2R_1} - \frac{\arccos\left[\frac{a+2b-c}{a+c}\right]}{2R_2} + \right. \\ + \frac{(-a+2b+c)\sqrt{(a-b)(c+b)}}{(a+c)^2\,R_1} + \\ \left. + \frac{(a+2b-c)\sqrt{(a+b)(c-b)}}{(a+c)^2\,R_2}\right]\,, \tag{A.36}$$

and $Ps = M$ so that

$$M = \frac{E^*\,(a+c)^2\,(a-c)}{8}\left[+\frac{\arccos\left[\frac{-a+2b+c}{a+c}\right]}{4R_1} + \frac{\arccos\left[\frac{a+2b-c}{a+c}\right]}{4R_2} + \right. \\ + \frac{\left(\frac{a^2-2b^2+c^2}{(a-c)} + \frac{a-2b-c}{2}\right)\sqrt{(a-b)(c+b)}}{3\,(a+c)^2\,R_1} - \\ \left. - \frac{\left(\frac{a^2-2b^2+c^2}{(a-c)} + \frac{a+2b-c}{2}\right)\sqrt{(a+b)(c-b)}}{3\,(a+c)^2\,R_2}\right]\,. \tag{A.37}$$

A.1.7 Case 'B' - The Rounded Punch with a Concave Central Segment

Consider a punch comprised of two convex edges of unequal radii and a concave middle portion as depicted in Figure A.2, case B. Additionally a moment might be

applied in order to introduce tilt. The solution found and presented for the generic three-segment punch still applies here, given the central curvature, $1/R$, is negative. Hence, the equations will not be repeated for brevity. Obviously, a requirement for the solution to be valid is that the contact remains simply connected, i.e. there is no separation in central segment.

A.1.8 Case 'C' - The Tilted Punch Comprised of Two Adjoined Unequal Half-Cylinders

The last case to be considered is the tilted rounded punch with unequal radii, i.e. the flat portion is removed from the indenter by taking the limit $b \to 0$.

The pressure distribution, $p(x)$, simplifies to the following expression

$$p(x) = -\frac{w(x)E^*}{2\pi}\left[\left(\frac{1}{R_1}+\frac{1}{R_2}\right)\frac{\pi}{2}+\left(\frac{1}{R_1}-\frac{1}{R_2}\right)\arcsin\left[\frac{a-c}{a+c}\right]+\right.$$
$$\left.+\left(\frac{1}{R_1}-\frac{1}{R_2}\right)\frac{x}{w(x)}\ln\left|\frac{x(a+c)}{2ac+(c-a)x+2\sqrt{ac(c-x)(a+x)}}\right|\right]. \quad \text{(A.38)}$$

The consistency condition is given by

$$\alpha = \left(\frac{1}{R_1}-\frac{1}{R_2}\right)\frac{\sqrt{ac}}{\pi}+\left(\frac{1}{R_1}-\frac{1}{R_2}\right)\frac{a-c}{2\pi}\arcsin\left[\frac{a-c}{a+c}\right]+$$
$$+\left(\frac{1}{R_1}+\frac{1}{R_2}\right)\frac{a-c}{4}\,. \quad \text{(A.39)}$$

Imposing normal and rotational equilibrium, the two side conditions are

$$\frac{8P}{E^*(a+c)^2} = \left(\frac{1}{R_1}-\frac{1}{R_2}\right)\frac{(c-a)\sqrt{ac}}{(a+c)^2}-\frac{1}{2}\left(\frac{1}{R_1}-\frac{1}{R_2}\right)\arcsin\left[\frac{a-c}{a+c}\right]-$$
$$-\left(\frac{1}{R_1}+\frac{1}{R_2}\right)\frac{\pi}{4}\,, \quad \text{(A.40)}$$

and

$$\frac{8Ps}{E^*(a+c)^2} = \frac{a-c}{12}\left(+\left(\frac{1}{R_1}-\frac{1}{R_2}\right)\frac{4\sqrt{ac}}{(a+c)^2}\left(\frac{a^2+c^2}{a-c}+\frac{a-c}{2}\right)+\right.$$
$$\left.+\left(\frac{1}{R_1}-\frac{1}{R_2}\right)3\arcsin\left[\frac{a-c}{a+c}\right]+\left(\frac{1}{R_1}+\frac{1}{R_2}\right)\frac{3\pi}{2}\right)\,. \quad \text{(A.41)}$$

A.2 Partial Slip Problems - Sequential Loading [Andresen et al., 2020e]

Figure 6.2 shows sequential and proportional loading for a P, Q, σ-problem neglecting the effect of a moment. The sequence in which the loads are applied greatly affects the procedure and the solution to a contact problem. For completeness, we look at the effects of a sequential load application in this appendix.

Consider the problem shown in Figure 6.1 b), and suppose that the contacting bodies are elastically similar. We assume initially, that the coefficient of friction, f, is sufficiently high to inhibit all slip. First, we apply the normal load, P and potentially a moment, M, and establish a contact of extent $[-a \quad b]$. In our analysis we will neglect the shear tractions induced by the application of the normal load as they will be much smaller in magnitude than the contact pressure when the bodies are elastically similar. Now we apply the external tangential loads $(Q, \sigma_{\mathrm{A}}, \sigma_{\mathrm{B}})$. These will be square root singular in character at the contact edges - symmetric when induced by a shear force and antisymmetric when induced by differential bulk tension, as shown in Figure A.3. The full-stick shear traction distribution is given by

$$q(x) = \frac{Q}{\pi\sqrt{(a+x)\,(b-x)}} + \frac{\sigma\,(2x+a-b)}{8\sqrt{(a+x)\,(b-x)}}\,, \tag{A.42}$$

where $\sigma = \sigma_{\mathrm{A}} - \sigma_{\mathrm{B}}$. Suppose we introduce a new coordinate, $s = a + x$, measured from the left hand contact edge, so that

$$q(s) = \frac{Q}{\pi\sqrt{s\,(b+a-s)}} + \frac{\sigma\,(2s-a-b)}{8\sqrt{s\,(b+a-s)}}\,, \tag{A.43}$$

and now take the limit $s \to 0$, so that

$$q(s)\sqrt{s} \to \frac{Q}{\pi\sqrt{(a+b)}} - \frac{\sigma(a+b)}{8\sqrt{(a+b)}}\,. \tag{A.44}$$

Similarly, if we measure $t = b - x$ from the left hand edge

$$q(t) = \frac{Q}{\pi\sqrt{t\,(a+b-t)}} + \frac{\sigma(a+b-2t)}{8\sqrt{t\,(a+b-t)}}\,, \tag{A.45}$$

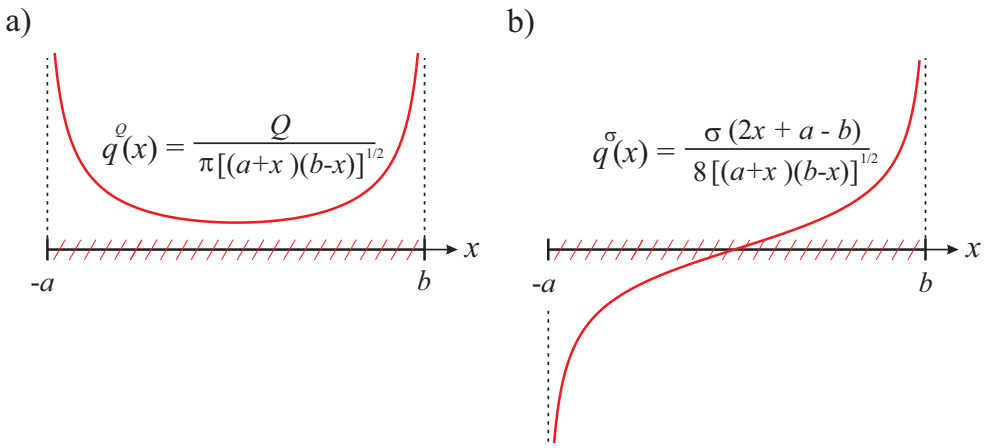


Figure A.3: Fully adhered shear tractions due to a) a shear force, Q and b) differential bulk tension, σ.

and, in the limit $t \to 0$

$$q(t)\sqrt{t} \to \frac{Q}{\pi\sqrt{(a+b)}} + \frac{\sigma\,(a+b)}{8\sqrt{(a+b)}}\,. \tag{A.46}$$

Therefore, by taking the output for $q(s)$ and $q(t)$ from a finite element analysis and plotting the left hand sides of limits (A.44) and (A.46) we can deduce the value of Q and σ. Of course, we know the value of the shear force, Q, by another route, equation (6.3), but this provides an independent check to our results.

We now turn our attention to a consideration of the absolute bulk tensions present. The general expression for the strain induced at the surface of a half-plane, under plane strain, by surface tractions, $p\,(x)$ and $q\,(x)$, is [Barber, 2010]

$$\varepsilon_{xx}^{p(x),q(x)}(x) = -\frac{2}{\pi E^*}\int_{-a}^{b}\frac{q\,(\xi)\,\mathrm{d}\xi}{x-\xi} + \frac{(1-2\nu)}{(1-\nu)\,E^*}\,p(x)\,, \tag{A.47}$$

where $E^* = E/\,(1-\nu^2)$, E is Young's modulus and ν is Poisson's ratio. We know the contact pressure rigorously, originating from the normal load, P, and moment, M. In any practical problem, the total surface strains, ε_{xx}, everywhere on the surface can be found using the finite element output. The contribution from the contact pressure (and therefore P, M) is given by

$$\varepsilon_{xx}^{P,M}(x) = \frac{(1-2\nu)}{(1-\nu)\,E^*}\,p(x)\,, \tag{A.48}$$

and as we have found a solution under no-slip conditions, so we can also find the implied surface strains resulting from the effects of an applied shear force, Q, and the shear tractions arising from differential bulk tension, σ, rigorously, *for once and for all*, from equation (A.42), which gives

$$\varepsilon_{xx}^{Q}(x) = -\frac{2Q}{\pi^2 E^*}\int_{-a}^{b}\frac{\mathrm{d}\xi}{(x-\xi)\sqrt{(a+\xi)\,(b-\xi)}} = 0\ , -a < x < b\ , \tag{A.49}$$

and

$$\varepsilon_{xx}^{\sigma}(x) = -\frac{\sigma_{\mathrm{A}}-\sigma_{\mathrm{B}}}{4\pi E^*}\int_{-a}^{b}\frac{(2\xi+a-b)\,\mathrm{d}\xi}{(x-\xi)\,\sqrt{(a+\xi)\,(b-\xi)}} = -\frac{\sigma_{\mathrm{A}}-\sigma_{\mathrm{B}}}{4E^*}\ , -a < x < b\ . \tag{A.50}$$

The total strain distribution within the fully stuck contact will therefore have four contributions, *viz.* the three just derived $\varepsilon_{xx}^{P,M}(x), \varepsilon_{xx}^{Q}(x), \varepsilon_{xx}^{\sigma}(x)$ together with the effect of the *average* remote bulk loads, i.e.

$$\varepsilon_{xx}^{\sigma_{\mathrm{A}}+\sigma_{\mathrm{B}}}(x) = \frac{\sigma_{\mathrm{A}}+\sigma_{\mathrm{B}}}{2E^*}\ , \tag{A.51}$$

giving, therefore, the sum of the bulk stresses. Notice that the results derived here should be robust in the sense that they are averaged and do not rely on 'spot' values. With sequential loading they are not geometry dependent: under full stick conditions the shear traction distribution is fully defined without knowing the relative profile of the contacting bodies.

A.3 Leading-order Asymptotic Form

Consider the expression for the contact pressure for an indenter under both an applied normal force, P, and an applied moment, M, as given by Eq. (6.43):

$$p(x) = \frac{1}{\pi}\int_{P_x}^{P}\left[\frac{1}{\sqrt{(a+x)\,(b-x)}} + \frac{4\,(2x+a-b)}{(a+b)^2\,\sqrt{(a+x)\,(b-x)}}\frac{\mathrm{d}M}{\mathrm{d}\tilde{P}}\right]\mathrm{d}\tilde{P}. \tag{A.52}$$

where $-a < x < b$. In this expression, the size of the contact is a function of both P and M with $a(P,M) = a$ and $b(P,M) = b$. We shall restrict ourselves to the case in which the loading is proportional, and in particular, we set

$$\frac{\mathrm{d}M}{\mathrm{d}P} = \gamma a. \tag{A.53}$$

For notational brevity, we introduce the shorthand notation

$$\bar{a}(P) = a(s, \gamma a s),\ \bar{b}(s) = b(s, \gamma a s). \tag{A.54}$$

We seek the coefficients of the square-root bounded terms as $x \to -a^+$, $x \to b^-$. We shall consider the right-hand contact point in detail to illustrate the methodology, but a similar analysis follows for the left-hand contact point. Suppose

$$x = b - \delta X \tag{A.55}$$

where $0 < \delta \ll 1$ and $X = O(1)$ strictly. Provided that $\bar{b}(P)$ is sufficiently well-behaved so as to have a Taylor expansion there, we know that

$$P_x = P - \delta \hat{P} \text{ where } \hat{P} = \frac{X}{\bar{b}'(P)} + O(\delta). \tag{A.56}$$

In particular, since we shall only require the leading-order term in the asymptotic expansion, it will be sufficient for us to assume that $X - \hat{P}\bar{b}'(P) = o(1)$ henceforth. In the integral, we set $\tilde{P} = P - \delta S$. Then,

$$p = \frac{\sqrt{\delta}}{\pi} \int_0^{\hat{P}} \left(1 + \frac{4\gamma a(b+a)}{(a+b)^2} + O(\delta)\right) \frac{1}{\sqrt{(a+b) + O(\delta)}} \frac{1}{\sqrt{X - S\bar{b}'(P) + O(\delta)}} \, \mathrm{d}S. \tag{A.57}$$

Assuming δ is small, we can expand each term in the integrand in terms of Taylor series, finding that

$$p = \frac{\sqrt{\delta}}{\pi\sqrt{a+b}} \left(1 + \frac{4\gamma a}{(a+b)}\right) \int_0^{X/\bar{b}'(P)} \frac{1}{\sqrt{X - S\bar{b}'(P)}} \, \mathrm{d}S + O(\delta^{3/2}), \tag{A.58}$$

where we have used the approximation for $\hat{P}$ in Eq. (A.56). Thus, after integrating and returning to the original variables, we see that

$$p(x) = \frac{2}{\bar{b}'(P)\pi\sqrt{a+b}} \left(1 + \frac{4\gamma a}{(a+b)}\right) \sqrt{b-x} + o\left(\sqrt{b-x}\right) \tag{A.59}$$

as $x \to b^-$.

By setting $x = -a + \delta X$ where $0 < \delta \ll 1$ and X is strictly order unity, a similar analysis yields

$$p(x) = \frac{2}{\bar{a}'(P)\pi\sqrt{a+b}} \left(1 - \frac{4\gamma a}{(a+b)}\right) \sqrt{a+x} + o\left(\sqrt{a+x}\right) \tag{A.60}$$

as $x \to -a^+$.

Naturally, a similar process also holds for the shear tractions, $q(x)$, as given by Eq. (6.44),

$$q(x) = \int_{P_x}^{P} \left[\frac{1}{\pi\sqrt{(a+x)(b-x)}} \frac{\mathrm{d}Q}{\mathrm{d}\tilde{P}} + \frac{(2x+a-b)}{8\sqrt{(a+x)(b-x)}} \frac{d\Delta\sigma}{\mathrm{d}\tilde{P}} \right] \mathrm{d}\tilde{P}. \tag{A.61}$$

We again assume proportional loading, defining

$$\frac{\mathrm{d}Q}{\mathrm{d}P} = \lambda, \ \frac{\mathrm{d}\Delta\sigma}{\mathrm{d}P} = \frac{\eta}{a}. \tag{A.62}$$

Then, an asymptotic analysis yields

$$q(x) = \frac{2}{\bar{b}'(P)\sqrt{a+b}} \left(\frac{\lambda}{\pi} + \frac{\eta(a+b)}{8a} \right) \sqrt{b-x} + o\left(\sqrt{b-x}\right) \tag{A.63}$$

as $x \to b^-$, and

$$q(x) = \frac{2}{\bar{a}'(P)\sqrt{a+b}} \left(\frac{\lambda}{\pi} - \frac{\eta(a+b)}{8a} \right) \sqrt{a+x} + o\left(\sqrt{a+x}\right) \tag{A.64}$$

as $x \to -a^+$.

Therefore, the desired ratios of the coefficients are given by

$$\frac{q(-a^+)}{p(-a^+)} = \frac{1}{8} \frac{\left(1+\left(\frac{b}{a}\right)\right)^2 \left[8\lambda - \pi\eta\left(1+\frac{b}{a}\right)\right]}{\left(1+\left(\frac{b}{a}\right)\right)^2 - 4\gamma\left(1+\frac{b}{a}\right)}, \tag{A.65}$$

as we approach the left-hand contact point, and

$$\frac{q(b^-)}{p(b^-)} = \frac{1}{8} \frac{\left(1+\left(\frac{b}{a}\right)\right)^2 \left[8\lambda + \pi\eta\left(1+\frac{b}{a}\right)\right]}{\left(1+\left(\frac{b}{a}\right)\right)^2 + 4\gamma\left(1+\frac{b}{a}\right)}, \tag{A.66}$$

as we approach the right-hand contact point, respectively.

A.4 Experimental Data

Test	Radius [mm]	a [mm]	p_0 [MPa]	P [N/mm]	Q/P [-]	σ_{mean} [MPa]	ΔQ [N/mm]	$\Delta\sigma$ [MPa]	K_N [MPa/mm$^{1/2}$]	ΔK_T LHS [MPa mm$^{1/2}$]	ΔK_T RHS [MPa mm$^{1/2}$]	N_f [-]	d LHS [µm]	d RHS [µm]
1	13	0.1	157	25	0.45	0	22	185	743	26	5	1.00E+07	47	10
2	25	0.19	157	47	0.45	0	42	185	512	36	8	1.00E+07	94	20
3	38	0.28	157	69	0.45	0	62	185	414	44	9	1.00E+07	141	29
4	50	0.38	157	94	0.45	0	84	185	362	51	11	1.29E+06	188	39
5	75	0.57	157	141	0.45	0	127	185	296	62	13	6.70E+05	282	59
6	100	0.76	157	187	0.45	0	169	185	256	72	15	8.50E+05	376	78
7	125	0.95	157	234	0.45	0	211	185	229	81	17	7.30E+05	470	98
8	150	1.14	157	281	0.45	0	253	185	209	88	18	6.70E+05	564	117
9	13	0.09	143	20	0.24	0	10	185	705	17	-3	1.00E+07	32	5
10	25	0.18	143	40	0.24	0	19	185	498	24	-4	1.00E+07	65	10
11	50	0.36	143	81	0.24	0	39	185	352	34	-5	1.00E+07	130	19
12	75	0.54	143	121	0.24	0	58	185	288	42	-6	1.00E+07	194	29
13	100	0.72	143	162	0.24	0	78	185	249	48	-7	5.06E+06	259	39
14	125	0.9	143	202	0.24	0	97	185	223	54	-8	1.22E+06	324	48
15	150	1.08	143	243	0.24	0	116	185	203	59	-9	1.28E+06	389	58
16	13	0.09	143	20	0.45	0	18	185	705	23	4	1.00E+07	44	7
17	25	0.18	143	40	0.45	0	36	185	498	33	5	1.00E+07	89	14
18	38	0.27	143	61	0.45	0	55	185	407	41	7	4.04E+06	133	22
19	50	0.36	143	81	0.45	0	73	185	352	47	8	1.50E+06	178	29
20	75	0.54	143	121	0.45	0	109	185	288	58	9	8.00E+05	267	43
21	100	0.72	143	162	0.45	0	146	185	249	66	11	6.10E+05	356	58
22	125	0.9	143	202	0.45	0	182	185	223	74	12	1.24E+06	444	72
23	150	1.08	143	243	0.45	0	218	185	203	81	13	1.08E+06	533	87
24	13	0.09	143	20	0.45	0	18	154	705	22	5	1.00E+07	41	10
25	25	0.18	143	40	0.45	0	36	154	498	31	8	1.00E+07	83	21
26	50	0.36	143	81	0.45	0	73	154	352	44	11	1.00E+07	165	41
27	75	0.54	143	121	0.45	0	109	154	288	54	13	1.20E+06	248	62
28	100	0.72	143	162	0.45	0	146	154	249	62	15	1.42E+06	331	83
29	125	0.9	143	202	0.45	0	182	154	223	69	17	1.02E+06	413	103
30	25	0.14	120	26	0.45	0	24	240	439	30	-2	1.00E+07	92	5
31	38	0.21	120	40	0.45	0	36	240	359	37	-2	1.00E+07	137	7
32	50	0.28	120	53	0.45	0	48	240	311	43	-2	1.00E+07	183	10
33	75	0.42	120	79	0.45	0	71	240	254	52	-3	1.00E+07	275	14
34	100	0.57	120	107	0.45	0	97	240	222	61	-3	1.00E+07	366	19
35	125	0.71	120	134	0.45	0	120	240	198	68	-4	1.57E+06	458	24
36	150	0.85	120	160	0.45	0	144	240	180	74	-4	1.23E+06	549	29

Table A.1: A summary of parameters and the observed number of cycles for the fretting fatigue experiments conducted by Nowell [Nowell, 1988] for Aluminium.

Test	Radius [mm]	a [mm]	p_0 [MPa]	P [N/mm]	Q/P [-]	σ_{mean} [MPa]	ΔQ [N/mm]	$\Delta\sigma$ [MPa]	K_N [MPa/mm$^{1/2}$]	ΔK_T LHS [MPa mm$^{1/2}$]	ΔK_T RHS [MPa mm$^{1/2}$]	N_f [-]	d LHS [µm]	d RHS [µm]
1	127	1.54	246	595	0.22	0	262	221	287	96	-1	3.14E+05	514	5
2	127	1.24	198	385	0.28	0	216	169	258	77	10	4.22E+05	459	61
3	127	1.31	208	427	0.31	0	265	221	265	97	7	2.41E+05	562	44
4	121	1.21	203	384	0.35	0	269	201	267	94	16	2.41E+05	542	92
5	121	1.37	231	497	0.31	0	308	221	284	105	14	2.17E+05	568	74
6	229	1.76	156	429	0.43	0	369	223	170	115	10	2.38E+05	1040	93
7	229	1.75	155	427	0.37	0	316	226	170	107	1	2.50E+05	966	9
8	127	1.4	223	490	0.23	0	226	170	274	78	7	6.68E+05	440	42
9	178	1.66	189	494	0.27	0	267	200	213	92	1	3.50E+05	666	7
10	178	1.66	189	493	0.27	0	266	200	213	92	1	4.34E+05	666	7
11	127	1.3	207	423	0.35	0	296	177	264	94	23	5.64E+05	548	133
12	127	1.51	240	569	0.31	0	353	204	284	109	20	5.45E+05	589	110
13	127	1.51	240	569	0.31	0	353	204	284	109	20	3.38E+05	589	110
14	178	1.53	174	418	0.38	0	318	172	204	95	20	5.83E+05	718	153
15	229	1.88	166	490	0.32	0	314	194	176	99	4	7.39E+05	861	39
16	178	1.75	200	551	0.34	0	374	226	218	117	11	4.56E+05	821	76
17	229	1.88	167	494	0.32	0	316	171	176	93	10	8.57E+05	815	92
18	127	1.28	204	410	0.52	0	426	232	262	131	38	4.65E+05	770	226
19	178	1.77	201	558	0.21	0	234	170	220	80	0	6.65E+05	558	3
20	178	1.77	201	558	0.21	0	234	170	220	80	0	7.49E+05	558	3
21	229	2	177	557	0.24	0	267	164	182	83	2	7.47E+05	707	14
22	229	2	177	557	0.25	0	278	164	182	85	3	7.30E+05	722	29
23	127	1.4	223	489	0.35	0	343	218	274	111	20	3.03E+05	623	110
24	229	1.73	153	417	0.31	0	258	162	169	82	7	8.67E+05	746	60
25	229	1.74	154	419	0.26	0	218	166	169	76	-1	7.68E+05	689	13
26	178	1.79	204	571	0.31	0	354	199	221	107	13	5.52E+05	742	87
27	229	1.99	176	551	0.34	0	375	219	181	114	5	3.21E+05	972	44
28	127	1.49	238	557	0.27	0	301	218	283	102	9	2.54E+05	558	46
29	229	1.87	166	487	0.33	0	322	222	176	107	-1	4.80E+05	933	5
30	127	1.4	224	494	0.36	0	356	196	274	109	27	4.64E+05	611	150
31	229	2.01	178	563	0.24	0	270	196	182	92	-6	4.63E+05	778	52
32	178	1.65	188	486	0.27	0	263	169	212	85	8	6.21E+05	613	55
33	178	1.53	174	419	0.36	0	302	195	204	97	12	4.60E+05	734	93
34	178	1.69	192	509	0.34	0	346	213	215	109	11	2.26E+05	780	79
35	178	1.53	175	421	0.38	0	320	221	204	107	10	3.31E+05	803	75
36	127	1.31	209	430	0.33	0	284	194	265	95	17	3.12E+05	552	96
37	127	1.5	239	560	0.27	0	303	171	284	93	19	3.82E+05	503	101

Table A.2: A summary of parameters and the observed number of cycles for the fretting fatigue experiments conducted by Szolwinski et al. [Szolwinski and Farris, 1998] for Aluminium.

Test	Radius [mm]	a [mm]	p_0 [MPa]	P [N/mm]	Q/P [-]	σ_{mean} [MPa]	ΔQ [N/mm]	$\Delta\sigma$ [MPa]	K_N [MPa/mm$^{1/2}$]	ΔK_T LHS [MPa mm$^{1/2}$]	ΔK_T RHS [MPa mm$^{1/2}$]	N_f [-]	d LHS [µm]	d RHS [µm]
1	50	0.46	136	100	0.29	55	79	90	388	37	15	1.41E+06	146	61
2	50	0.46	136	100	0.34	63	92	104	388	43	18	1.11E+06	170	72
3	50	0.46	136	100	0.41	74	111	122	388	51	22	4.20E+05	204	88
4	50	0.46	136	100	0.29	74	79	122	388	41	11	3.58E+05	161	46
5	50	0.46	136	100	0.36	88	98	144	388	50	15	2.46E+05	197	60
6	50	0.46	136	100	0.61	105	166	171	388	75	34	1.42E+05	299	136
7	50	0.46	136	100	0.59	113	160	185	388	75	31	1.15E+05	298	122
8	50	0.46	136	100	0.49	121	133	198	388	68	20	9.96E+04	269	80
9	50	0.46	136	100	0.59	121	160	198	388	77	29	8.66E+04	304	116

Table A.3: A summary of parameters and the observed number of cycles for the fretting fatigue experiments conducted by Hojati-Talemi et al. [Hojjati-Talemi et al., 2014] for Aluminium.

Test	Radius [mm]	a [mm]	p_0 [MPa]	P [N/mm]	Q/P [-]	σ_{mean} [MPa]	ΔQ [N/mm]	$\Delta\sigma$ [MPa]	K_N [MPa/mm$^{1/2}$]	ΔK_T LHS [MPa mm$^{1/2}$]	ΔK_T RHS [MPa mm$^{1/2}$]	N_f [-]	d LHS [µm]	d RHS [µm]
1	8.2	4.19	565	1200	0.13	400	312	229	2163	117	-48	5.56E+04	83	34
2	4.9	4.13	665	1200	0.13	400	312	229	3050	117	-48	6.09E+04	59	24
3	4.9	4.13	665	1200	0.13	400	312	160	3050	92	-23	1.23E+05	46	12
4	4.9	4.13	665	1200	0.13	280	312	160	3050	92	-23	2.19E+05	46	12
5	4.9	4.13	665	1200	0.13	280	312	160	3050	92	-23	3.45E+05	46	12
6	4.9	4.13	665	1200	0.13	280	312	160	3050	92	-23	4.74E+05	46	12
7	4.9	4.13	665	1200	0.13	280	312	160	3050	92	-23	2.15E+05	46	12
8	4.9	4.13	665	1200	0.13	280	312	160	3050	92	-23	3.04E+05	46	12
9	4.9	4.13	665	1200	0.13	280	312	160	3050	92	-23	2.11E+05	46	12
10	4.9	4.13	665	1200	0.13	210	312	120	3050	78	-9	1.00E+07	39	4
11	4.9	4.13	665	1200	0.13	163	312	93	3050	68	1	1.00E+07	34	0
12	13	4.25	478	1200	0.13	187	312	107	1575	73	-5	1.00E+07	71	5
13	13	4.25	478	1200	0.13	400	312	229	1575	117	-49	8.81E+04	115	48
14	13	4.25	478	1200	0.13	280	312	160	1575	92	-24	4.53E+05	90	24
15	13	4.25	478	1200	0.13	233	312	133	1575	83	-15	1.00E+07	81	14
16	13	4.25	478	1200	0.13	327	312	187	1575	102	-34	1.83E+05	100	33
17	13	4.34	665	1950	0.13	400	507	229	1867	139	-29	6.23E+04	115	24
18	13	4.34	665	1950	0.13	327	507	187	1867	123	-14	2.61E+05	102	11
19	13	4.34	665	1950	0.13	233	507	133	1867	104	6	8.19E+05	86	5
20	13	4.34	665	1950	0.13	210	507	120	1867	99	11	1.45E+06	82	9
21	8.2	4.19	565	1200	0.13	400	312	229	2163	117	-48	6.12E+04	83	34
22	8.2	4.19	565	1200	0.13	327	312	187	2163	102	-33	1.54E+05	72	24
23	8.2	4.19	565	1200	0.13	280	312	160	2163	92	-24	2.31E+05	66	17
24	8.2	4.19	565	1200	0.13	257	312	147	2163	87	-19	1.00E+07	62	13
25	8.2	4.19	565	1200	0.13	233	312	133	2163	83	-14	1.00E+07	59	10
26	8.2	4.19	565	1200	0.26	257	624	147	2163	122	16	2.02E+05	87	11
27	8.2	4.19	565	1200	0.26	233	624	133	2163	117	20	7.54E+05	83	14
28	8.2	4.19	565	1200	0.26	280	624	160	2163	127	11	1.65E+05	90	8
29	8.2	4.19	565	1200	0.26	327	624	187	2163	136	1	1.25E+05	97	1
30	8.2	4.19	565	1200	0.26	373	624	213	2163	146	-9	6.81E+04	104	6
31	8.2	4.19	565	1200	0.26	210	624	120	2163	112	25	4.29E+05	80	18
32	8.2	4.19	565	1200	0.26	187	624	107	2163	107	30	5.89E+05	76	21
33	8.2	4.19	565	1200	0.26	140	624	80	2163	98	40	2.07E+06	69	28
34	8.2	4.19	565	1200	0.26	93	624	53	2163	88	49	1.00E+07	63	35
35	8.2	4.19	565	1200	0.26	233	624	133	2163	117	20	2.69E+05	83	14
36	8.2	4.22	665	1550	0.13	373	403	213	2355	122	-33	1.04E+05	79	22
37	8.2	4.22	665	1550	0.13	327	403	187	2355	112	-24	1.43E+05	73	15

Table A.4: A summary of parameters and the observed number of cycles for the fretting fatigue experiments conducted by Dini [Dini, 2003] for Titanium - part A.

Test	Radius [mm]	a [mm]	p_0 [MPa]	P [N/mm]	Q/P [-]	σ_{mean} [MPa]	ΔQ [N/mm]	$\Delta\sigma$ [MPa]	K_N [MPa/mm$^{1/2}$]	ΔK_T LHS [MPa mm$^{1/2}$]	ΔK_T RHS [MPa mm$^{1/2}$]	N_f [-]	d LHS [µm]	d RHS [µm]
38	8.2	4.22	665	1550	0.13	257	403	147	2355	97	-9	2.81E+05	64	6
39	8.2	4.22	665	1550	0.13	210	403	120	2355	88	1	1.00E+07	57	0
40	8.2	4.22	665	1550	0.13	233	403	133	2355	93	-4	6.17E+05	60	3
41	8.2	4.22	665	1550	0.13	280	403	160	2355	102	-14	5.53E+05	67	9
42	8.2	4.22	665	1550	0.13	210	403	120	2355	88	1	1.00E+07	57	0
43	13	4.25	478	1200	0.13	257	312	147	1575	87	-19	5.04E+06	85	19
44	13	4.34	665	1950	0.13	280	507	160	1867	114	-4	2.17E+05	94	3
45	13	4.34	665	1950	0.13	257	507	147	1867	109	1	2.63E+05	90	1
46	4.9	4.13	665	1200	0.13	280	312	160	3050	92	-23	2.31E+05	46	12
47	4.9	4.13	665	1200	0.13	257	312	147	3050	87	-18	7.15E+05	44	9
48	4.9	4.13	665	1200	0.13	233	312	133	3050	82	-13	4.17E+05	42	7
49	4.9	4.13	665	1200	0.13	233	312	133	3050	82	-13	1.00E+07	42	7
50	4.9	4.13	665	1200	0.13	327	312	187	3050	102	-33	1.21E+05	51	16
51	4.9	4.13	665	1200	0.13	350	312	200	3050	106	-37	7.68E+04	54	19
52	13	4.34	665	1950	0.13	187	507	107	1867	94	16	4.98E+05	77	13
53	13	4.34	665	1950	0.13	187	507	107	1867	94	16	7.80E+05	77	13
54	13	4.34	665	1950	0.13	163	507	93	1867	89	20	1.00E+07	73	17
55	8.2	4.19	565	1200	0.39	327	936	187	2163	170	35	8.92E+04	121	25
56	8.2	4.19	565	1200	0.39	280	936	160	2163	161	45	1.40E+05	114	32
57	8.2	4.19	565	1200	0.39	233	936	133	2163	151	55	2.77E+05	108	39
58	8.2	4.19	565	1200	0.39	187	936	107	2163	142	64	4.16E+05	101	46
59	8.2	4.19	565	1200	0.39	140	936	80	2163	132	74	1.17E+06	94	53
60	8.2	4.19	565	1200	0.13	147	312	1026	2163	406	-337	3.08E+04	288	240
61	8.2	4.19	565	1200	0.13	187	312	1307	2163	507	-439	1.17E+04	361	312
62	8.2	4.19	565	1200	0.39	93	936	53	2163	122	84	6.01E+06	87	59
63	8.2	4.22	665	1550	0.13	490	403	280	2355	146	-58	4.05E+04	95	38
64	8.2	4.22	665	1550	0.13	513	403	293	2355	151	-62	3.64E+04	98	41
65	8.2	4.22	665	1550	0.13	560	403	320	2355	160	-72	2.51E+04	105	47
66	8.2	4.19	565	1200	0.26	467	624	267	2163	165	-28	4.06E+04	117	20
67	8.2	4.19	565	1200	0.26	490	624	280	2163	170	-33	3.96E+04	121	23
68	8.2	4.19	565	1200	0.26	513	624	293	2163	175	-38	3.43E+04	124	27
69	8.2	4.19	565	1200	0.26	560	624	320	2163	184	-47	2.82E+04	131	34

Table A.5: A summary of parameters and the observed number of cycles for the fretting fatigue experiments conducted by Dini [Dini, 2003] for Titanium - part B.

A.5 Range of Asymptotic Multipliers

The asymptotic multipliers, K_N and ΔK_T, lend themselves particularly well for characterising the fretting fatigue strength as they are the equivalents of a combined mode I/mode II loading, as explained in §7.4. In Figures A.4 and A.5 those experiments which led to run outs ($> 10^7$ cycles), are highlighted. Their position at the bottom of the spectrum suggest that the fretting fatigue strength is predominantly controlled by the underlying value of ΔK_T with a secondary effect of the corresponding K_N value. The slip zone size is a result of the combined loading and is therefore chosen to be the guiding parameter in our subsequent visualisation of the fretting fatigue strength.

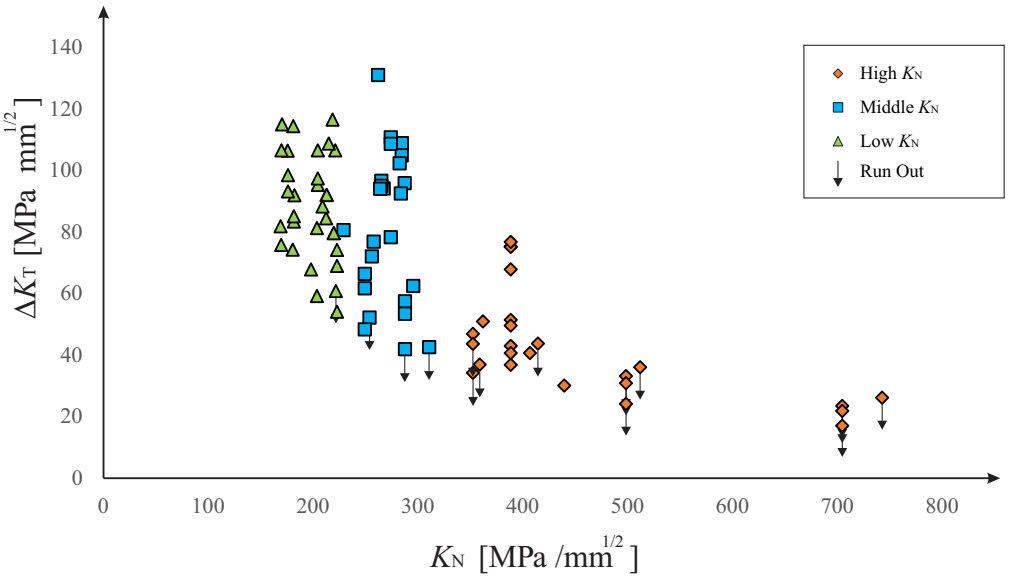


Figure A.4: Range of K_N values plotted against the corresponding values of ΔK_T for the pooled data set of Aluminium alloys.

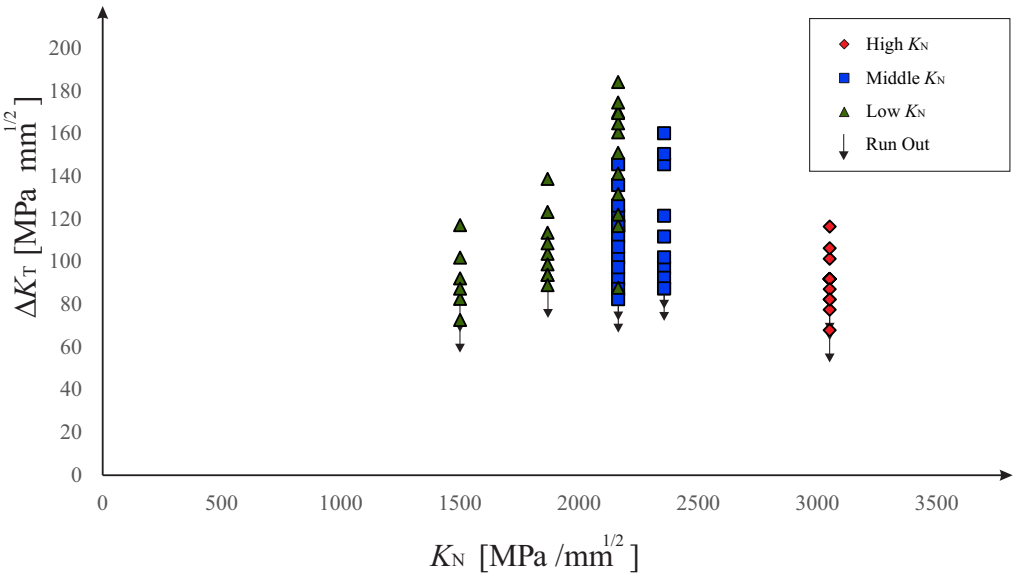


Figure A.5: Range of K_N values plotted against the corresponding values of ΔK_T for Titanium.

Bibliography

[Amontons, 1699] Amontons, G. (1699). De la resistance cause dans les machines. *Mémoires de l'Académie royale des sciences*, **41**:206 – 222.

[Anderson et al., 2016] Anderson, P., Hirth, J., and Lothe, J. (2016). *Theory of Dislocations (third edition)*. Cambridge University Press.

[Andresen et al., 2020a] Andresen, H., Fleury, R., Moore, M., and Hills, D. (2020a). Explicit and asymptotic solutions for frictional incomplete half-plane contacts subject to general oscillatory loading in the steady-state. *J. Mech. Phys. Solids, under review*.

[Andresen and Hills, 2020] Andresen, H. and Hills, D. (2020). A review of partial slip solutions for contacts represented by half-planes including bulk tension and moments. *Tribology Int.*, **143**:106050.

[Andresen et al., 2019a] Andresen, H., Hills, D., Barber, J., and Vázquez, J. (2019a). Frictional half-plane contact problems subject to alternating normal and shear loads and tension in the steady state. *Int. J. Solids Struct.*, **168**:166 – 171.

[Andresen et al., 2020b] Andresen, H., Hills, D., Barber, J., and Vázquez, J. (2020b). Steady state cyclic behaviour of a half-plane contact inpartial slip subject to varying normal load, moment, shear load, and moderate differential bulk tension. *Int. J. Solids Struct.*, **182-183**:156 – 161.

[Andresen et al., 2020c] Andresen, H., Hills, D., and Moore, M. (2020c). The steady state partial slip problem for half plane contacts subject to a constant normal load using glide dislocations. *Eur. J. Mech/A Solids*, **79**:103868.

[Andresen et al., 2019b] Andresen, H., Hills, D., and Vázquez, J. (2019b). Closed-form solutions for tilted three-part piecewise-quadratic half-plane contacts. *Int. J. Mech. Sci.*, **150**:127 – 134.

[Andresen et al., 2020d] Andresen, H., Hills, D., Wormsen, A., and Macdonald, K. (2020d). Fretting Fatigue design of subsea connectors; a generalised approach to testing. *Proceedings of the ASME 2020 39th International Conference on Ocean, Offshore and Arctic Engineering*, **39**, in press.

[Andresen et al., 2020e] Andresen, H., Moore, M., and Hills, D. (2020e). Representation of incomplete contact problems by half-planes. *Eur. J. Mech/A Solids, accpeted for publication.*

[Arrieta and Wackers, 2004] Arrieta, H. and Wackers, P. (2004). Modelling attempts to predict fretting-fatigue life on turbine components. *RTO Applied Vehicle Technology Panel Symposium Proceedings*, **22**:1 – 12.

[Banerjee et al., 2009] Banerjee, N., Hills, D., and Dini, D. (2009). The derivation and application of a semi-infinite flat and rounded asymptotic frictionless contact. *Int. J. Mech. Sci.*, **51**:662 – 666.

[Barber, 1983] Barber, J. (1983). The solution of elasticity problems for the half-space by the method of green and collins. *Appl. Sci. Research*, **40**:135 – 157.

[Barber, 2010] Barber, J. (2010). *Elasticity (third edition).* Springer.

[Barber, 2018] Barber, J. (2018). *Contact Mechanics.* Springer.

[Barber et al., 2011] Barber, J., Davies, M., and Hills, D. (2011). Frictional elastic contact with periodic loading. *Int. J. Solids Struct.*, **48**:2041 – 2047.

[Basquin, 1910] Basquin, O. H. (1910). The exponential law of endurance test. *Proc. American Soc. Test. and Mat.*, **10**:625 – 630.

[Bramhall, 1973] Bramhall, R. (1973). *Studies in Fretting Fatigue.* PhD thesis, University of Oxford.

[Cattaneo, 1938] Cattaneo, C. (1938). Sul contato di due corpo elastici. *Atti Accad. Naz. Lincei, Cl. Sci. Fis., Mat. Nat., Rend.*, **27**:342 – 348, 434 – 436, 474 – 478.

[Ciavarella, 1998] Ciavarella, M. (1998). The generalised cattaneo partial slip plane contact problem, part i theory, part ii examples. *Int. J. Solids Struct.*, **35**:2349 – 2378.

[Ciavarella et al., 1998] Ciavarella, M., Hills, D., and Monno, G. (1998). The influence of rounded edges on indentation by a flat punch. *Proc. Instn. Mech. Engrs.*, **212**:Part C.

[Comninou, 1976] Comninou, M. (1976). Stress singularity at a sharp edge in contact problems with friction. *J. Appl. Math. Phys.*, **27**:493 – 499.

[Coulomb, 1785] Coulomb, C. (1785). Theorie des machines simples. *Mémoires de mathématique et de physique, presentés à l'Académie royale des sciences*, **41**:161 – 342.

[Dini, 2003] Dini, D. (2003). *Studies in Fretting Fatigue with particular application to almost complete contacts*. PhD thesis, University of Oxford.

[Dini and Hills, 2004] Dini, D. and Hills, D. (2004). Bounded asymptotic solutions for incomplete contacts in partial slip. *Int. J. Solids Sruct.*, **41**:7049 – 7062.

[Dini et al., 2005] Dini, D., Sackfield, A., and Hills, D. A. (2005). Comprehensive bounded asymptotic solutions for incomplete contacts in partial slip. *J. Mech. Phys. Solids*, **53 (2)**:437 – 454.

[Dundurs, 1969] Dundurs, J. (1969). Discussion of edge-bonded dissimlar orhtogonal wedges under normal and shear loading (by d. bogey. *J. Appl. Mech.*, **36**:342 – 348, 650 – 652.

[Erdogan et al., 1973] Erdogan, F., Gupta, G., and Cook, T. (1973). *Numerical Solution of singular integral equations (Methods of Analysis and Solutions of Crack Problems)*. Ed. G.C. Sih, Noordhoff.

[Fenner and Field, 1958] Fenner, A. and Field, J. (1958). La fatigue dans les conditions de frottement. *Rev. Met.*, **55**:75 – 485.

[Fenner and Field, 1960] Fenner, A. and Field, J. (1960). A study of the onset of fatigue damage due to fretting. *Proc. NE Coast Inst. of Engineers and Shipbuilders*, **76**:183 – 195.

[Fleury et al., 2016a] Fleury, R. M. N., Hills, D. A., and Barber, J. R. (2016a). A corrective solution for finding the effects of edge rounding on complete contact between elastically similar bodies. Part I: Contact law and normal contact considerations. *Int. J. Solids Struct.*, **85 - 86**:89 – 96.

[Fleury et al., 2016b] Fleury, R. M. N., Hills, D. A., and Barber, J. R. (2016b). A corrective solution for finding the effects of edge rounding on complete contact between elastically similar bodies. Part II: Near-edge asymptotes and the effect of shear. *Int. J. Solids Struct.*, **85 - 86**:97 – 104.

[Fleury et al., 2017] Fleury, R. M. N., Hills, D. A., Ramesh, R., and Barber, J. R. (2017). Incomplete contacts in partial slip subject to varying normal and shear loading, and their representation by asymptotes. *J. Mech. Phys. Solids*, **99**:178 – 191.

[Hertz, 1881] Hertz, H. (1881). Über die Berührung fester elastischer Körper. *Journal für die reine und angewandte Mathematik*, **92**:156 – 171.

[Hibbeler, 2016] Hibbeler, R. (2016). *Mechanics of Materials*. Pearson Publications.

[Hills and Andresen, 2020] Hills, D. and Andresen, H. (2020). *Fundamentals of Elastic Contacts. In: M. Paggi and D.A. Hills, ed., Modeling and Simulation of Tribological Problems in Technology (1st ed.)*. Springer Int. Publish.

[Hills et al., 2011] Hills, D., Davies, M., and Barber, J. (2011). An incremental formulation for half-plane contact problems subject to varying normal load, shear, and tension. *J. Strain Ana.*, **46**:436 – 443.

[Hills et al., 1996] Hills, D., Kelly, P., Dai, D., and Korsunsky, A. (1996). *Solution of Crack Problems*. Kluwer Academic Publishers.

[Hills and Nowell, 1987] Hills, D. and Nowell, D. (1987). Mechanics of fretting fatigue tests. *Int. J. Mech. Sci.*, **29**:355 – 365.

[Hills and Nowell, 1994] Hills, D. and Nowell, D. (1994). *Mechanics of Fretting Fatigue*. Springer.

[Hills et al., 1993] Hills, D., Nowell, D., and Sackfield, A. (1993). *Mechanics of Elastic Contacts*. Butterworth-Heinemann.

[Hojjati-Talemi et al., 2014] Hojjati-Talemi, R., Wahab, M., De Pauw, J., and De Baets, P. (2014). Prediction of fretting fatigue crack initiation and propagation lifetime for cylindrical contact configuration. *Tri. Int.*, **76**:73 – 91.

[Hull and Bacon, 2011] Hull, D. and Bacon, D. (2011). *Introduction to Dislocations*. Butterworth-Heinemann.

[Jäger, 1997] Jäger, J. (1997). Ein neues Prinzip der Kontaktmechnik. *ZAMM*, **77, S1**:143 – 144.

[Johnson, 1985] Johnson, K. (1985). *Contact Mechanics*. Cambridge University Press.

[Karuppanan and Hills, 2008] Karuppanan, S. and Hills, D. (2008). Frictional complete contacts between elastically similar bodies subject to normal and shear load. *Int. J. Solids Struct.*, **17**:4662 – 4675.

[Krenk, 1975] Krenk, S. (1975). On the use of the interpolation polynomial for solutions of singular integral equations. *Quarterly of Applied Mathematics*, **32 (4)**:479 – 484.

[Lau, 1964] Lau, M. (1964). *On the stress distribution of cylindrical elastic bodies in contact*. PhD thesis, Doktorsavhandlingar, University of Goteborg, Chalmers Tekniska Hogskola.

[Lopes and Hills, 2019] Lopes, J. and Hills, D. (2019). The axisymmetric frictional receding contact of a layer pressed against a half-space by pressure outside a disk. *Eur. J. Mech. A/Solids*, **77**:103787.

[McDowell, 1953] McDowell, J. (1953). Fretting corrosion tendencies and several combinations of materials. *Symposium on Fretting Corrosion, ASMT*, **144**:24 – 39.

[Mindlin, 1949] Mindlin, R. (1949). Compliance of elastic bodies in contact. *AASME Trans. J. Appl. Mech.*, **16**:259 – 268.

[Mindlin and Dereiewicz, 1953] Mindlin, R. and Dereiewicz, H. (1953). Elastic spheres in contact under varying oblique forces. *J. of Applied Mechanics*, **20**:327 – 344.

[Mindlin et al., 1951] Mindlin, R., Mason, W., Osmer, T., and Dereiewicz, H. (1951). Effect of an oscillating tangential force on the contact surfaces of elastic spheres. *Proc. First Nat. Congress of Applied Mechanics*, pages 203 – 208.

[Moore and Hills, 2020] Moore, M. and Hills, D. (2020). Extending the Mossakovskii Method to Contacts supporting a Moment. *J. Mech. Phys. Solids*, **141**:103989.

[Moore and Hills, 2018] Moore, M. R. and Hills, D. (2018). Solution of half-plane contact problems by distributing climb dislocations. *Int. J. Solids Struct.*, **147**:61 – 66.

[Moore et al., 2018] Moore, M. R., Ramesh, R., Hills, D., and Barber, J. (2018). Half-plane partial slip contact problems with a constant normal load subject to a shear force and a differential bulk tension. *J. Mech. Phys. Solids*, **118**:245 – 253.

[Mossakovskii, 1953] Mossakovskii, V. (1953). Application of the reciprocity theorem to the determination of the resultant forces and moments in three-dimensional contact problems. *PMM*, **17**:477 – 482.

[Mossakovskii, 1954] Mossakovskii, V. (1954). The fundamental mixed problem of the theory of elasticity for a half-space with a circular line separating the boundary conditions. *Prikl Mat I Mekhanika*, **18 (2)**:187 – 196.

[Mugadu et al., 2002] Mugadu, A., Hills, D., and Limmer, L. (2002). An asymptotic approach to crack initiationin fretting fatigue of complete contacts. *J. Mech. Phys. Solids*, **50**:531 – 547.

[Nowell, 1988] Nowell, D. (1988). *An Analysis of Fretting Fatigue*. PhD thesis, University of Oxford.

[NTSB, 2019] NTSB (2019). Left engine failure and subsequent depressurization southwest airlines flight 1380. *NTSB/AAR-19/03*, National Transportation Safety Board.

[Paris, 1963] Paris, P. C. Erdogan, F. (1963). A critical analysis of crack propagation laws. *J. Basic Eng.*, **85(4)**:528 – 533.

[Ruiz and Nowell, 2000] Ruiz, C. and Nowell, D. (2000). Desinging against fretting fatigue in aeroengines. *Eur. Struct. Integrity Soc.*, **26**:73 – 95.

[Sackfield et al., 2005] Sackfield, A., Dini, D., and Hills, D. (2005). The finite and semi-infinite tilted, flat but rounded punch. *Int. J. Solids Struct.*, **42**:4988 – 5009.

[Sackfield et al., 2003] Sackfield, A., Mugadu, A., Barber, J. R., and Hills, D. A. (2003). The application of asymptotic solutions to characterising the process zone in almost complete frictionless contacts. *J. Mech. Phys. Solids*, **51 (7)**:1333 – 1346.

[Sackfield et al., 2001] Sackfield, A., Truman, C., and Hills, D. (2001). The tilted punch under normal and shear load (with application to fretting tests). *Int. J. Mech. Sci.*, **43**:1881 – 1892.

[Southwest, 2018] Southwest (2018). *Southwest Reports Second Quarter Profit*, http://investors.southwest.com/news-and-events/news-releases/2018/07-26-2018-113124751:last retrieved 15 June 2020.

[Szolwinski and Farris, 1998] Szolwinski, M. and Farris, T. (1998). Observation, analysis and prediction of fretting fatigue in 2024-t351 aluminum alloy. *Wear*, **221**:24 – 36.

[Timoshenko, 1983] Timoshenko, S. (1983). *History of Strength of Materials*. Dover Publications.

[Tomlinson, 1927] Tomlinson, G. (1927). The rusting of steel surfaces in contact. *Proc. Royal Soc. London Series A, Containing Papers of a Mathematical and Physical Character*, **115**:472 – 483.

[Truman et al., 1995] Truman, C., Sackfield, A., and Hills, D. (1995). Contact mechanics of wedge and cone indenters. *Int. J. Mech. Sci.*, **37**:261 – 275.

[Vazquez et al., 2010] Vazquez, J., Sackfield, A., Hills, D., and Dominguez, J. (2010). The mechanical behaviour of a symmetrical punch with compound curvature. *J. Strain Ana.*, **45**:209 – 222.

[Warlow-Davies, 1941] Warlow-Davies, E. (1941). Fretting Corrosion and Fatigue Strength: Brief Results of Preliminary Experiments. *Proceedings of the Institution Mech. Eng.*, **115**:32 – 38.

[Waterhouse, 1972] Waterhouse, R. (1972). *Fretting Corrosion*. Pergamon.

[Waterhouse, 1981] Waterhouse, R. (1981). *Fretting Fatigue*. Applied Science Publishers.

[Waterhouse, 1984] Waterhouse, R. (1984). Fretting Wear. *Wear*, **100**:107 – 118.

[Weertman and Weertman, 1993] Weertman, J. and Weertman, J. (1993). *Elementary dislocation theory*. Oxford University Press.

[Williams, 1952] Williams, M. (1952). Stress singularities resulting from various boundary conditions in angular corners of plates in extension. *J. Appl. Mech.*, **19**:526 – 528.

[Wöhler, 1870] Wöhler, A. (1870). Über die Festigkeitsversuche mit Eisen und Stahl. *Zeitschrift für Bauwesen*, **20**:73 – 106.